Technical Report
for
Research Project T9234-07
"Modeling Pile Foundations for Seismic Analysis"

Determination of Rheological Parameters of Pile Foundations for Bridges for Earthquake Analysis

by

Sukomal Modak and William F. Cofer
Washington State Transportation Center (TRAC)
Washington State University
Department of Civil & Environmental Engineering
Pullman, WA 99164-2910

Washington State Department of Transportation
Project Manager
Keith Anderson

Prepared for

Washington State Transportation Commission
Department of Transportation
and in cooperation with
U.S. Department of Transportation
Federal Highway Administration

July 1997

TECHNICAL REPORT STANDARD TITLE PAGE

1. REPORT NO.	2. GOVERNMENT ACCESSION NO.	3. RECIPIENT'S CATALOG NO.
WA-RD 406.1		

4. TITLE AND SUBTITLE	5. REPORT DATE
Determination of Rheological Parameters of Pile Foundations for Bridges for Earthquake Analysis	July 1997
	6. PERFORMING ORGANIZATION CODE
7. AUTHOR(S)	8. PERFORMING ORGANIZATION REPORT NO.
Sukomal Modak and William F. Cofer	
9. PERFORMING ORGANIZATION NAME AND ADDRESS	10. WORK UNIT NO.
Washington State Transportation Center (TRAC) Civil and Environmental Engineering; Sloan Hall, Room 101 Washington State University Pullman, Washington 99164-2910	11. CONTRACT OR GRANT NO. T9234-07
12. SPONSORING AGENCY NAME AND ADDRESS	13. TYPE OF REPORT AND PERIOD COVERED
Washington State Department of Transportation Transportation Building, MS 7370 Olympia, Washington 98504-7370	Technical Report
	14. SPONSORING AGENCY CODE

15. SUPPLEMENTARY NOTES

This study was conducted in cooperation with the U.S. Department of Transportation, Federal Highway Administration.

16. ABSTRACT

Current seismic design criteria for highway bridges generally require that the effects of earthquake loading be evaluated using either an equivalent static load approach for simple bridges or a dynamic analysis for more complex bridges. These provisions usually provide detailed explanations and commentaries on techniques which are judged to be suitable for static and dynamic modeling of the bridge superstructure and supporting columns or piers. There is, however, a significant lack of guidance on exactly how the boundary conditions and soil-structure-interaction should be incorporated into the model.

The purpose of this study is to present a simple analytical model of pile and pile group foundations for use as boundary conditions in a numerical model for seismic analysis of highway bridges. Both the axial and lateral response are considered. This simple model consists of a set of springs, dashpots, and masses for each degree-of-freedom on a pile, and it is based upon the Winkler hypothesis. The spring behavior is established by using the finite element method for static load conditions. The lumped dashpot constants and masses are based on realistic approximations. The effect of a sliding interface, nonlinearity of the soil and geometric, hysteresis, and viscous damping of the soil have been considered.

The *p-y* curves for lateral and axial vibration of single piles of 0.457m (18") and 0.610m (24") diameter based on plane analysis for different depths have been presented. Similar curves for direct-lateral, shear-lateral, and axial vibrations have also been presented for two-pile groups with three different spacings.

Using these *p-y* curves, pile responses have been obtained which have been compared with those obtained from a rigorous analysis. Good agreement has been observed for a single pile response. The comparison justifies the use of this simple model.

17. KEY WORDS	18. DISTRIBUTION STATEMENT
Key words: bridge, earthquake, pile, group, finite element	No restrictions. This document is available to the public through the National Technical Information Service, Springfield, VA 22616

19. SECURITY CLASSIF. (of this report)	20. SECURITY CLASSIF. (of this page)	21. NO. OF PAGES	22. PRICE
None	None	303	

DISCLAIMER

The contents of this report reflect the views of the authors, who are responsible for the facts and the accuracy of the data presented herein. The contents do not necessarily reflect the official views or policies of the Washington State Transportation Commission, Department of Transportation, or the Federal Highway Administration. This report does not constitute a standard, specification, or regulation.

TABLE OF CONTENTS

LIST OF TABLES

LIST OF FIGURES

1. INTRODUCTION AND RESEARCH APPROACH

1.1 Context and Problem Statement

Bridges are important links in modern transportation and communication systems. Highway bridges have suffered heavy damage in recent earthquakes. Most of the damage was caused by excessive forces at the supports and by weakness of the substructure. Deficiencies in details at connections, insufficient length of bearing at supports, inappropriate design of hinges, embankment movement, liquefaction, and inadequate restraining devices have been the causes of many failures (Mizuno 1987).

Most design codes express the dynamic effects of the ground motion as a set of equivalent static forces. The equivalent lateral forces are proportional to the superstructure weight. The proportionality constant is expressed in terms of different factors, which include the regional seismicity, the importance and the ductility of the structure, the soil conditions, and the vibration characteristics of the structure. This design procedure has proven to be inadequate, and design codes are being constantly revised on the basis of lessons learned from the 1964 Alaska Earthquake, the 1971 San Fernando Earthquake, the 1985 Mexico Earthquake, the 1989 Loma Prieta Earthquake, and the 1994 Northridge Earthquake. Research has been valuable for improving the seismic performance of bridges.

The increasing use of pile foundations, the significant damage to pile-supported structures in major earthquakes, limitations in understanding, and the uncertainty in the prediction of soil-pile-structure interaction under dynamic loads all contribute to recent interest in the dynamic-response analysis of soil-pile-structure systems.

The objectives of the study presented herein are to increase the safety of the piles and the structures they support, and to better understand the interaction between the piles and the structures under both critical and operational conditions. A rational, dynamic, frequency independent lumped parameter soil-pile interaction model has been developed for both lateral and axial vibration of single piles and two-pile groups. Special

attention was paid to the nonlinearity of soil, the formation of gaps and slippage, radiation damping, and pile-group behavior. The model allows time domain nonlinear analysis to be conducted in a relatively simple manner. Since the model can reproduce the dynamic effects by itself, its parameters are defined from the static behavior of a pile-soil system by reasonable *p-y* curves developed under the static condition and obtained from finite element analysis adopting the Winkler hypothesis.

1.2 Research Objectives

The specific objectives of the research reported herein are as follows:

1. To obtain equivalent stiffness properties for single piles and pile groups that can be used to model the nonlinear behavior of pile foundations for the seismic analysis of bridge superstructures. Specifically, an objective is to define nonlinear stiffness characteristics for typical soils and pile configurations to be used as input to seismic bridge analysis software.

2. To define the dynamic pile interaction effects for groups of two piles.

3. To obtain lumped mass properties for piles and pile groups.

1.3 Background

1.3.1 Dynamic Soil-Structure Interaction

The effects of an earthquake are usually classified as primary, when due directly to the causative process, such as faulting or volcanic action, and secondary, when due to the ground motion resulting from the passage of seismic waves. The secondary effects include those associated with landslides, soil liquefaction, and low frequency structural vibration in which inertial effects are predominant (Derecho 1991). The foundation effects discussed in this thesis fall under the last category (Derecho 1991).

Ground conditions at the site affect the earthquake response of structures. Two aspects of this influence are important: (1) *site effect* — the amplifying (or attenuating) effect of local geology on the intensity as well as its filtering effect on the frequency characteristics of the transmitted seismic waves, and (2) *soil-structure-interaction* — the effect of soil properties in the immediate vicinity of a structure on the structural

response. Soil-structure interaction includes the effect of the underlying soil in modifying the response of a structure in relation to its behavior when founded on an essentially rigid base, as well as the effect of the presence of the structure in modifying the ground motion at the site in relation to the free-field motion (Derecho 1991).

From the analytical standpoint, one may view soil structure interaction as consisting of two distinct effects: (a) *inertial interaction*, which arises from the motion of the foundation relative to the surrounding soil associated with the transmission of inertial forces from the structure to the adjoining soil; and (b) *kinematic interaction*, which can occur in the absence of inertial forces, that arises when a relatively stiff structural foundation can not conform to the distortion of the soil generated by the passage of seismic waves (Derecho 1991).

In the standard analysis of building and bridge structures, it is assumed that the motion experienced by the base of a structure during an earthquake is the same as the *free-field ground motion* that would occur at the level of the foundation if no structure was present. Strictly speaking, this assumption is true only for a structure supported on essentially rigid ground. For structures supported on soft soil, the foundation motion generally is different from the free-field motion due to kinematic interaction. In addition, a structure with a flexible base has less effective stiffness than the idealized structure, so that the period of the actual structure is higher than that of the idealized structure which affects inertial interaction. A flexibly supported structure also differs from a rigidly supported structure in that a substantial part of its vibrational energy may be dissipated into the supporting medium by the radiation of waves and by hysteretic action in the soil. This affects the damping characteristics of the structure. The importance of the latter factor increases with increasing intensity of ground-shaking.

In typical dynamic structural analysis, either the load or the displacement is specified at every point of the structure. In soil-structure-interaction problems, neither the load nor the displacement is known at the boundary or at other points of the structure. When the wave front of the incident wave propagating in the soil encounters the structure, scattering of the wave front occurs. This leads to a load acting on the structure which will cause motion, accompanied by the generation of a radiation wave in the soil and a relief of the loading on the structure. All of these mechanisms are coupled: the motion of the structure depends on the loading acting on it, and the loading, in turn, is affected by the structural

motion. The same applies to soil. In a dynamic analysis, it is insufficient to prescribe a zero displacement at a large distance from the structure, as is routinely done in statics. Rather, an *energy absorbing boundary* must be specified so that once the waves leave the zone of interest, they will not return during the time of the analysis. It is thus ensured that only outgoing waves are present in the actual interaction analysis. This avoids an infinite energy buildup and it will result in damping, called *radiation damping*, occurring even in an elastic unbounded system. Excellent summaries of currently available approaches to the analysis of soil-structure interaction problems are given in the literature (Seed et al. 1975, Seed et al. 1977, Seed & Lysmer 1977, Roesset & Tassoulas 1982, Wolf 1985, Derecho 1991). Brief descriptions of the two general approaches to analysis that are currently used are given below.

1.3.1.1 Complete or Direct Methods

For methods under this category, the motion of the soil mass and the structure is determined simultaneously. A complete soil-structure interaction problem typically consist of two parts. A *site response analysis* involves the determination of the temporal and spatial variation of all motions within a site from a single specified control motion at some control point within the site where an observed or estimated motion is available. A *source problem*, on the other hand, involves the determination of the response of a structure to specified forces or displacements within a source region (Derecho 1991). The interaction analysis then consists of the superposition of these two cases. Complete methods (Idriss & Sadigh 1976, Lysmer et al. 1977) generally employ the finite element method of model representation.

It is not possible to include the source in the analytical model in earthquake response analysis, in general. In one approach, referred to as a *pseudo-interaction analysis* (Lysmer 1978), this difficulty is overcome by defining the seismic environment in terms of specified loads or displacements on an external boundary. The site response problem is solved first by deconvolution of the surface control motion to some level below the ground surface where it can be assumed that the presence of the structure will not influence the ground motion. This step is depicted in Figure 1.1.a. The second step, shown in Figure 1.1.b, consists of using the base motion computed in the first step as a specified boundary motion for a finite element analysis of the soil-structure system.

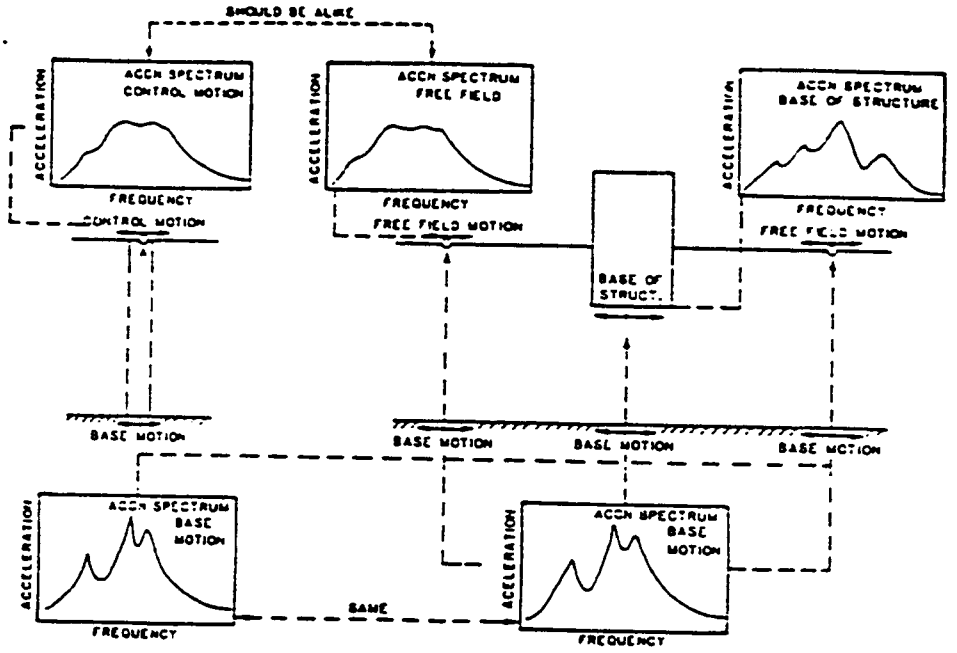

Figure 1.1 Schematic representation of pseudo-interaction method based on finite element analysis. (a) Soil deposit model, (b) Finite element model of soil-structure system. (After Lysmer et al. 1977)

1.3.1.2 Substructure Methods

In this approach, the complicated soil-structure interaction problem are broken into more manageable parts. These methods are simpler and cheaper to perform than direct methods. Here, the soil mass is treated as a continuum (half-space) and the structure is treated as a discretized model. The half-space is analyzed first, usually in the frequency domain, and the impedance (force-displacement relationship) and scattering properties at the soil-structure interface are established (Bielak 1974, Luco 1974, Veletsos 1977). Some models assume linear visco-elastic properties for the soil to simulate the energy loss due to hysteresis in the soil. The solution of this part of the problem has gained great impetus with the development of the *Fast Fourier Transform* algorithm. In the second step, the properties determined in the first step are used as boundary conditions in a dynamic analysis of the structure with a loading that depends on the free-field motions. In recent years, several substructure methods have appeared, in which the half-space solution is obtained using finite element models with transmitting boundaries (Gutierrez & Chopra 1978, Lysmer & Kuhlemeyer 1969, Kausel 1988).

The basic substructure method has provided reasonable solutions for cases involving a single structure at the surface of a uniform half-space. However, its application to the more practical case of a structure embedded in a layered half-space has not been fully explored, primarily because of the extreme complexity required in its formulation. For each dynamic degree of freedom, the standard lumped-parameter system to model the soil consists of a mass, a spring, and a damper in parallel which is attached to a rigid support. For time domain analysis, all coefficients should be frequency independent.

Discrepancies between reported results of analysis using the direct method on one hand and the substructure method on the other have been ascribed to differences in the definition of the problem (Singh et al. 1980, Chopra 1980). These differences include the idealization of the soil region, the idealization of the structure, the idealization of the structural foundation, and differences in the definition of the earthquake input.

1.3.1.3 The Strengths and Limitations of Different Methods

An important aspect of the seismic design of bridges is the evaluation of the dynamic interaction between the structure and the surrounding soil. This is usually accomplished in one of two ways, either by representing the effects of the soil on the structural response

by a series of springs and dashpots representing a theoretical half-space surrounding the structure (substructure or load-transfer method) or by modeling the soil-structure system by a finite element method (complete or direct method).

Thus, depending on the method of analysis used, structural response may be seriously overestimated or underestimated, the former leading to serious over design and lack of economy and the latter leading to potentially hazardous conditions. In a few cases, of course, both methods may lead to the same degree of safety and economy. It is the purpose of this section to present an evaluation, and to suggest appropriate methods of analysis for design purposes. For a complete discussion, the reader is referred to Seed et al. (1975).

Substructure Analyses

These analyses can be made in various ways, but essentially they are all based on evaluations of structures resting on the surface of an infinite half-space. The most common method is to represent the effects of the soil around the structure by a series of interaction springs and dashpots. Values of spring constants and damping values are determined by first examining the response of the structure resting on an idealized half-space and then determining the spring constants and damping values which, with the half-space removed, would lead to the same response values. In practice, damping values of 7%-10% are commonly assumed for strong earthquake shaking. Having determined the springs and dashpots, the dynamic analysis is carried out by specifying the motion developed in the soil surrounding the spring-dashpot system. In another slightly more complicated form of this approach, the spring and dashpot values are translated into impedance functions. This approach offers the advantage that the control method can be specified in the free-field away from the structure and variation in ground motions in the vicinity of the structure can be taken into account.

While half-space analyses of this type seem reasonable, they necessarily involve a number of assumptions and limitations. For example, in soil-structure-interaction analyses, energy is dissipated in the structure as structural damping and in the soil as material damping. Energy is also lost by radiation of waves from the base of the structure into the surrounding soil — a phenomenon called *radiation* or *spatial* or *geometric* damping. It is an extremely important factor in foundation vibration problems, but it is of

relatively minor importance in studies of earthquake response. Available analytical results are based on the assumption that the soil has no material damping properties. In fact, material damping is very high in soils and, thus, an important factor affecting the soil-structure response is omitted from consideration. To overcome this deficiency, it is customary to make some assumption concerning the magnitude of material damping effects and incorporate them with other damping effects in the final analysis.

Half-space analyses can only be made at the present time for deposits with one or two layers, and even two-layer analyses are very complicated. In general, most sites involve several layers of different types of soil underlain by rock. The presence of the underlying rock layer would prevent energy from dissipating continuously through the base. The assumption of a single soil layer radically over-simplifies the conditions for most deposits and, again, may inadequately reflect the radiation damping in stratified deposits. Indeed, because radiation damping effects are not evaluated accurately and material damping effects are not evaluated at all, the combined effects of these two sources of damping must be estimated for design purposes, rather than rationally determined. In view of the uncertainty involved, a conservative choice of an overall damping value is usually made.

In order to determine appropriate values of spring constants, it is necessary to know the moduli of soils adjacent to the structure. However, the deformation moduli of soil depend very much on the strain level induced in them and depth of embedment. The substructure analysis method provides no means for determining the strains induced in the soils, thereby prohibiting the selection of an appropriate modulus of deformation. Some design companies advocate the use of soil moduli compatible with the strains induced in the soil by earthquake motions in the free-field; others use moduli determined at extremely low strains. Furthermore, in analyzing the response of embedded structures, some organizations use spring constants appropriate for near-surface conditions while others use higher values which reflect the influence of the depth of embedment. The wide difference in results inevitably leads to considerable uncertainty in the selection of design criteria.

Since half-space solutions are only available for structures resting on the ground surface, there is no simple means for determining spring constants and dashpots for embedded structures. Spring constants for embedded structures can be determined with reasonable accuracy by static finite element analyses, but dashpot characteristics cannot

be found from a static analysis. Also, for embedded structures, interaction-spring analyses are invariably based on the assumption that motions around the structure are the same as those below the base; i.e. the motions are the same everywhere in the surrounding soil. Clearly, this could only be so if the surrounding soil were rigid or very stiff. However, ground motions vary considerably at depths during earthquakes.

The existence of soil-structure interaction effects in a response problem necessarily means that the presence of the soil affects the movements of the structure and, conversely, the presence of the structure affects the movements of the soil. Thus, for a soil-structure system, the ground motions at points below the base of the structure are different from those in the free-field at the same level. While it is possible to determine the effect of the structure on the motions developed below its base using the impedance function approach, interaction-spring analyses are often based on the assumption that the motions below the base of the interaction-springs are the same as those in the free-field. This is tantamount to assuming that soil-structure interaction affects the motions in the structure without simultaneously affecting the motions in the soil, which is inconsistent.

Finally, the response of a structure may be influenced to a very significant extent by the presence of adjacent structures. While it is possible to consider such effects in half-space analyses, they are not normally considered in interaction-spring analyses.

Finite element methods of analysis

In an effort to overcome some of the limitations of the half-space or interaction-spring method of analysis, finite element methods of analysis have been developed and used to solve soil-structure interaction problems. The control motion is typically specified at some point in the free-field. As a first step, therefore, it is necessary to determine the motions that would have to be developed in an underlying rock-like formation in order to produce the specified motions at the control point. This can be accomplished readily by means of a wave propagation analysis of a column in the free-field using an appropriate computer program such as SHAKE (Schnabel et al. 1972).

It may be seen that this method of analysis does not suffer from many of the limitations of the interaction-spring approach. For example:

1. The analysis can take into account the deformability of the soil around the structure and the variations of accelerations in the soil profile.

2. The analysis does not involve the use of the same motions below the structure as in the free-field.

3. The analysis procedure provides a means for determining the motions in the soil adjacent to the structure.

4. Soil properties (both damping and moduli) can be determined in a rational way.

5. Material damping can be incorporated in the analysis.

6. Radiation damping can be included appropriately.

7. The effects of adjacent structures can be considered. However, while eliminating these limitations of the interaction-spring approach, finite element analysis can introduce other limitations that can lead to deficiencies in the computed response values. These are often due to limitations of the computational techniques used, and it is important to recognize them in evaluating the significance of the results obtained.

For example, for strong shaking, the material damping of the soil will typically be much larger than that in the structure, and it will vary to some extent with depth and lateral distance from the structure. Furthermore, the damping may vary in different parts of the structure itself. Clearly, it is desirable, in analyzing situations of this type, to use a finite element analysis procedure which has the capability of considering a different and completely specified damping value in each element of the mesh. Few analytical procedures currently in use have this capability. Finite element analyses are often performed on the basis of mode superposition procedures. In this approach, the damping ratio must be the same for all elements. Accordingly, when this analysis procedure is used, some compromise value between the lower values appropriate for the structure and the higher values appropriate for the soil deposit is usually adopted. For strong shaking, this value may be in the order of 7%-10%. Variable damping capabilities in the analysis procedure are highly desirable when finite element with secant modulus procedures are used.

One of the means available for considering the variation of damping in different elements in a soil-structure system is to incorporate damping using a Rayleigh damping matrix of the form $[C] = \alpha[M] + \beta[K]$, in which $\mathbf{M}$ = the mass matrix; $\mathbf{K}$ = the stiffness

matrix; and α and β are *Rayleigh damping coefficients.* Thus, damping is expressed as a linear combination of the mass and stiffness matrices of the system. It can be shown that the use of this damping matrix is equivalent to using a modal analysis in which the fraction of critical damping in the nth mode is

$$\xi_n = \frac{a_0}{2\,\omega_n} + \frac{a_1 \omega_n}{2}, \qquad [1.1]$$

where ω_n is the circular frequency of the nth mode of vibration and a_0 and a_1 are arbitrary constants which are obtained from two conditions. For example, if the damping ratios ξ_m and ξ_n corresponding to modal frequencies ω_m and ω_n are given, Equation 1.1 can be written in the form expressing the two conditions as

$$\begin{Bmatrix} \xi_m \\ \xi_n \end{Bmatrix} = \frac{1}{2} \begin{bmatrix} 1/\omega_m & \omega_m \\ 1/\omega_n & \omega_n \end{bmatrix} \begin{Bmatrix} a_0 \\ a_1 \end{Bmatrix}, \qquad [1.2]$$

from which

$$\begin{Bmatrix} a_0 \\ a_1 \end{Bmatrix} = 2 \left\{ \frac{\omega_m\, \omega_n}{{\omega_n}^2 - {\omega_m}^2} \right\} \begin{bmatrix} \omega_n & -1\omega_m \\ -1/\omega_n & 1/\omega_m \end{bmatrix} \begin{Bmatrix} \xi_m \\ \xi_n \end{Bmatrix}. \qquad [1.3]$$

However, in general, ξ can be defined for as many frequencies as desired as

$$\xi_n = \frac{1}{2\omega_n} \sum_b a_b\, {\omega_n}^{2b}. \qquad [1.4]$$

In principle, the value of b may range from $-\infty$ to $+\infty$, but in practice it is desirable to select values as near as possible to zeros. If damping ratios are specified for k frequencies, only k terms are considered. In general, the relationship may be written as

$$\{\xi\} = (1/2)\ [Q]\ \{a\}, \qquad [1.5]$$

where Q is a square matrix involving different powers of the modal frequencies. The above equation can be used to solve for $\{a\}$ as

$$\{a\} = 2\ [Q]^{-1}\ \{\xi\}. \qquad [1.6]$$

In effect, the proportion of critical damping varies with frequency and it increases as the frequency increases. A major advantage of analysis methods using Rayleigh damping is that they can be modified to permit the inclusion of variable damping (Idriss et al. 1974). While this method of approach is extremely useful for the analysis of certain types of problems, the frequency-dependence of the damping can lead to very high values of

damping at high frequencies, as shown in Figure 1.2, with the result that these frequencies are effectively damped out completely from the structural response (Clough & Penzien 1975). This may be of little importance in analyzing the response of structures such as earth dams, where the induced stresses are controlled mainly by the first few modes, but it can be a serious limitation in the analysis of a structure containing critical equipment with high-frequency characteristics, such as nuclear power plants. Thus, the formulation of damping in the analysis of soil-structure systems requires the utmost care in cases for which high frequency effects are important.

Another aspect of finite element analysis requiring careful control in cases where high frequency effects are important is the choice of element size for the finite element mesh, especially in the vertical direction. It has been found (Kuhlemeyer & Lysmer 1973) that the dimension of the element in the direction of wave propagation has a major influence on the frequency of motions that can be transmitted, with large elements being unable to transmit motion with short wavelengths, leading to a marked reduction in response for higher frequencies. In fact, Kuhlemeyer and Lysmer proposed the empirical rule that the required mesh size for effective transmission of any motion should be not more than one-quarter, or preferably one-eighth, of the wave length of the motion. This requires the use of very small element sizes for transmission of frequencies of the order of 20-30 cps, as is required in nuclear power plant studies.

The extent of the finite element mesh is especially important in considering the effects of radiation damping. If the boundaries of the mesh are placed too close to the structure, some of the energy which should dissipate from the system will be reflected back, thereby changing the response. This difficulty can be overcome by the use of energy absorbing boundaries (Isenberg 1970, Lysmer & Drake 1971, Lysmer & Kuhlemeyer 1969, Kausel 1988) or by the use of a sufficiently extensive mesh. If the material damping in the soil is relatively high, energy radiating outward from the vicinity of the structure is absorbed relatively quickly and free-field conditions are developed within a distance of 120–150m (400–500 ft). However, if the soil damping is low, the effects of wave motions generated by the structure may be felt a considerable distance away (Seed et al. 1975).

In analyzing soil-structure response using the finite element method, it is customary to assume that the motions in the system are generated by the upward propagation of waves from an underlying boundary. This is particularly true in cases for which the

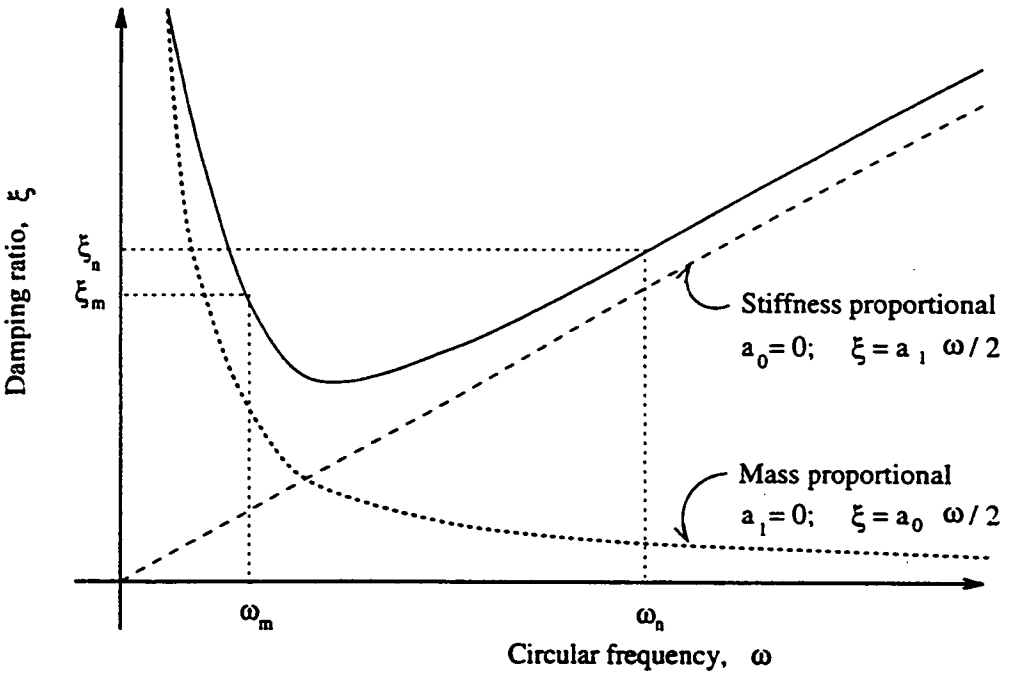

Figure 1.2 Relationship between damping ratio and frequency for Rayleigh damping. (Redrawn after Clough and Penzien 1975)

control motion is specified at some point in the ground and vertical wave propagation analyses are used to compute the corresponding motion in an underlying stiff soil or rock formation. The same base rock motion is then used to excite the soil-structure system. While this may not be a completely accurate picture of the source of earthquake excitation in the soil mass, it is probably a reasonably good representation of the actual condition. Thus, while it is a potential source of error, it is consistent with the normal simplification of complex engineering systems used for engineering analysis purposes.

In addition to the limitations presented, complications in evaluating dynamic response also arise from uncertainties in determining soil properties and the characteristics of the ground motion. Thus, the problem of ground and structural response to earthquake excitation is extremely complicated. Consequently, it is pointed out that even sophisticated analyses do not have the capability to incorporate many important aspects of actual conditions (Seed et al. 1975).

Conclusion The following conclusions may be drawn with regard to soil-structure interaction effects for embedded structures:

1. The errors and assumptions that must be made in using the half-space theory, or interaction-spring analysis, to evaluate the response of deeply embedded structures may make those approaches very approximate for these conditions.

2. The finite element method, properly performed with due regard to the extent and fineness of the mesh and variations of damping characteristics, is the best analytical tool currently available.

3. Although it is revealed that the FEM gives the most accurate result for SSI analyses, it is not advisable to use FEM for routine design of bridges. Because of the heavy involvement of computer time and data synthesis, it is likely to be too cumbersome for a design engineer to handle this large volume of numerical results obtained from FEM unless analysis and design are performed by integrated computer programs.

4. The results of any analysis of the seismic response of deeply embedded structures must be interpreted with good judgment before being adopted for design.

1.3.1.4 Dynamic Soil-Pile-Structure Interaction Parameters

The following parameters influence the response of pile supported structures subjected to earthquake excitation (Gazetas et al. 1991, Derecho 1991, Hadjian et al. 1992).

- **Soil Profile**
  1. Shear wave velocity, V_s
  2. Bulk density, ρ_s
  3. Poisson's ratio, ν_s
  4. Damping ratio, β_s
  5. Material nonhomogeneity
  6. Markedly layered media
- **Pile Tip Condition**
  1. Floating (friction) pile
  2. End-bearing pile
- **Physical attributes**
  1. Pile diameter, d
  2. Pile length, L
  3. Pile spacing ratio, s/d
  4. Pile slenderness ratio, L/d
  5. Pile-soil material stiffness ratio, E_p/E_s
  6. Pile-soil mass density ratio, ρ_p/ρ_s
  7. Pile batter, α
  8. Angle of loading for a pile-group, θ
- **Nonlinear Effects**
  1. Time history of free-field motion

2. Lateral resistance of soil per unit length of pile, p-y curves
3. Axial resistance of soil per unit length of pile, t-z curves
4. Quality of pile-cap contact with the soil
5. Pile-soil separation and gapping
6. Pile-soil slippage and friction
7. Stress induced radial nonhomogeneity of soil
8. Cracking of concrete pile sections
9. Pile installation procedure
10. Initial stresses

1.3.2 Current Practice

Typically, dynamic effects in design are circumvented due to a lack of practical analysis methods, or ignored due to the seldom substantiated assumption that they are negligible. For the majority of applications, the state-of-practice is considerably less developed than the state-of-the-art. This stems primarily from the very complex nature of the dynamic problem, particularly for earthquake loads. Another contributing factor is the shared, but not well defined, responsibility between the structural and geotechnical engineers and, in particular, the lack of adequate integration of their respective contributions. It is generally believed that the additional cost of detailed dynamic evaluation is not justified considering the fact that a correct analysis is not simple. The level of application of the current state of knowledge in practice is idealized in Figure 1.3. A brief review of seismic code requirements for pile foundations and available computer codes has been included herein. A detailed survey is available in Hadjian et al. (1992).

1.3.2.1 Review of Seismic Code Requirements for Pile Foundations

Code provisions have addressed soil-pile-structure interaction effects during earthquakes for a number of years. Code provisions covering the design of pile foundations for seismic loads have developed from two somewhat different backgrounds. One approach, following recommendations developed by the Structural Engineers Association of California (SEAOC), is contained in the current Uniform Building Code (1991) requirements published by International Conference of Building Officials (1991). The other approach,

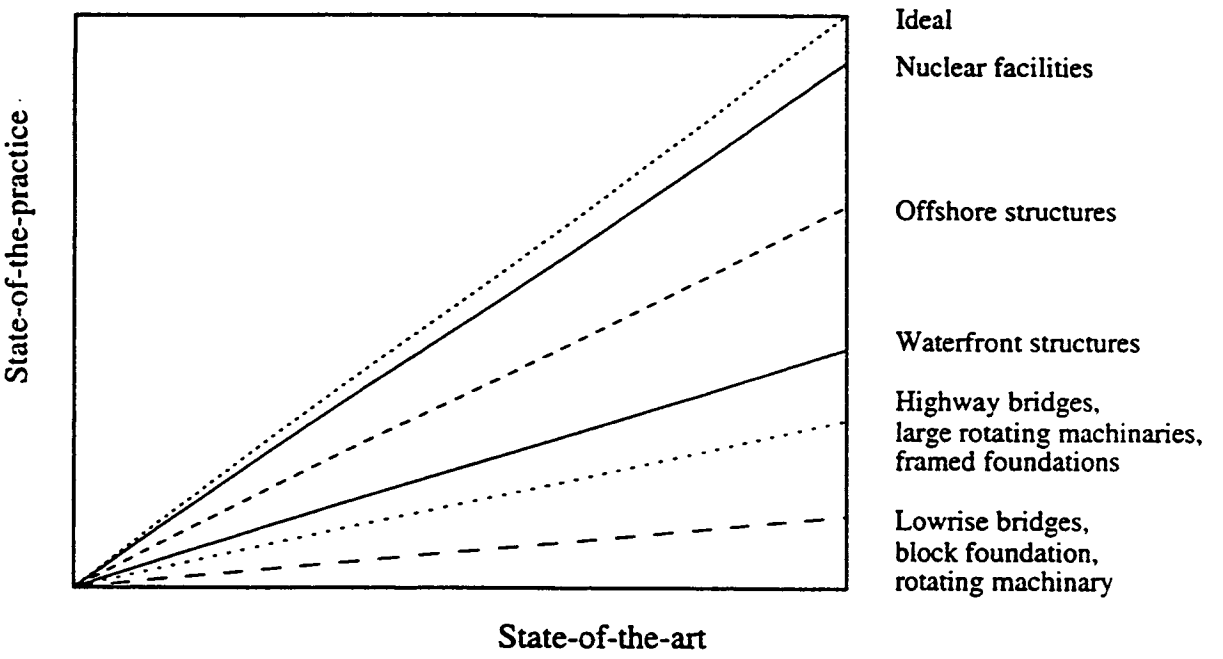

Figure 1.3 State-of-the-practice lags state-of-the-art in considering the pile-structure interaction. This lagging is most severe for low rise buildings and bridge foundations. (Redrawn after Hadjian et al. 1992)

stemming from the Applied Technology Council (ATC) recommended provision, is contained in the recent NEHRP (1991) document. A brief review of these code provisions for piles, soil-pile-structure interaction effects during earthquakes, is provided below.

Uniform Building Code (UBC 1991)

The UBC provides specific design requirements for piles subject to seismic forces, but gives only minimal requirements and guidance for determining design seismic forces for pile-supported structures. The seismic design requirements are adopted primarily from the recommended provisions of the current SEAOC "Blue Book".

Design provisions include the following requirements:

1. Individual pile caps and caissons of all structures subjected to seismic forces are to be interconnected by ties designed for a minimum horizontal force equal to 10% of the larger column vertical load (2908b).

2. Special provisions for Seismic Zones 3 and 4 (2910) include allowing greater than a one-third increase in stress allowable for soils (pile-soil friction and bearing) when substantiated by geotechnical data, omitting the force F_t concentrated at the top of the building for overturning moment at the base when using the static force procedure for regular buildings, and the design of piles and caissons for flexure (e.g., ductile detailing for 120% of the flexural length for concrete) when the tops of the piles will be displaced by earthquake motions.

3. Consideration of the effects of soil-pile-structure interaction on building response is required only for structures located on soft soils (profile type S4) with a period greater than 0.7 seconds (2335b4B). For this case, the dynamic lateral force procedure is required for both regular and irregular buildings. However, no specific requirements are imposed on the mathematical modeling of the foundation for dynamic analysis (2335c). Since any structure may be designed using the dynamic lateral force procedure (2333h) and there are no restrictions that a fixed-base model be used, the effects of soil-pile-structure interaction may always, if desired, be scaled up close to or equal to the base shear determined by the static force procedure (2335e3). Thus, any potential reduction in design forces due to consideration of soil-pile-structure interaction can seldom be realized in design.

NEHRP (1991)

The interest in soil-structure interaction effects during earthquakes seems to have been initiated in 1972 by the applied Technology Council following the 1971 San Fernando Earthquake. A cooperative program, including participants from the public and private sector, design professionals, researchers, federal agency representatives, staffs from model code organizations, and representatives from state and local governments throughout the United States, was initiated to present the current state-of-knowledge in research and engineering practice as they pertain to the seismic design and construction of buildings. The ATC 3-06 (1978) document was the result of this pioneering work. A review of ATC 3-06 indicates that if adequate ductility was provided, piles designed (statically) to vertical loads and code specified lateral loads (base shear) were expected to perform their function during earthquakes.

The 1991 NEHRP document, *Recommended Provisions for the Development of Seismic Regulations for New Buildings*, as well as previous editions, is primarily based on the early work. ATC 3-06 recommended specific pile design provisions for four seismic performance categories (A, B, C, D, the latter category comparing roughly to California design practice for normal buildings other than hospitals). NEHRP provisions have added an additional category E, restricted to essential facilities in zones of relatively high seismicity.

Specific design requirements of the NEHRP document for piles subject to seismic forces are similar to the UBC (1991). Provisions include foundation ties for pile caps, drilled piers, and caissons (7.4.3), and reinforcing for 120% of the flexural length (point of fixity to pile cap) to achieve ductility for pile foundations in relatively soft soil profiles in high seismic areas (7.5). A reduction factor of 0.75 may be used for foundation overturning moment at the foundation soil interface for all building heights when using the equivalent lateral force procedure (4.5). A 10% reduction is allowed when using the modal analysis procedure (5.10).

Special provisions that may be used to incorporate the effects of soil-structure interaction by modifying the dynamic properties of the structure and evaluating the response of the modified structure to the free-field ground motion are provided (Appendix to Chapter 6: NEHRP 1991). The soil-structure interaction effects result in an increase in the natural period of the structure caused by the flexibility of the foundation soil and a change

(usually an increase) in radiation and material damping in the soil. Two procedures for incorporating soil-structure interaction effects are presented: (1) *Equivalent Lateral Force Procedure*, and (2) *Modal Analysis Procedure*. Both methods lead to a decrease in design values of base shear, lateral forces, and overturning moments, but may increase lateral displacements and secondary forces associated with P-Δ effects. A reduced base shear of no less than 70% of the base shear determined from the equivalent lateral forces procedure may be used, based on an effective building period and increased damping for the soil structure system.

The effective period is based on lateral and rocking foundation stiffness using soil properties compatible with soil strain levels associated with the design earthquake motion (Chapter 6: NEHRP 1991). Lateral and rocking stiffness for pile foundations are computed by evaluating the static stiffness of individual piles. These may be determined from field tests or analytically, by treating each pile as a beam on an elastic foundation.

It is indicated in the provisions that more elaborate procedures would be justified only for structures of major importance or if soil-structure interaction is of definite consequence in design. In this case, techniques that might be considered include better estimates of soil properties and foundation stiffness, and finite element modeling of the structure-soil system taking due account of the nonlinear effects in both the structure and the supporting medium. It is emphasized that, while more elaborate procedures may be appropriate in special cases for design verification, they involve their own approximations and they do not eliminate the uncertainties that are inherent in the modeling of the structure-foundation-soil system, in the specification of the design ground motion, or in the properties of the structure and soil.

1.3.2.2 Review of Current Software for Pile Analysis

In this section, some of the computer programs for analysis of pile foundations, as identified by Hadjian et al. (1992), are described. It is not an exhaustive list.

COM624

This program computes the deflection and bending moment of a pile under static lateral loads as a function of depth. It is assumed that the pile is a linearly elastic beam and it is supported as a beam on inelastic foundation (Reese & Sullivan 1984). The behavior of the soil surrounding the laterally loaded pile is described in terms of p-y

curves, which relate soil resistance to pile deflection at various depths below the surface. In general, the curves are nonlinear and depend on several parameters, including depth, soil shear strength, and number of load cycles. Solution of the governing differential equation is based on the finite difference method. This program can handle different types of boundary condition including specified lateral load, moment, slope, and rotational restraint.

LPILE — Analysis of Piles and Drilled Shafts Under Lateral Load

LPILE is a special purpose program based on rational procedures for analyzing a pile under lateral loading (Ensoft Inc. 1991). The program is similar to COM624. LPILE computes deflection, shear, bending moment, and soil response with respect to depth. The nonlinear *p-y* curves may be input by the user, or the program will generate them internally following published recommendations for various types of soils.

The following features are included in this program: multiple load cases, different boundary conditions, resistance from pile base, and nonprismatic piles.

APILE2 — Analysis of Vertically Loaded Piles

The program uses a well-known *t-z* method for pile-soil interaction analysis with nonlinear *t-z* curves. It has the capability of handling negative skin friction. The principal output is the pile-head movement as a function of applied load but, for any given load, load transfer and movement can also be obtained as a function of the length of the pile.

GROUP — Analysis of Piles

This program computes the distribution of loads to piles in a group. Batter piles and vertical piles can be included in the same group. Three boundary conditions are handled for the pile-head: pinned, fixed head, and elastic restraint. *p-y* curves can be input by the user or they can be generated internally. If desired, the pile-soil-pile interaction can be taken into account by introducing reduction factors for the *p-y* curves for single piles. The deflection, bending moment, shear, and soil resistance are computed as a function of depth for each pile. The solution is two-dimensional. The results satisfy the conditions of both equilibrium and compatibility with nonlinear soil response. Iterative techniques are employed in solving the nonlinear difference equations.

DYNA

This program calculates the response of rigid foundations to all types of dynamic loads which can be produced by rotating or reciprocating machines, earthquake, or traffic (Novak et al. 1985). The foundation stiffness and damping coefficients are returned for the possible use in soil-structure interaction analysis. Capabilities are included for soil layering, a weak zone around embedded foundations and piles, pile interaction in a group, interaction between degrees of freedom, and other features. The analysis is linear. Nonlinearity can be included approximately by modeling the weakened zones around the footing or pile and by adjusting the values of soil shear modulus and internal damping according to the level of the stress.

For a group of piles, it is assumed that the piles are embedded in a layered medium. The tip conditions may range from end bearing to floating. Pile heads may be fixed or pinned. The piles may be of step wise variable cross-section, and they may be battered. The piles may have a weakened cylindrical zone around them. For a group of closely spaced piles, the effect of pile-soil-pile interaction (the group effect) on stiffness and damping of the group is evaluated approximately, using the static interaction coefficients defined by Poulos (1968, 1971, 1979, 1980).

PILAY2 — Stiffness and Damping of Piles in Layered Media

For a vertical pile embedded in layered soil, the program evaluates dynamic stiffness and damping, internal forces, and displacements for all vibration modes (Novak & Aboul-Ella 1978*a*). With stiffness and damping available, the response of pile supported footings and structures to dynamic loads can be predicted using the same techniques as those applied with shallow foundations. Any number of soil layers having different properties can be considered and soil material damping is included in all vibration modes. Displacements and internal forces in the pile are given for all modes. The pile can be of variable cross section, or Franki type, and it can stick out of the ground. Any tip condition can be considered and the head can be either fixed or pinned.

SPASM — Seismic Pile Analysis with Support Motion

This program was developed for the response analysis of piles due to earthquake ground motion. Wave loadings and mud-slide effects may also be considered. The single pile member is represented in the analysis by a discrete element mechanical model which is restricted to linearly elastic behavior. The soil-pile coupling at each node along the

embedded length of the pile is represented by a multi-element assemblage of friction blocks, springs, and dashpots. The program allows either degradation or hardening of resistance as a function of deflection and of the number of reversals of deflection in the range beyond an initially elastic condition. Furthermore, the formation of gaps is allowed in order to properly represent the expected soil-pile interplay in the upper layers of the soil. Simplified superstructure effects can be simulated by increased stiffness along the pile member within the structural system and by coupled rotational restraints at appropriate joints.

It uses Crank-Nicolson type of implicit numerical solution. The computer program is formulated to allow interfacing with either a superstructure program or a free-field motion program.

1.3.3 Review of Previous Research

The complexity of dynamic pile behavior led Terzaghi and Peck (1967) to state that

> "... theoretical refinements in dealing with pile problems.... are completely out of place and can be safely ignored."

However, in spite of this pessimistic evaluation, a number of analytical and numerical approaches to the analysis of pile dynamic behavior have been developed. These approaches have provided a much sounder theoretical basis for pile design than the equivalent cantilever concept or other purely empirical methods which dominated the field for decades. Nevertheless, some differences between the various theoretical approaches exist, and the experiments that have been reported are sometimes inconclusive. Also, some uncertainties are inevitable when applying an idealized theory to field conditions. Thus, it may be useful to review some of the approaches in order to examine the differences among them and summarize what can be learned from experiments and observations.

There are different dynamic loads that can act on piles including earthquake forces, wave forces, wind forces, and machine imbalance. Here, earthquake loading is the primary concern.

In this section, the topics that are discussed include the properties and behavior of single piles and pile groups, interaction with the cap, pile experiments, pile-structure interaction, and other topics. The subject of pile dynamics has received a comprehensive treatment in the state of the art reports by many researchers (Tajimi 1977, De Beer et al.

1977, O'Neill & Dobry 1980, Nogami 1987, Prakash & Sharma 1990, Novak 1991). A brief presentation follows in the following subsections which are organized in the way that is similar to that done by Novak (1991).

1.3.3.1 Dynamic Behavior of Single Piles

The earliest systematic, theoretical studies of dynamic soil-pile interaction are due to many researchers (Parmelee et al. 1964, Tajimi 1966, Penzien 1970, Novak 1974). Parmelee et al. (1964) and Penzien (1970) employed a non-linear discrete model and a static theory to describe the dynamic elastic stress and displacement fields. Tajimi (1966) used a linear visco-elastic stratum of the Kelvin-Voigt type to model the soil and, in his analysis of the horizontal response, neglected the vertical component of the soil motion. Novak (1974) assumed linearity and an elastic soil layer composed of independent infinitesimally thin horizontal layers extending to infinity. Nogami and Konagai (1987, 1988) developed a lumped parameter model which included linear and nonlinear springs, along with dampers, for radiation damping. It was developed for time domain analysis of laterally loaded single piles. A similar lumped parameter model for axial vibration of single piles was developed by Nogami and Konagai (1986, 1987, 1988) and Kagawa (1991). The different approaches adopted and the results that they yield are briefly discussed below.

Single Piles in Homogeneous Soil

Analytical and numerical approaches have been formulated in terms of continuum mechanics for the analysis of interaction between the pile and soil, schematically depicted in Figure 1.4. Even for the idealistic assumptions of linear elasticity or visco-elasticity, homogeneous soils, and the pile being welded to the soil, the problem is very difficult to solve. Thus, approximate procedures were formulated first. Tajimi's (1966) solution of the horizontal response of an end-bearing pile in a homogeneous layer, the first of its kind, neglected the vertical component of the motion. Novak (1974) formulated a very simple approach based on plane strain soil reactions, which can be interpreted as a dynamic Winkler medium or a complex plane-strain transmitting boundary placed directly next to the pile. Material damping was later included in closed form expressions for the soil reactions (Novak et al. 1978). The application of the same approach to the vertical response of floating piles (Novak 1977) indicated great sensitivity of the pile behavior to

the tip condition and showed that floating piles generate more radiation damping, but less stiffness, than end-bearing piles. Torsional response was also examined in this way (Novak & Howell 1977, Novak & Howell 1978) and the importance of material damping for this vibration mode was demonstrated.

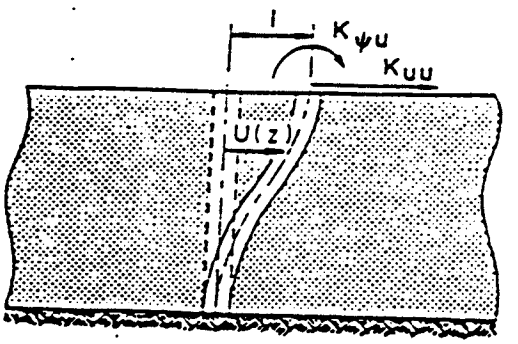

Figure 1.4 Schematic diagram of pile-soil interaction representing impedance functions for pile-head horizontal displacement. (After Novak 1991)

A somewhat more rigorous solution, similar to that of Tajimi (1966), was formulated by Nogami and Novak (1976) for the vertical response and, later, for the horizontal response (Novak & Nogami 1977). These approximate solutions offered basic insight into the behavior of the soil-pile system. However, more accurate solutions, based on the solution of the governing equations of a three dimensional continuum, were also formulated (Kobori et al. 1977, Sen et al. 1985, Pak & Jennings 1987). Rajapakse and Shah (1987*a*, 1987*b*, 1989) evaluated the accuracy of some of the existing solutions and concluded that continuum models based on harmonic line loads may not be sufficiently accurate. Therefore, they generated an extensive set of charts for impedances of floating piles.

Makris and Gazetas (1991) investigated the phase wave velocities and displacement phase difference in a harmonically oscillating pile. For lateral inertial loading, they found that significant vibration occurs at the top (depth of 5-10 diameters). The phase

difference between pile displacements at various depths was shown to be insignificant for both vertical and lateral load and, therefore, waves emanated nearly simultaneously from the periphery of an oscillating pile.

Mamoon and Banerjee (1992) adopted an efficient, but approximate, hybrid boundary element technique to model single elastic piles in elastic half-space. This method can also handle some types of nonlinearities. Mamoon and Banerjee (1990) also investigated the angle of incidence of traveling S-H waves on the response of single-piles and pile-groups. It has been revealed that, at the low frequency range, piles and pile groups essentially follow the ground motion and, at higher frequencies, they seem to be remain relatively still. An obliquely incident wave was shown to produce higher displacements than a vertically incident one. In the low frequency range, vertically incident waves produce higher rotations of the pile head than those that are obliquely incident. The cap displacements were not as sensitive to the difference in the angle of incidence. The practical significance of all such curves is that, by multiplying a given free-field design response spectrum with the appropriate interaction curve, one may obtain a design response spectrum that can be used as an input motion at the base of the structure on the pile foundation.

Haldar and Bose (1990) found that the dynamic soil distributed stiffnesses along the pile in lateral vibrations of a floating finite pile are higher than those for an infinite pile obtained by Baranov (1967). On the basis of the assumption that the vertical component of the displacement vanishes for lateral vibration of piles in a uniform elastic soil medium, this study indicated that soil stiffness does not vary significantly along the pile. The same conclusion has been made both for the real and imaginary part of the impedance function.

Abendroth et al. (1989a, 1989b) have composed several design alternatives for pile behavior. The alternatives included an equivalent-cantilever column based on horizontal stiffness, maximum moment, or elastic buckling load, and finite element analysis.

Valsangkar and Pradhanang (1987) conducted an investigation of the effect of axial force on the lateral response of end bearing piles, assuming a constant coefficient of subgrade reaction as is usually encountered in stiff cohesive soils under small displacements. The results indicate that an axial force which is less than the critical Euler buckling load has a negligible influence on natural frequency response, but it usually decreases the first fundamental frequency. The findings indicated that the existing method of free vibration analysis neglecting axial load is reasonably valid.

Some dynamic soil reaction values for plane-strain cases of rigid, massless, infinitely long piles in elastic, homogeneous, and visco-elastic soil were given by Novak et al. (1978). Nogami and Novak (1980) investigated the soil reaction on the basis of a continuum model. They concluded that, at frequencies higher than the fundamental frequency of the soil deposit ($a_0 > (1/2)(r_0/h)$, where r_0 = pile radius, h = pile length = soil deposit depth), the soil medium can be treated as uncoupled springs and dashpots distributed along the length of the pile. At any particular frequency, such a treatment is more favorable for stiffer piles and deeper soil deposits. The constants of these springs and dashpots can be obtained from a cylindrical plane-strain condition and, therefore, they are independent of the parameters of the pile.

A finite layer solution has been obtained by Lee and Small (1991*a*, 1991*b*) for isotropic and cross-anisotropic, horizontally layered elastic soil. The dynamic soil-reaction characteristics of axially loaded single piles were studied by Kagawa (1991) to find simple models for a beam-on-Winkler-foundation-type analysis of axially loaded single piles.

Finite element modeling has been applied to piles by many researchers (Kuhlemeyer 1976, Kuhlemeyer 1979*b*, Kuhlemeyer 1979*a*, Blaney et al. 1976, Wolf & von Arx 1978, Waas & Hartmann 1981, Sanchez-Salinero 1982, Faruque & Desai 1982, Muqtadir & Desai 1986, Sayegh & Tso 1988, Brown & Shie 1990, Brown & Shie 1991, Trochanis et al. 1991*b*, Trochanis et al. 1991*a*, Brown & Shie 1991). Boundary element approaches have also been developed (Banerjee 1978, Banerjee & Sen 1987). Ready to use charts and formulae have been produced for homogeneous soils (Kuhlemeyer 1979*a*, Kuhlemeyer 1979*b*, Roesset 1980, Dobry et al. 1982, Novak & El Sharnouby 1983). Thus, a considerable amount of data on piles in linear, homogeneous media is available. Although some differences in this data exist from the practical point of view, they agree reasonably well. It has been found from nonlinear finite element analysis that pile-soil slippage is practically the only source of nonlinear behavior and energy dissipation under axial loading, as yielding occurs within a narrow region of soil surrounding the piles (Trochanis et al. 1991*b*).

Much of the attention has been focused on the pile-head *complex dynamic stiffness (impedance function)* because it has a strong influence on the response of pile supported structures. The impedance functions are defined as amplitudes of harmonic forces (or moments) that have to be applied to the pile head in order to generate a harmonic motion with a unit amplitude in the specified direction, as is schematically depicted in Figure 1.4

for the case of horizontal impedance. The complex stiffness can be expressed in any of the following ways, i.e.

$$K = K_1 + iK_2 = k + i\omega C \qquad [1.7]$$

in which K_1 and K_2 are the real and imaginary parts of the complex stiffness, respectively, and $i = \sqrt{-1}$ = complex operator, $k = K_1$ = true stiffness, $C = K_2/\omega$ = coefficient of equivalent viscous damping, and ω = circular frequency. All of the parameters in Equation 1.7 depend on frequency or the dimensionless frequency $a_0 = r_o\,\omega\,/V_s$ where r_o = pile radius and V_s = soil shear wave velocity. An example of the horizontal impedance of end-bearing piles is shown for two soil-pile stiffness ratios in Figure 1.5. In this figure, V_c is the primary wave velocity in the pile, L is the pile length, ν is the Poisson's ratio, D is 2β where β is the soil material damping ratio, and $\bar{\rho}$ is the ratio of the soil specific mass to pile specific mass. The depressions visible in Figure 1.5a practically disappear for higher soil material damping.

Interesting features of the pile impedance follow from the theoretical solution indicated in Figure 1.5. For example, pile-head dynamic stiffness varies little with frequency, except for very heavy piles or very weak soils, in which case it diminishes with frequency in a parabolic manner and can even become negative for endbearing piles vibrating below the fundamental frequency of the soil layer. Also, the geometric damping is absent because no progressive waves are generated in an elastic medium, leaving soil and pile material damping as the only source of energy dissipation. Apart from this low frequency region, a fully embedded slender pile, not supporting any additional mass, is usually overdamped and consequently does not exhibit any marked resonance peak in dynamic tests.

Single Piles in Nonhomogeneous Soil

Comparing experiments with theoretical predictions has repeatedly shown that if the soil is assumed to be homogeneous, both pile stiffness and damping can be grossly overestimated (Novak & Grigg 1976, Novak & Sheta 1982). The reasons for the deficiencies of the theory based on the assumption of soil homogeneity are local non-linearity and pile-soil slippage, schematically depicted in Figures 1.6 and 1.7. Single piles under horizontal loading, as in Figure 1.6, are particularly sensitive to these two factors. Observations of this kind led to the development of approaches better suited for nonhomogeneous soils.

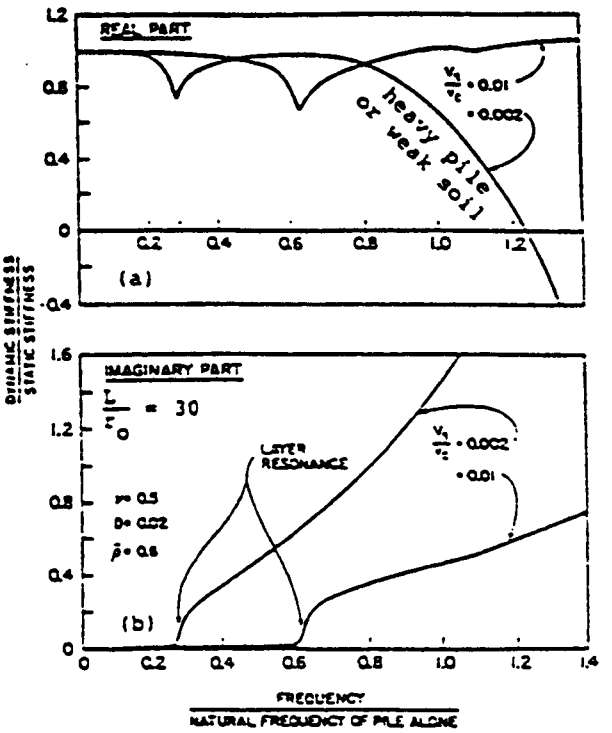

Figure 1.5 Typical horizontal pile-head impedance of endbearing pile. The real part remains almost constant for low frequency. The imaginary part is negligible for low frequency. (After Novak and Nogami 1977)

A significant improvement in the finite element model was formulated by Roesset and his co-workers (Blaney et al. 1976, Roesset & Angelides 1979), who placed the consistent, frequency dependent boundary, derived by Kausel et al. (1975), directly to the pile or outside the cylindrical finite element zone around the pile. This approach was then used by Krishnan et al. (1983) and Gazetas (1984) for extensive parametric studies.

Significant further progress was made by Kaynia (1982) and Kaynia and Kausel (1982, 1991) who based their solution of piles in generally layered media on the formulation of displacement fields due to uniformly distributed forces on a cylindrical surface (so called barrel load). Banerjee & Sen (1987) presented a boundary element solution for piles embedded in a semi-infinite, nonhomogeneous soil in which the soil modulus, $E_s(z)$, varies linearly with depth, z. Banerjee and Sen's results suggest that, unlike in layered soils, the frequency variations of the impedance functions, normalized by static stiffness, are quite smooth and affected very little by nonhomogeneity. The actual magnitude of the stiffness and damping diminishes with $E_s(o)$, however.

Other methods suitable for linear, generally layered media are based on a semi-analytical finite element approach. These methods treat the wave propagation in the horizontal direction analytically and, in the vertical direction, a finite element idealization including auxiliary sublayers are employed (Shimizu et al. 1977, Novak & Nogami 1977, Takemiya & Yamada 1981, Waas & Hartmann 1981, Waas & Hartmann 1984, Mizuhata & Kusakabe 1984). The pile is modeled by beam elements.

A much simpler and more versatile solution, particularly well suited for high frequencies, was formulated by Novak and Aboul Ella (1978*a*) who extended the plane strain approach to include layered media and incorporated it in the code, PILAY. This code was used later by Novak & El Sharnouby (1983) to generate design charts and tables for parabolic soil profiles, as well as homogeneous ones. Roesset et al. (1986) also found the plane-strain approach to work very well for high frequencies. For very low frequencies, an adjustment to the plane-strain soil reaction was made for the vertical and horizontal directions as discussed by Novak & El Sharnouby (1983) and implemented in the code, PILAY. The plane-strain approach works well for high frequencies because in a layer, elastic waves tend to propagate more horizontally as the frequency increases, as in a wave guide.

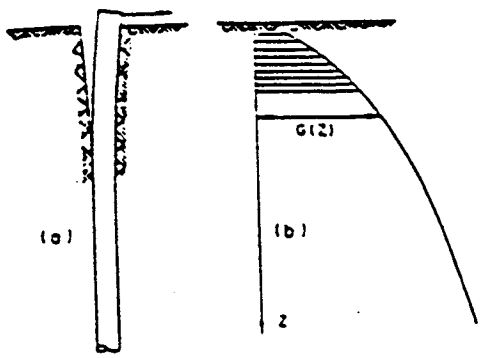

Figure 1.6 Schematic diagram of pile separation and soil modulus reduction towards ground surface. The overall effect is to reduce the resistance to horizontal movements. (After Novak 1991)

While the consideration of a free separation length in the analysis may produce the reduction in both pile stiffness and damping often observed in experiments, a better measure of this effect, or a complementary one, may be to account for soil nonhomogeneity in the radial direction. A simple way of doing this is to assume a weak, cylindrical boundary zone around the pile, as shown in Figure 1.7. The zone is homogeneous and features a soil shear modulus, G_i, smaller than that of the outer zone, and greater material damping. The purpose of such a zone is to account in a very approximate way for soil nonlinearity in the region of the highest stresses, pile separation, slippage, and other deficiencies of the pile-soil interface. Such a zone was proposed by Novak & El Sharnouby (1983). In their plane-strain solution, the mass of the boundary zone was neglected in order to prevent wave reflections from the fictitious interface between the cylindrical zone and the outer region. These reflections occur with non-zero weak zone mass, and result in undesirable undulations in both stiffness and damping of the composite medium. The difficulty with wave reflections can be avoided by providing for a continuous transition of stresses from the inner zone to the outer region. Such a solution has been explored by the researchers (Lakshmanan & Minai 1981, Dotson & Veletsos 1990, Mizuhata & Kusakabe 1984). The latter authors found that even with the weak zone, the experimental resonance amplitude measured on a $43.2m$ long pile was five times larger than the theoretical value while the resonance frequency was predicted quite well. This is consistent with other observations and indicative of the need to account for pile separation.

Wolf & Weber (1986) conducted a more rigorous study of the effect of soil tension exclusion, also assuming the circular cavity in the unbounded thin layer to be plane strain. They found that soil separation hardly affects horizontal stiffness, K_h, but reduces damping, C_h by more than fifty per cent, a result quite similar to that of Novak & Sheta (1980). In addition, if shear is eliminated and, hence, slipping is allowed in the zone of contact, stiffness is also strongly reduced. Many other authors have studied the interface behavior (Mamoon 1990, He 1990).

Recognizing the separation effect and allowing for it in an approximate way, a reasonable agreement between the theoretical results and experiments can be obtained. This is exemplified in Figure 1.8, comparing the theoretical and experimental responses of a concrete pile $7.5m$ in length and $0.32m$ in diameter. The soil was multi-layered and a cylindrical weak zone was assumed when calculating the responses using the code

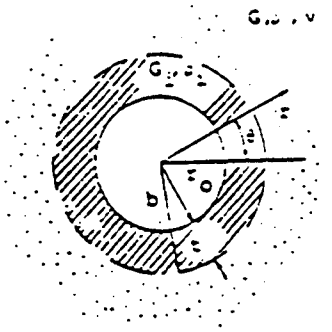

Figure 1.7 Cylindrical boundary around a single pile. Weak zone with lower shear modulus is next to the pile representing soil nonlinearity in a approximate way. (After Novak 1991)

DYNA3. In this code, the weak zone is analyzed as massless, but its mass is added to that of the pile in full or in part. Similar tests and comparisons were reported (Gle 1981, Woods 1984).

Nonlinear Response of Single piles

The theories discussed earlier are essentially linear and quite adequate for small displacements. At large displacements, piles behave in a nonlinear fashion because of soil nonlinearity at high strain, gapping, slippage, and friction. To incorporate these factors in a continuum theory is extremely difficult and, therefore, lumped mass models are most often used when nonlinear analysis is required. Such models, employed by Penzien (1970), Matlock et al. (1978), Matlock & Foo (1980) and a number of authors, feature nonlinear springs, nonlinear dampers, gaps, and coulomb friction blocks. The combination of these elements makes it possible to generate a variety of nonlinear force displacement relationships. An example of a lumped mass model formulated by Penzien (1970), is shown in Figure 1.9. Models of this type are very versatile, but it is difficult to relate the characteristics of the discrete elements to standard geotechnical parameters of soil. To overcome this difficulty, various nonlinear soil resistance-deflection relationships, known as p-y curves for lateral response and t-z curves for axial response, have been recommended in the literature. For applications in offshore structures, the American Petroleum Institute (1986) specifies the p-y curves for clay as well as sand, for both static and cyclic loading. Extensive data on p-y curves and nonlinear pile response were obtained by Yan (1990), using model piles and the hydraulic gradient similitude method to reproduce the prototype conditions.

Cyclic loading is defined as repetitive loading with very low frequency so that no significant inertial forces and radiation damping arise. It provides basic insight into the material degradation due to soil plasticity and mechanical degradation due to gapping associated with large displacements. Many studies have been devoted to this type of loading, but only a few may be mentioned here. Trochanis et al. (1988) found theoretically a dramatic decrease in pile stiffness due to gapping. Morrison & Reese (1988) conducted an extensive full scale investigation of piles and pile groups. Summarizing their observations, Swane & Poulos (1982) postulated that, during cyclic lateral loading, the two forms of degradation lead to an increase in the pile deflection and bending stresses. However, if this degradation stabilizes, the pile is said to "shakedown" to a

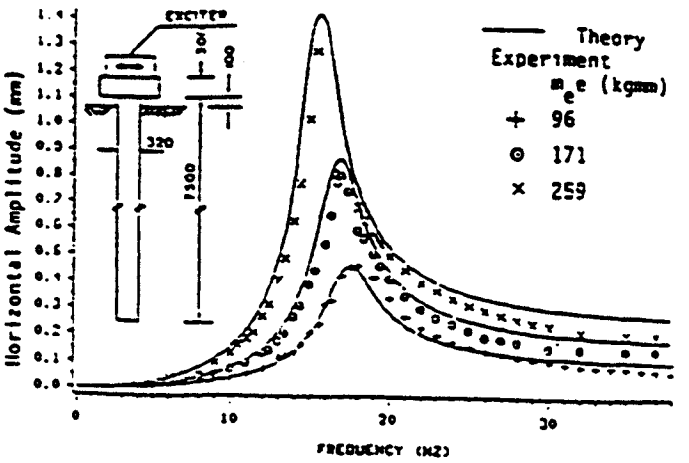

Figure 1.8 Theoretical and experimental horizontal response of concrete pile for three levels of harmonic excitation. Close agreement was found using a weak zone. (After El Marasafawai et al. 1990)

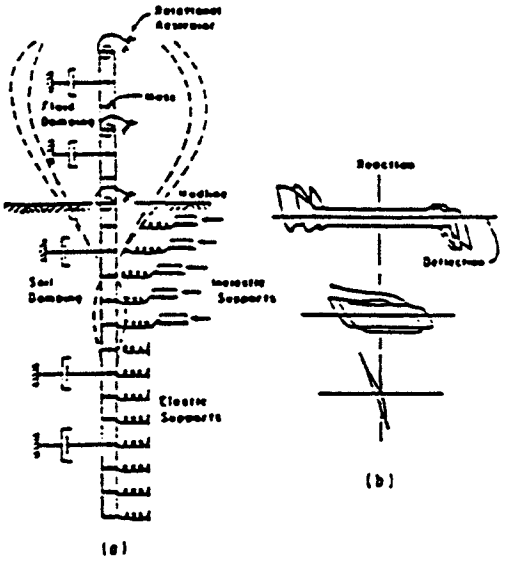

Figure 1.9 Nonlinear lumped mass model of pile. (After Penzien 1970)

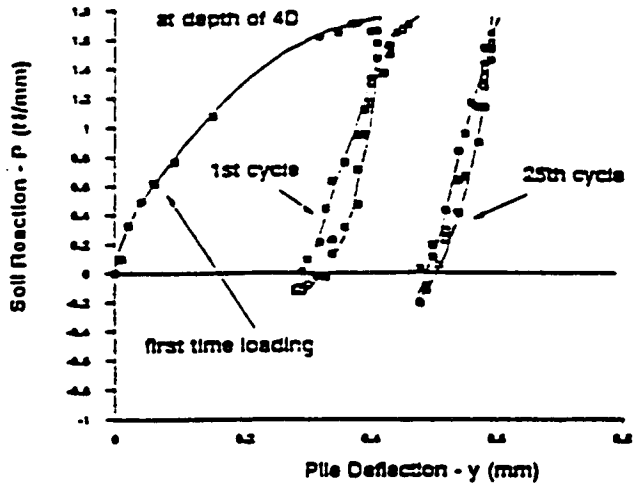

Figure 1.10 Example of *p-y* curve under cyclic loading (After Yan 1990)

state of permanent strains and residual stresses and it will react elastically to any further cyclic loading of the same intensity. When the pile does not stabilize into an elastic or inelastic response, the pile deflection continues to increase and incremental collapse may result. The two situations are depicted in Figure 1.11. The shakedown phenomenon is favorable from the point of view of the applicability of the various linear theories for dynamic response analysis. It explains why, with adequate adjustments, particularly for pile separation, such theories may give reasonable results, even in cases where overall strong nonlinearity of the response is clearly manifested.

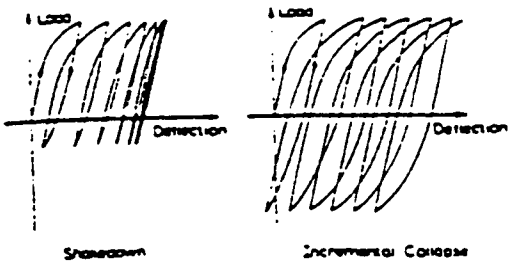

Figure 1.11 Pile stabilization (shakedown) and incremental collapse under cyclic loading with constant amplitude. (After Swane and Poulos 1982)

The nonlinear pile stiffness characteristics were investigated for both horizontal and vertical dynamic response by Angelides & Roesset (1980) using toroidal finite elements in the region surrounding the soil and the consistent boundary matrix. Even neglecting slippage and gapping, they demonstrated the dramatic reduction in pile horizontal stiffness and equivalent damping with increasing pile force. The p-y curves, also used for comparison, gave lower stiffness values because they accounted for gapping and a high number of load cycles, N, while only 10 load cycles were applied by Angelides and Roesset. The effect of a stable gap on soil resistance to pile steady state vibration is schematically depicted in Figure 1.12. The reduction of the equivalent linear stiffness and the necking

of the loop are evident. Progressive degradation occurs under incrementally increasing loads when the hysteresis loops exhibit different shapes for sand and clays. In clay, the gap may expand with each cycle, giving rise to the characteristic elongated loops with reduced radiation damping.

Time Domain Analysis

The procedures for the frequency domain dynamic analysis of pile foundations are well developed. Transient analysis of pile foundations, however, has received very little attention, although many real dynamic and/or seismic responses involve transient motions. Moreover, unless a solution in the time domain is developed, the nonlinearities involved can not be modeled. Analytical approaches for laterally loaded piles have developed in two separate directions. The first of these retains the conceptual model of treating the soil restraint as discrete springs, as shown in Figure 1.9. The model is improved by allowing the spring stiffness to vary along the length of the pile (Reese & Matlock 1956) and, subsequently, by replacing the linear springs by nonlinear p-y curves (Matlock 1970, Reese et al. 1975, Reese & Sullivan 1984). The limitations of this approach are twofold. First, difficulties exist in choosing appropriate p-y curves for a given combination of pile size and soil type. Second, the replacement of the soil continuum by discrete springs precludes the extension of the analysis to pile groups, since interaction between neighboring piles may not be taken into account. The second approach is to use the boundary element formulation. The first general three dimensional time domain direct boundary element formulation for transient dynamic analysis was given by Banerjee & Ahmed (1985) and Banerjee et al. (1986). The use of constant temporal variation was published by Ahmad & Banerjee (1988) for general three dimensional transient elasto-dynamic analysis, which was transformed to the axisymmetric case by Wang (1989) and Wang & Banerjee (1990). Mamoon & Banerjee (1992) adopted an efficient, but approximate, hybrid boundary element technique to model single elastic piles in elastic half-space for time domain analysis.

Few attempts have been made to develop the transient analysis of pile foundations, principally because of the formidable computing requirements. Nogami and Konagai (1986, 1987, 1988) and (Mitwally & Novak 1988) were the first to present approximate procedures for axial and flexural dynamic analyses of piles. Under axial vibration, much of the nonlinearity that is observed is due to slip and friction. It was extended to allow

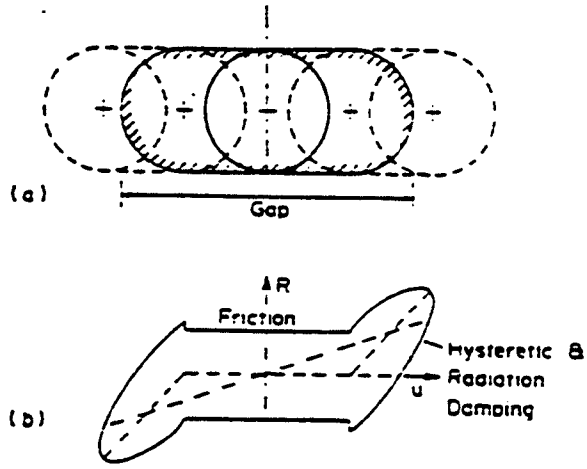

Figure 1.12 Schematic of (a) Pile under steady-state vibration in stable gap, and (b) corresponding soil reaction, R, vs. pile displacement, u for stable cycle. (After Novak 1991)

for nonlinear analysis (Nogami et al. 1992). Numerous assumptions and approximations were adopted in their approach to facilitate the development of a simple practical method of calculation. Rather significant ones involved the formulation of the soil-pile interaction force and the solution of the governing equation of pile motion. Adopting Winkler's hypothesis, the soil response to the pile motion was formulated through a simplified mechanical model based on Winkler's assumption, the parameters of which were determined from the consideration of plane-strain wave propagation. One of the advantages of these models is that their properties are specified in terms of standard geotechnical parameters.

1.3.3.2 Pile Groups

Piles are usually used in groups. If they are not very widely spaced, they interact with each other, generating phenomena known as *pile-soil-pile interaction*, or *group effects*. These effects have attracted much interest in recent years (Kaynia 1982, Ostadan 1983, Mamoon 1990, Hassini 1990). The effect of a pile group on foundation stiffness and damping is illustrated in Figure 1.13.

Linear Behavior of Pile Groups

Under static loads, pile interaction increases group settlement, redistributes the loads on individual piles, and reduces bearing capacity unless this reduction is counteracted by densification of the soil within the group due to pile driving. The first suggestion regarding these effects can probably be attributed to Sooysmith (1896). The investigation of static group effects was put on a rational basis, relying in continuum mechanics, by Poulos (1971, 1979) and Butterfield & Banerjee (1971). Extensive data on static group effects are available in many works (Poulos & Davis 1980, Butterfield & Douglas 1981, El Sharnouby & Novak 1985, El Sharnouby & Novak 1986, El Sharnouby & Novak 1990). The static data are useful, even to those interested in dynamics, because at low frequencies, and particularly below the fundamental frequency of a stratum, the dynamic stiffness is usually quite close to the static stiffness.

The techniques employed for dynamic pile-groups are extensions of the approaches used for single piles and most of them are limited to linear interaction. The methods rely on the availability of a Green's function, with which the load transfer from the pile surface to soil can be calculated. These loading conditions include point loads, line loads, ring loads, disk loads, and cylindrical (barrel) loads. Applying this loading to individual segments into which the pile is discretized, the soil dynamic displacement field

is established, yielding the soil dynamic flexibility matrix. The soil stiffness matrix is then obtained by inverting the dynamic flexibility matrix. In this process, the presence of the pile cavities outside the loaded segment is usually ignored, which implies that wave scattering among the piles is not accounted for and the soil displacements are calculated either for the pile axes or as an average of the circumferential values. Then the soil stiffness matrix is combined with the pile structural stiffness matrix and the soil-pile system can be analyzed for any type of excitation. Different authors have proposed various refinements or implications to this procedure.

The first theoretical analysis of pile-soil-pile interaction was conducted by Wolf & von Arx (1978) who employed an axisymmetric finite element formulation to establish the dynamic displacement fields due to ring loads. Waas and Hartmann (1981, 1984) formulated an efficient semi-analytical method which uses ring loads and is well suited for thin layered media, properly accounting for the far field. Kaynia (1982, 1982) and Kaynia and Kausel (1982, 1991) improved the accuracy by combining the cylindrical loads as a boundary element formulation with the consistent stiffness matrix of layered media to account for the far-field. The thin layer method was used by many researchers (Shimizu et al. 1977). Boundary element solutions, employing Green's function for generally layered media, were formulated (Banerjee & Sen 1987, Banerjee et al. 1987, Mamoon et al. 1988, Mamoon 1990, Mamoon & Ahmed 1990, Mamoon & Banerjee 1990). Simpler solutions based on the dynamic Winkler medium were developed (Nogami 1980, Nogami 1985, Sheta & Novak 1982). The advantage of the latter approach is that it makes it possible to include the weak zone (Sheta & Novak 1982) and nonlinearity (Nogami et al. 1992).

Basic Features of Dynamic Group Effects

The main features of dynamic group effects have emerged from the theoretical solutions. For example, both stiffness and damping are strongly frequency dependent, and they can be either reduced or increased due to pile-soil-pile interaction. Their values, as a function of frequency, may exhibit very sharp peaks and they are affected even for very large pile spacing. Some of these features can be observed in the example of a 4×4 group whose normalized dynamic stiffness is displayed for different spacings in Figure 1.13. The normalization is done using the product (number of piles $\times$ single pile stiffness), and it yields a ratio expressing group efficiency. As can be seen in Figure 1.13,

the group properties and their variation in frequency depend strongly on the spacing ratio, s/d. This is so because pile interaction depends on the ratio of the wave length to spacing. A group solution including the weak zone around the piles dulls the peaks but does not eliminate them. On the other hand, soil nonhomogeneity can make the peaks either more pronounced, or duller (Gazetas & Makris 1991), depending on conditions such as frequency and spacing.

Makris & Gazetas (1992) proposed a simplified procedure for estimating the dynamic interaction between two vertical piles subjected to both inertia and kinematic loading. It is shown that for a homogeneous stratum, pile-soil-pile interaction effects are far more sign)ficant for inertial than for kinematic loading. Makris & Gazetas (1991) demonstrated that the *dynamic group efficiency* with increasing soil nonhomogeneity tends to reduce the respective resonant peaks and leads to an interaction function for axial vibration.

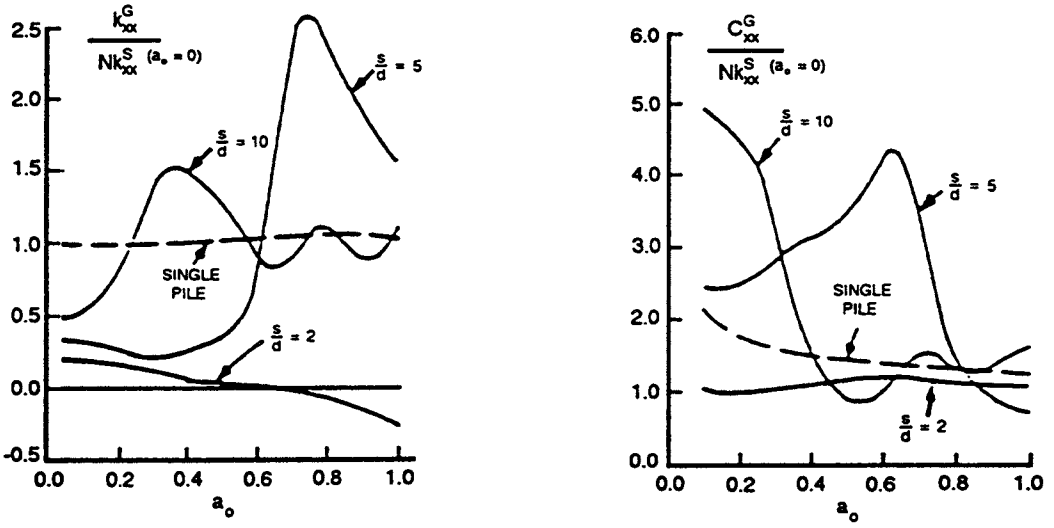

Figure 1.13 Normalized dynamic stiffness and damping of 4 x 4 pile group for different ratios of spacing to diameter, *s/d*. (After Kaynia and Kausel 1982; L/d = 15, E_p/E_s = 1000, $\rho_s/\rho_p = 0.7$).

Fan et al. (1991) considered pile-soil and pile-soil-pile interaction for vertically propagating, harmonic S-waves. It was shown that, under kinematic interaction, the effects of the pile group configuration, number of piles in a group, and relative spacing between piles are usually insignificant for lateral displacement but quite important for pile cap rotation, which determines "effective" seismic input motion. A more general formulation

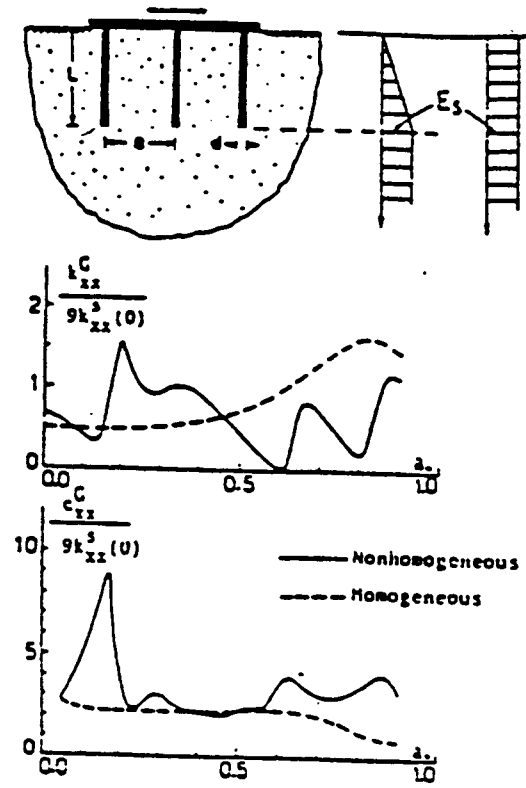

Figure 1.14 Vertical response of 2×2 group of closely spaced piles: theory vs. experiment. (After Sheta and Novak 1982; $L = 3.4$m, $d = 60.3$mm)

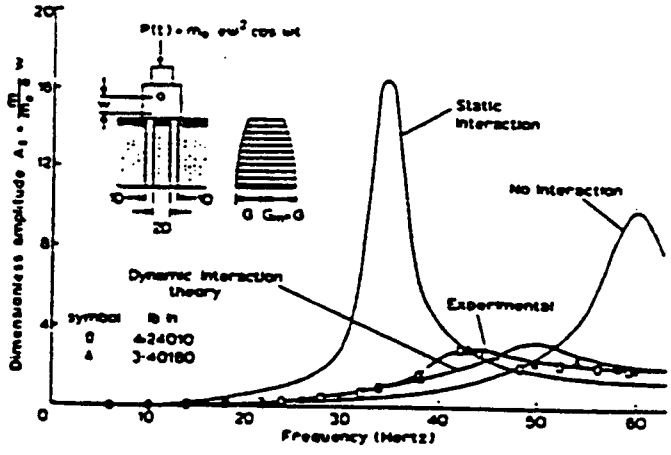

Figure 1.15 Theoretical and experimental lateral response in the Y-direction for a group of six concrete piles. (After El Marsafawi et al. 1990; $L = 7.5$m, $d = 0.32$m)

has been presented by Kaynia & Kausel (1991) for the dynamic response analysis of piles and pile groups in a layered elastic half-space. In their investigation, Green's function for layered media was evaluated numerically by the application of an integral transform technique. Toki et al. (1991) studied nonlinear seismic soil-pile interaction with a hybrid procedure that used a pseudo-dynamic testing (PDT) method which was modified to account for frequency dependence. Kaynia & Kausel (1991) investigated the effects of pile to cap fixity and pile spacings on the kinematic interaction of pile foundations. They concluded that, under vertically incident SH waves, pile groups closely follow the ground motion. The increasing angle of incidence reduces the horizontal motion, but increases torsional group response. Rayleigh waves and SV waves with angles between 30 and 60 degrees produce large rocking motions in pile groups.

Chow & Teh (1991) analyzed the behavior of vertically loaded pile groups, embedded in a homogeneous soil with the pile cap in contact with the ground. The load carried by the cap is significantly affected by the distribution of the soil's Young's Modulus. Pressley & Poulos (1986) analyzed pile groups for simplified conditions for the load and the structure. Muqtadir & Desai (1986) analyzed piles and pile groups using three-dimensional finite element analysis for nonlinear-elastic and elastic-plastic hardening behavior of soil. Nogami (1985) presented a simple approach to analyze the flexural vibration of grouped piles using a pile-head flexibility matrix of grouped piles in layered elastic soil. He used plane-strain stiffness as the Winkler spring. El Sharnouby & Novak (1985) presented a simple method for the analysis of large pile groups for the static and low frequency vibration cases. In their analysis, they took the static stiffness and proportional damping for stiffness and damping constants, even for interaction. They also used the static interaction factor obtained by Selby & Arta (1991) conducted a finite element analysis of piles and pile groups. They observed the stiffness and the redistribution of pile moments due to nonlinear effects. Blaney & O'Neill (1991) suggested a field testing procedure of slow cyclic load tests and plucking tests of a single pile and integrated these test results with a simplified SDOF analysis to produce response functions for the dynamic design of pile groups.

Trbojevic et al. (1981) presented a simple procedure for conducting dynamic analyses of dense pile groups based on the complex response method in the frequency domain. The soil was treated as a linear visco-elastic material with hysteretic damping. El Marsafawi

et al. (1992a, 1992b) compared the response of two-pile groups obtained from dynamic experiments and those obtained by theoretical analyses. They concluded that the vibration of the pile groups displays moderate nonlinearity even for small displacement amplitudes ($0.01d$). The linear theory, combined with soil properties derived from shear wave velocity measurements, gives reasonable estimates of single-pile and pile group stiffness for small displacement amplitudes. The damping may be grossly overestimated unless some corrections are made for separation and other deficiencies. The prediction of group response is better than that of the single pile since it is less dependent on the soil properties of the topmost layer. Chow (1987) investigated axial and lateral response of pile groups embedded in nonhomogeneous nonlinear soil using the finite element procedure. Ottaviani (1975) used the finite element method to study the behavior of vertically loaded single piles and pile groups in a homogeneous linear elastic medium. A few observations on nonlinear analysis will be made later herein.

With the pile-soil-pile interaction theories being so complex, it is of importance to examine how the theories perform when compared with experiments. Figure 1.14 shows one such comparison based on a group of four closely spaced model piles, tested in the field and evaluated using plane-strain theory for soil reactions with a weak zone. The response was also evaluated both with interaction ignored and assuming static interaction. Both of these assumptions proved to be inadequate. The dynamic interaction theory gives far better results. On a test group of 102 small scale model piles, encouraging results were obtained (Novak & El Sharnouby 1984). For six full scale piles, accurate results were also obtained, but the weak zone and separation had to be included for a satisfactory match. Successful experiments, conducted on a group of 56 full scale piles were reported by Masuda et al. (1986). Kobori et al. (1991) also found the theory to be of sufficient applicability. Thus, it may be concluded that the linear theory works quite well as long as the experiments do not deviate too much from the theoretical assumptions. Often, however, a correction for separation, gapping, and nonlinearity is needed, at least in the form of the weak zone and a pile free length.

Interaction Factors

For the pile group analyses discussed earlier, the computing requirements were quite severe, particularly for larger groups. Therefore, Kaynia & Kausel (1982) formulated the concept of the dynamic interaction factor as an extension of the static interaction factor

approach. In this approach, interaction is considered between only two piles at a time, and the group properties are obtained by superposition. Dynamic interaction factors are dimensionless, frequency dependent complex numbers, defined as

$$\alpha_{ij} = \frac{Dynamic\ displacement\ of\ pile\ j}{Static\ displacement\ of\ pile\ i} \qquad [1.8]$$

in which the displacement of pile j is caused by a unit harmonic load on pile i, and the static displacement of pile i is established for an isolated pile. The displacement is either translation or rotation. Examples of the real and imaginary parts of the interaction factors, calculated using the Kaynia & Kausel (1982) method, are plotted for homogeneous soil in Figure 1.16. The interaction factors are oscillatory in character, i.e. their magnitudes become negative as well as positive. A negative value of the imaginary part indicates a possible increase in group damping, characterized by group efficiency greater than unity. For a limited selection of parameters, a complete set of interaction factors is available for floating piles in homogeneous soil (Kaynia & Kausel 1982), and for vertical vibration in soil with linearly increasing modulus with depth (Banerjee et al. 1987).

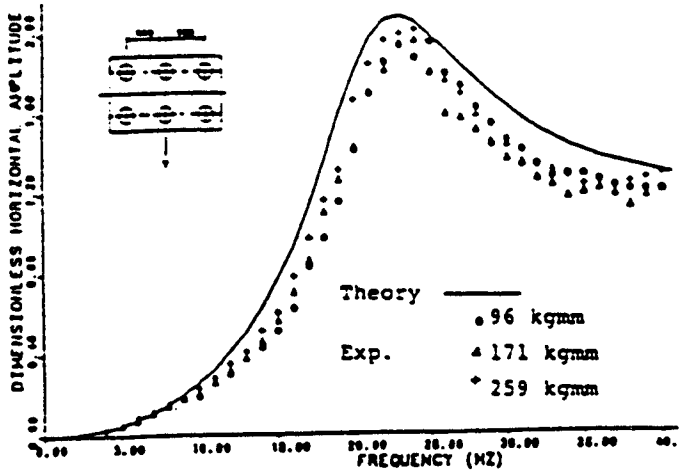

Figure 1.16 Vertical dynamic interaction factor for various dimensionless spacings and frequencies. (After Kaynia and Kausel 1982)

The interaction factors can be expressed in terms of amplitude, α, and phase angle, ϕ, i.e.

$$\alpha = \alpha_1 + \alpha_2 i = |\alpha| e^{i\phi} \qquad [1.9]$$

As an example, the interaction factors from Figure 1.16 are presented in this form in Figure 1.17. This latter form makes interpolation of interaction factors easy for intermediate pile spacing.

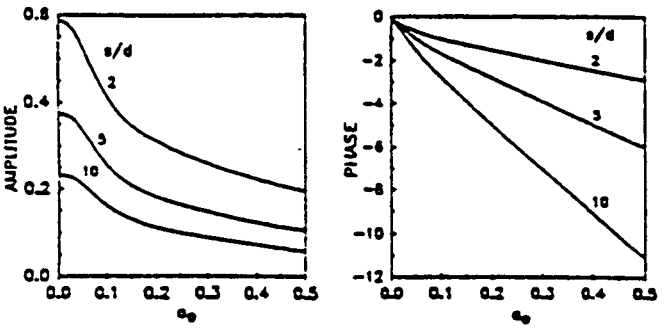

Figure 1.17 Vertical dynamic interaction factors in terms of amplitude and phase. (After Novak 1991)

Correcting the available interaction factors for pile length, endbearing, and other effects, a very efficient but approximate procedure for group analysis is obtained. For example, the vertical or horizontal dynamic stiffness of a group with a rigid cap becomes

$$K^G = \bar{K} \sum_i \sum_j \epsilon_{ij} \qquad [1.10]$$

$$\epsilon_{ij} = [\alpha]^{-1} \qquad [1.11]$$

in which $\bar{K}$ is the static stiffness of a single pile and ϵ_{ij} are the elements of the inverted matrix $[\alpha]$. For all the vibration modes, the corresponding formulas are given by Novak & Mitwally (1990).

The interaction factor approach would be mathematically accurate if the interaction factors as well as the single pile properties were calculated with all piles present in the system, which is not normally done. However, the results may be adequate for most applications. Kaynia & Kausel (1982) found that the accuracy of the interaction factor approach is quite sufficient for a homogeneous medium. For a nonhomogeneous medium, they observed that the approach is less accurate. The interaction effects may be overestimated in the static vertical response of endbearing pile-groups (El Sharnouby & Novak 1985).

A remarkably simple approximate method for dynamic interaction factor evaluation was proposed by Dobry & Gazetas (1988), and extended for non-homogeneous soils (Gazetas et al. 1991). For homogeneous soils, these authors assumed that the displacement field around the vibrating pile and, thus also, the displacement of the neighboring pile (the interaction factor), were governed by the law of cylindrical wave propagation. Then, the vertical interaction factor is simply

$$\alpha_v = \left(\frac{r_0}{s}\right)^{\frac{1}{2}} e^{-\left\{\frac{\beta\omega}{V_s}(s-r_0)\right\}} e^{-\left\{\frac{i\omega s}{V_s}\right\}} \qquad [1.12]$$

where β is the soil hysteretic damping ratio. In their comparisons with the more rigorous solutions for floating piles, the authors obtained a very reasonable, although not quite perfect, agreement.

Nonlinear Analysis of Pile Groups

Nonlinear dynamic analysis of pile groups has received much less attention than linear analysis. Nogami & Konagai (1987) developed a group analysis method assuming that, in the vertical vibration response, nonlinearity stems mainly from slippage at the soil pile interface. They represented the soil using a dynamic Winkler model. They found that this nonlinearity reduces the wave interference effects, making the stiffness less frequency dependent, and produces residual skin friction and residual axial force in the pile under transient loading. Then, Nogami and Konagai (1988, 1992) extended the concept of the dynamic Winkler medium further to include horizontal response, slippage, gapping, and inelastic soil behavior to be able to generate a variety of degrading hysteresis loops.

In most analyses, it is observed that under large displacements, most of the action occurs right around the pile and, consequently, pile-soil-pile interaction is not very significant. Some insight into this observation can be obtained from static experiments.

Figure 1.18 show the results of field tests conducted on free-headed test steel pipe piles of 0.1016m in outer diameter and 3.05m in length. The soil was mainly stratified silty sand to silty gravel. Figure 1.18 shows that the interaction factor diminishes with increasing deflection, dropping to about one half of the original value at a deflection of about 3.5 percent of the diameter. This reduction varies with spacing and the angle of incidence. If the pile is unloaded and reloaded, the interaction factors for small displacements become much smaller than the original ones, due to gaps generated by the preceding large displacements, and then its values asymptotically approach those from the first loading. It can be concluded that under large displacements, pile-soil-pile interaction is reduced but not eliminated.

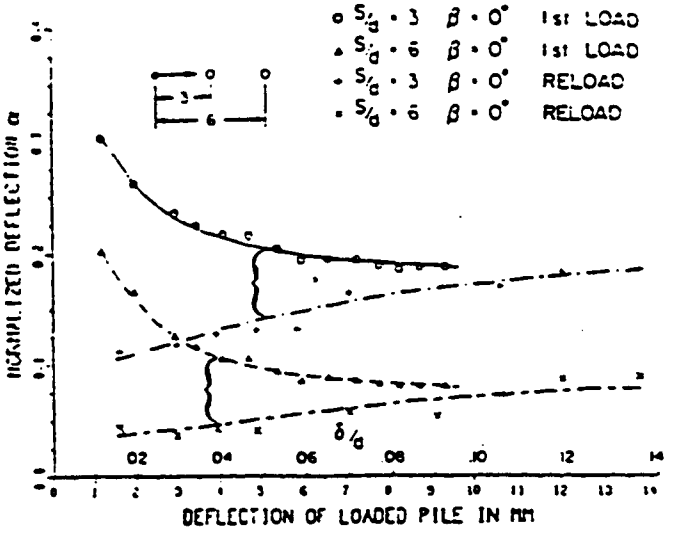

Figure 1.18 Horizontal static interaction factors for first loading and reloading (After Janes and Novak 1989)

1.3.3.3 Other Factors Affecting Pile Behavior

Among other factors that affect pile response, the important ones are pile batter, soil-pile-cap interaction, and soil liquefaction. Those are briefly discussed in the following sub-sections.

Pile Batter

Pile batter is often used to increase the horizontal stiffness of the group. For machine foundations and other structures, this is sometimes useful. However, under earthquake loading, pile batter may not always be beneficial, because it restricts the pile's ability to sway and yield, resulting in greater seismic forces and possible damage to the piles and the cap. Little information is available on the dynamic effects of the batter. As a very approximate practical approach, the pile can be analyzed first as if it were vertical, and the stiffness matrix obtained in this way can be taken as valid for the inclined element coordinates. Then, this matrix can be transformed into global coordinates, being horizontal and vertical, to give the battered pile stiffness matrix in these coordinates. More details on this are given by Novak (1980). For static conditions, Poulos (1980) employed a similar technique. He recommended the evaluation of interaction between two vertical piles whose distance is equal to the separation measured on the inclined piles at $L/3$ from the top.

One of the few dynamic solutions of pile groups with batter was produced by Mamoon (1990) using an approximate analytical formulation, denoted as method I where the soil domain is modeled as an elastic half-space. An example of Mamoon's result is shown in Figure 1.19, comparing the normalized vertical stiffness (real part) of a 3×3 group of vertical piles with that of a similar group featuring piles with a 15 degree batter in one plane. (Notice that the vertical scale is not the same for both cases.) Kaynia's solution of the vertical group is displayed for comparison. The comparison of cases (a) and (b) suggests that for the separation $s/d = 5$ and higher frequencies, the inclination of the piles causes a significant reduction in the real part of the impedance. For the peak, this reduction is about 43 percent. Also a slight shift in the peak can be noticed. The batter effect results in an increase in the imaginary parts of the impedances.

Soil-Pile-Cap Interaction

In most situations, piles have caps, and soil-pile-cap interaction may occur. The cap influence depends not only on the size and embedment of the cap, but also on the quality of its contact with the soil. Considering the behavior of actual soils under static and dynamic loading, it may be speculated that this contact will be well maintained in stiff clays and dense sands; but in loose to moderately dense sands, the cap base may separate from the soil, and, in soft clays, the contact in the cap base as well as the cap sides can be lost. Finally, the separation of the base is more likely for endbearing piles.

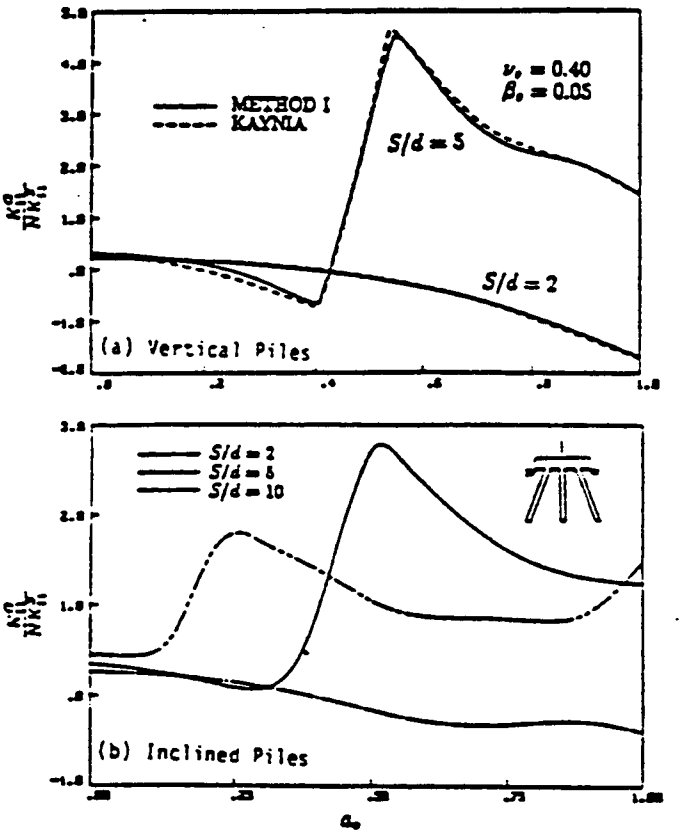

Figure 1.19 Real part of vertical impedance of a 3 × 3 group for (a) vertical piles, (b) piles with 15 degree inclination (L/d = 15, E_p/E_s =1000, ρ_s/ρ_p =0.7) (After Mamoon 1990)

The few dynamic analyses that have been reported invariably presume full contact and perfect elasticity and, thus, their results should be applied with some allowance for the actual soil behavior. Banerjee & Sen (1987) observed a rather small effect of the cap on the vertical impedances of single piles and groups of two and four floating-piles, respectively. This is a valid conclusion for the stiff piles that they analyzed ($E_p/E_s = 10,000$). For more flexible piles, the cap may cause a more significant increase in pile impedances, as can be deduced from static analysis (Figure 1.20).

An extensive theoretical study of dynamic cap effects was conducted by Mamoon (1990). He included cap inertia in his analysis, but ignored the shear stresses in the mat base, even for the horizontal response. The principal observation is that, for some conditions, cap inertia can reduce or eliminate the sharp peaks in the impedances, typical for pile groups without caps.

Effects of Soil Liquefaction on Pile Behavior

Piles are often used in loose saturated sands and silts. If such deposits liquefy due to increased pore water pressure during an earthquake, the piles lose much of their lateral and vertical support which can result in a substantial increase in bending moments, loss of stability, and failure. Damage of this type occurred in the Niigata and Alaska earthquakes of 1964 and elsewhere.

Only a relatively few studies have been devoted to this important subject (Seed & Idriss 1969*a*, Zienkiewicz et al. 1978, Finn et al. 1970, Finn et al. 1971, Zienkiewicz et al. 1991, Nomura et al. 1991, Kagawa 1992).

Kagawa (1992) presented a theoretical study of pile behavior during liquefaction. The potential significance of the impact of liquefaction on the dynamic response of pile foundations has been studied by Kagawa (1992) through a numerical study. Results of this study demonstrated that, due to liquefaction, the pile-head acceleration may be amplified or it may be attenuated, pile-head displacement and pile moment will be greatly amplified in most cases, and the depth at which the maximum pile moment occurs increases significantly.

1.3.3.4 Soil-Pile-Structure Interaction

Once the properties of the pile foundations are established, they can be incorporated into the examination of pile structure interaction just as with other types of foundations.

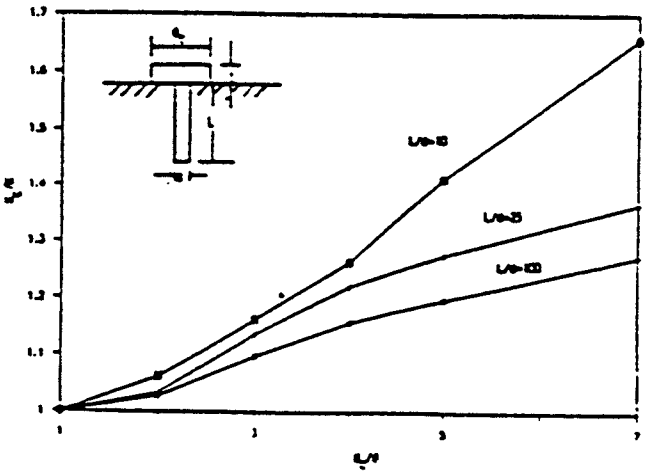

Figure 1.20 A cap increases the static stiffness for short piles. (K_1 K_0 = stiffness with and without cap; d_1 d_0 = dia. of pile and cap, $\nu = 0.5$, $E_p/E_s = 1000$) (After Liu and Novak 1990)

A number of studies have been devoted to this subject. As there is a difference between direct excitation of the structure by external loads and excitation by seismic motions of the ground, these two cases are discussed separately in this thesis.

Pile-Structure Interaction Under External Loads

Typical examples of direct external loads are Figure 2.3. The near-field element in the unbalanced forces acting on machine foundations, wind forces on buildings, wave forces on offshore towers, and inertial loading from support movement due to earthquake excitation. In such cases the pile foundation impedance can be superimposed on the structural system matrices to give the governing equations of the pile-structure system in the standard form, i.e.

$$[M]\{\ddot{u}\} + [C]\{\dot{u}\} + [K]\{u\} = \{P(t)\} \qquad [1.13]$$

in which $[M]$, $[C]$, and $[K]$ are the mass, damping, and stiffness matrices incorporating the structure and foundation properties, and, in some cases, other factors such as hydrodynamic effects, aerodynamic damping properties etc.; $\{u\}$ and $\{P(t)\}$ are the displacement and loading vectors, respectively. Dynamic pile-soil-pile interaction reduces the resonance frequencies only slightly. However, it provides damping which attenuates the peak response (Novak 1991).

Pile-Soil-Pile Interaction Under Seismic Loading

The evaluation of soil-pile-structure interaction is needed to establish the forces expected to act on the structure and the piles in a seismic event. Such studies can be done experimentally or theoretically. Experimental investigations are most often conducted on models using shaking table tests, less often in a centrifuge. The tests require careful scaling and a special design of the test bin boundaries which are to prevent wave reflections (the box effect). Shaking table tests of pile supported structures have been reported, e.g., Mizuno et al. (1984) and Nomura et al. (1991), pile scaling has been examined by Kana et al. (1986); and the modeling of the free-field conditions in centrifuge tests has been investigated by Cheney et al. (1990).

For design purposes, the theoretical analysis of pile structure interaction is more practical and it is conducted much more often. Adequate for routine designs, a simple procedure is based on substructuring and the following assumptions: the input ground motion is given for the pile heads and it is not affected by the presence of the piles and

their cap; soil-pile interaction analysis is conducted separately to yield the pile foundation impedances; and the seismic response is obtained from Equation 1.13 using standard analysis, even response spectra. For shear buildings, all the matrices in Equation 1.13 may be rearranged to take the form that is common to shallow foundations. This type of analysis, known as *inertial interaction* analysis, usually indicates that the pile foundation flexibility and dissipative properties result in the reduction of the seismic forces as well as the base shear and an increase in the building response, just as in the case of shallow foundations (Novak & El Hifnawy 1984).

The assumption of the input ground motion not being affected by the presence of the piles is based on the idea that the dominant seismic wave lengths are much larger than the pile diameter and, given the bending flexibility of slender piles, the piles will follow the horizontal motion of the ground. A more comprehensive examination of these assumptions involves consideration of the wave scattering effect, known as *kinematic interaction.* A few researchers have examined this phenomenon. Gazetas (1984) conducted an extensive parametric study of the response of single endbearing piles exposed to harmonic shear waves propagating upward from the bedrock. He defined the kinematic interaction factors as

$$I_u = u_p/u_0 \qquad [1.14]$$

$$I_\phi = \phi_p\, r_0/u_0 \qquad [1.15]$$

in which u_p and u_o are the absolute values of the horizontal displacements, relative to the bedrock, of the embedded pile head and the ground surface motion in the absence of piles, respectively, and ϕ_p is the absolute value of pile head rotation. The magnitude of I_u depends on the soil profile, the stiffness ratio, E_p/E_s, the slenderness ratio, L/d, and the frequency ratio, f/f_1; where f = wave frequency and f_1 = fundamental horizontal frequency of the soil layer. For a parabolic soil profile, f_1 equals $0.56(V_s/L)$. When there is no kinematic interaction, $I_u = 1$. Synthesizing his numerical results, Gazetas found it possible to express the kinematic interaction factors for each soil profile in terms of a dimensionless frequency parameter. For the parabolic soil profile, this parameter becomes

$$F_B = (f/f_1)\,(E_p/E_s)^{0.16}\,(d/L)^{0.35}. \qquad [1.16]$$

In terms of this parameter, the kinematic interaction factor for translation assumes the form plotted in Figure 1.21. As can be seen, for small f/f_1, E_p/E_s, and d/L, the kinematic interaction factor is close to unity; for large values of these ratios, it drops to about 0.5. This suggests that the kinematic interaction is either negligible or is on the conservative side. Only for the homogeneous soil profile, a slight amplification of I_u may occur at low frequencies. The effect of the angle of incidence was examined by Mamoon and his group (Mamoon & Ahmed 1990, Mamoon 1990).

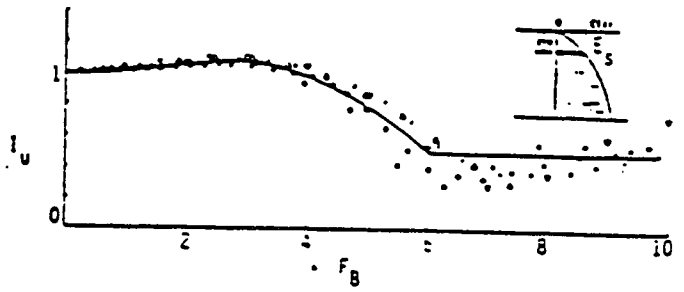

Figure 1.21 Kinematic interaction factor for parabolic soil profile as a function of dimensionless frequency parameter, F_B. [$(E_s = E_s(z = d))$ (After Gazetas 1984)]

For pile groups, kinematic interaction may be more significant. Waas & Hartmann (1984) examined a single pile and a large group of 356 piles and concluded that, while a single pile follows the earthquake motion of soil with little deviation, a large group of stiff piles in soft soil shows a response significantly different from the free-field motion. Significant kinematic interaction effects were also observed for a similar pile group by Wolf & von Arx (1982) who considered horizontally traveling waves. Thus, for important projects such as nuclear power plants, a complete analysis including kinematic interaction may be desirable. Such a complete response analysis of a pile-supported structure, in which the kinematic interaction is evaluated beforehand to give the ground motion for the inertial interaction calculation is schematically indicated in Figure 1.22 with M representing the

mass of the structure and a_0 representing input bedrock acceleration. Analysis of this type has been conducted Waas & Hartmann (1984), Hadjian et al. (1990) and Kobori et al. (1991).

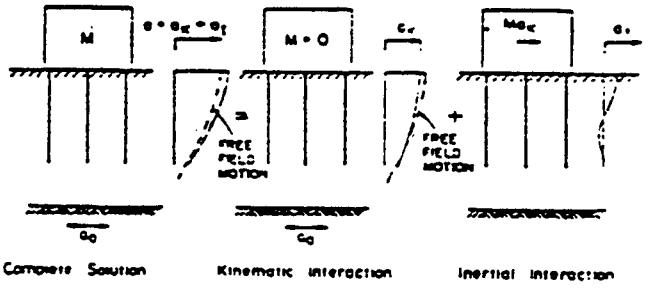

Figure 1.22 Schematic of seismic response analysis including kinematic interaction (After Novak 1991)

The two step response analysis shown in Figure 1.22 indicates that pile stress comes from two sources, i.e. pile deflection due to ground motion and inertial interaction. One limitation of the accuracy of most kinematic interaction studies is that they assume soil linearity. It is well known that for strong earthquakes, linear site response analysis can yield unrealistic displacements and stresses.

One more complication may occur if the piles are not adequately connected to the cap or if this connection fails in a severe earthquake. Then the cap may uplift, modifying the seismic forces on the structure, substantially increasing the forces on the peripheral piles that maintain the connections. These piles can become overloaded and may fail. Uplift of the tip of an endbearing pile, which was not socketed, from the bearing stratum may have similar but less severe results. More data on the uplift effects are reported by El Hifnawy & Novak (1986).

1.3.3.5 Mechanical Behavior of Soil

Accurate modeling of boundary value problems of soil-structure interaction using numerical (finite element) procedures requires a detailed knowledge of the constitutive behavior of the soil. A comprehensive general stress-strain relation for soils would be very complex simply because of the large number of parameters that affect the behavior of soil.

The whole problem of the behavior of soil structures is dependent on the soil skeleton-pore water pressure interaction. In the classical work of Biot (1941), the governing equations for such phenomena were first formulated, but further development was needed to provide full forms suitable for non-linear finite element analysis (Zienkiewicz & Shiomi 1984, Zienkiewicz 1985*a*, Zienkiewicz 1985*b*). But the soil-skeleton and pore-water interaction is too complicated to consider in the current work. and this interaction is neglected.

Constitutive Models

A number of constitutive models for soils have been published and evaluated. and they are well established in the geotechnical engineering community (Chen & Saleeb 1982, Chen & Baladi 1985, Chen & Han 1988, Lubliner 1990). Classical plasticity models (Drucker et al. 1957, Schofield & Wroth 1968, Roscoe & Burland 1968) can reproduce basic trends of soil under monotonic loading, but they fail when applied to more complex situations. Modified plasticity theories are able to eliminate most of these difficulties (Dafalias & Herrmann 1982, Hirai 1987, Zienkiewicz et al. 1991). Among the models, the cap plasticity model has been used widely in recent years in finite element analysis programs for a number of geotechnical engineering applications (DiMaggio & Sandlar 1971, Sandler et al. 1976, Sandler & Rubin 1979, Chen & McCarron 1983, Daddazio et al. 1987, McCarron & Chen 1987, Simo et al. 1988, Hofstetter et al. 1993). From a theoretical point of view, the cap model is particularly appropriate to soil behavior, because it is capable of treating the conditions of stress history, stress path dependency, dilatancy, and the effect of the intermediate principal stress.

In this research, a simple, isotropic, generalized cap model with an elliptic cap and without strain softening has been used. Considering the importance of this model, it, along with the determination of its parameters, is described in Appendix D.

Shear Modulus and Damping of soil

The shear modulus and damping in soils are important to the analysis of all soil vibration problems. In particular, the modulus and damping for small strain amplitude are necessary for the analysis of foundation vibrations. For the analysis of earthquake effects, the modulus and damping for a range of strain amplitudes are needed.

Current methods of determining the dynamic response of a horizontal saturated sand layer are based on total stress procedures. The significant ground motions are assumed to be shear waves propagating vertically and the appropriate shear modulus, G, for use in the analysis, may be determined from an equation of the form (Seed & Idriss 1975).

$$G = 1000\ K_2\ (\sigma_m)^{1/2} \qquad [1.17]$$

in which K_2 is a parameter that varies with shear strain and σ_m is the mean normal effective stress. The value of K_2 is depicted in Figure 1.23. The initial effective stresses are used in the computation of the initial value of G and, thereafter, G is modified to take into account its dependence on shear strains. Although the pore water pressure increase during shaking decreases the effective stresses in a layer, the effect of decreasing mean normal effective stress on the shear modulus, G, is not taken into account in the total stress methods of analysis.

In fundamental studies of effective stress-strain relations for sands, Seed & Idriss (1975) and Hardin & Drnevich (1972) showed the shear modulus, G, to be a function of the mean normal effective stress and the shear-strain. On the basis of extensive resonant column tests performed on a range of soil, Hardin & Drnevich (1972) concluded the following:

1. The shear modulus decreases and damping ratio increases very rapidly with increasing strain amplitude as shown in Figure 1.23. However, the rate of decrease or increase depends on many parameters, and a single relationship between modulus or damping and strain amplitude is not sufficient. The initial rates of decrease in modulus or increase in damping are higher for: (1) lower effective mean principal stress; (2) higher void ratio; and (3) lower number of cycles of loading. The initial rates are also higher for cohesive than for cohesionless soils.

2. The shear modulus increases and the damping ratio decreases with increasing effective mean principal stress. For very small strain amplitudes, the modulus varies

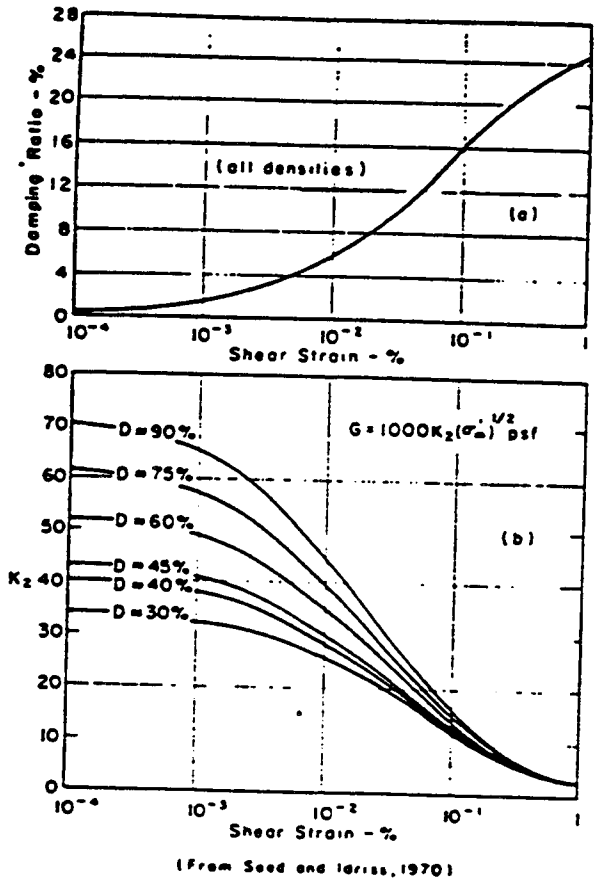

Figure 1.23 Moduli and damping ratio for sand (After Seed and Idriss 1970)

with the 0.5 power of effective mean principal stress. But, at large strain amplitudes, the modulus depends primarily on the strength of the soil and the variation is more nearly with the 1.0 power. The damping decreases approximately with the 0.5 power of effective mean principal stress independent of strain amplitude. The deviatoric component of the ambient state of stress in the soil has a much smaller effect than the effective mean principal stress.

3. The modulus decreases and the damping ratio decreases with increasing void ratio in undisturbed cohesive soils. The effect is accounted for by a factor, F(e), which is a function of the void ratio, e.

4. The shear modulus decreases for cohesive soils and increases slightly for cohesionless soils with the number of cycles of loading. The damping ratio decreases approximately with the logarithm of the number of cycles of loading in both cohesive and cohesionless soils, up to about 50,000 cycles. Beyond this, there appears to be a fatigue mechanism involved that causes the damping to increase with the number of cycles.

5. The effect of degree of saturation on the modulus and damping in cohesionless soils is small, but the modulus of cohesive soils increases rapidly with a decreasing degree of saturation.

6. Thixotropic effects cause the modulus to increase and the damping ratio to decrease with time, particularly in cohesive soil. The recovery of the modulus and damping with time after high amplitude cyclic loading is also significant.

7. For undisturbed cohesive soil, damping is increased only slightly with frequency within the range considered. Hardin and Black (1966, 1968) have shown that dry cohesionless soils are almost unaffected by frequency from essentially zero to a few hundred cycles per second. Although frequencies above 0.1 Hz have a relatively minor effect on the modulus and damping in cohesive soils, the behavior should be expected to change drastically for much lower frequencies where creep phenomena are involved.

8. The effect of preconsolidation pressure is to increase G_{max} over the normally consolidated value, depending on the plasticity index, PI, of the soil, with almost no

effect of overconsolidation for $PI = 0$. An equation for G_{max} including this effect is given by Hardin & Black (1969). The effect of overconsolidation on the behavior at larger strain amplitudes was shown by Hardin & Drnevich (1972).

In saturated sands, the progressive development of pore water pressure during cyclic loading continuously diminishes the level of effective stress and, hence, the shear modulus and the resistance to deformation is also diminished.

During cyclic loading, the slips at grain contacts result in volumetric compaction and increased values of K_o, the coefficient of effective lateral stress. Both effects stiffen the sand against further deformation. It is also probable that the slips at grain contacts result in a more stable sand structure under the existing effective stress regime. The processes, leading to increased resistance, are referred to collectively as hardening. The effect has been noted in dry sands and in saturated undrained sand at the strain levels typical of ground shaking.

In summary, the important factors which must be considered when computing the response of saturated sand layers to a given earthquake are (a) the initial shear modulus in-situ; (b) the variation of shear modulus with shear strain; (c) contemporaneous generation and dissipation of pore water pressures; (d) changes in effective mean normal stress; (e) damping; and (f) hardening. All of these factors except damping are taken into account in this thesis using the geologic cap model.

1.4 Research Approach

1.4.1 Finite Element Analysis of Pile Cross Sections

The objective of the work of this thesis was to develop the nonlinear spring properties that can be applied for Winkler analyses of arbitrary single piles and pile groups. Several Finite Element analyses were performed for circular piles of 0.457m (18″) and 0.610m (24″) diameters.

DYNA3D, a finite deformation, large strain Finite Element code for dynamic analysis in three dimensions was used for these analyses. Isoparametric solid elements with single point integration controlling "zero energy" modes were used to model both the soil and the pile cross-sections. The piles were modeled as rigid disks for 2D models and assumed to be linearly elastic for 3D models, while soil was assumed to be elasto-plastic. The

plastic behavior was represented using the Geologic Cap Model (DiMaggio & Sandlar 1971, Sandler et al. 1976, Sandler & Rubin 1979, Simo et al. 1988, Hofstetter et al. 1993). The pile-soil interfaces were modeled by using sliding interface elements which permit sliding with separation, closure, and friction.

Plane-stress/plane-strain models Two dimensional models, that included cross-sections of single piles, sets of two piles at various spacings, and typical pile cap models, were analyzed with pseudo-static harmonic loads. Maximum values of the loads were were such that reasonable force-displacement curves could be obtained. Plane-stress and plane-strain models were considered in order to provide bounds for soil layers near the surface and for those at greater depths. The reason for using the plane-strain condition is that previous research has shown that the force-displacement behavior of a thin layer based on plane-strain conditions provides a reasonable response for piles with moderate to high frequency vibration. The pile cap model was analyzed with plane-stress assumptions only, because at this depth no restraint would be available to attain plane-strain conditions in practice. From the results, equivalent spring/damper models were developed to simulate the effect on the piles and pile caps of the surrounding soil and pile-soil-pile interaction for lateral loading. A typical finite element model is shown in Figure 2.2 for computation of lateral resistance provided by the soil to a single pile. Similarly, finite element models, shown in Figures 2.17 and 2.15, were used for a square pile cap and two-pile groups, respectively, to compute lateral resistance.

Axisymmetric models Axisymmetric models are appropriate to obtain stiffness and damping properties in the axial direction of a single pile. In order to separate the effects of soil deformation and pile-soil slippage from the axial deformation of the pile and the stiffness of the soil beneath the tip, thin cylindrical layers of the pile were modeled with a layer of soil of same thickness. The model was loaded harmonically with pseudo-static axial force while pressure was applied to the soil to simulate overburden for various depths. Only shear deformation was allowed in the soil. From these analyses, spring/damper models for axial loading on a single pile were developed as a function of depth. A typical finite element model is shown in Figure 2.10, which is used to find soil resistance to vertical displacement of a single pile.

Three-dimensional models The axial pile-soil-pile interaction effects can not be modeled with axisymmetric assumptions. Therefore, three dimensional models were utilized to consider the axial behavior of sets of two piles within a finite layer of soil. As with the axisymmetric models, pseudo-static axial force was applied harmonically to one of the piles to obtain stiffness/damping properties that can be assumed to exist between adjacent piles.

1.4.2 Development and Verification of the Winkler Model

Several equivalent Winkler pile models were developed using the nonlinear spring elements obtained in this work for the near field and the spring/damper elements of Nogami et al. (1992) for lateral vibration. The main objective was to investigate the ability of this simplified approach to accurately model the nonlinear, dynamic response of single piles. The lumped parameter model of the pile was excited at the top with an impulsive lateral load and the free vibration response was noted. The computer runs were performed by the bridge analysis software, NEABS, described in an earlier report (McGuire, Cofer, Marsh, and McLean 1994).

An equivalent three dimensional finite element model of a single pile and surrounding soil was developed and loaded at the top with the same impulsive lateral load. As with the two dimensional models, nonlinear soil material properties, sliding interfaces at soil-pile interfaces, and non-reflecting boundaries were used. The response of the pile was noted and used for comparison with the load transfer models.

2. MODEL BASICS AND FINDINGS

2.1 General

A rational, dynamic, nonlinear soil-pile interaction model has been developed for a single pile and a two-pile group for lateral and axial vibration. Nonlinearities arising from the nonlinear stress-strain relationship of soil and from the pile-soil interface, which is susceptible to separation and friction, were considered. These were formulated as simple combinations of frequency independent masses, springs, and dashpots. Therefore, time domain nonlinear analysis may be conducted in a relatively simple manner. The model has been developed by adopting Winkler's hypothesis, i.e., the soil response at a given depth depends only on the reaction of the pile to soil at that specific depth. Figures 2.1 and 1.9 show typical Winkler pile models.

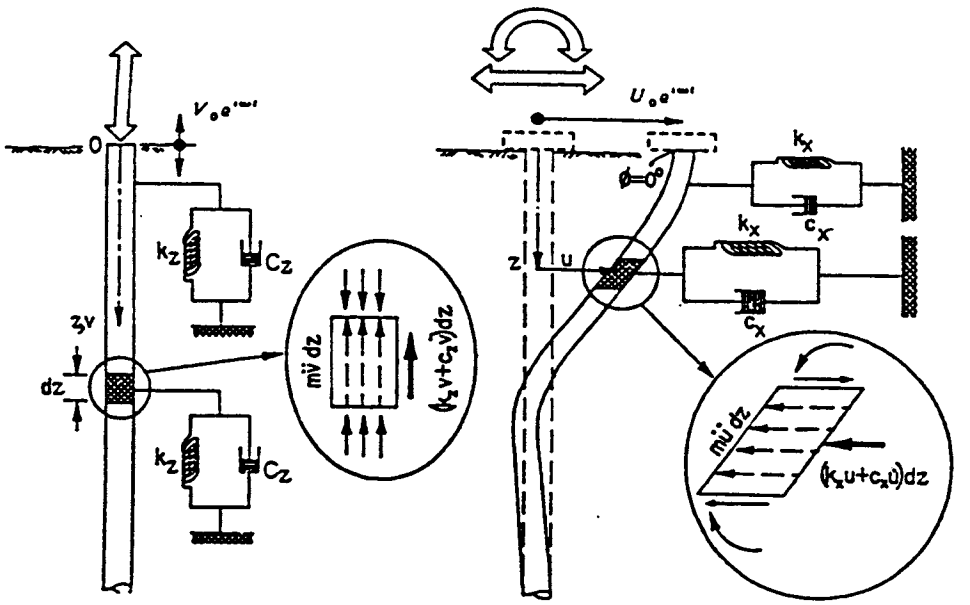

Figure 2.1 A typical discrete soil-pile model based on Winkler's hypothesis. (After Makris and Gazetas 1991)

For the development of the mass, spring, and dashpot models, pile segment(s) in a soil layer of finite thickness have been considered. A finite element discretization of the soil-pile combination was made using 8-node, quadrilateral, isoparametric elements. Due consideration was given for the near-field region of soil in which large strains may occur. In the far-field region, the soil was assumed to remain essentially elastic because of small strain development. Elastic behavior is, therefore, appropriate for the far-field. Pile segments have no (or little) deformation in comparison with the soil, and they are considered to be rigid where appropriate. A sliding interface was assumed to exist between the pile and soil during analyses for lateral vibration. However, to avoid instability, this interface was not included in the models for determining axial vibration response.

Due consideration was given for the initialization of geo-static stresses within the model. The properties of soil were obtained from conventional laboratory tests. The test results are summarized in Appendix C. Pseudo-static perturbations in the form of forces on single pile segments and pile segments within the two-pile groups were simulated using the finite element program, DYNA3D. The response was measured in the form of displacement and reactive forces in single pile models, and in the form of reactive forces in pile group models. The force and displacement histories were obtained from the post-processor, TAURUS, analyzed, plotted, and presented in this thesis in Appendix E. The force-displacement curves were simplified using simple parameters such as elastic or unloading stiffness, elasto-plastic stiffness, yield force, hardening coefficient, and a gap parameter. These simple parameters, called *bilinear parameters* afterwards, are also presented in Appendix E.

2.2 Modeling of a Single Pile

For modeling a single pile, the model proposed by Nogami et al. (1992) for lateral vibration and that proposed by Nogami and Konagai (1986, 1987, 1988) for axial vibration were applied with some modifications. Those models are described in Appendices A and B, respectively.

The lateral and axial vibrations were modeled on the basis of finite element analysis of a circular thin soil layer of unit thickness and diameter $40d$ (where d is the diameter of the pile). Within the range of stress developed, it was assumed that the pile segment is relatively rigid. Therefore, the pile was modeled as a rigid disk, surrounded by a mesh

representing the soil, as shown in Figures 2.2 and 2.11. Soil within a radius of $4d$ from the pile center was modeled with a nonlinear geologic cap material model. The remainder of the soil was modeled with consistent elastic properties because soil strains are assumed to be small away from the pile. All parameters for modeling of the soil properties were appropriate for the depth considered and for the existing K_0-stress condition. There was a *sliding interface* between the pile and soil. The sliding interface was modeled to mimic gap formation, impact within a gap. and sliding with friction. The interface was not modeled by using any element; rather it is resolved in the solution algorithmic phase in the explicit finite element program, DYNA3D. The K_0-stress state was taken as the initial condition. The main analyses were performed using DYNA3D because its material library includes the geologic cap model. The stress initialization was done by incorporating the initial stress output file from the implicit finite element companion program, NIKE3D.

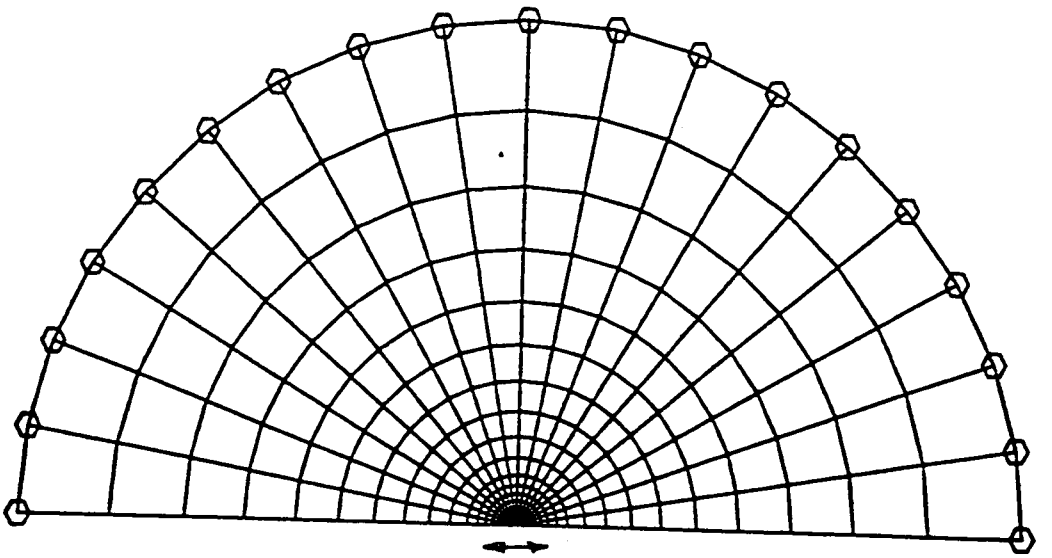

Figure 2.2 Finite element mesh used for the analysis of 2D soil-pile layer for lateral vibration of single pile. Symmetry has been used.

2.2.1 Lateral Vibration of a Single Pile

The model is based on the model proposed by Nogami et al. (1992) in which the pile is modeled as beam on inelastic Winkler-type foundation modified for dynamic analysis. It

is based on a thin layer solution. In this model, there are two nodes at each layer: a *pile node* and an *auxiliary node*. The model consists of a nonlinear near-field spring, a linear near-field viscous damper, lumped masses at the pile and auxiliary nodes, three linear far-field springs and three linear far-field dampers. The model is shown in Figure 2.3. The detail of the near- and far-field elements are shown in Figure 2.4. The model is described in Appendix A in details. Nogami et al. (1992) provided explicit expressions for the far-field element parameters in terms of elastic soil properties. In this thesis the major emphasis goes to the formulation of the nonlinear near-field springs and the lumped masses. The spring characteristics were obtained using a finite-element approach. The lumped masses were obtained by using a consistent formulation with assumed shape functions and a lumping procedure.

2.2.1.1 Characteristics of the Near-Field Spring

For very large depths, the plane-strain condition is appropriate while, for very small depths, the plane-stress condition may be used. It has been shown that for moderate to high frequency vibration, plane-strain soil impedance is appropriate for the linear elastic case (Novak 1974, Novak & Nogami 1977, Novak et al. 1978, Novak & Aboul-Ella 1978*a*, Novak & Aboul-Ella 1978*b*). Plane-strain analyses for several depths, represented by vertical effective stresses of 6.9, 17.3, 34.5, 68.9, 137.8, 275.6, 551.2, and 1102.4 kPa (1, 2.5, 5, 10, 20, 40, 80, and 160 psi) were performed. But for very small depths, the plane-strain case can not be realized. So, the plane-stress condition is assumed to be more appropriate where vertical pressure will not change with lateral pile movement. Plane-stress analyses were used for 4 vertical stresses: 6.9, 17.3, 34.5, and 68.9 kPa (1, 2.5, 5, and 10 psi). The basic soil parameters were needed exactly for these specific vertical confining pressures. These are interpolated from Tables C.4 through C.7. The resulting soil properties are tabulated in Tables D.1 through D.2. The resulting cap parameters for those soils at different layers are presented in Table D.3. In Table D.1, some averaging was used to obtain a set of uniform values throughout the depths. The averaging procedure is described in Appendix D. In the following sections, the derivation of the coefficients for the near-field and the far-field elements is described.

To develop the nonlinear near-field spring, the pile segment was forced to move laterally either in the plane-stress or plane-strain condition during the computer simulation

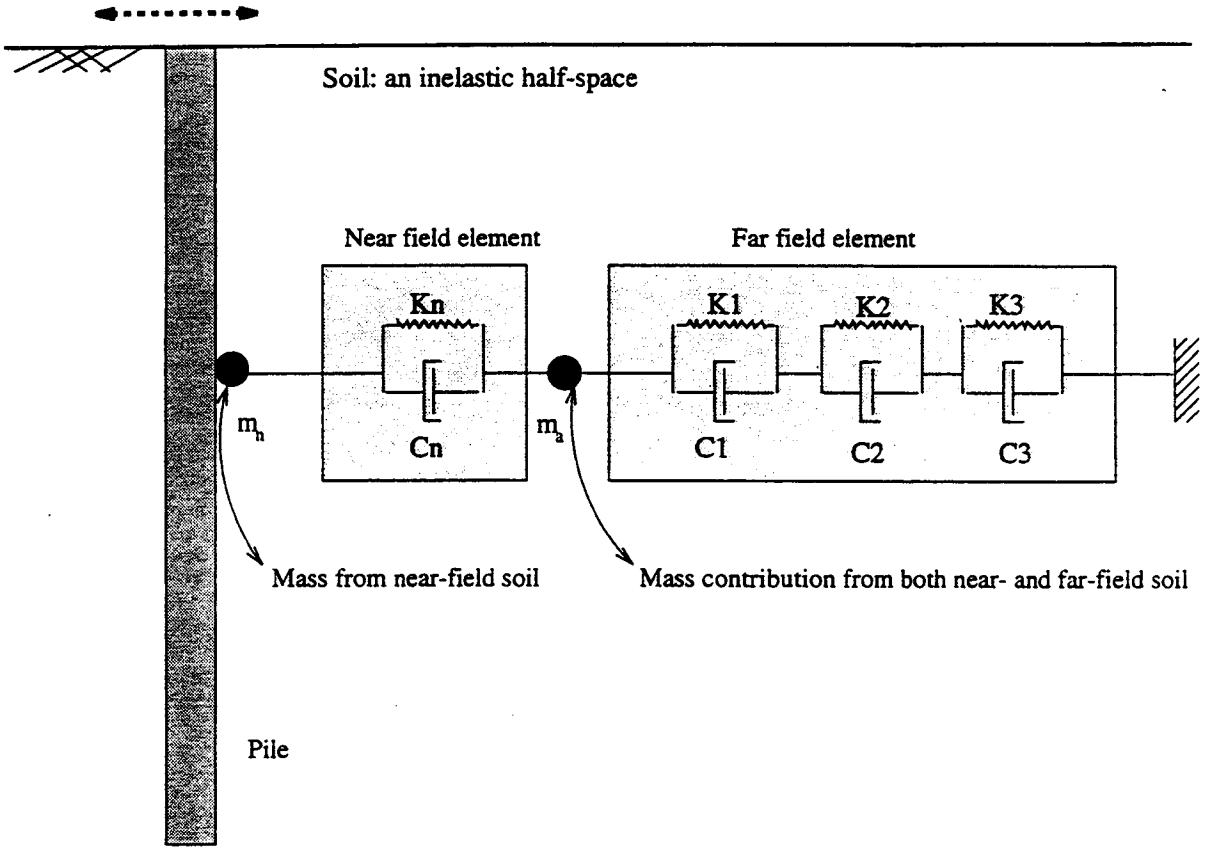

Figure 2.3 A model for lateral vibration of single pile. The model consists of springs, dashpots, and masses to represent.

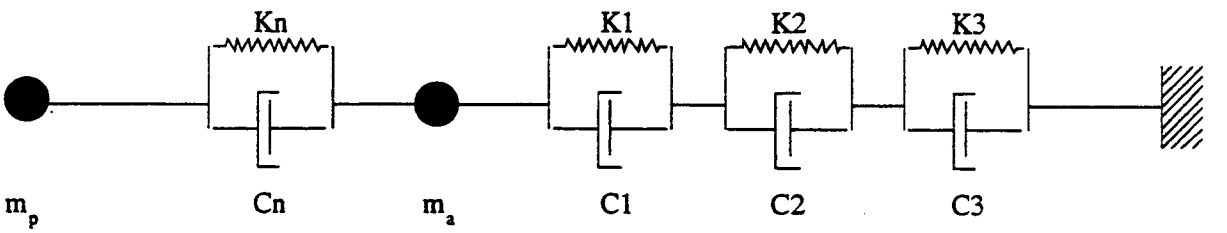

Figure 2.4 A combination of springs, dashpots, and masses to represent the near-field and far-field element for modeling lateral vibration of a single pile. (After Nogami and Konagai 1992)

of a lateral load test using the finite element mesh, shown in Figure 2.2, and the displacement of the segment was observed using TAURUS. The lateral force-displacement behavior for a single pile or pile-groups is represented by p-y curves, where p is lateral force per unit length of pile and y is lateral displacement. Moreover, a similar relationship is represented by the t-z relation for vertical response of a single pile or pile-groups, where t is axial force per unit length of pile and z is axial displacement. A typical p-y curve is shown in Figure 2.5 for two cycles of the load, and it includes nonlinearities from hysteretic and gap behavior.

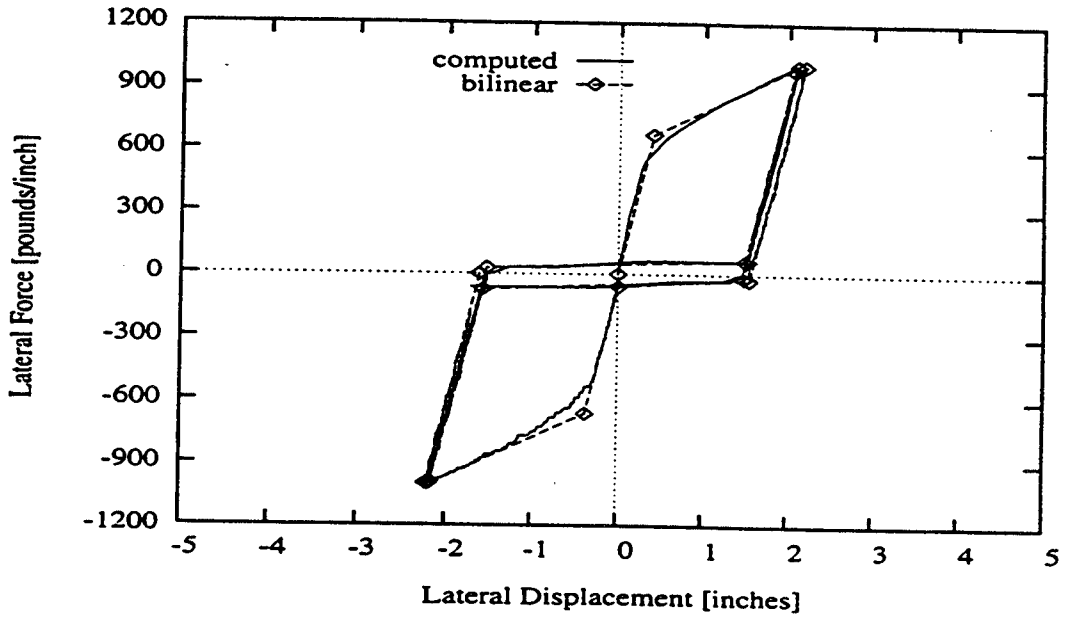

Figure 2.5 A typical p-y curve for the near-field spring, shown as lateral force per length of pile (pounds/inch) versus displacement (inches)

Initially, when a pile segment moves laterally in a thin layer of soil, the force-displacement relationship remains linear elastic. When the force level exceeds the elastic range, it leaves a gap behind it and plastic deformation continues. It is shown in Figure 2.6. The slope of the p-y curve changes to represent plastic behavior. Upon unloading, the pile segment moves back elastically until the "zero" force state is almost reached. Then, with reverse loading, the pile moves back, through the gap created before, with very small resistance. Here, the slope of the p-y curve is called the *first gap stiffness.* With increasing reverse load, the pile segment reaches the rear end of the gap, after which the loading behavior is elastic until reverse plastic loading occurs. The slope of

reverse plastic loading is similar to that of the loading elasto-plastic slope. At the same time, the rear end of the gap moves more. Reverse loading becomes elastic again until the "zero" force state is again reached. Then it moves back through the gap.

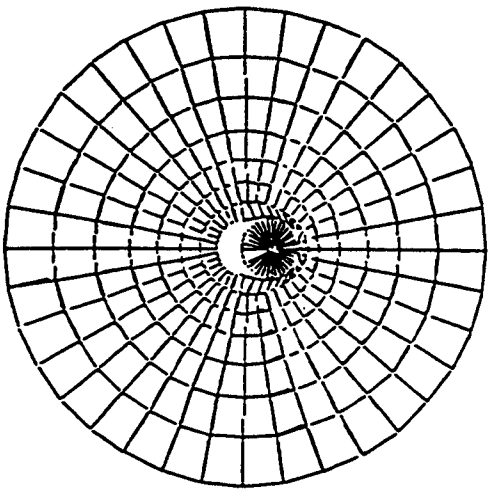

Figure 2.6 A pile leaves a gap behind it when plastic deformation continues during lateral·motion.

A comprehensive determination of near-field spring constants has been made for piles with diameters of $0.457m$ (18″) and $0.610m$ (24″), respectively, using soil parameters determined from laboratory tests performed on soil samples taken from a Snohomish river site in Washington State. Most of the soil samples were silty (MH, ML, SM). The soil was uniform from depths of 3m (10′) to 9m (30′). Constant soil parameters for this range of depths were used, with modification for confining pressures. These thin-layer *p-y* curves were produced for 6.9, 17.3, 34.5, 68.9, 137.8, 275.6, 551.2, and 1102.4 kPa (1, 2.5, 5, 10, 20, 40, 80, and 160 psi) of vertical effective stress, assuming drained conditions. In all cases, the coefficient of earth pressure at rest, K_0, was assumed to be 0.5, and the coefficient of friction in the interface was assumed to be 0.4. The *p-y* curves for very small vertical stresses, 6.9, 17.3, 34.5, and 68.9 kPa (1, 2.5, 5, and 10 psi) were developed for the plane-stress condition. All *p-y* curves are presented in Figures E.1 through E.4.

For the analysis of pile vibration using NEABS as modified by McGuire (1993), the *p-y* curve is simplified as a combination of several linear segments with (see Figure 2.7):

1. initial stiffness, K_1,

2. yield force, F_y,

3. hardening stiffness without gap, K_2,

4. unloading stiffness without gap, K_3,

5. hardening stiffness with gap, K_4,

6. unloading stiffness with gap, K_5, and

7. hardening parameter, β, and

8. a gap parameter representing the capability on the trailing edge to follow the leading edge of the gap, γ.

This simplified representation of *p-y* curves, shown in Figure 2.7, will be called as *bilinear p-y* curves. The parameters K_1 and K_3 are found to be more or less the same for all the *p-y* curves. Also, K_5 can not be determined from a load controlled test. Its value has a minor significance in practice, and should be in between K_4 and K_1. K_5 can be taken to be equal to K_1. The hardening parameter, β, represents the way in which the *p-y* curve hardens for reverse loading with elasto-plastic load increments. For isotropic hardening, β equals one, and for kinematic hardening, β equals zero. Intermediate values of β represent mixed hardening. The gap parameter, γ, represents the behavior of the movement of the leading and the trailing edge of the gap. Effectively, it relates the plastic movement of soil, $u_{plastic}$ and the generated gap, u_{gap}.

$$\gamma = \frac{u_{gap}}{u_{plastic}} \qquad [2.1]$$

Figure 2.5 shows the matching between the *p-y* and its linearized version. The matching is excellent and it validates the use of *bilinear parameters* to represent any *p-y* curve with gap formation.

The simplified parameters which can reproduce the *p-y* curves for lateral vibration of single piles are presented in Tables 2.1 and 2.2. The tables show that the stiffness increases with confining pressure almost linearly in both plane-stress and plane-strain conditions. The stiffness values are almost independent of the pile diameter. This is

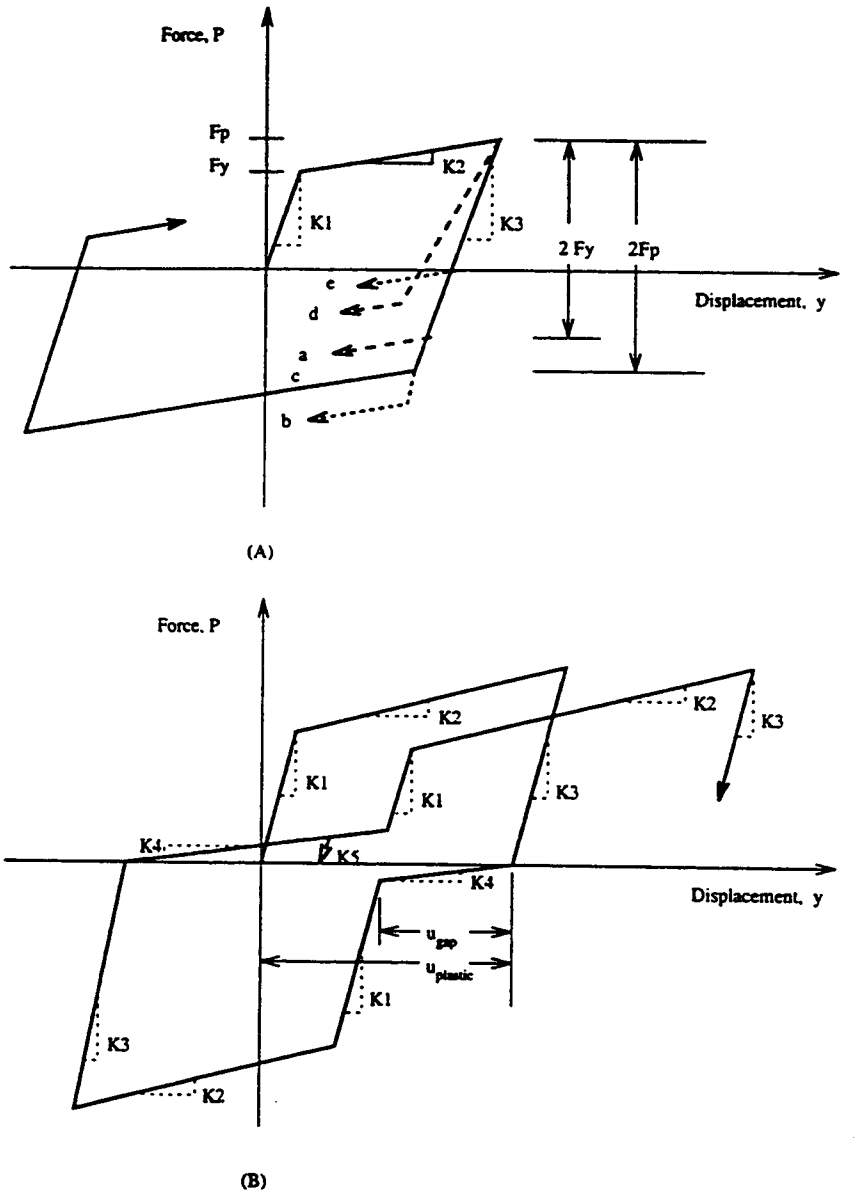

Figure 2.7 A linearized idealization of p-y curves

because the region of soil considered in the near-field zone is 40 times the diameter of the pile. For larger diameters, larger models were used. Initial stiffness is usually less in the plane-stress case than in plane-strain case. The yield force increases with confining pressure. The yield forces are proportional to the diameters in both the plane-stress and plane-strain cases. Hardening occurs for all the p-y curves. The effect of the gap is more significant in the plane-strain case than in the plane-stress case.

Table 2.1 NEABS parameters for p-y curves for a single pile vibrating laterally for different confining pressures. [$d = 0.457m$, $K_0' = 0.50$, $f = 0.40$, isotropic hardening, drained condition]

Vertical pressure, *psi*	**Initial stiffness,** lbs/in^2	**Post-yield stiffness,** lbs/in^2	**Initial yield force** lbs/in	**First Gap stiffness,** lbs/in^2	**Hardening parameter,** β	**Gap parameter,** γ
Plane-strain condition						
1	174.	46.	135.	5.	0.42	1.06
2.5	423.	71.	215.	7.	0.33	1.02
5	832.	117.	315.	11.	0.43	1.01
10	1692.	183.	529.	48.	0.62	1.19
20	2160.	291.	1034.	69.	0.60	1.13
40	2594.	617.	2062.	131.	0.49	1.03
80	3704.	1112.	4537.	314.	0.10	1.09
160	5474.	1865.	8711.	695.	0.41	1.02
Plane-stress condition						
1	157.	49.	143.	14.	0.33	0.54
2.5	389.	78.	218.	15.	0.58	0.71
5	868.	140.	354.	52.	0.15	0.73
10	1479.	195.	559.	100.	0.54	0.63

Table 2.2 NEABS parameters for p-y curves for single pile vibrating laterally for different confining pressures. [$d = 0.610m$, $K_0' = 0.50$, $f = 0.40$, isotropic hardening, drained condition]

Vertical pressure, *psi*	**Initial stiffness,** lbs/in^2	**Post-yield stiffness,** lbs/in^2	**Initial yield force** lbs/in	**First Gap stiffness,** lbs/in^2	**Hardening parameter,** β	**Gap parameter,** γ
Plane-strain condition						
1	179.	44.	175.	7.	0.55	1.07
2.5	429.	73.	278.	7.	0.35	1.03
5	857.	116.	419.	10.	0.43	1.03
10	1653.	192.	668.	19.	0.50	0.99
20	1921.	241.	1321.	76.	0.49	1.30
40	2762.	600.	2735.	159.	0.54	1.11
80	3931.	1384.	4484.	337.	0.43	1.05
160	5397.	1988.	12250.	702.	0.16	1.05
Plane-stress condition						
1	159.	53.	189.	24.	0.50	0.64
2.5	431.	70.	270.	28.	0.74	0.80
5	776.	100.	494.	37.	0.64	0.85
10	1913.	302.	581.	287.	0.58	0.40

2.2.1.2 Characteristics of Near-field Dampers

A damper represents one means of dissipating energy. It is very difficult to estimate damping constants from the finite element analysis of any structure for which viscosity of the material is actually unknown. For most cases, it is obtained from a field test. Moreover, a field test for a thin layer of soil and pile segment combination for either plane-stress or plane-strain conditions with initial K_0-stress would be extremely difficult. It is easy to specify the damping coefficient as a fraction of critical damping, i.e. as a proportional damping. Then the damping constant is

$$C = 2 \xi K / \omega_{ave}. \qquad [2.2]$$

where, K_i = initial or unloading-reloading stiffness,
ω_{ave} = average loading frequency, and
ξ = material damping ratio.

The stiffness value, K, may be represented by the elastic stiffness or an unloading-reloading stiffness. The circular frequency for the actual earthquake loading may be estimated from the earthquake acceleration history of the free-field motion by counting the number of peaks, either maxima or minima, by counting the number of crossings of the zero acceleration level, by Fourier analysis of the acceleration time history for kinematic interaction analysis, or by considering the modal frequency of the structure involving predominantly foundation movement for inertial loading. Engineering judgment is needed to compute the ω_{ave}. The damping coefficient, ξ is merely estimated as 0.01 to 0.10, still based on engineering judgment and the magnitude of displacement at that particular level. The value of ξ can be obtained from the curves prepared by Hardin & Drnevich (1972) and Seed & Idriss (1969*b*). However, before using these curves, the average strain within the radius r_0 to r_1 should be known. The average value of strain should be taken as a function of the maximum displacement. Since the value of the displacement is unknown, the selection of the value of β becomes iterative. One may observe that the value of C is frequency dependent and, therefore, C must be defined for an estimated frequency. For higher frequencies of loading, the specified value of C represents higher values of ξ. Also, higher frequencies of loading are damped out due to the discretization of the structure by finite elements. However, high frequency loads have relatively less importance for bridge design. For a high amplitude of loading, excessive cyclic deformation will induce a hysteretic dissipation of energy due to the nonlinear

effect of the spring which will be taken care of by the nonlinear springs. This dissipation of energy will be much more important than that dissipated in the damper. So, it is reasonable to estimate the damping constant by the use of Equation 2.2.

2.2.1.3 Characteristics of Nodal Masses

Near-field masses are obtained from a lumped mass procedure. The model has two nodes: a *pile node* and an *auxiliary node*. The mass of the pile node consists of the mass of the pile itself along with the contribution of the mass from the near-field soil. The contribution of the mass from soil is computed from the consistent mass matrix developed for the annular segment of soil with inner and outer radius r_0 and r_1, respectively, where r_0 is the radius of the pile and r_1 is the inner radius of the near-field zone. r_1 can be chosen arbitrarily such that all of the nonlinearity is contained within the near-field zone and the p-y curves should be consistent with this zone. In all cases, r_1 was taken as $40d$. where d is the pile diameter. The nodes are assumed to exist at the pile center and at the outer boundary. All points of the outer boundary of radius r_1 are assumed to have equal displacement and share the same degrees of freedom. The shape function in cylindrical coordinates is assumed to vary as a function of the nth power of r and it is not a function of the θ coordinate at all. The consistent mass matrix for two nodes is

$$[M] = \left\{\frac{(\pi\rho r_0^2)(m-1)}{(n+1)(2n+1)}\right\} \begin{bmatrix} (2n+1)m+1 & \frac{n}{n+2}\{(2n+1)m+3\} \\ \frac{n}{n+2}\{(2n+1)m+3\} & m+(2n+1) \end{bmatrix} \quad [2.3]$$

where, m = r_1/r_0,
r_1 = radius of near field zone,
r_0 = radius of rigid pile,
n = power in the shape function (Nogami assumed $n = 1$).

In his analysis, Nogami assumed $n = 1$ arbitrarily. Using the HRZ lumping scheme, described in Appendix F, the contribution of the soil to the nodes as lumped mass is represented by the mass matrix,

$$[\mathrm{M}] = \left\{\frac{(\pi\rho r_0^2)(m-1)}{2(n+1)(m+1)}\right\} \begin{bmatrix} \{(2n+1)m+1\} & 0 \\ 0 & \{m+(2n+1)\} \end{bmatrix} \quad [2.4]$$

The values of $\frac{m_{11}}{m_{11}+m_{22}}$ are plotted in Figure 2.8 as a function of n and m. Having the mass contributions from soil, the nodal mass at the pile node can be obtained by adding the nodal contribution from soil to the mass of the pile itself, as

$$m_p = \pi\rho_s {r_0}^2 \left\{\frac{(m-1)\{m+(2n+1)\}}{2(n+1)(m+1)} + \frac{\rho_p}{\rho_s}\right\} s \quad [2.5]$$

where s = spacing of the nodes in the vertical direction.

The mass at the auxiliary node, m_a, can be obtained by adding two contributions, one from near-field soil and the other from far-field soil.

$$m_a = m_{11} + m_f \qquad [2.6]$$

where, m_{11} = first diagonal element of [M], and

m_f = mass contribution from far-field soil.

The mass contribution, mf, can be obtained from the equation

$$mf = \pi \rho r_1^2 \xi_m (\nu) \qquad [2.7]$$

where $\xi_m (\nu)$ is a function of Poisson's ratio, and it can be obtained from Figure 2.9 and Table 2.3.

2.2.1.4 Characteristics of the Far-Field Elements

The far-field element consists of the far-field mass contribution, m_f, springs, K_1, K_2, and K_3, and dampers, C_1, C_2, and C_3. Those are shown in Figure 2.4. The far-field element has been adopted from Nogami et al. (1992), as discussed in Appendix A. The mass contribution from the far-field, m_f, can be obtained from the Equation 2.7. The spring and damping constants are defined as:

$$\begin{Bmatrix} K_1 \\ K_2 \\ K_3 \end{Bmatrix} = G \xi_k(\nu) \begin{Bmatrix} 3.518 \\ 3.581 \\ 5.519 \end{Bmatrix} \qquad [2.8]$$

$$\begin{Bmatrix} C_1 \\ C_2 \\ C_3 \end{Bmatrix} = \frac{G r \xi_k(\nu)}{V_s} \begin{Bmatrix} 113.0973 \\ 25.133 \\ 9.362 \end{Bmatrix} \qquad [2.9]$$

where, G = Shear modulus of soil of the pertinent layer, and

$\xi_k (\nu)$ and $\xi_m (\nu)$ = Function of Poisson's ratio ν. It is obtained from Figure 2.9 or from Table 2.3 as a function of Poisson's ratio, and

V_s = Shear wave velocity in soil.

The spring constants and damping constants are basically frequency dependent. However, the aforementioned values work well for the range of frequency, $0.02 < a_o < 2.0$, where a_o is the nondimensional frequency and it is defined as $a_o = r_o \omega / V_s$, the commonly encountered frequency range for earthquake loading. The details are described by Nogami et al. (1992).

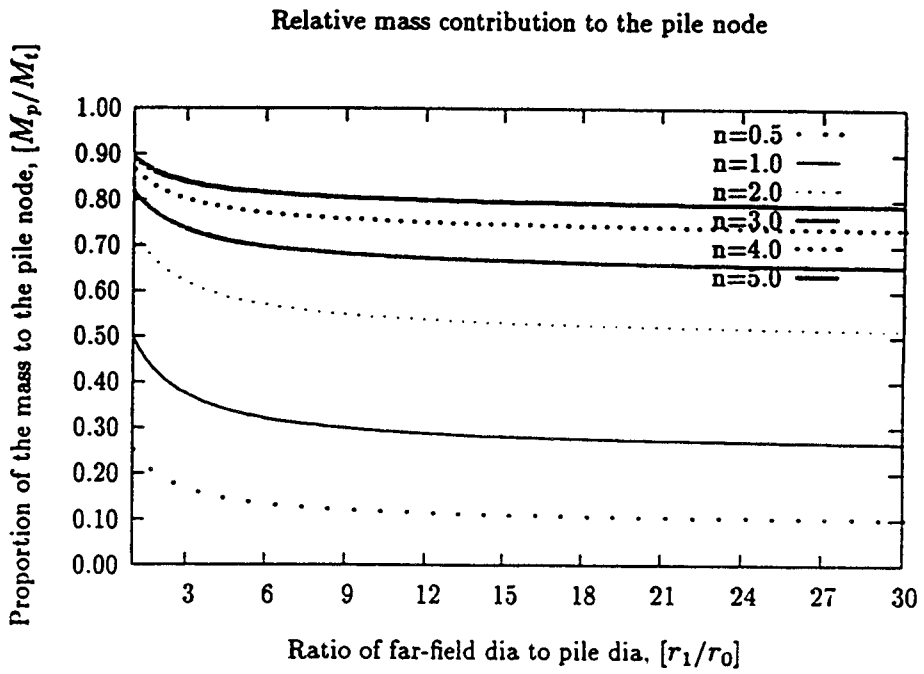

Figure 2.8 Contribution of near-field mass of soil to the ends of near-field spring element

Table 2.3 Functions $\xi_k(\nu)$ and $\xi_m(\nu)$. (After Nogami 1992)

Poisson's ratio, ν	Function $\xi_k(\nu)$	Function $\xi_m(\nu)$
0.50	2.000	1.0000
0.49	1.940	0.7828
0.48	1.883	0.6420
0.47	1.831	0.5336
0.46	1.784	0.4464
0.45	1.741	0.3740
0.43	1.667	0.2628
0.40	1.580	0.1428
0.35	1.476	0.0352
0.25	1.351	000000
0.20	1.311	000000
0.10	1.252	000000
0000	1.213	000000

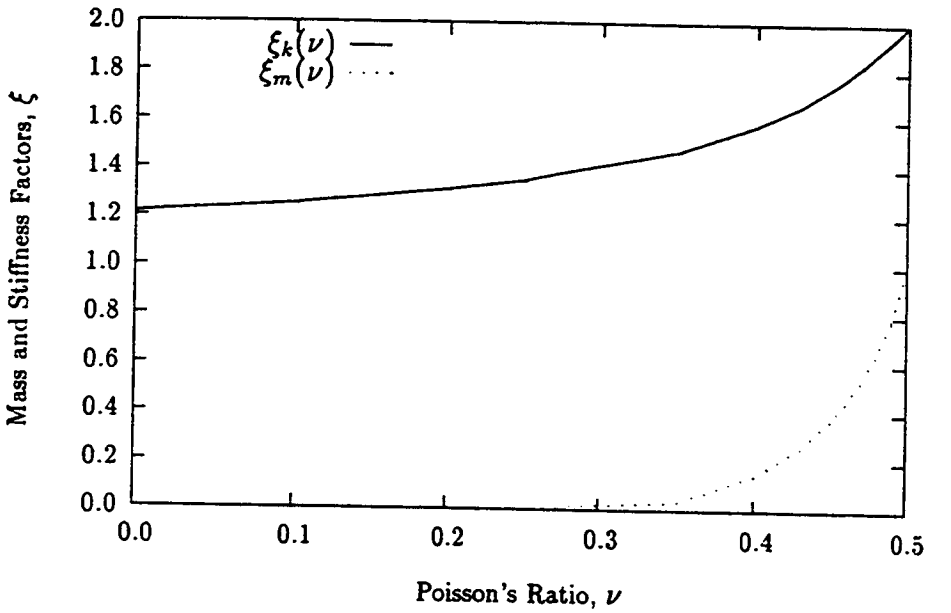

Figure 2.9 Mass and Stiffness factors for a single pile vibrating in the lateral mode

2.2.2 Axial Vibration of Single Pile

This model is basically an extension of that proposed by Nogami and Konagai (Nogami & Konagai 1986, Nogami & Konagai 1988, Mitwally & Novak 1988), which has been described in Appendix B. The model was originally developed for elastic soil and pile conditions, and extended to include nonlinear behavior. Analogous to the model for lateral vibration, the model consists of two nodal masses at the pile node and an auxiliary node, a nonlinear near-field spring, a linear near-field damper, three linear far-field springs, and three far-field dampers, as shown in Figure 2.10.

The thin layer solution and Winkler hypothesis is once again the basis of the development of the model for axial vibration response. Moreover, it is assumed that during axial vibration of a single pile in semi-infinite soil, all points move only in the vertical direction. This simplifies the problem of 3D vibration to 2D vibration, and allows the thin layer solution to be considered as an approximate solution of more complicated 3D vibration. This assumption is a reasonable one if the pile is long. When the pile is long enough, the thin layer moves vertically, and subsequent layers move in the same way, maintaining compatibility in an approximate manner, since each layer does not move equally. Resistances of different magnitudes develop at different depths depending on the shear modulus and pile displacement magnitudes.

For the assumption of no lateral displacement, only the shear deformation is included, rather than bending deformation of thin soil layers. This makes the stiffness of the soil spring proportional to the thickness, rather than the third power of thickness. This assumption applies to the skin resistance only. For the determination of the tip resistance, the pile tip is assumed to be on a nonlinear half-space with appropriate effective overburden pressure. The latter topic will be discussed in Section 2.5. The following subsections describe the model for skin resistance behavior for axial vibration.

2.2.2.1 Characteristics of the Nonlinear Spring

To develop the nonlinear spring characteristics, a finite element model was developed for a thin layer elasto-plastic soil and a rigid pile segment. Figure 2.11 shows a typical finite element model used to generate the nonlinear spring characteristics for axial vibration. Since the 3D computer program, DYNA3D, was used, it was necessary to take a sector of a thin circular segment. Soil within 8d of the pile was modeled with the geologic

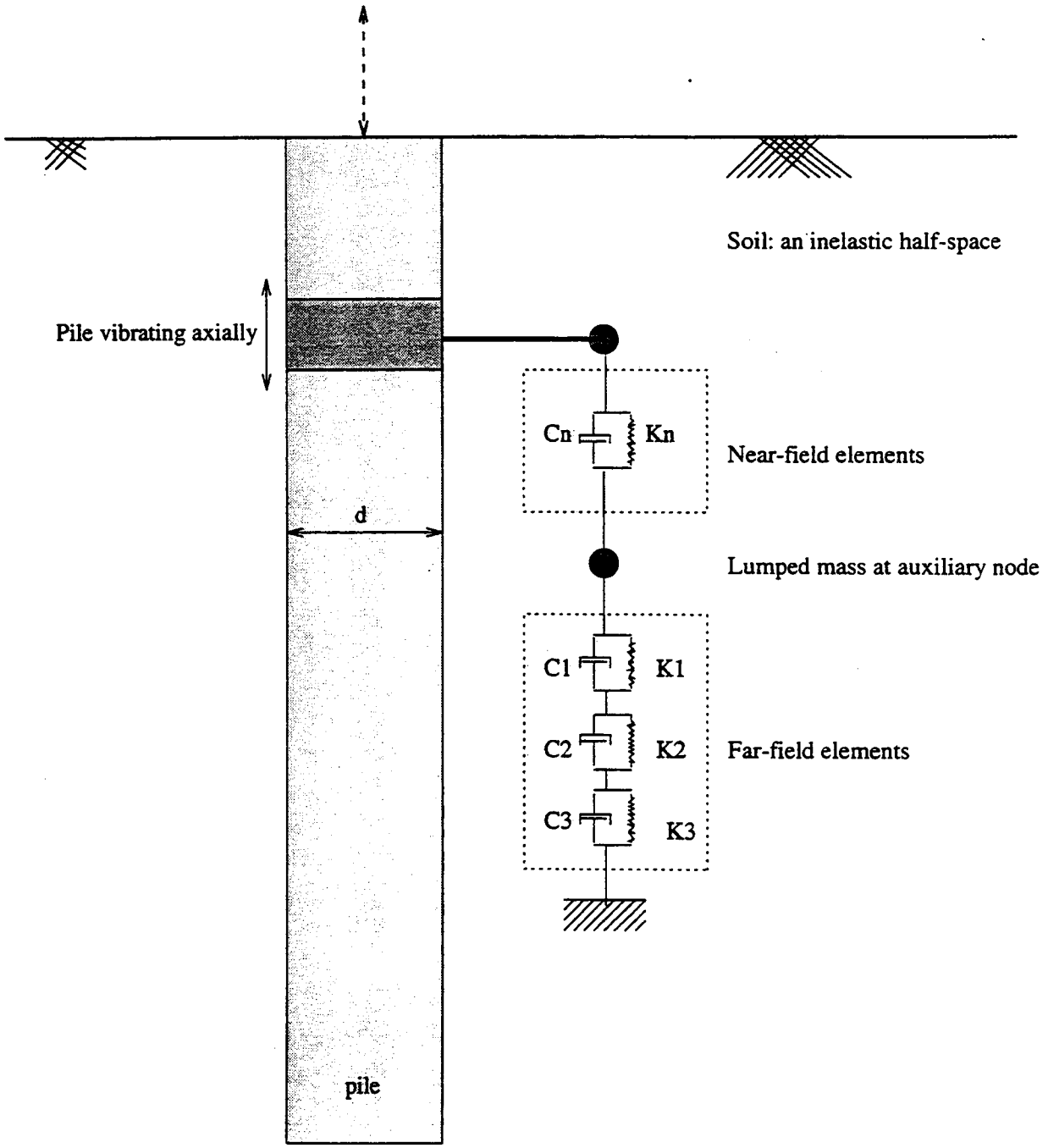

Figure 2.10 A model for axial vibration of single pile.

cap model. It was observed that soil displacement at a large distance (20 diameters) from the pile center was negligibly small and, therefore, an artificial, no displacement boundary was placed there. A pseudo-static load was applied along the pile axis to observe the resulting displacement. No sliding interface was assumed to exist between the pile and soil because initial observations showed that it induces instability. The initial K_0-state of stress was assumed as the initial condition. The overburden pressure was always maintained to ensure the confining effect.

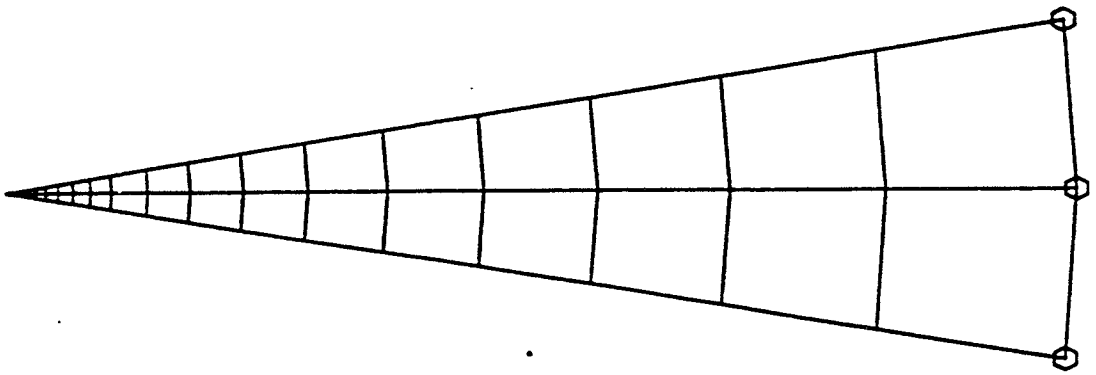

Figure 2.11 Finite element mesh used for the analysis of 2D soil-pile layer for axial vibration of single pile.

All nodes along the boundary were assumed to be fixed, and the rest of the nodes were allowed to move only vertically. The resulting *force (per unit thickness)–displacement* behavior, represented by t-z curves, were produced with 8 different confining pressures for soil of the Snohomish river site. These curves are presented in Figures E.5 and E.6 for piles of 18″ (0.457m) and 24″ (0.610m) diameters. Most of the curves were obtained for a linear range of forces, because within the nonlinear range, the t-z response is non-hardening. So, it becomes unstable when it reaches or exceeds the yield force in a load controlled simulation. Moreover, it was almost impossible to precisely estimate the yield force.

The bilinear parameters for the t-z curves are presented in Tables 2.4 and 2.5. The tables show that the initial stiffness increases with increasing confining pressure. However, they are not proportional. Also, comparing the tables, it can be observed that the stiffness of the near-field spring is almost independent of pile-diameters, although higher stiffness could be expected for larger pile diameters. The reason is that a larger soil region was included in the model for the larger pile diameter, as explained in the previous section. However, the yield force is almost proportional to the pile diameters. Since almost all the piles are analyzed in the linear range, it is necessary to estimate the strength of the near-field springs. The strength of the springs may be obtained from the equation

$$t_{max} = (2\pi rt)\tau_{max}. \qquad [2.10]$$

The value of τ_{max} may be obtained from recommended values presented in Table 2.6. Finally, this spring behavior should be elastic perfectly plastic, without hardening. The gap parameters are not needed for this case.

Table 2.4 NEABS parameters for t-z curves for single pile vibrating axially for different confining pressures. [$d = 0.457m$, $K_0' = 0.50$, isotropic hardening, drained condition]

Vertical pressure, *psi*	Initial stiffness, lbs/in^2	Post-yield stiffness, lbs/in^2	Initial yield force *lbs/in*	Hardening parameter, β
1	155.			
2.5	285.	3.	279.	0.000
5	810.	21.	352.	0.000
10	1020.	0.	552.	0.000
20	1246.	0.	955.	0.000
40	2093.			
80	2621.			
160	3774.			

Table 2.5 NEABS parameters for t-z curves for single pile vibrating axially for different confining pressures. [$d = 0.610m$, $K_0' = 0.50$, isotropic hardening, drained condition]

Vertical pressure, *psi*	**Initial stiffness,** lbs/in^2	**Post-yield stiffness,** lbs/in^2	**Initial yield force** lbs/in	**Hardening parameter,** β
1	153.			
2.5	398.	45.	357.	0.000
5	807.			
10	1618.			
20	1934.			
40	2092.			
80	2625.			
160	3768.			

Table 2.6 Shaft resistance f_s for bored pile, determination from laboratory strength data (After Poulos 1989)

Soil type	Equation	Remarks	References
Clay	$f_s = \alpha c_u$	$\alpha = 0.45$ (London Clay) $\alpha = 0.70$ times value for driven displacement pile	Skempton (1959) Fleming et al. (1985)
	$f_s = K \tan \delta \sigma'_v$	K is lesser of K_0 or $0.5\ (1 + K_0)$	Fleming et al. (1985)
		$K/K_0 = 2/3$ to 1: K_0 depends on OCR; δ depends on interface material	Stas and Kulhawy (1984)
Silica Sand	$f_s = \beta \sigma'_v$	$\beta = 0.10$ for $\phi' = 33°$ $\beta = 0.20$ for $\phi' = 35°$ $\beta = 0.35$ for $\phi' = 37°$	Mayerhof (1976)
		$\beta = F \tan(\phi' - 5°)$ where $F = 0.7$ (Compression) $F = 0.5$ (Tension)	Kraft & Lyons (1974)
Uncemented Calcareous Sand	$f_s = \beta \sigma'_v$ $f_s \leq f_{slim}$	$\beta = 0.50$ to 0.8 $f_{slim} = 60$ to 100 kN/m^2	Polous (1988)

2.2.2.2 Characteristics of the Damper

Proportional damping can be used in the same way as for lateral vibration. The damping ratio is for the material damping alone. The explicit value of C can be computed as

$$C = 2\xi K_i/\omega \qquad [2.11]$$

where, K_i = initial or unloading-reloading stiffness,
ω = average loading frequency obtained from counts of peaks or 0 crossing, fourier analysis of acceleration time history for kinematic interaction, or the modal frequency which dominates foundation movement of the bridge foundation system, and
ξ = effective material damping ratio.

2.2.2.3 Nodal Lumped Masses

For a thin layer of soil with a pile segment, only two degrees of freedom are needed to model the vibration: the pile node and an auxiliary node. During the axial vibration of the pile, the whole layer of soil vibrates along with the pile. Therefore, some inertial resistance comes from the soil, and for the sake of modeling, a certain part of the soil layer should be assumed to contribute to the inertial resistance of the pile. For a point in a soil layer at a large distance away from the pile, the amplitude decays and becomes less important. A shape function may, therefore, be applied to compute the soil contribution. The shape function assumed here is the approximate displacement shape of the same layer of elastic soil with a rigid pile segment. The resulting consistent mass matrix is

$$[\mathrm{M}] = \left\{ \frac{2\pi\rho_s t {r_1}^2}{[\ln (r_1/r_0)]^2} \right\} \begin{bmatrix} f_{11}(m) & f_{12}(m) \\ f_{21}(m) & f_{22}(m) \end{bmatrix} \qquad [2.12]$$

where

$$f_{11}(m) = 1/4 - \{1 + 2(\ln m) + 2(\ln m)^2/m^2\}, \qquad [2.13]$$

$$f_{12}(m) = (3/4)(m^2 - 1)(\ln m)(1/m^2) - f_{11}(m), \qquad [2.14]$$

$$f_{22}(m) = f_{11}(m) + (1/2)(1 - 1/m^2)\{1 - 3/(\ln m)\}\ , \qquad [2.15]$$

$$m = r_1/r_0\ . \qquad [2.16]$$

After HRZ lumping, the following consistent mass matrix, was obtained (see Appendix F):

$$[\mathrm{M}'] = \left\{\pi({r_1}^2 - {r_0}^2)\,\rho_s\,t\right\} \begin{bmatrix} f'_{11}(m) & 0 \\ 0 & f'_{22}(m) \end{bmatrix} \quad [2.17]$$

where

$$f'_{11}(m) = \frac{f_{11}(m)}{f_{11}(m) + f_{22}(m)}, \text{and} \quad [2.18]$$

$$f'_{22}(m) = \frac{f_{22}(m)}{f_{11}(m) + f_{22}(m)}. \quad [2.19]$$

[2.20]

and the contribution of mass from near-field soil to the pile, m_p, and to the auxiliary node, m_a, are

$$m_p = \pi r_0^2 \rho_s\, t(m^2-1) f'_{11}(m), \text{and} \quad [2.21]$$

$$m_a = \pi r_0^2 \rho_s\, t(m^2-1) f'_{11}(m), \text{respectively.} \quad [2.22]$$

The value of $f'_{11}(m)$ is plotted in Figure 2.12 as a function of m. However, the above expressions will only work well for low frequency vibration. The shape function that was assumed will not represent the actual displacement behavior during high frequency vibration for which the mass contribution of the soil would be lower than this due to both positive and negative contributions of the soil from wave effects. The effect of soil mass would be further reduced for nonlinear soil, because most of the effects are local during nonlinear vibration.

2.3 Modeling of Pile Groups

For the vibration of two-pile groups, in addition to the near-field and far-field elements considered for a single pile, it is necessary to consider interface springs between the piles. Also, the number of auxiliary nodes at which the near-field and far-field elements are connected would be more than one, as opposed to the model of a single pile. Here, it may be expected that each external pile should be connected to the far-field elements through auxiliary nodes. Also, near-field soil mass would be distributed between the pile nodes and the auxiliary nodes. The emphasis of this thesis is given to the determination of the near-field and interaction-springs for the pile groups. In general, there are 3

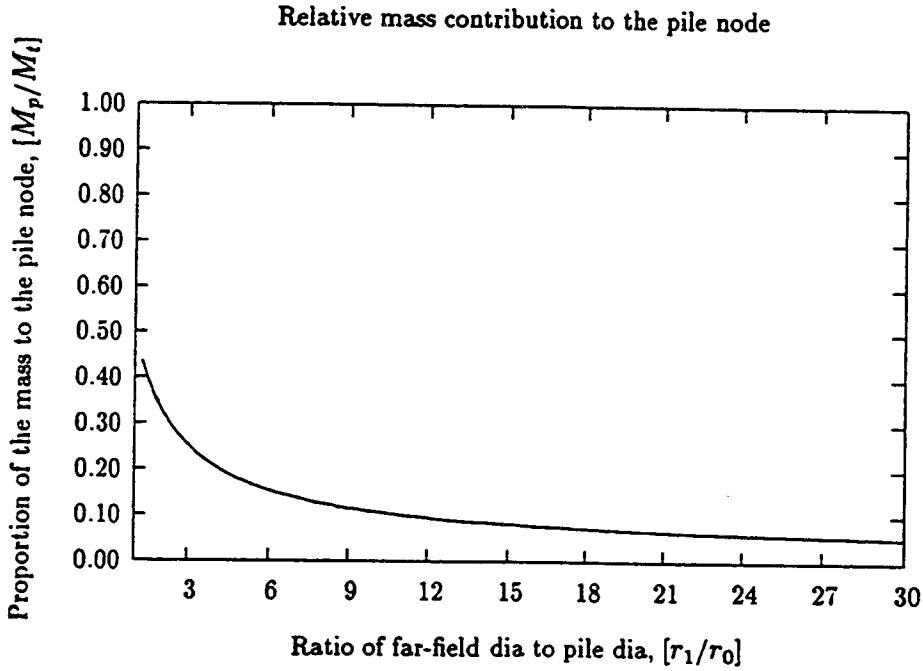

Figure 2.12 Lumped mass contribution to the pile for pile segment vibrating in-plane in soil media

near-field nonlinear springs required for each pile node, 3 nonlinear interaction-springs required for each pile-soil-pile connection, and three sets of far-field elements required for each external pile for modeling of 3D vibration of a general pile group.

For the sake of modeling, it is expected that three interaction-springs (i.e., direct-lateral, shear-lateral, and axial springs) between two isolated piles for general vibration will be required to represent the interaction between neighboring piles. So, in a large group, each pile will be connected with neighboring piles by direct-lateral, shear-lateral, and axial interaction-springs. For even closely spaced pile groups, say with $2d$ clear spacing (i.e., $3d$ center spacing), the far neighbors will have a $5d$ clear spacing (i.e., $6d$ center spacing). For this spacing, interaction can be neglected. For this interaction model, it is assumed that the consideration of interaction between neighboring piles only is sufficient for engineering accuracy. For the interaction of more than two-pile groups, the interaction-spring behavior may be obtained from that of two piles. The Winkler hypothesis was once again the basis of this approximate model for the pile-soil-pile interaction for axial and lateral vibration for earthquake loading.

2.3.1 Characteristics of Springs in Two-Pile Groups

There are three basic types of springs in pile group models. These include *nonlinear near-field springs*, *nonlinear interacting springs*, and *linear far-field springs*. Nonlinear near-field springs are required for those connecting piles with surrounding soil, and nonlinear interacting-springs are required for those connecting the piles themselves.

The non-linear spring elements for the modeling of a two-pile group with near-field and interaction-springs are shown in Figure 2.13 for uniaxial lateral vibration and in Figure 2.14 for biaxial lateral vibration. From Figure 2.13, it is observed that one load case is necessary to determine the force displacement behavior for the three near-field springs required for direct-lateral vibration. The load case, in which one segment is moved and the other is kept fixed, is required to get the interaction-spring, K2, and the near-field spring, K1, characteristics. Then, it may be considered that the behavior of K3 and K1 are same both in compression and tension.

For the two-pile groups with vibration in both direct-lateral and shear-lateral directions, two types of additional springs are required. One is an interaction shear-spring and the other is a near-field spring for connecting pile-segments with the surrounding soil.

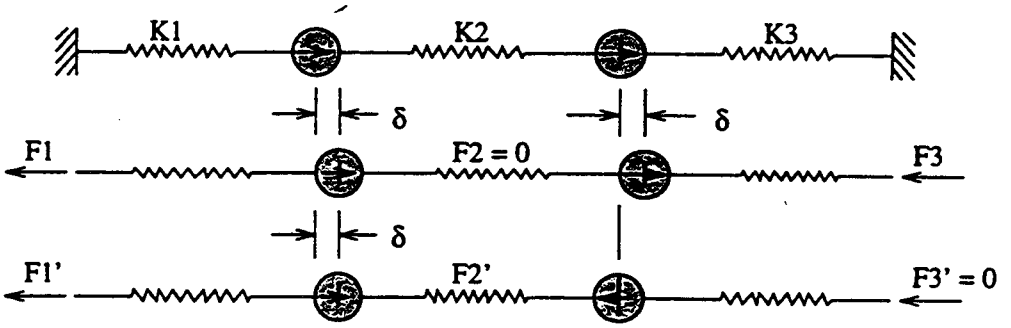

Figure 2.13 Model for direct-lateral vibration of a two-pile group moving laterally along the line which passes through the piles

Moreover, one additional load case is required to establish the behavior of the springs K4 and K6, as shown in Figure 2.14.

As expected, the behavior of spring K1 in tension is the same as that of K3 in compression. However, they should have different yield forces in tension and compression. On the other hand, springs K2, K4, K5, and K6 are expected to behave in the same manner in both tension and compression. Also, spring K6 should behave similarly in positive and negative shear. Moreover, as the spacing between two piles, s, increases, the stiffness of the interaction-springs, K2 and K6, are expected to diminish, and K1, K3, K4, and K5 should tend to those for a single pile. Then, K1, K3 and K4 should have the same yield strengths.

2.3.1.1 Direct-Lateral Vibration

The characteristics of the interaction-springs for different confining pressures and for drained conditions are determined for soil taken from the Snohomish river site. For the determination of the direct interaction-spring constants for lateral vibration, plane-strain conditions were assumed for all depths represented by 6.9, 17.3, 34.5, 68.9, 137.8, 275.6, 551.2, and 1102.4 kPa (1, 2.5, 5, 10, 20, 40, 80, and 160 psi) vertical stresses. Plane-stress was assumed for confining pressures 6.9 and 34.5 kPa (1 and 5 psi). Due attention was given to the initial K_0-stress condition and constitutive modeling of elastic and elasto-plastic soil. The displacement at a distance of 20d from the pile was assumed to be zero, and a zone of radius $4d$ was assumed to be the zone of nonlinearity. Within the nonlinear zone, soil was modeled using the geologic cap model, while, beyond the nonlinear zone,

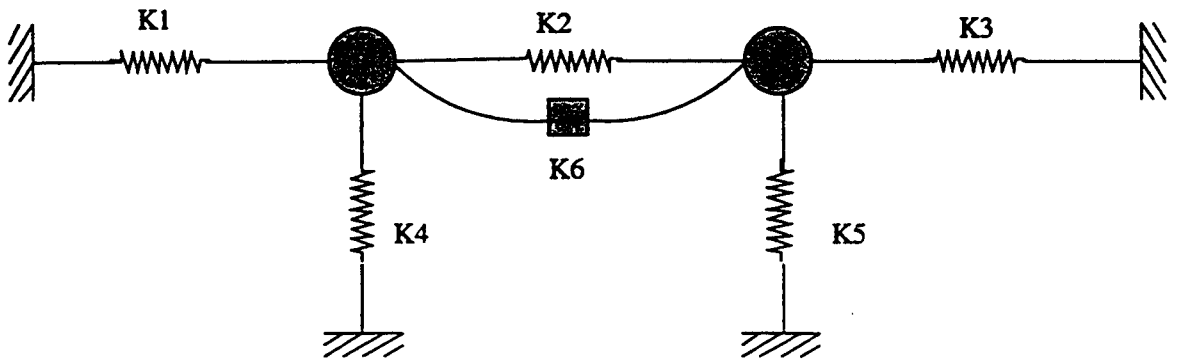

(A)

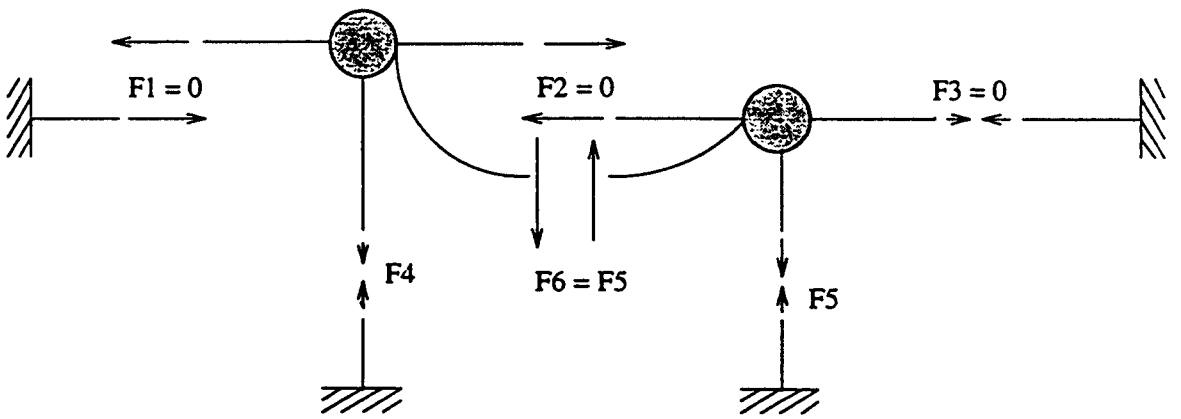

(B)

Figure 2.14 A more general model for vibration of a two-pile group for direct-lateral and shear-lateral vibration.

it was modeled using the elastic model. At the boundary of these zones, the observed strains were small, implying that the elastic constitutive model of soil is applicable in the far field. Moreover, the pile-soil interface was modeled with sliding interface elements with a coefficient of friction, $f = 0.4$. The finite element model is shown in Figure 2.15. The condition of symmetry was used to save computer time.

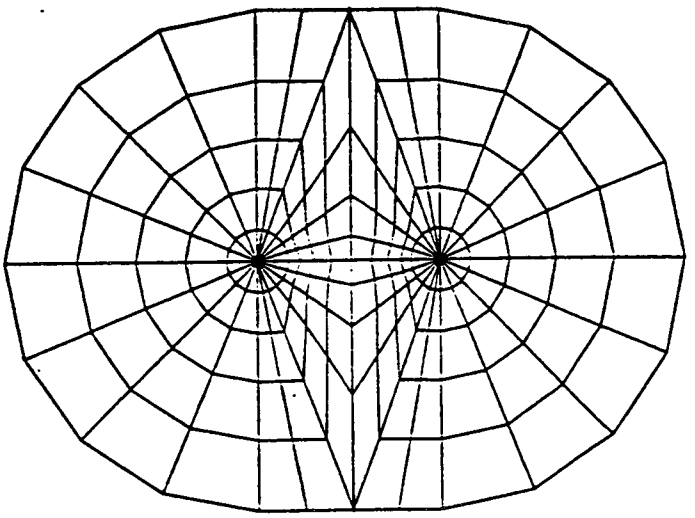

Figure 2.15 Finite element mesh used for the analysis of 2D pile-soil-pile layer.

A pseudo-static load was applied on one rigid segment of the pile either toward the other pile or in the reverse direction, varying sinusoidally with a very low frequency and low rate of loading, keeping the other pile fixed. The resulting displacement in the first pile, and active or reactive force on both piles, were observed and analyzed to establish the p-y behavior of the two-pile group. The resulting p-y behavior of the interaction-springs and the near-field springs are presented in Figures E.7 through E.22 for soil from the Snohomish river site. The NEABS parameters for those spring were computed, and they are presented in Tables 2.7 through 2.9. The values of K_1, K_2, K_4, F_Y, γ, and β given in these tables refer to Figure 2.7. The value of σ'_{v0} refers to initial effective confining pressure in the layer. The spacing, s, is expressed in terms diameters, d.

From the tables, one may observe that the stiffness of the interaction and near-field springs increases with confining pressure. The stiffness of the interaction-springs decreases with increasing spacing. The stiffness of the near-field springs increases with

increasing spacing. The stiffness of the near-field springs is almost of the same magnitude as that for isolated solitary piles. Although the stiffness does not depend on the pile diameter, the yield force does. The yield force of the near-field springs is less than, but of similar magnitude to, that of a single pile. The reason is that a single pile gets better inelastic redistribution. The yield force of the near-field springs is higher than that of the interaction-springs. All of the springs displayed hardening, and the gap effect was shown to be very significant.

Logically, one would assume that, when the stiffness value of the interaction spring becomes small in comparison with that of the near-field spring, group effects diminish, which occurred at a spacing of between 2d and 4d.

Table 2.7 NEABS parameters for p-y curves for near-field springs for two-pile groups vibrating laterally for different confining pressures. [$d = 0.457m$, $K_0' = 0.50$, $f = 0.40$, isotropic hardening, drained condition]

s	σ'_{v0} psi	K_1 lbs/in^2	K_2 lbs/in^2	F_y lbs/in	K_4 lbs/in^2	β	γ
Plane-strain condition							
2d	2.5	267.	72.	116.	19.	0.26	1.21
2d	5	582.	101.	147.	25.	0.68	1.31
2d	10	1344.					
2d	20	1609.	781.	64.	141.	0.74	1.04
2d	40	1924.					
2d	80	2647.					
2d	160	3755.					
4d	1	115.	42.	69.	5.	0.63	1.19
4d	2.5	288.	47.	116.	12.	0.40	1.03
4d	5	570.	36.	200.	33.	0.88	1.39
4d	10	1120.	162.	214.	54.	0.74	1.09
4d	20	1357.	271.	406.	46.	0.57	1.01
4d	40	1752.	418.	936.	77.	0.70	1.04
4d	80	2468.	675.	2053.	200.	0.71	1.00
4d	160	3505.	1363.	3830.	389.	0.79	0.87
8d	1	165.					
8d	2.5	304.	59.	154.	6.	0.15	1.05
8d	5	609.	88.	220.	9.	0.36	1.04
8d	10	1451.	184.	285.	66.	0.53	1.12
8d	20	1709.	264.	423.	55.	0.77	1.15
8d	40	1835.	518.	1102.	103.	0.61	0.95
8d	80	2727.	814.	2785.	254.	0.14	1.01
8d	160	3864.	1434.	5073.	546.	0.67	0.83
Plane-stress condition							
4d	1	126.					
4d	5	660.					
8d	1	145.					
8d	5	725.					

Table 2.8 NEABS parameters for p-y curves for near-field springs for two-pile groups vibrating laterally for different confining pressures. [$d = 0.610m$, $K_0' = 0.50$, $f = 0.40$, isotropic hardening, drained condition]

s	σ'_{v0} psi	K_1 lbs/in^2	K_2 lbs/in^2	F_y lbs/in	K_4 lbs/in^2	β	γ
Plane-strain condition							
2d	1	116.	76.	66.	9.	0.39	1.16
2d	2.5	305.	29.	159.	22.	0.49	1.20
2d	5	646.	143.	124.	37.	0.38	1.67
2d	10	1218.	122.	262.	64.	0.74	1.23
2d	20	1751.	271.	562.	62.	0.49	1.14
2d	40	2179.	578.	774.	106.	0.66	1.11
2d	80	2654.	873.	1279.	212.	0.95	1.08
2d	160	3859.	1479.	2889.	501.	1.02	1.04
4d	1	127.					
4d	2.5	281.	52.	157.	6.	0.22	1.05
4d	5	561.	78.	221.	8.	0.48	1.04
4d	10	1179.	39.	330.	76.	1.18	1.13
4d	20	1633.	238.	623.	53.	0.44	1.07
4d	40	1944.	442.	1016.	103.	0.82	1.09
4d	80	2608.	943.	2219.	219.	0.42	0.97
4d	160	3886.	1299.	5521.	421.	0.56	0.93
8d	1	125.	57.	182.	4.	0.12	1.15
8d	2.5	304.	63.	197.	7.	0.12	1.07
8d	5	607.	92.	351.	34.	0.15	1.09
8d	10	1361.	23.	426.	107.	0.16	1.06
8d	20	1684.	249.	812.	64.	0.19	0.98
8d	40	2021.	507.	1188.	121.	0.90	1.09
8d	80	2789.	1213.	2216.	319.	0.43	0.95
8d	160	3899.	1532.	7669.	610.	0.50	0.96
Plane-stress condition							
2d	1	110.	79.	26.	18.	0.87	1.08
4d	1	124.	128.	9.	10.	0.27	1.15
4d	5	579.	157.	197.	24.	0.24	1.06
8d	1	142.					
8d	5	627.	159.	277.	34.	0.39	1.06

Table 2.9 NEABS parameters for p-y curves for interaction-spring between two-pile groups vibrating laterally for different confining pressures. [$d = 0.457m$, $K_0' = 0.50$, $f = 0.40$, isotropic hardening, drained condition]

s	σ'_{v0} psi	K_1 lbs/in^2	K_2 lbs/in^2	F_y lbs/in	K_4 lbs/in^2	β	γ
Plane-strain condition							
2d	2.5	206.	7.	89.	14.	47.84	1.14
2d	5	490.	42.	157.	22.		0.99
2d	10	2277.					
2d	20	2190.	132.	509.	141.	0.26	0.69
2d	40	3246.					
2d	80	5031.					
2d	160	8021.					
4d	1	95.	24.	64.	9.	0.08	0.63
4d	2.5	225.	23.	114.	3.	0.19	0.97
4d	5	414.	79.	173.	16.	0.14	1.04
4d	10	1040.	79.	266.	46.	0.06	0.92
4d	20	1073.	39.	682.	27.		0.96
4d	40	1516.	149.	1319.	59.		0.90
4d	80	2172.	361.	2504.	150.		0.77
4d	160	3188.	573.	5223.	332.		0.61
8d	1	110.					
8d	2.5	156.	22.	80.	3.	0.46	0.90
8d	5	324.	33.	123.	5.	0.51	0.90
8d	10	717.	39.	224.	48.		0.96
8d	20	812.	72.	582.	26.		1.02
8d	40	1122.	112.	1050.	58.		0.99
8d	80	1483.	333.	1732.	144.	0.39	0.86
8d	160	2094.	609.	3785.	302.		0.73
Plane-stress condition							
4d	1	119.					
4d	5	732.					
8d	1	76.					
8d	5	459.					

Table 2.10 NEABS parameters for p-y curves for interaction-spring between two-pile groups vibrating laterally for different confining pressures. [$d = 0.610m$, $K_0' = 0.50$, $f = 0.40$, isotropic hardening, drained condition]

s	σ'_{v0} psi	K_1 lbs/in^2	K_2 lbs/in^2	F_y lbs/in	K_4 lbs/in^2	β	γ
Plane-strain condition							
2d	1	117.	35.	72.	9.		0.78
2d	2.5	305.	29.	159.	22.	0.50	1.01
2d	5	849.	95.	214.	83.	0.57	0.78
2d	10	1331.	90.	375.	47.		0.94
2d	20	1636.	79.	689.	48.	0.87	1.00
2d	40	2375.	120.	1683.	83.	0.36	0.96
2d	80	3433.	360.	3766.	179.		0.87
2d	160	5041.	697.	8133.	427.		0.77
4d	1	103.	66.	59.	45.	0.19	1.08
4d	2.5	231.	28.	141.	5.	0.32	0.88
4d	5	483.	36.	225.	6.	0.40	0.92
4d	10	1079.	169.	326.	45.	0.23	0.95
4d	20	1092.	64.	835.	51.	0.37	0.98
4d	40	1575.	153.	1782.	84.		0.87
4d	80	2241.	205.	3481.	164.		0.81
4d	160	3238.	612.	6813.	340.		0.66
8d	1	62.	14.	74.	2.		1.08
8d	2.5	160.	26.	96.	4.	0.57	0.89
8d	5	348.	35.	77.	30.	1.28	1.10
8d	10	744.	158.	275.	24.		0.99
8d	20	851.	75.	655.	49.	0.56	1.10
8d	40	1068.	136.	1488.	90.		1.00
8d	80	1439.	61.	2856.	139.		0.92
8d	160	2103.	558.	4785.	339.	0.34	0.73
Plane-stress condition							
2d	1	112.	47.	57.	12.	0.52	0.64
4d	1	101.	55.	45.	34.	0.75	1.02
4d	5	532.	90.	171.	22.	0.62	0.65
8d	1	68.	22.	47.	18.	0.94	1.11
8d	5	352.	55.	135.	20.	0.88	0.63

2.3.1.2 Shear-Lateral Vibration

For the computation of shear-lateral interaction spring behavior, the two piles with soil were modeled within the finite element framework. The same mesh, as shown in Figure 2.15, is used without the symmetry. The piles were considered to be rigid while the soil was considered to be elasto-plastic near the pile and elastic away from the pile. Due consideration was given for the initial K_0-stress condition and sliding interfaces. From this thin layer finite element model, the interaction behavior was obtained using the same procedure as that used for that of direct interaction springs. The resulting p-y behavior of the interaction-springs and the near-field springs is presented in Figures E.23 through E.38 for soil from the Snohomish river site. The NEABS parameters for those spring were computed, and they are presented in Tables 2.11 through 2.14. The values of K_1, K_2, K_4, F_Y, γ, and β given in these tables refer to Figure 2.7. The value of σ'_{v0} refers to initial effective confining pressure in the layer. The spacing, s, is expressed in terms diameters, d.

From the tables, it is observed that the stiffness of the interaction and near-field springs increases with confining pressure. The stiffness of the interaction-springs decreases with increasing spacing. The stiffness of the near-field springs increases with increasing spacing. The stiffness of the near-field springs is almost of the same magnitude as that for isolated solitary piles. Although the stiffness does not depend on the pile diameter, the yield force does. The stiffness of the interaction-spring for shear-lateral vibration is much less than that for direct-lateral vibration. This essentially means that the direct-lateral interaction is much more prominent than shear-lateral interaction. The yield force of the near-field springs is less than, but of similar magnitude to, that of a single pile. The reason is that a single pile gets better inelastic redistribution. The yield force of the near-field springs is higher than that of the interaction-springs. All of the springs displayed hardening property, and the gap effect was shown to be very significant.

Table 2.11 NEABS parameters for p-y curves for near-field spring between two-pile groups vibrating laterally in shear-direction for different confining pressures. [$d = 0.457m$, $K_0' = 0.50$, $f = 0.40$, isotropic hardening, drained condition]

s	σ'_{v0} psi	K_1 lbs/in^2	K_2 lbs/in^2	F_y lbs/in	K_4 lbs/in^2	β	γ
Plane-strain condition							
2d	1	112.	40.	73.	6.	0.36	1.10
2d	2.5	264.	54.	126.	6.	0.28	1.06
2d	5	536.	91.	182.	6.	0.33	1.03
2d	10	999.	151.	291.	27.	0.39	1.14
2d	20	1425.	298.	470.	40.	0.33	1.01
2d	40	1892.	584.	903.	87.	0.38	1.05
2d	80	2604.	1038.	1971.	228.	0.27	1.06
2d	160	3490.	1814.	4632.	584.	0.17	1.01
4d	1	119.	40.	83.	5.	0.27	1.08
4d	2.5	277.	51.	134.	5.	0.23	1.05
4d	5	557.	86.	195.	6.	0.29	1.03
4d	10	1052.	145.	305.	27.	0.41	1.15
4d	20	1582.	305.	501.	41.	0.35	1.08
4d	40	1935.	593.	1022.	101.	0.36	1.04
4d	80	2602.	1026.	2369.	237.	0.19	1.02
4d	160	3724.	1799.	5226.	509.	0.10	0.93
8d	1	128.	40.	109.	5.	0.09	1.08
8d	2.5	297.	53.	159.	5.	0.15	1.04
8d	5	597.	92.	229.	6.	0.25	1.02
8d	10	1147.	151.	354.	33.	0.36	1.16
8d	20	1618.	336.	593.	54.	0.32	1.03
8d	40	2094.	677.	1194.	127.	0.35	1.00
8d	80	2876.	1142.	2803.	307.	0.13	0.98
8d	160	4023.	1961.	6309.	741.	-0.06	0.97
Plane-stress condition							
2d	1	138.	103.	7.	109.	0.23	3.60
2d	5	635.	451.	12.	377.	0.93	4.63
4d	1	125.					
4d	5	525.					
8d	1	122.					
8d	5	579.	126.	165.	18.	0.45	0.97

Table 2.12 NEABS parameters for p-y curves for near-field springs for two-pile groups vibrating laterally in shear-direction for different confining pressures. [$d = 0.610m$, $K_0' = 0.50$, $f = 0.40$, isotropic hardening, drained condition]

s	σ_{v0}' psi	K_1 lbs/in^2	K_2 lbs/in^2	F_y lbs/in	K_4 lbs/in^2	β	γ
Plane-strain condition							
2d	1	111.	40.	104.	6.	0.24	1.06
2d	2.5	261.	53.	175.	5.	0.37	1.07
2d	5	539.	90.	236.	8.	0.32	1.03
2d	10	1067.	92.	319.	78.	0.50	1.11
2d	20	1555.	225.	765.	77.	0.13	1.10
2d	40	1808.	430.	1234.	128.	0.70	1.13
2d	80	2500.	924.	2541.	270.	0.50	1.11
2d	160	3550.	1561.	6187.	677.	0.42	1.03
4d	1	120.	24.	121.	6.	0.70	1.07
4d	2.5	272.	44.	188.	5.	0.46	1.07
4d	5	562.	72.	254.	5.	0.69	1.07
4d	10	869.	77.	468.	28.	0.72	1.17
4d	20	1566.	303.	730.	50.		1.03
4d	40	2062.	545.	1328.	103.	0.49	1.09
4d	80	2587.	881.	2784.	820.	0.79	0.38
4d	160	4102.	1632.	5136.	489.	0.67	0.93
8d	1	127.	41.	147.	8.		1.13
8d	2.5	291.	49.	222.	5.	0.24	1.06
8d	5	621.	102.	296.	14.	0.40	1.08
8d	10	985.	137.	543.	57.	0.13	1.20
8d	20	1638.	302.	870.	58.	0.03	0.97
8d	40	2149.	685.	1619.	143.	0.24	1.08
8d	80	2809.	1363.	3016.	295.	0.29	0.91
8d	160	4239.	2256.	7211.	760.	0.09	0.89
Plane-stress condition							
2d	1	111.					
2d	5	640.					
4d	1	112.	29.	115.	10.	0.55	0.98
4d	5	542.	107.	232.	27.	0.54	0.96
8d	1	107.	27.	135.	32.		1.00
8d	5	658.	132.	281.	25.	0.27	1.05

Table 2.13 NEABS parameters for p-y curves for interaction-spring between two-pile groups vibrating laterally in shear-direction for different confining pressures. [$d = 0.457m$, $K_0' = 0.50$, $f = 0.40$, isotropic hardening assumed, drained condition]

s	σ'_{v0} psi	K_1 lbs/in^2	K_2 lbs/in^2	F_y lbs/in	K_4 lbs/in^2	β	γ
Plane-strain condition							
2d	1	88.	21.	48.	4.	0.63	1.00
2d	2.5	207.	20.	102.	4.	0.49	0.98
2d	5	426.	31.	163.	4.	0.39	0.97
2d	10	903.	57.	267.	27.	0.61	1.06
2d	20	1169.	121.	536.	52.	0.28	0.86
2d	40	1578.	194.	1064.	84.	0.22	0.90
2d	80	2261.	334.	1961.	186.	0.33	0.82
2d	160	2977.	559.	3807.	495.	0.40	0.69
4d	1	85.	20.	65.	4.	0.37	1.01
4d	2.5	206.	22.	109.	4.	0.28	1.00
4d	5	429.	34.	164.	5.	0.37	0.99
4d	10	827.	65.	257.	25.	0.56	1.11
4d	20	1055.	140.	510.	42.	0.22	0.98
4d	40	1330.	211.	991.	102.	0.14	1.00
4d	80	1836.	391.	1747.	163.	0.33	0.91
4d	160	2455.	682.	3345.	401.	0.31	0.83
8d	1	64.	15.	57.	3.	0.32	1.01
8d	2.5	163.	22.	85.	4.	0.29	1.01
8d	5	341.	35.	131.	4.	0.40	0.99
8d	10	639.	64.	214.	25.	0.54	1.13
8d	20	779.	132.	444.	33.	0.02	1.01
8d	40	933.	161.	846.	107.		1.06
8d	80	1291.	343.	1384.	120.	0.31	0.94
8d	160	1728.	632.	2471.	360.	0.34	0.93
Plane-stress condition							
2d	1	201.					
2d	5	762.					
4d	1	110.					
4d	5	392.	48.	159.	12.	0.18	0.89
8d	1	63.	18.	55.	6.	0.16	0.80
8d	5	315.	55.	124.	18.	0.34	0.91

Table 2.14 NEABS parameters for p-y curves for interaction-springs for two-pile groups vibrating laterally in shear-direction for different confining pressures. [$d = 0.610m$, $K_0' = 0.50$, $f = 0.40$, isotropic hardening, drained condition]

s	σ'_{v0} psi	K_1 lbs/in^2	K_2 lbs/in^2	F_y lbs/in	K_4 lbs/in^2	β	γ
Plane-strain condition							
2d	1	90.	18.	85.	5.	0.41	0.99
2d	2.5	209.	17.	164.	4.	0.37	1.00
2d	5	479.	32.	230.	7.	0.39	0.97
2d	10	1190.	164.	310.	61.	0.41	0.93
2d	20	1304.	66.	722.	60.	0.85	1.01
2d	40	1602.	160.	1535.	119.		0.92
2d	80	2051.	206.	2894.	219.	0.30	0.84
2d	160	2855.	413.	5269.	487.	0.67	0.69
4d	1	88.	21.	85.	4.	0.31	1.02
4d	2.5	194.	19.	154.	3.	0.31	1.01
4d	5	411.	37.	232.	8.	0.44	0.88
4d	10	874.	99.	297.	14.	0.55	1.14
4d	20	1165.	177.	595.	56.	0.49	1.05
4d	40	1342.	252.	1171.	94.	0.39	0.95
4d	80	2054.	681.	2882.	728.	0.33	0.76
4d	160	2502.	747.	4436.	368.	0.25	0.79
8d	1	68.	16.	72.	4.	0.30	1.03
8d	2.5	155.	20.	120.	3.	0.35	1.03
8d	5	325.	35.	192.	8.	0.43	1.06
8d	10	742.	115.	217.	5.	0.54	1.15
8d	20	838.	169.	503.	57.	0.46	1.10
8d	40	992.	244.	1061.	85.	0.16	0.87
8d	80	1354.	303.	2025.	111.		0.99
8d	160	1727.	640.	3468.	240.	0.16	0.81
Plane-stress condition							
2d	1	154.					
2d	5	995.					
4d	1	81.	13.	88.	8.	0.50	0.84
4d	5	405.	36.	207.	23.	0.64	0.88
8d	1	59.	45.	87.	8.		1.20
8d	5	336.	57.	155.	16.	0.49	0.95

2.3.1.3 Axial Vibration

Pile groups for axial vibration are modeled in the same way that they were modeled for lateral vibration. The only difference is that all piles are connected to the surrounding soil by near-field shear springs, and the piles are connected to themselves by interaction shear-springs. These interaction springs resist relative vertical displacements and they are expected to behave in the same way for both directions of loading. The near-field elements, such as near-field mass and dampers, and far-field elements connecting the pile to soil, are still applied. For the determination of the spring characteristics, it is further assumed that no point in the soil should move laterally during axial vibration of piles in pile groups.

For the determination of axial interaction and near-field springs, two piles were modeled once again within the finite element framework. The same mesh, as shown in Figure 2.15, was used with an axis of symmetry. No sliding interface was assumed to exist to avoid instability and the condition of symmetry was utilized. No lateral displacement boundary condition was used. Vertical displacement of soil at a distance of $20d$ from the pile or further apart was neglected by using an artificial, no-displacement boundary. Vertical stresses were maintained to simulate confining effects. Perturbation was given only in one pile, and the resulting displacement of the pile and the reactive forces in both pile segments were observed and analyzed to obtain the interaction characteristics. t-z curves are computed for the effective vertical stresses of 6.9, 17.3, 34.5, 68.9, 137.8, 275.6, 551.2, and 1102.4 kPa (1, 2.5, 5, 10, 20, 40, 80, and 160 psi) for drained behavior of the soil, and for center spacing of $2d$, $4d$, and $8d$. The resulting t-z behavior of the interaction-springs and the near-field springs are presented in Figures E.39 through E.50 for soil from the Snohomish river site. The NEABS parameters for those springs were computed, and they are presented in Tables 2.15 through 2.18. The values of K_1, K_2, F_Y, and β given in these tables refer to Figure 2.7. The value of σ'_{v0} refers to initial effective confining pressure in the layer. The spacing, s, is expressed in terms diameters, d.

From the tables, it is observed that the stiffness of the interaction and the near-field springs increases with confining pressure. The stiffness of the interaction-springs decreases with increasing spacing. The stiffness of the near-field springs increases with increasing spacing. The stiffness of the near-field springs is almost of the same magnitude

as those for isolated solitary piles. Although the stiffness does not depend of the pile diameter, the yield force does. The yield force of the near-field springs is less than, but of similar magnitude to, the yield force for a single pile. The reason is that a single pile gets better inelastic redistribution. The yield force of the near-field springs is higher for higher spacing. The hardening of the springs with displacements is insignificant. During the analysis, it was assumed that the interface is perfect and no gap is formed. The results show that slippage occurs, causing a perfectly plastic t-z behavior.

Table 2.15 NEABS parameters for t-z curves for near-field springs for two-pile groups vibrating axially for different confining pressures. [$d = 0.457m$, $K_0' = 0.50$, isotropic hardening, drained condition]

s	σ'_{v0} psi	K_1 lbs/in^2	K_2 lbs/in^2	F_y lbs/in	β
2d	1	96.			
2d	2.5	243.			
2d	5	490.	119.	159.	
2d	10	975.	332.	208.	0.50
2d	20	1183.			
2d	40	1265.			
2d	80	1580.			
2d	160	2206.			
4d	1	98.			
4d	2.5	252.			
4d	5	512.	69.	173.	
4d	10	1023.	347.	236.	0.00
4d	20	1227.			
4d	40	1326.			
4d	80	1652.			
4d	160	2317.			
8d	1	105.			
8d	2.5	269.			
8d	5	549.	190.	208.	0.10
8d	10	1094.	447.	287.	0.10
8d	20	1312.			
8d	40	1418.			
8d	80	1766.			
8d	160	2480.			

Table 2.16 NEABS parameters for t-z curves for near-field springs for two-pile groups vibrating axially for different confining pressures. [$d = 0.610m$, $K_0' = 0.50$, isotropic hardening, drained condition]

s	σ'_{v0} psi	K_1 lbs/in^2	K_2 lbs/in^2	F_y lbs/in	β
2d	1	95.			
2d	2.5	240.			
2d	5	487.			
2d	10	976.			
2d	20	1169.			
2d	40	1265.			
2d	80	1584.			
2d	160	2222.			
4d	1	98.			
4d	2.5	252.			
4d	5	505.			
4d	10	1022.			
4d	20	1227.			
4d	40	1325.			
4d	80	1660.			
4d	160	2303.			
8d	1	104.			
8d	2.5	272.			
8d	5	538.			
8d	10	1095.			
8d	20	1309.			
8d	40	1418.			
8d	80	1773.			
8d	160	2482.			

Table 2.17 NEABS parameters for t-z curves for interaction-spring between two-pile groups vibrating axially for different confining pressures. [$d = 0.457m$, $K_0' = 0.50$, isotropic hardening, drained condition]

s	σ'_{v0} psi	K_1 lbs/in^2	K_2 lbs/in^2	F_y lbs/in	β
2d	1	212.	99.	103.	0.48
2d	2.5	538.	71.	160.	
2d	5	1059.	86.	241.	0.29
2d	10	2171.	313.	320.	0.33
2d	20	2607.	1074.	453.	0.35
2d	40	2845.	1231.	893.	0.43
2d	80	3543.	1475.	1760.	0.48
2d	160	5005.	2640.	1003.	0.06
4d	1	148.			
4d	2.5	372.			
4d	5	754.	72.	221.	0.43
4d	10	1502.	309.	296.	0.54
4d	20	1804.			
4d	40	1949.			
4d	80	2424.			
4d	160	3415.			
8d	1	100.			
8d	2.5	250.			
8d	5	508.	170.	183.	0.48
8d	10	1013.	432.	250.	0.66
8d	20	1214.			
8d	40	1312.			
8d	80	1631.			
8d	160	2295.			

Table 2.18 NEABS parameters for t-z curves for interaction-spring between two-pile groups vibrating axially for different confining pressures. [$d = 0.610m$, $K_0' = 0.50$, isotropic hardening, drained condition]

s	σ'_{v0} psi	K_1 lbs/in^2	K_2 lbs/in^2	F_y lbs/in	β
2d	1	216.			
2d	2.5	542.			
2d	5	1101.	183.	283.	0.52
2d	10	2192.	737.	348.	0.31
2d	20	2633.	1272.	572.	0.34
2d	40	2846.	1511.	1132.	0.36
2d	80	3557.	1841.	2273.	0.41
2d	160	5037.	1243.	1640.	0.23
4d	1	148.			
4d	2.5	372.			
4d	5	762.			
4d	10	1505.	850.	331.	0.36
4d	20	1804.			
4d	40	1949.			
4d	80	2439.			
4d	160	3436.	1055.	1588.	0.59
8d	1	101.			
8d	2.5	250.			
8d	5	520.			
8d	10	1014.			
8d	20	1212.			
8d	40	1311.			
8d	80	1640.			
8d	160	2296.			

2.3.2 Modeling of Near-Field Dampers

The damping constants for the near-field elements were based on Rayleigh's proportional damping for the dominant loading frequency. This loading frequency comes from the earthquake loading. This loading frequency can be obtained by counting the number of maxima, minima, crossings, or from the Fourier analysis of the acceleration history. The initial or unloading spring stiffness is the basis of the damping coefficient.

$$C = 2\xi K/\omega \qquad [2.23]$$

2.3.3 Modeling of Near-Field Masses

The nodes corresponding to pile segments can have a mass from the pile itself and a contribution from the soil. The concept of tributary area may be used for the determination of lumped masses. The contribution from the soil to an interior pile segment may be considered to come from the hatched region, as shown in Figure 2.16. Then for the piles at the center,

$$m_p = \rho_\rho \pi r_0^2 + \rho_s(S_1S_2 - \pi r_0^2) \qquad [2.24]$$

For piles on the sides and in the corners of the group, the mass contribution of the soil also comes from a large distance. This contribution to the mass can be estimated by considering tributary area and an approximate shape function. The consistent mass matrices can then be developed. The HRZ lumping scheme may be followed to get a diagonal mass matrix, which is then used to identify the contribution of soil to the lumped nodal masses. According to this procedure, the mass contribution from soil, and the total masses in side and corner piles, may be defined. For piles on the side,

$$m_p = (\pi r_0^2 \rho_s)\left\{\frac{2LS_1}{\pi r_0^2}\frac{n^2}{(2n^2+n+1)}\frac{S_1S_2}{2\pi r_0^2}+\left(\frac{\rho_\rho}{\rho_s}-1\right)\right\}. \qquad [2.25]$$

For piles in the corner,

$$m_p = (m_{p,single} + S_1S_2\rho_s)/4 + 2\ (\text{soil contribution from sides}) + \pi r_0^2 \rho_p\left(1-\frac{\rho_s}{4\rho_\rho}\right). \qquad [2.26]$$

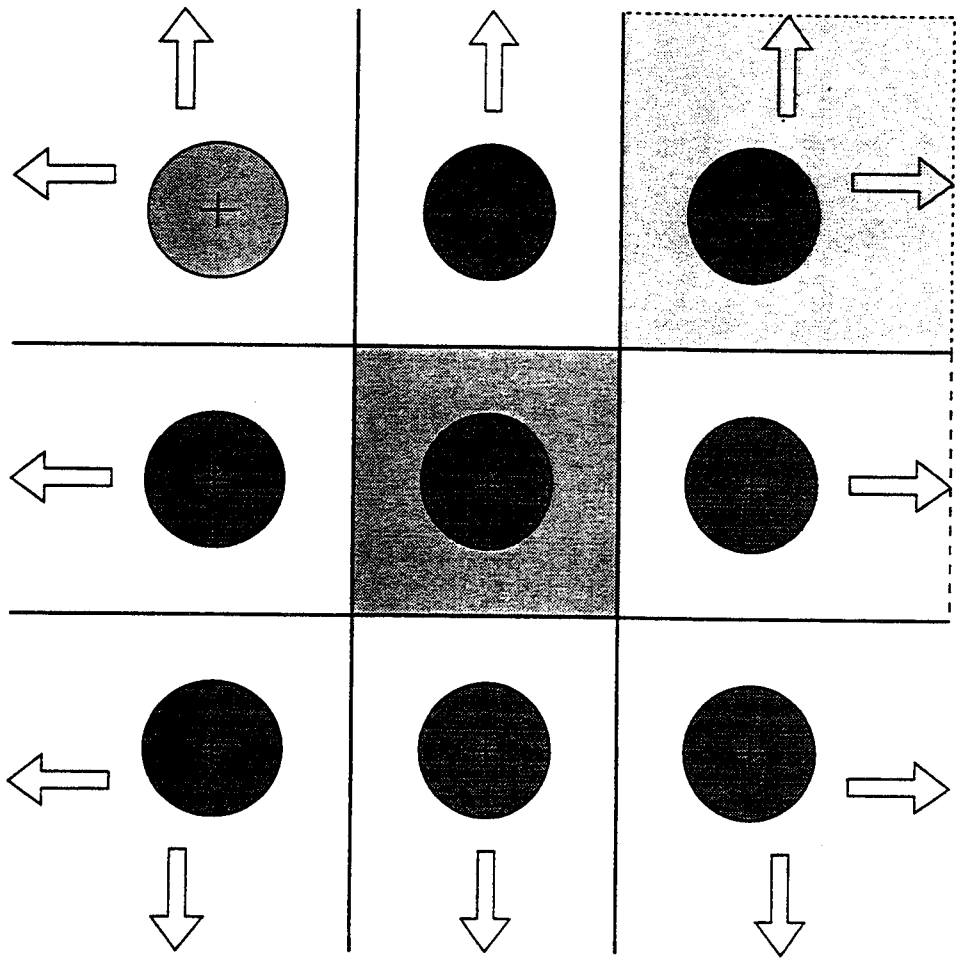

Figure 2.16 Concept of tributory area employed to find approximate mass contributions from soil to the piles in a pile group

2.3.4 Estimation of the Far-Field Elements

In the estimation of the far-field elements, it may be assumed that the waves produced by the inner piles of the group are reflected by the piles around them. Thus, the radiation energy dissipated from the inner piles comes back into the system. On the other hand, it may be assumed that the waves generated by the surrounding piles either at the sides or at the corners of the group do not come back.

Therefore, modeling of the far-field for a pile group can be done by connecting far-field elements to the surrounding piles with the near-field elements through the auxiliary nodes. Furthermore, for the sake of modeling, it may be assumed that piles in the group do not interact with each other at the far-field. So, the far-field elements connecting a pile in a pile group may be assumed to be those for a single pile. Alternatively, the far-field spring stiffnesses, damping coefficients, and the lumped masses for a single pile which is equivalent to the pile group can be distributed along the external pile using a reasonable ad hoc procedure. In this case, a reasonable equivalent radius of the pile group would be required.

2.4 Pile Cap Behavior

In almost no cases are solitary piles used. Piles come in groups and they are usually connected at the top with sufficiently rigid caps. If the cap is above the ground and it is not connected to the soil, it will not contribute to the lateral resistance. On the other hand, if it is connected to the soil and embedded in it, it will produce lateral resistance. It can produce lateral resistance in two ways: bearing and shearing along the vertical surface, and shearing along the bottom surface.

At the surface, the confining pressure is small. The soil is normally soft (that is why piles are necessary) and the vertical surfaces will contribute little to the pile-group resistance compared to that of the piles. For the modeling of this resistance, p-y curves were developed for circular and rectangular pile caps of different dimensions in the same way as done for single piles, and they are useful for lateral vibration analysis. During the analysis, rigid behavior of the cap, elasto-plastic and elastic behavior of the soil in the near- and far-zones respectively, sliding interfaces, and plane-stress conditions were considered. Displacement of the soil at a distance of $20d$ or $20a$ (d, a = Dimensions of

the circular and square caps, respectively) was considered to be negligible by providing an artificial, no displacement boundary. The resulting p-y curve was generated for four different sizes of square and four different sizes of circular pile-caps for the soil of the Snohomish river site. The resulting p-y behavior of the near-field springs are presented in Figures E.51 through E.52. The NEABS parameters for those springs were computed, and they are presented in Table 2.19.

Because soil layers were considered to be independent within the framework of the Winkler hypothesis, the shearing resistance at the bottom of the pile cap should be zero, because both layers of soil above and below the cap bottom will move the same amount during lateral vibration. The cap and pile segment will produce bearing resistance, and the bottom surface of the cap should move automatically without any resistance. However, the deformed shape of the soil layer for the movement of pile-groups will differ from that required for the movement of the cap bottom. This difference will produce some resistance. Only a relatively small effective part of the cap bottom will produce this lateral resistance. This effective area should be less than the cap bottom area less the sum of the pile cross-sectional areas. The approximate stiffness of this p-y curve may be determined from elastic solutions available in the literature. The ultimate value of p. i.e. P_{ult}, will depend on the actual vertical load carried by the cap itself and the coefficient of friction.

During bridge vibration, the rocking component will produce a nonuniform distribution of bearing stress. This spatial and temporal variation of bearing stress makes it too cumbersome to develop a realistic p-y curve for the cap bottom. Moreover, for soft soil conditions, when the pile tip takes a higher contribution than the skin friction, vibration may cause the soil to be compacted and a gap may be produced between the pile-cap bottom and the soil. Then, the contribution of the shearing of the cap bottom will be negligibly small. On the other hand, a finite element analysis of the shear resistance produced by the cap bottom in shear would require a complete 3D analysis of different dimensions and shapes of the pile cap, the soil conditions, and confining pressures. An extensive use of computer time would not produce an appreciable result. That is why it is left to the judgment of the designer.

For the vertical movement of the pile cap, resistance comes from bearing at the cap bottom and the side shear resistance of the vertical surface of the cap. For resistance of

the cap bottom, only a part of the cap area is effective. This area should be the gross area of the cap bottom less the sum of the pile cross-sectional areas. Also the rocking component of the cap motion will interact with the model making the problem more complicated. The exact determination of the T_c-Z_c curve for the cap bottom would be cumbersome and it would not be cost-effective with respect to computer time. It is left up to the judgment of the designer.

The side shear resistance to vertical movement was also developed for both circular and rectangular caps in the same manner as for the single pile segment. No sliding interface was assumed to exist. Very little confining pressure was considered. No lateral movement of the soil was assumed. The resulting p-y behavior of the near-field springs are presented in Figures E.53 through E.54. The NEABS parameters for those spring were computed, and they are presented in Table 2.20.

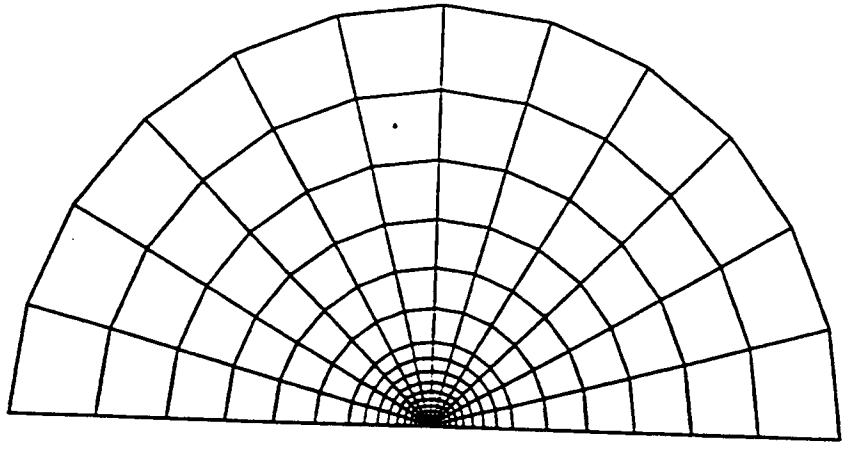

Figure 2.17 A FE model for square pile-cap

2.5 Pile Tip Response

The vertical force-displacement relation for axial response, T_t-Z_t, of the pile-tip is much more important for end-bearing piles than friction piles. Pile tip vertical response is also important for lateral response of pile groups. The lateral response for the pile

Table 2.19 NEABS parameters for P_c-Y_c curves for pile-caps vibrating laterally for different sizes and shapes. [$K_0' = 0.50$, $f = 0.40$, isotropic hardening, drained condition]

Size (shape), $in(S/C)$	**Initial stiffness, lbs/in^2**	**Post-yield stiffness, lbs/in^2**	**Initial yield force lbs/in**	**First Gap stiffness, lbs/in^2**	**Hardening parameter, β**	**Gap parameter, γ**
Circular in plan						
d=200	260.	80.	244.	146.	0.37	0.64
d=300	240.	101.	329.	140.	0.74	0.46
d=400	311.	74.	398.	161.	0.37	0.42
Square in plan						
a=50	227.	33.	273.	25.	-0.49	1.36
a=100	242.	45.	378.	32.	0.08	1.51
a=200	213.	28.	1209.	36.	-0.68	1.72
a=300	253.	22.	1915.	47.	-1.13	1.34

S = Square, C = Circular, a = Lengh, d = Diameter

Table 2.20 NEABS parameters for T_c-Z_c curves for pile-caps vibrating axially for different sizes and shapes. [$K_0' = 0.50$, isotropic hardening, drained condition]

Size (shape), $in(S/C)$	**Initial stiffness, lbs/in^2**	**Post-yield stiffness, lbs/in^2**	**Initial yield force lbs/in**	**Hardening parameter, β**
Circular in plan				
d=100	202.	161.	502.	-0.06
d=200	203.	161.	1004.	-0.06
d=300	253.	315.	2983.	0.96
d=400	219.	25.	2617.	2.59
Square in plan				
a=50	213.	171.	209.	0.96
a=100	253.	157.	296.	0.83
a=200	348.	767.	3241.	0.96
a=300	292.	208.	882.	-1.67

S = Square, C = Circular, a = Lengh, d = Diameter

tip, P_t-Y_t, is important for determining the lateral response of end-bearing piles and pile groups. For the determination of the lateral response of the pile tip, an actual 3D analysis is required. However, the result has little significance. The lateral force-displacement behavior for the perfectly elastic condition is available in the literature (Wolf 1988, pages 20–25) and will be adopted. It might be possible to use the bearing capacity as the strength of the vertical spring.

Alternatively, the use of the pile tip response may be avoided by considering soil column as part of the pile with soil material properties. The near-field and the far-field elements can be added to this extended soil column. Nogami and Konagai (1986, 1987) adopted this concept in their work.

The interaction between pile-tips might also be considered. However, the designer may adopt the elastic interaction factors. In that case, one should keep in mind that interaction effects reduce with increasing plasticity, and elastic interaction factors are the upper limits of those factors.

3. INTERPRETATION, APPRAISAL, AND APPLICATION

3.1 General

In this chapter, the results obtained by numerical and analytical techniques used in the previous chapter have been interpreted, assessed, and evaluated. An evaluation of the applicability of the proposed near- and far-field elements has been described in detail in this chapter. The limitations and the areas of application have also been discussed.

3.2 Calibration of the Model

The models developed and described in the previous chapter for single piles and pile groups with or without caps were mostly based on the following assumptions:

- The lateral reaction of a single pile or of a pile in a pile group depends only on the lateral displacement or relative lateral displacement of that pile or those piles at that particular level (Winkler hypothesis). This means that the distributed lateral neighboring springs do not interact with each other.

- The axial reaction of a single pile or of a pile in a pile-group depends only on the axial displacement or relative axial displacement of that pile or those piles at that particular level (Winkler hypothesis). This also means that the neighboring distributed axial springs do not interact each other.

- The near-field discrete masses can be obtained from tributary area and shape function concepts.

- The damping coefficients can be determined from proportional damping, initial spring stiffness, and the dominating frequency of loading or response.

- The loading frequency is as small as normally encountered in practice for loading arising from earthquake excitation.

The first two assumptions work well for most cases because the pile itself is a stiff and strong element which connects those reactive springs. The displacement at one point in a pile induces displacement at other points due to some rigid body movement within a small length of the pile. This rigidity of the pile forces the springs to interact.

The lumped masses are based on some physically conceivable assumptions. A small error in the computation of masses is not expected to produce a large error for low frequency loading, such as that from earthquake excitation. Some researchers (Penzien 1970) have obtained "accurate" results without considering the lumped mass contributed by soil. Therefore, the third assumption is a reasonable one.

The damping coefficient can not be obtained from finite element or other numerical techniques unless the viscosity parameters are known. The typical stiffness-proportional or Rayleigh damping procedure is usually adopted. The near-field damping ratio basically depends on the strain amplitude in the soil. An average strain amplitude must be obtained to get this damping ratio from the equations derived by Seed and Idris (1979) or Hardin & Drnevich (1972). The total uncertainty comes from the selection of the damping ratio, dominant frequency, and spring stiffness values. A reasonable value of loading frequency can be obtained from the earthquake loading by peak counting or crossing counting, or by using a Fourier analysis of the accelerogram record, although it is not a purely harmonic load. Although the above assumptions and approximations are based on realistic bases of physical attributes, they should be subjected to evaluation.

3.3 Evaluation of the Model for Lateral Response of a Single Pile

The model proposed in the previous chapter has been evaluated by simulating one full scale loading test. The response obtained from the full scale model simulation of pile-soil interaction with sliding interfaces for lateral loading are compared with those obtained from the proposed model for the same conditions. The details are described as follows.

A single pile of diameter 0.632m (d = 24") was modeled in two different ways, one using complete finite element discretization of the full pile-soil combination and the other using the proposed finite layer model. The other was modeled using discrete elements with lumped masses, non-linear springs, and linear dashpots. The models are presented in Figures 3.1 and 3.2. The length of the pile was 22.5d. In the finite element model,

the diameter and the length of the soil domain was $20d$ and $36d$, respectively. The soil non-linearity, slippage, gap formation, and initial geo-static stress were considered. The damping was assumed to come from geometric damping and hysteretic damping. The infinite soil domain was simulated using a finite soil domain with non-reflecting boundaries. The condition of symmetry was utilized. The pile was assumed to be linearly elastic.

The basic soil parameters were needed exactly for these specific vertical confining pressures. These are interpolated from Tables D.1 through D.2. The depth independent parameters are exactly same as those given in Table D.1. The depth dependent parameters are given in 3.1 The resulting cap parameters for those soils at different layers are presented in Table 3.2.

The other was modeled using discrete elements with lumped masses, non-linear springs, and linear dashpots. In the discrete model, the lumped masses, non-linear springs, and linear dashpots were used to model the same pile. For the nonlinear near-field springs, the p-y curves computed in Chapter 2 and presented in Table 2.2 were used. The p-y curves were scaled by the thickness of the layer to get the proper resistance. Similarly, the linear spring and damping constants are computed according to the Equation A.1 and A.2. The lumped masses are computed according to Section 2.2.1.3. The proportional damping was used for the near-field damper. The resulting parameters are given in Tables 3.3 through 3.6.

The vibration was simulated for harmonic forced transient response. The forcing function is a half-sine wave with an amplitude of 150 kips, as shown in Figure 3.3. The analysis was done to obtain the response for 2 seconds. The duration of loading was 1 second. Peak load was attained at time $t = 0.5$ second. The pile displacement shapes at different times obtained from both the full scale finite element model and from the discrete model are presented in Figures 3.4 through 3.6. The pile head displacement histories are plotted in Figures 3.7 and 3.8. The curvature values along the pile are also plotted in Figures 3.9 and 3.10.

It is observed that the results obtained from the FE model compare well with those obtained from the lumped model with high damping. Although no Rayleigh damping was assumed in the FE model, the result show high damping in the response. The reason might lie in the fact that the energy is dissipated at a high rate through the non-reflecting

Table 3.1 Depth dependent basic soil parameters used for FE analysis of lateral vibration of a single pile

h	OCR	Strength	
		$\sigma'_{v0,con}$	$\frac{S_u}{\sigma'_{v0,con}}$
ft		psi	
00.5	3.50	0.668	11.67
01.5	3.50	0.668	11.67
02.5	3.00	0.668	11.67
03.7	3.00	0.668	11.67
05.2	2.50	0.668	11.67
07.0	2.50	0.668	11.67
09.0	2.50	0.668	11.67
11.5	2.00	0.668	11.67
14.5	2.00	0.612	15.42
18.0	2.00	0.612	15.42
23.0	1.50	0.575	31.40
29.5	1.00	0.551	36.26
35.5	1.00	0.551	36.26
40.0	1.00	0.551	36.26
43.0	1.00	0.551	36.26
44.5	1.00	0.551	36.26
45.5	1.00	0.551	36.26
47.0	1.00	0.551	36.26
49.5	1.00	0.551	36.26
53.0	1.00	0.551	36.26
57.5	1.00	0.551	36.26
63.5	1.00	0.551	36.26
71.0	1.00	0.551	36.26

Table 3.2 The cap parameters obtained from the basic soil properties.

h ft	W	R	D	X_0 psi	E psi	ν	K psi	G psi
00.5	0.238	0.269	1.377	-0.717	85.181	0.100	35.492	38.719
01.5	0.238	0.269	0.459	-2.151	255.542	0.100	106.476	116.156
02.5	0.235	0.269	0.275	-3.586	431.659	0.100	179.858	196.208
03.7	0.235	0.269	0.186	-5.307	638.855	0.100	266.189	290.388
05.2	0.231	0.269	0.132	-7.458	912.007	0.100	380.003	414.549
07.0	0.231	0.269	0.098	-10.040	1227.702	0.100	511.543	558.046
09.0	0.231	0.269	0.076	-12.908	1578.474	0.100	657.698	717.488
11.5	0.227	0.269	0.060	-16.494	2055.259	0.100	856.358	934.209
14.5	0.233	0.584	0.044	-22.410	2526.483	0.100	1052.701	1148.401
18.0	0.233	0.584	.032	-30.525	3070.981	.108	1306.801	1385.405
23.0	0.243	0.712	0.025	-40.276	3173.476	0.170	1601.447	1356.501
29.5	0.238	0.910	0.018	-54.715	3306.719	0.238	2100.027	1335.978
35.5	0.238	0.910	0.015	-68.124	3429.713	0.274	2527.151	1346.243
40.0	0.238	0.910	0.013	-78.180	3521.959	0.294	2847.494	1361.032
43.0	0.238	0.910	0.012	-84.885	3583.455	0.305	3061.056	1373.087
44.5	0.238	0.910	0.011	-88.237	3614.204	0.310	3167.837	1379.626
45.5	0.238	0.910	0.011	-90.472	3634.703	0.313	3239.025	1384.149
47.0	0.238	0.910	0.011	-93.824	3665.451	0.317	3345.806	1391.157
49.5	0.238	0.910	0.010	-99.411	3716.699	0.324	3523.774	1403.366
53.0	0.238	0.910	0.009	-107.233	3788.445	0.333	3772.930	1421.398
57.5	0.238	0.910	0.008	-117.290	3880.690	0.342	4093.273	1445.873
63.5	0.238	0.910	0.008	-130.699	4003.684	0.352	4520.397	1480.231
71.0	0.238	0.910	0.009	-147.460	4157.426	0.363	5054.302	1525.204

Table 3.3 The properties of the nonlinear springs.

Node	h in	σ'_v psi	K_1 lb/in	K_2 lb/in	F_y lb	K_4 lb/in	β	γ
1	0	0.00	570.00	126.00	810.00	42.00	0.55	1.00
2	12	0.71	1857.08	448.34	1961.47	84.00	0.55	1.05
3	24	1.42	2993.56	626.08	2448.37	84.00	0.49	1.06
4	36	2.13	5520.42	988.91	3793.19	105.00	0.40	1.04
5	54	3.20	9882.97	1531.11	5715.91	141.15	0.37	1.03
6	72	4.27	15366.51	2171.72	7932.41	191.56	0.41	1.03
7	96	5.69	23208.60	3036.12	10882.02	269.86	0.44	1.02
8	120	7.11	35805.93	4443.93	15728.15	414.15	0.46	1.01
9	156	9.25	55198.46	6500.54	22699.91	635.27	0.49	1.00
10	192	11.38	70981.83	8348.46	31846.88	1128.90	0.50	1.03
11	240	14.23	105978.27	12762.97	56644.43	2585.90	0.50	1.12
12	312	18.50	146694.27	18223.21	95378.09	5259.37	0.49	1.25
13	396	23.48	148835.43	21844.17	112805.38	6510.58	0.50	1.27
14	456	27.03	119703.33	19830.87	98183.74	5680.05	0.51	1.23
15	504	29.88	84109.82	15059.38	72698.33	4211.82	0.51	1.21
16	528	31.30	43131.81	7989.39	38159.79	2212.19	0.52	1.19
17	540	32.01	29113.51	5479.49	26043.41	1510.22	0.52	1.19

Table 3.4 The properties of the linear springs.

Node	h	σ'_v	$\xi_k(\nu)$	G	V_s	K_1	K_2	K_3
1	0	0.00	1.252	38.72	810.00	1023.24	1041.56	1608.15
2	12	0.71	1.252	116.16	1961.47	6139.36	6249.30	9648.81
3	24	1.42	1.252	196.21	2448.37	10370.46	10556.18	16298.55
4	36	2.13	1.252	290.39	3793.19	19185.37	19528.94	30152.33
5	54	3.20	1.252	414.55	5715.91	32866.13	33454.69	51653.45
6	72	4.27	1.252	558.05	7932.41	51616.61	52540.95	81122.29
7	96	5.69	1.252	717.49	10882.02	75844.84	77203.06	119200.15
8	120	7.11	1.252	934.21	15728.15	123442.72	125653.32	194006.47
9	156	9.25	1.252	1148.40	22699.91	182094.25	185355.17	286185.08
10	192	11.38	1.258	1385.41	31846.88	257514.99	262126.54	404718.70
11	240	14.23	1.293	1356.50	56644.43	370224.99	376854.94	581857.29
12	312	18.50	1.341	1335.98	95378.09	491607.53	500411.18	772625.93
13	396	23.48	1.376	1346.24	112805.38	469213.20	477615.83	737430.30
14	456	27.03	1.401	1361.03	98183.74	362239.72	368726.67	569307.39
15	504	29.88	1.426	1373.09	72698.33	247979.58	252420.37	389732.54
16	528	31.30	1.426	1379.63	38159.79	124580.26	126811.23	195794.28
17	540	32.01	1.426	1384.15	26043.41	83325.79	84817.98	130957.45

Table 3.5 The properties of the linear dampers.

Node	ν	$\xi_k(nu)$	G psi	V_s in/sec	C_1 lb-sec/in	C_2 lb-sec/in	C_3 lb-sec/in
1	0.10	1.252	38.72	502.36	31430.80	6984.70	2601.79
2	0.10	1.252	116.16	870.11	108879.03	24195.60	9012.82
3	0.10	1.252	196.21	1130.87	2141508.25	31446.61	11713.81
4	0.10	1.252	290.39	1375.77	215190.33	47820.58	17813.09
5	0.10	1.252	414.55	1643.78	308533.70	68563.77	25539.89
6	0.10	1.252	558.05	1907.18	417634.58	92808.67	34571.07
7	0.10	1.252	717.49	2162.53	541203.66	120268.76	44799.91
8	0.10	1.252	934.21	2467.62	771943.36	171544.79	63900.14
9	0.10	1.252	1148.40	2735.91	1027049.66	228235.68	85017.40
10	0.11	1.258	1385.41	3005.00	1322379.59	293865.25	109464.31
11	0.17	1.293	1356.50	2973.48	1921310.98	426962.53	159042.82
12	0.24	1.341	1335.98	2950.91	2570756.04	571285.18	212802.76
13	0.27	1.376	1346.24	2962.22	2444277.39	543178.52	202333.08
14	0.29	1.401	1361.03	2978.45	1876739.07	417057.55	155353.23
15	0.31	1.426	1373.09	2991.61	1279112.92	284250.33	105882.77
16	0.31	1.426	1379.63	2998.72	641077.52	142463.18	53067.29

Table 3.6 The properties of the lumped masses.

Node	h in	ν	$\xi_m(\nu)$	m_t slug	m_{p1} slug	m_a slug	m_{p2} slug	m_f slug
1	0	0.10	0	16.24	4.26	11.98	0.59	0.00
2	12	0.10	0	32.48	8.52	23.97	1.18	0.00
3	24	0.10	0	32.48	8.52	23.97	1.18	0.00
4	36	0.10	0	40.60	10.65	29.96	1.47	0.00
5	54	0.10	0	48.72	12.78	35.95	1.77	0.00
6	72	0.10	0	56.84	14.90	41.94	2.06	0.00
7	96	0.10	0	64.96	17.03	47.93	2.36	0.00
8	120	0.10	0	81.21	21.29	59.91	2.95	0.00
9	156	0.10	0	97.45	25.55	71.90	3.54	0.00
10	192	0.11	0	113.69	29.81	83.88	4.13	0.00
11	240	0.17	0	162.41	42.58	119.83	5.89	0.00
12	312	0.24	0	211.14	55.36	155.78	7.66	0.00
13	396	0.27	0.007	194.89	51.10	143.79	7.07	55.97
14	456	0.29	0.014	146.17	38.33	107.85	5.31	83.95
15	504	0.31	0.021	97.45	25.55	71.90	3.54	83.95
16	528	0.31	0.021	48.72	12.78	35.95	1.77	41.98
17	540	0.31	0.021	32.48	8.52	23.97	1.18	27.98

boundary. In the lumped model, it is required to add a damper with the nonlinear near-field spring. But it is very difficult, if not impossible, to compute the damping parameter for the near-field element. This research concentrated on the spring parameters. The damping parameters are still unknown and here they are adjusted to obtain a similar level of damping to those obtained in FE model. Also, the FE model is itself an idealization.

The damping shown by the FE model may also be a computational artifact. DYNA3D uses a simple 8-node element which is subject to "hour-glass zero energy" modes. To suppress these hour-glass modes, artificial damping is used as a tool. This artificial damping is not intended to affect the response significantly. However, the parameters used to specify the artificial damping are not unique. Although the recommended values were used, a parametric study is necessary to confirm/disprove this possibility. Although the FE model provides a better idealization of the pile and soil than the lumped model. the FE model is also not "exact". Both of the models are subject to scrutiny. because the most realistic response is to be found only by experiment. The lumped model provides a response of the same order as that given by the FE model and we can conclude that the lumped model is a reasonable practical alternative to complex finite element models.

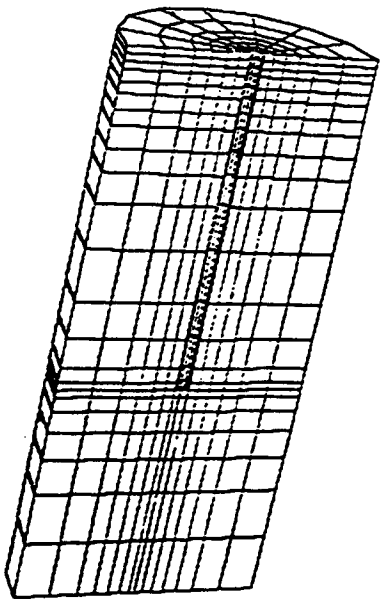

Figure 3.1 The FEM model used for the analysis of lateral vibration of a single pile.

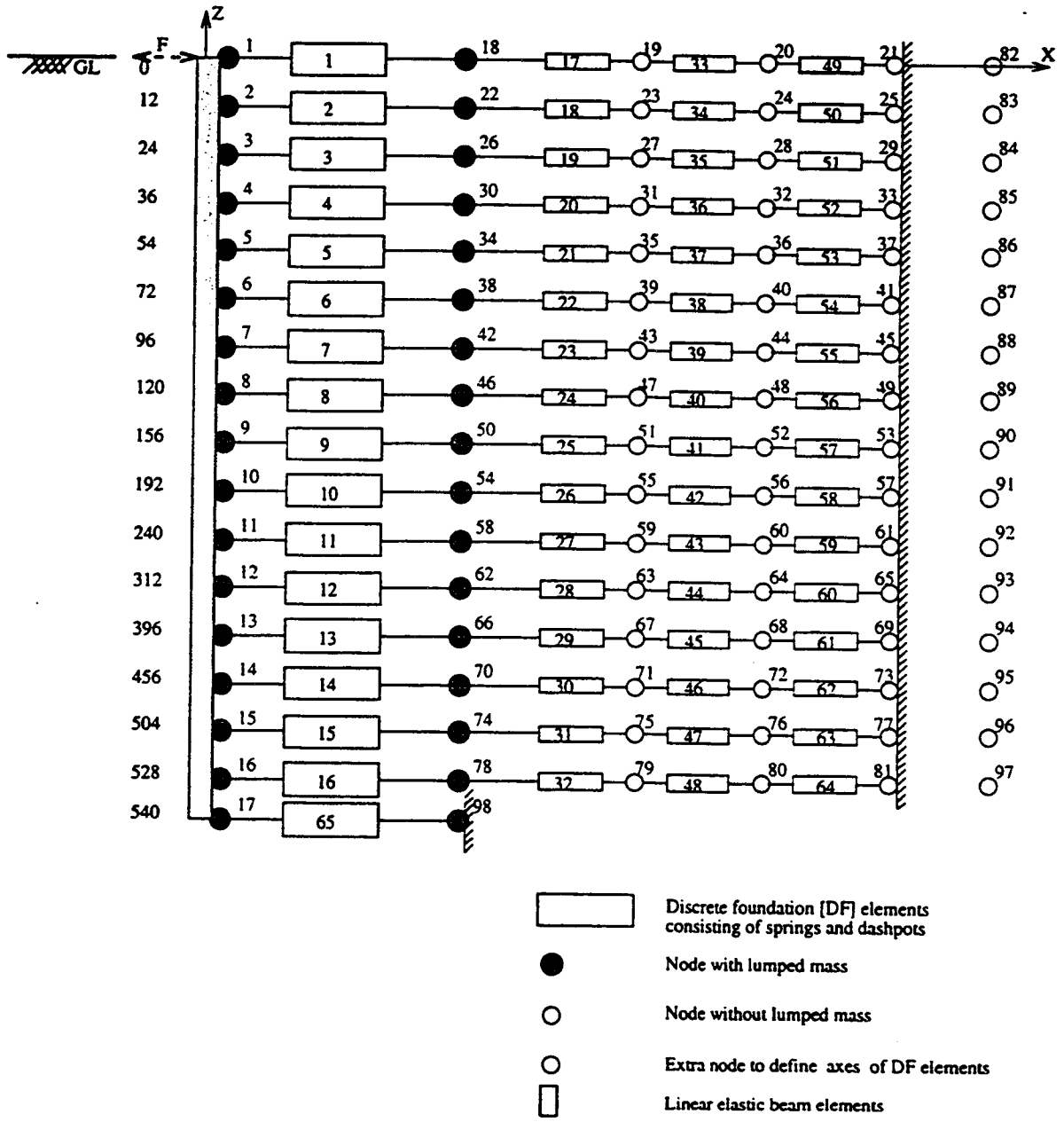

Figure 3.2 The lumped models used for the analysis of lateral vibration of a single pile.

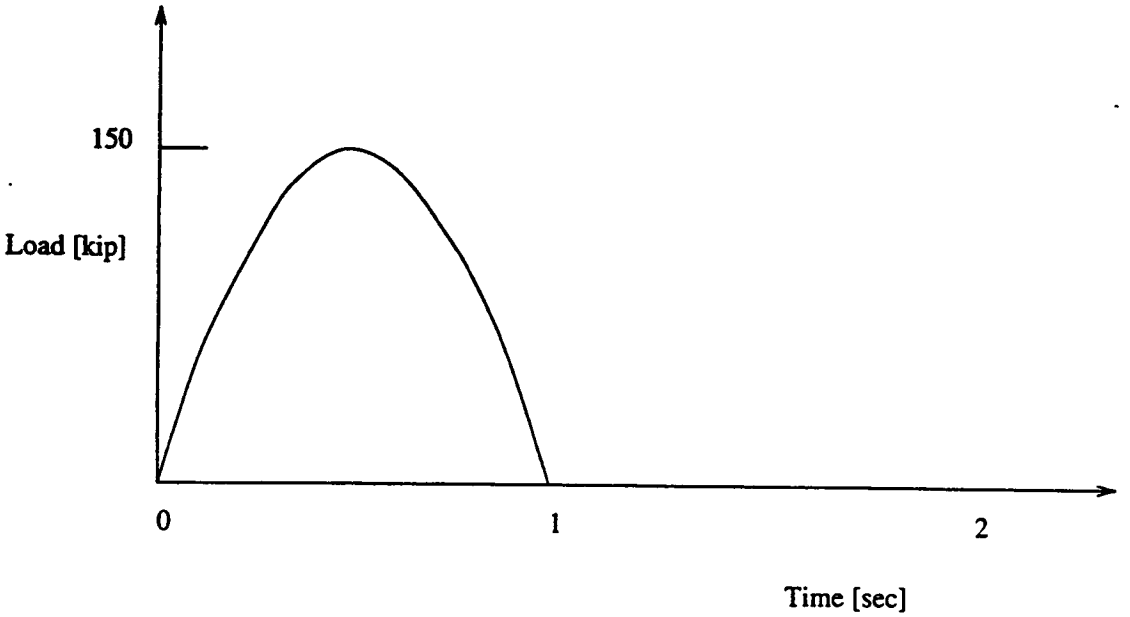

Figure 3.3 The load history used to analyze the lateral vibration of the single pile.

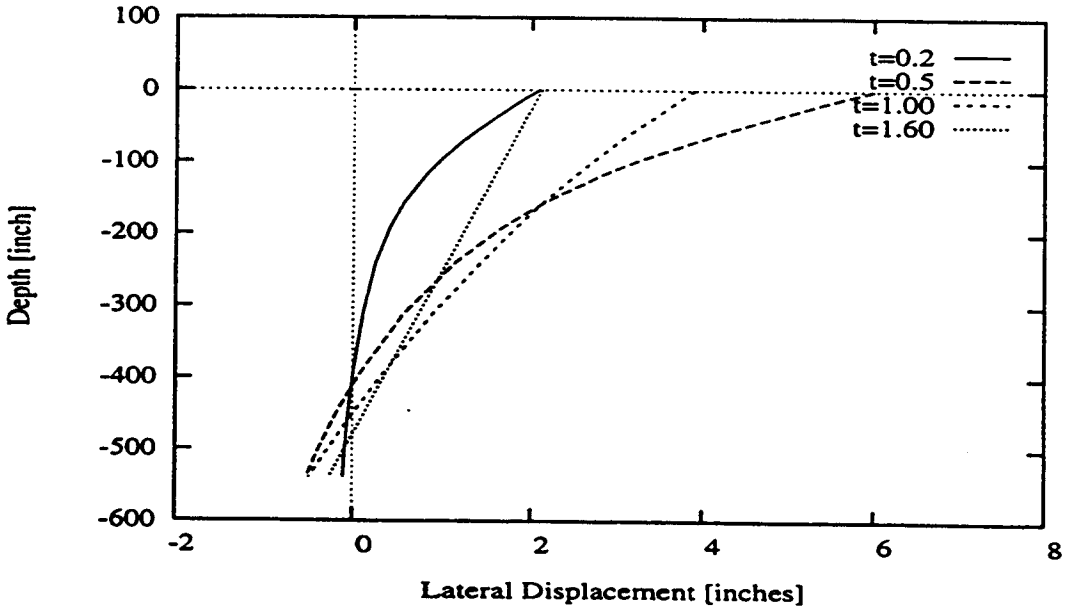

Figure 3.4 The pile displacement shapes obtained from the full scale finite element model

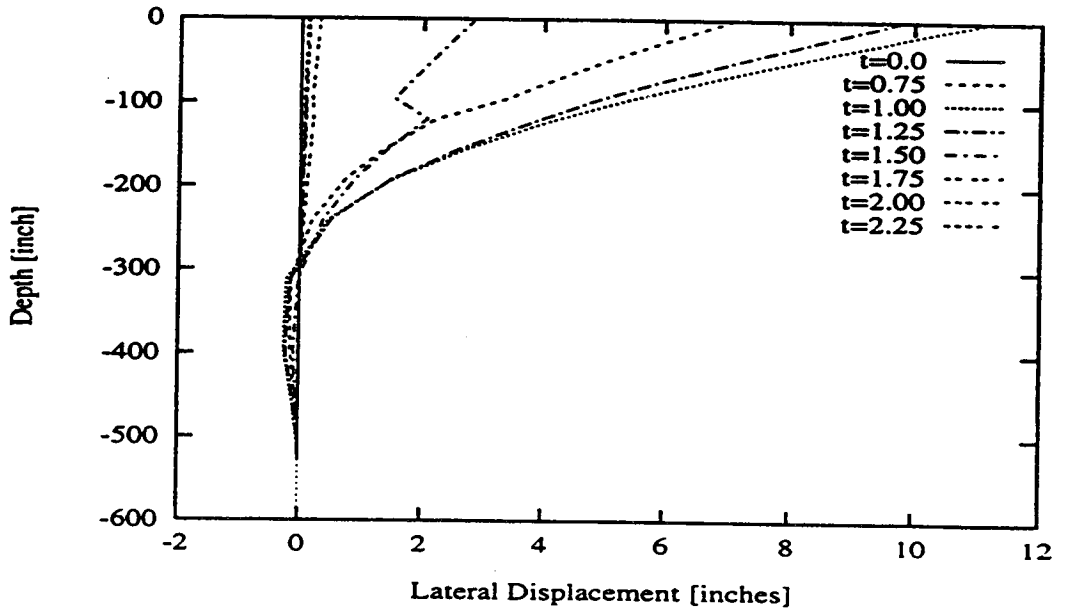

Figure 3.5 The pile displacement shapes obtained from the discrete model for small damping

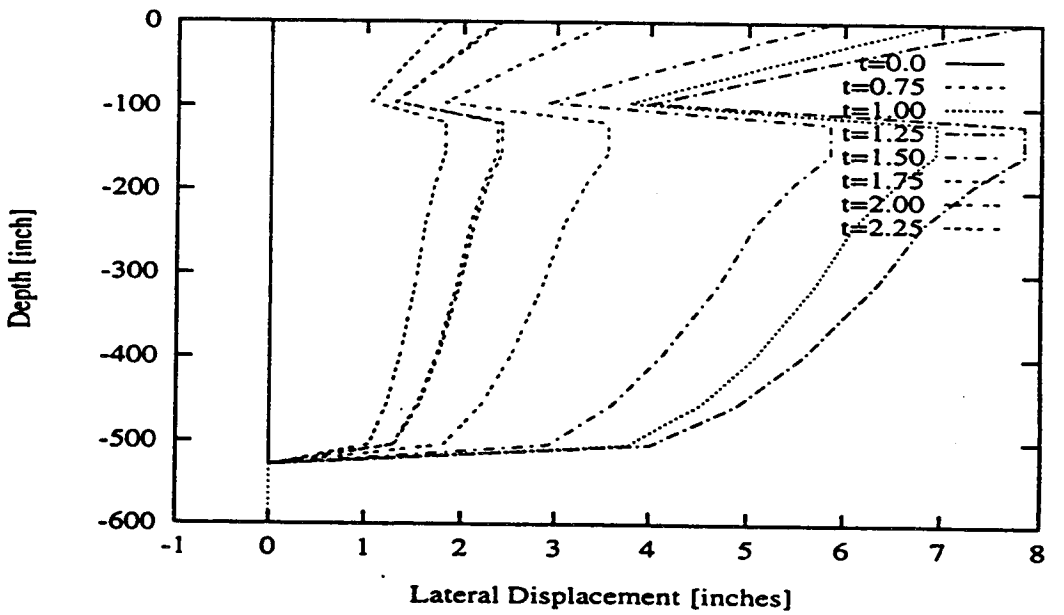

Figure 3.6 The pile displacement shapes obtained from the discrete model for large damping

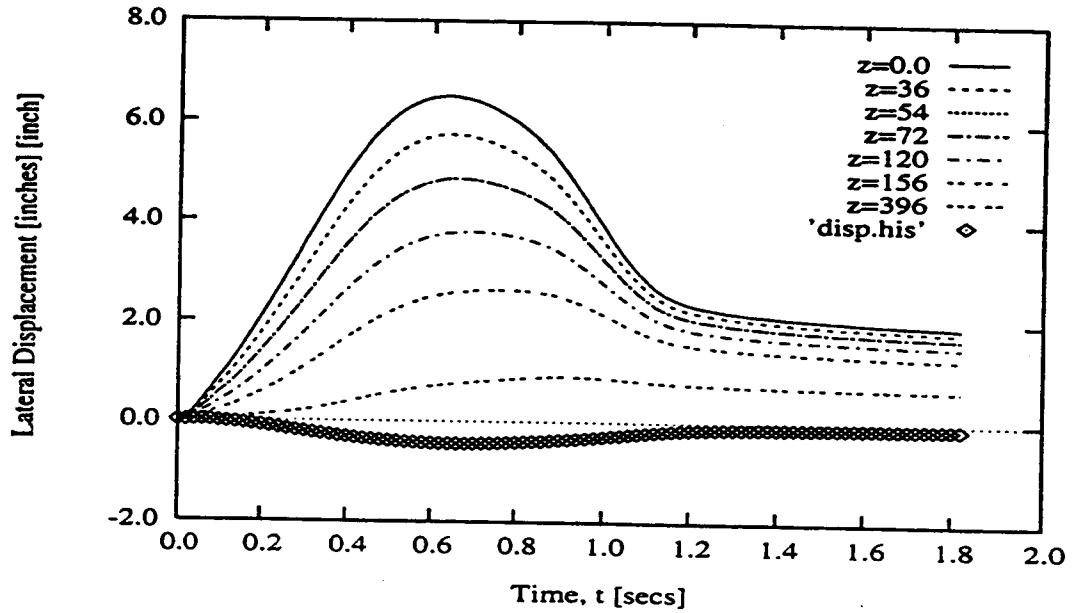

Figure 3.7 The pile displacement histories at different depths obtained from the full scale finite element model

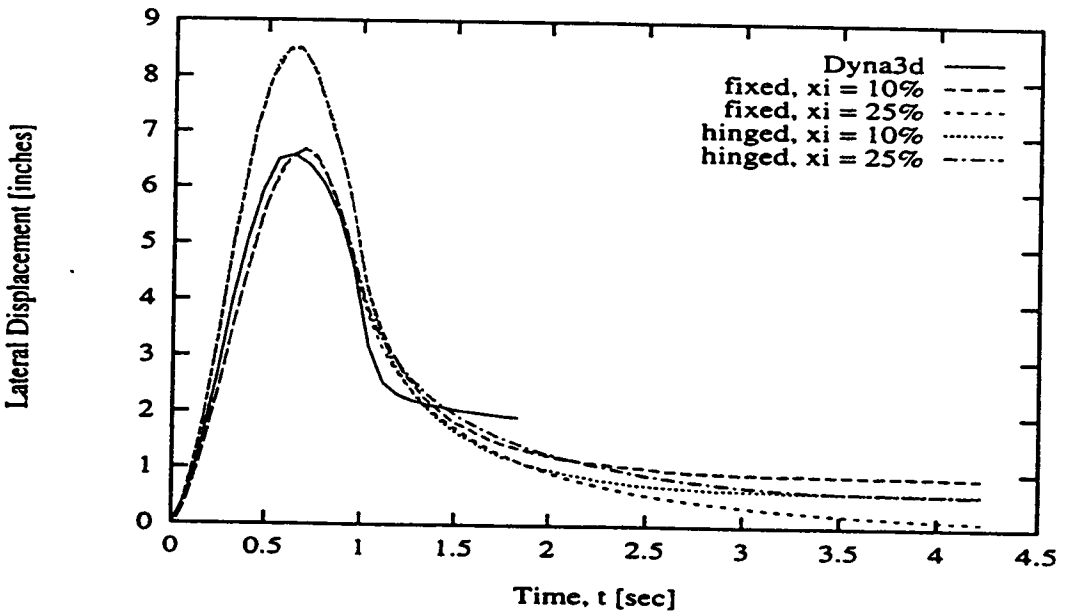

Figure 3.8 The pile head displacement histories obtained from the discrete model

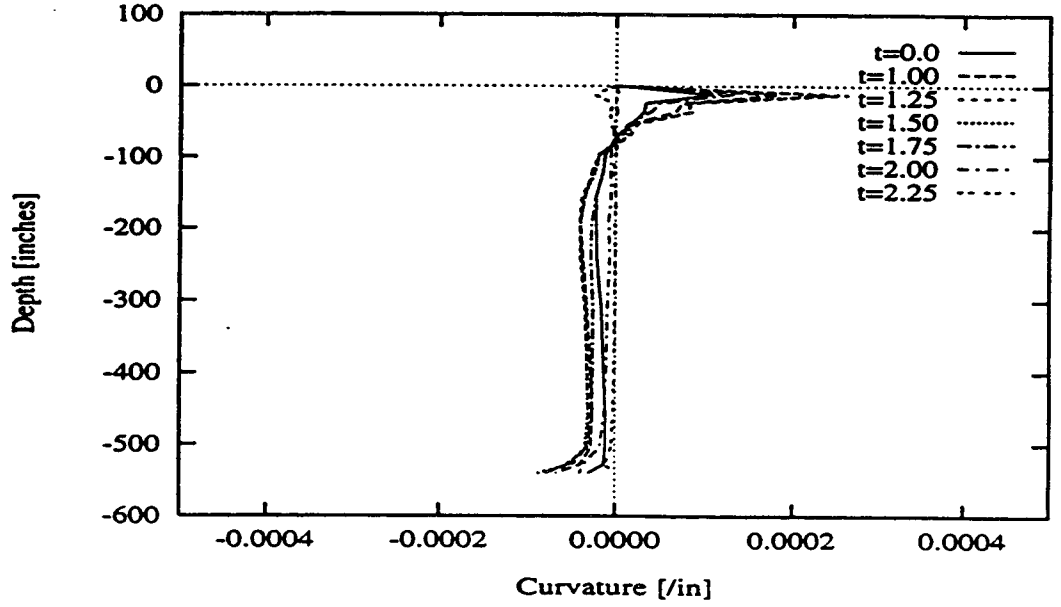

Figure 3.9 Curvature profile, at the time of the peak load attainment, obtained from the full scale finite element model

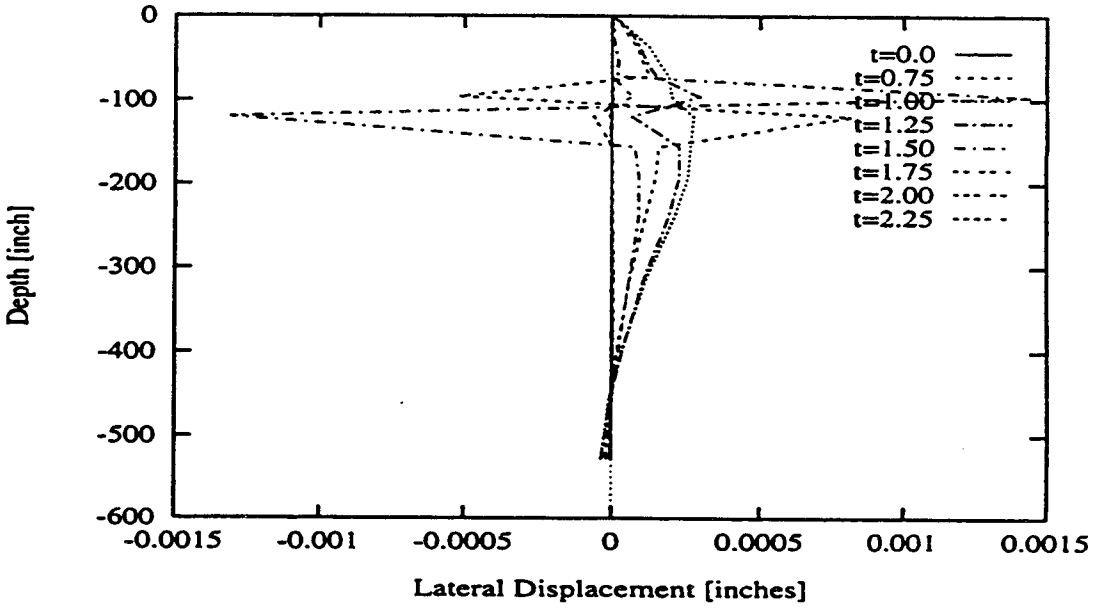

Figure 3.10 Curvature profile, at the time of the peak load attainment, obtained from the discrete model

3.4 Limitations of the Model

The model proposed in this thesis for the analysis of vibration of a single pile and a pile group is subject to the simplifications and approximations specified in Section 3.2. It is a very simplified model for piles and pile groups subjected to earthquake inertial and kinematic loading, and it may be easily adopted by any time domain finite element program which can handle discrete elements such as discrete mass, general nonlinear springs, and linear dashpots. However, the user should be aware of the following further limitations.

3.4.1 Coupling Between Layers

This model is based on the Winkler hypothesis. For the derivation of the reactive independent lateral springs, plane-strain assumptions for high depths and plane-stress assumptions for the upper region with constant vertical pressure were used. For axial vibration, no point is assumed to vibrate horizontally. For the hypothesis, proposed by Winkler, if a displacement is induced in one spring, the neighboring spring is not assumed to be subjected to any loading unless the neighboring springs have some displacement of themselves, i.e. the springs will not interact with each other, because there is no coupling spring between discrete masses. This coupling exists practically through the shearing resistance of soil layers. However, this limitation does not seriously deteriorate the response of the pile, because the pile itself acts as a large coupling element due to its shearing and bending stiffness.

3.4.2 Interaction Between Near-Field Springs in the Same Layer

In reality, the behavior of one near-field spring will heavily depend on the load level of the neighboring nonlinear spring. As an example, a single pile may be modeled by two springs in orthogonal directions for biaxial lateral vibration. The *p-y* curve obtained for uniaxial vibration is attributed to both springs, as shown in Figure 3.11. The lateral displacement degrees of freedoms are defined as δ_1 and δ_2. If, at any time, $\delta_2 = 0$ while δ_1 has a finite value, a force will develop in the $K1$ spring as a function of δ_1.

$$F_1 = F(\delta_1), \text{ and} \qquad [3.1]$$

$$F_2 = F(\delta_2 = 0) = 0. \qquad [3.2]$$

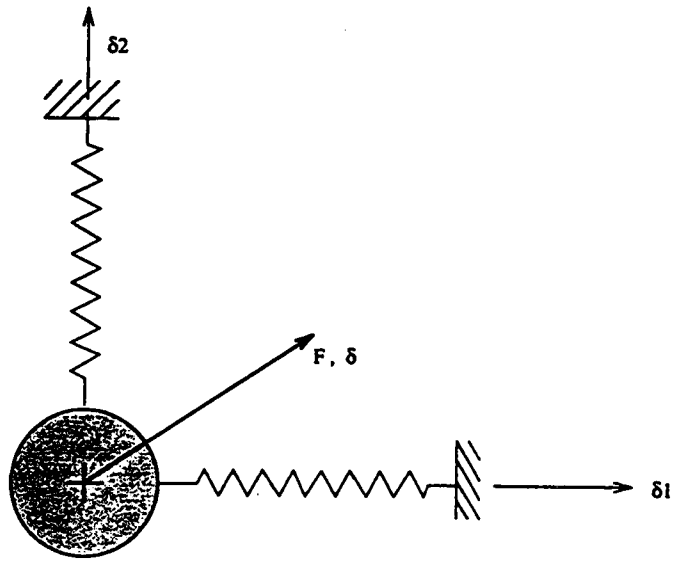

(a)

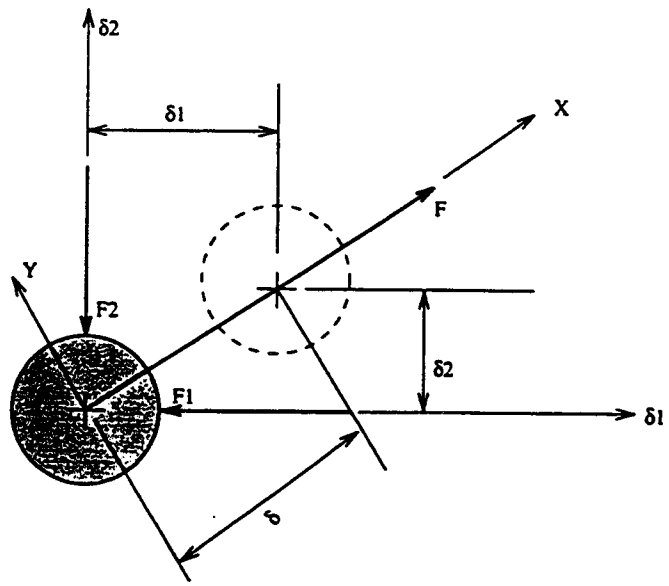

(b)

Figure 3.11 A demonstration of the effect of the interaction between the near-field springs in the same layer

Similarly, if at any time $\delta_1 = 0$ while δ_2 has a finite magnitude, then

$$F_1 = F(\delta_1 = 0) = 0, \text{ and} \quad [3.3]$$

$$F_2 = F(\delta_2). \quad [3.4]$$

This function $F(.)$ is the same for both pure cases of uniaxial vibration. But, for biaxial lateral vibration, the displacement δ has two components, δ_1 and δ_2, in two orthogonal directions.

$$\delta = \left\{\delta_1^2 + \delta_2^2\right\}^{1/2} \quad [3.5]$$

The force in the direction of X, the direction of δ, will actually be $F(\delta)$, as for uniaxial vibration. So, the component in the orthogonal directions will be

$$F_1 = \frac{F(\delta).\,\delta_1}{\delta}, \quad [3.6]$$

$$F_2 = \frac{F(\delta).\,\delta_2}{\delta} \quad and \quad [3.7]$$

$$F = \left\{F_1^2 + F_2^2\right\}^{1/2}. \quad [3.8]$$

For linear structures,

$$F_1 = F(\delta).\frac{\delta_1}{\delta} = F(\delta.\frac{\delta_1}{\delta}) = F(\delta_1), \quad [3.9]$$

$$F_2 = F(\delta).\frac{\delta_2}{\delta} = F(\delta.\frac{\delta_2}{\delta}) = F(\delta_2) \quad and \quad [3.10]$$

$$\frac{F(\delta_1)}{F(\delta_2)} = \frac{\delta_1}{\delta_2}. \quad [3.11]$$

and for non-linear structures,

$$F_1 = F(\delta).\frac{\delta_1}{\delta} \neq F(\delta.\frac{\delta_1}{\delta}) \neq F(\delta_1), \quad [3.12]$$

$$F_2 = F(\delta).\frac{\delta_2}{\delta} \neq F(\delta.\frac{\delta_2}{\delta}) \neq F(\delta_2), \; and \quad [3.13]$$

$$\frac{F(\delta_1)}{F(\delta_2)} \neq \frac{\delta_1}{\delta_2}. \quad [3.14]$$

The above formulas show that for linear F-δ curves, the reactions considering interaction are the same as those obtained without interaction. But for nonlinear structures,

these reactive values cannot be obtained from their own displacements. They are subject to the interaction equations:

$$F(\delta) = \left\{F(\delta_1)^2 + F(\delta_2)^2\right\}^{1/2}, \text{ and} \quad [3.15]$$

$$\frac{F(\delta_1)}{F(\delta_2)} = \frac{\delta_1}{\delta_2}. \quad [3.16]$$

For the same example, the yield strength, F_y, for individual springs may be examined, assuming the yield displacements, δ_y. If the spring stiffness does not harden with plastic loading, and

$$\begin{aligned} \delta_1 &= \delta_2 = \delta_y, \\ F_{1y} &= F(\delta_y) = F_y, \text{ and} \\ F_{2y} &= F(\delta_y) = F_y, \end{aligned}$$

then the equivalent uniaxial force is $\sqrt{2}F_y$. This expression indicates that, when $\delta_1 = \delta_2$ and no interaction between springs is considered, (for the perfectly plastic case), the yield strength is overestimated by as much as $\sqrt{2}$ times the actual yield strength. However, this is the worst case, because for other combinations of δ_1 and δ_2, this factor will be less.

On the whole, by considering no interaction between the near-field springs in the same layer, the stiffness is over-predicted while the displacement is under-predicted if the load exceeds the elastic limits at any spring. However, for small load the model can predict the actual behavior, even though no interactions between springs are considered. In the explicit form of biaxial lateral vibration finite element programs, these interaction equations can be considered as constrained equations. It is expected that the reduction of yield strength of the near-field springs can minimize the error caused from the interaction.

3.4.3 Effect of Pore-Water Pressure

The analysis can be done, so far, for two standard conditions of soil: the undrained condition and the drained condition. For intermediate conditions of state, i.e. for unsaturated soil, it is still difficult to predict stress-strain and volume change-pore pressure behavior. However in this thesis, analysis is done for only drained conditions. Soil below the ground water table and a few feet above it can be assumed to be saturated and, depending on the grain size, an undrained or drained analysis is appropriate there. For soil well above the GWT, drained analysis is appropriate. Engineering judgment is required for partially saturated soil. It can be observed that for a degree of saturation less

than 60%, the pore-pressure factor, β, is very small and essentially undrained behavior is appropriate for small load increases. Even for 85% saturation, $\beta < 0.04$ for most soils. However, a complete analysis will require the history of the development and dissipation of pore-water at every point during the vibration of piles. A finite element analysis with the capability of handling two problems of the determination of stress-field and the determination of pore-water pressure field subject to stress change and seepage with the known displacement and/or stress and seepage boundary conditions is appropriate. But these details are too cumbersome to consider in the design of bridge foundations. Therefore, the proposed simplified model is expected to provide acceptable response within engineering accuracy.

3.4.4 The Effect of Soil Liquefaction

Some soils, such as saturated silt and sand of low relative density, are subject to liquefaction when the earthquake excitation exceeds a critical value which is appropriate for the soil of the site. The proposed model did not consider the potentiality of strength and stiffness reduction due to the soil liquefaction. In fact, a spring which varies the strength and stiffness with load and time is appropriate there. This analysis is too cumbersome and too extensive to consider for bridge foundation analysis, and it is left to the judgment of the geotechnical engineer.

3.4.5 Sensitivity of Soil

The model cannot predict the behavior of piles in a sensitive soil by itself. The user is expected to produce correct *p-y* behavior for specific soil, pile diameter, and group configurations if the soil is sensitive. The model can not predict the thixotropic behavior of soil by itself. Once again, the user is expected to use his/her own judgment.

3.4.6 Pile Installation Procedure

The *p-y* curve for near-field soil is developed for initial geo-static states of stress, where the coefficient of earth pressure, K, is assumed to be the coefficient of earth pressure at rest, K_o. However, a large amount of disturbance with strength and stiffness reduction in sensitive soil, and strength and stiffness increase with time due to thixotropic behavior occur in practice. For driven piles, an increase in K occurs, and for bored piles, a

decrease in K is expected. The user should consider the pile installation procedure in his/her analysis.

3.4.7 Pile Batter

The model represented in this thesis is only for vertical piles. However, it is expected that batter piles can be modeled by the near-field and far-field elements specified in this thesis for vertical piles. It is also expected that the pile foundation response can be obtained for earthquake response within engineering accuracy. It is advisable that the lateral and axial springs be placed in the lateral and axial direction of the batter piles instead of placed horizontally and vertically. The interaction-spring can be placed in the horizontal direction. When specifying the interaction-spring p-y behavior, it should be kept in mind that the spacing is not constant between two batter piles or between a vertical and a batter pile. However, batter piles do not perform well for resisting earthquake load. It increases lateral rigidity, inducing higher load in the structure.

3.4.8 Piles in Sloping Ground

All p-y curve characteristics determined in this research are for vertical piles in leveled horizontal ground. For sloping ground, the p-y behavior is expected to change.

3.4.9 Strength and Stiffness Degradation of Soil

The effect of strength and stiffness degradation has not been considered in this research. It should be considered for the p-y curves.

3.4.10 Kinematic Interaction Effect

The model presented in this thesis was developed primarily for inertial earthquake loading. It is expected that it can reproduce the behavior of pile foundations for kinematic loading as well. However, this model should be used for kinematic loading with caution. For a kinematic type of loading, it is expected that the ends of the far-field element will represent the actual far-field. Moreover, it is expected that far-field displacement or acceleration boundary condition would be specified at those nodes.

3.5 Application Areas

The model proposed in this thesis is primarily developed for vertical single piles and pile groups embedded in horizontal ground. Therefore, engineering judgment is required to apply this model for batter piles and pile groups, or piles in sloping ground. The nonlinear springs are developed only for soil with drained conditions. The soil below the ground water table and, depending upon capillary action, several feet above the ground water table may be assumed to be saturated, and the undrained loading condition is expected. Soils with a degree of saturation less than 60% are assumed to be dry for small load increments, and then the drained condition of loading is expected.

4. CONCLUSIONS AND RECOMMENDATIONS

4.1 Conclusions

The main objective of this research was to develop a simplified lumped parameter model of pile foundations for bridges for the time domain analysis of the response due to earthquake excitation. Lumped parameters such as nonlinear near-field springs, linear near-field dampers, linear far-field springs and dampers, and lumped masses are used to model a single pile. For pile groups, interaction-springs and dampers are also used to include group effects. The properties of the model have been evaluated for soil at a Snohomish river bridge site. It is well recognized that each simplification involves some approximations. The limitations of the proposed model along with ways to eliminate, or at least to reduce them, have been discussed in Section 3.4.

4.2 Recommendations

On the basis of the studies done herein, recommendations are made in the following sections.

4.3 Recommended Models

The model, shown in Figure 2.4, is proposed for a single pile under uniaxial lateral vibration. The model, shown in Figure 2.10, is proposed for a single pile under axial vibration. The model, shown in Figure 2.14, is proposed for a 2-pile group under biaxial lateral vibration. The springs that are shown in Figure 2.14 are the nonlinear near-field springs and interaction-springs. One dashpot with proportional damping should be associated with each nonlinear spring in parallel. One end of the nonlinear spring and dashpot is connected with the pile, and the other with an auxiliary node having a lumped mass, which is connected with the far-field element. Far-field elements consist of

three lumped masses connected with three linear springs and dashpots. The springs are associated with the dampers connected in parallel.

Only the far end of the far-field elements is assumed to be fixed for inertial interaction. The characteristics of the far-field springs and dashpots, the lumped masses, and the near-field damper for a single pile have been presented in explicit form in Section 2.2. For pile-groups, each pile is connected with nonlinear near-field springs to the surrounding soil, and with nonlinear interaction-springs to nearby piles. For three dimensional vibration, two piles are connected by a set of three interaction-springs: one for axial interaction, one for shear lateral interaction, and the other for direct lateral interaction. For large pile groups, inner piles are not connected with the far-field elements. However, the behavior of nonlinear springs is site specific. Finite element analysis is required to establish their force-displacement behavior. The p-y curves for the near-field elements presented in this thesis were developed for soil at the Snohomish-river-crossing-bridge-site for piles of diameters 0.457m (18″) and 0.610m (24″). The curves are described herein in Figures E.1 through E.54 in Appendix E. The simple bilinear parameters for these curves are presented in Tables 2.1, 2.2, 2.4, 2.5, and 2.7 through 2.20.

4.3.1 Recommended Near-Field Spring

The exact force-displacement behavior of the near-field springs for axial and lateral vibration of single piles and pile groups are presented in Figures E.1 through E.54 in Appendix E. However, simplified p-y behavior is needed in some computer programs. The program, NEABS (McGuire et al. 1994) can only handle bilinear springs with gap options. The characteristic parameters for the simplified p-y curves are presented in Tables 2.1, 2.2, 2.4, 2.5, and 2.7 through 2.20 for the drained condition of loading.

4.3.2 Recommended Dampers

It is not possible to establish damping characteristics by the finite element method, unless viscosity properties are properly known. Therefore, it is recommended that Rayleigh's conventional proportional damping or just the stiffness proportional damping procedure be used.

4.3.3 Recommended Masses

The explicit expression for nodal lumped masses is based on tributary area and an assumed shape function, and it is presented in Section 2.2.1.3 for lateral vibration of single pile, in Section 2.2.2.3 for axial vibration of single pile, and in Section 2.3.3 for general vibration of two-pile groups. The explicit expression for lumped masses in far-field nodal points is adopted from (Nogami & Konagai 1986, Nogami & Konagai 1987, Nogami et al. 1992) for vibration of a single pile. These are presented in Appendices A and B.

4.3.4 Recommended Far-Field Elements

The explicit expressions for the far-field masses, springs, and dashpots are presented in Appendices A and B. Those were obtained from (Nogami & Konagai 1986, Nogami & Konagai 1987, Nogami et al. 1992).

5. IMPLEMENTATION

5.1 General

The proposed model can be implemented in any explicit finite element computer program which can handle discrete elements such as: linear and nonlinear springs, linear dashpots, lumped mass, and a beam element with or without geometric stiffness. However, the nonlinear springs should have special features such as gap stiffness in addition to usual the nonlinear stiffness behavior. The program NEABS, which has been modified (McGuire et al. 1994) as a companion phase of the present research, has all the capabilities required for the proposed model. Therefore, this version of NEABS is recommended.

5.2 Recommendation for Further Research

In this research, near-field and interaction springs have been developed for only two specified diameters of piles, leveled ground conditions, vertical piles and pile groups, for drained conditions, and a site-specific soil. The spring elements must be generalized for design. It is anticipated that standard *p-y* curves will be used as near-field elements for single piles. However, research is needed to determine the most appropriate manner in which to apply the pile interaction elements, testing is necessary to validate the approach, and the results must be put into a form that is amenable for design.

An improved analysis method could be developed on the basis of knowledge gained in this project. The issues that could be considered include (a) the suitability of existing *p-y* curves for defining soil stiffness values; (b) the form of the elements to be used between piles in pile groups; and (c) ease of use in design. A two-stage approach could be considered, similar to that proposed in the accompanying summary report, in which a relatively complex model can be used to obtain coefficients for use in a simplified model. The complex model consists of the piles themselves, connected with *p-y* springs, masses, and dashpots, the coefficients of which would be based on soil properties and, for elements connecting piles in a group, pile spacing. Although this model would be suitable for analysis of the structure, the number of elements required would make it unwieldy for use in design. To obtain a simpler foundation

model, two approaches could be considered. For the first, the foundation could be modeled in the complex fashion, with a very gross approximation of the structure added to include its dynamic effects. The motion of the foundation at the ground surface could be measured and applied in a separate analysis to a more realistic structural model. For the other approach, a model of the foundation could be generated and loaded harmonically with several frequencies. From the response, an equivalent foundation element could be derived and applied in a separate analysis at the base of the structural model.

A computer program that could incorporate the new analysis method could also be developed. It is anticipated that it would be an extension of WSU-NEABS. For future research, the elements could be enhanced and the program streamlined to be efficient and focused for pile analysis only. In addition, pre- and post-processors could be written to facilitate data entry and interpretation of results in a graphical, easy to use format.

LIST OF REFERENCES

LIST OF REFERENCES

Abendroth, R. E., Greimann, L. F. & Ebner, P. B. (1989a), 'Abutment pile design for jointless bridges', *Journal of Structural Engineering* **115**(11), 2914–2929.

Abendroth, R. E. & Greimann, L. F. (1989b), 'Rational design approach for integral abutment bridge piles', *Transportation Research Record* **1223**, 12–23.

Ahmad, S. & Banerjee, P. K. (1988), 'Time-domain transient elastodynamic analysis of 3-d solids by bem.', *International Journal for Numerical Methods in Engineering* **26**(8), 1709–1728.

Angelides, D. & Roesset, J. M. (1980), Nonlinear dynamic stiffness of piles, Technical Report R80-13, MIT, Department of Civil Engineering, Cambridge, Massachusetts.

API (1986), *Recommended Practice for Planning, Designing, and Constructing Fixed Offshore Platforms*, 16th edn, American Petrolium Institute, Dallas, TX.

Applied Technology Council (1978), Tentative provisions for the development of seismic regulations for buildings : a cooperative effort with design professions, building code interests, and the research community., Technical report, Applied Technology Council and Structural Engineers Association of California and United States National Bureau of Standards, Washington, D. C. ATC 3-06 or NSF 78-7 or NBS Special Publication 510.

Atkinson, J. H. & Bransby, P. L. (1978), *The Mechanics of Soils — An Introduction to Critical State Soil Mechanics*, McGraw-Hill, Maidenhead, England.

Banerjee, P. K. (1978), Analysis of axially and laterally loaded pile foundations, *in* C. R. Scott, ed., 'Developments in Soil Mechanics', Applied Science Publication, London, chapter 9, pp. 317–346.

Banerjee, P. K. & Ahmed, S. (1985), Advanced three-dimensional dynamic analysis by boundary elements, *in* T. A. Cruse, A. Pifko & H. Armen, eds, 'Proceeding ASME Conference on Advanced Boundary Element Analysis', Vol. AMD 72, ASME, New York, NY, pp. 65–81.

Banerjee, P. K. & Sen, R. (1987), Dynamic behavior of axially and laterally loaded piles and pile groups, *in* P. K. Banerjee & R. Butterfield, eds, 'Dynamic Behavior of Foundations and Buried Structures (Developments in Soil Mech Found Engineering)', Vol. 3, Elsevier Applied Science, London, chapter 3, pp. 95–133.

Banerjee, P. K., Mamoon, S. M. & Manolis, G. D. (1986), 'Transient elastodynamic analysis of three-dimensional problems by boundary element method', *Earthquake Engineering and Structural Dynamics* **14**(4), 933–949.

Banerjee, P. K., Sen, R. & Davies, T. G. (1987), Static and dynamic analysis of axially and laterally loaded piles and pile groups, *in* S. M. Sayed, ed., 'Geotechnical Modeling and Applications (Dean Alexander Vesic Memorial Volume)', Gulf Publication Company, Houston, chapter 7, p. 322.

Baranov, V. A. (1967), 'On the calculation of an embedded foundation (in Russian)', *Vipiosy Dinamikii Piochnosti* **14**, 195–209.

Bielak, J. (1974), 'Earthquake response of building foundation systems', *Earthquake Engineering and Structural Dynamics* **3**(2), 121–138.

Biot, M. A. (1941), 'General theory of three dimensional consolidation', *Journal of Applied Physics* **12**, 155–164.

Blaney, G. W. & O'Neill, M. W. (1991), 'Procedures for prediction of dynamic lateral pile group response in clay from single pile tests', *Geotechnical Testing Journal, ASTM* **14**(1), 3–12.

Blaney, G. W., Kausel, E. & Roesset, J. M. (1976), 'Dynamic Stiffness of Piles', *in* C. S. Desai, ed., 'Proceedings 2nd International Conference on Numerical Methods in Geomechanics', ASCE, New York, NY, Blacksburg, Virginia, pp. 1001–1012.

Brown, D. A. & Shie, C.-F. (1990), 'Three dimensional finite element model of laterally loaded piles', *Computers and Geotechnics* **10**(1), 59–79.

Brown, D. A. & Shie, C.-F. (1991), 'Some numerical experiments with a three dimensional finite element model of a laterally loaded pile', *Computers and Geotechnics* **12**(2), 149–162.

Butterfield, R. & Banerjee, P. K. (1971), 'The elastic analysis of compressible piles and pile groups', *Geotechnique* **21**, 43–60.

Butterfield, R. & Douglas, R. A. (1981), Flexibility coefficient for the design of piles and pile groups, Technical Notes 108, Construction Industry Research and Inf. Assoc., Six Storey's Gate, London, England.

Chen, W.-F. & Baladi, G. Y. (1985), *Soil Plasticity : Theory and Implementation*, Developments in Geotechnical Engineering, 38, Elsevier, Amsterdam : New York.

Chen, W.-F. & Han, D.-J. (1988), *Plasticity for Structural Engineers*, Springer-Verlag, New York, NY.

Chen, W. F. & McCarron, O. W. (1983), Modelling of soils and rocks based on concepts of plasticity, *in* 'Proc., Symp. on Recent Developments in Laboratory and Field Tests and Analysis of Geotechnical Problems', Bankok, Thailand, pp. 467–510.

Chen, W.-F. & Saleeb, A. F. (1982), *Constitutive Equations for Engineering Materials*, Vol. 1, John Wiley and Sons Inc., New York, NY.

Cheney, J. A., Brown, R. K., Dhat, N. R. & Hor, O. Y. Z. (1990), 'Modeling free-field conditions in centrifuge models', *Journal of Geotechnical Engineering* **116**(9), 1347–1367.

Chopra, A. K. (1980), Soil-structure interaction - on interrelationship of analytical methods, *in* '7th World Conference on Earthquake Engineering', Istanbul, Turkey. State-of-the-Art Panel Report.

Chow, Y. K. (1987), 'Axial and lateral response of pile groups embedded in nonhomogeneous soils', *International Journal for Numerical and Analytical Methods in Geomechanics* **11**(6), 621–638.

Chow, Y. K. & Teh, C. I. (1991), 'Pile-cap-pile-group interaction in nonhomogeneous soil', *Journal of Geotechnical Engineering* **117**(11), 1655–1668.

Clough, R. W. & Penzien, J. (1975), *Dynamics of structures*, McGraw-Hill, New York.

Cook, R. D., Malkus, D. S. & Plesha, M. E. (1989), *Concepts and Applications of Finite Element Analysis*, third edn, Wiley, New York.

Daddazio, R. P., Ettouney, M. M. & Sandler, I. S. (1987), 'Nonlinear dynamic slope stability analysis', *Journal of Geotechnical Engineering* **113**(4), 285–298.

Dafalias, Y. R. & Herrmann, L. R. (1982), Bounding surface formulation of soil plasticity, *in* G. N. Pande & O. C. Zienkiewicz, eds, 'Soil Mechanics — Transient and Cyclic Load', John Wiley and Sons, pp. 253–283.

De Beer, E. et al., eds (1977), *Proceedings of Specialty Session, 10, The Effects of Horizontal Loads on Piles Due to Surcharge or Seismic Effects, IX ICSMFE*, Tokyo.

Derecho, A. T. snd Huckelbridge, A. A. (1991), Soil-structure interaction – a brief overview, *in* S. K. Ghosh, ed., 'Earthquake-Resistant Concrete Structures: Inelastic Response and Design', SP 127, American Concrete Institute, Detroit, Michigan, pp. 239–259.

DiMaggio, F. L. & Sandlar, I. S. (1971), 'Material models for granular soils', *Journal of Engineering Mechanics, ASCE* **97 (EM3)**, 935–950.

Dobry, R. & Gazetas, G. (1988), 'Simple method for dynamic stiffness and damping of floating pile groups', *Geotechnique* **38**(4), 557–574.

Dobry, R., Vincente, E., O'Rourke, M. J. & Roesset, J. M. (1982), 'Horizontal stiffness and damping of single piles', *Journal of Geotechnical Engineering Division, ASCE* **108**(GT3), 439–459.

Dotson, K. W. & Veletsos, A. S. (1990), 'Vertical and torsional impedence for radially inhomogeneous viscoelastic soil layers', *Soil Dynamics & Earthquake Engineering* **9**(3), 110–119.

Drucker, D. C., Gibson, R. E. & Henkel, D. J. (1957), 'Soil mechanics and work hardening theories of plasticity', *Transactions, ASCE* **122**, 338–346.

Drucker, D. C. & Prager, W. (1952), 'Soil mechanics and plastic analysis of limit design', *Quarterly Applied Mathematics* **10**(2), 936–950.

El Hifnawy, L. & Novak, M. (1986), 'Uplift in seismic response of pile supported buildings', *Journal of Earthquake Engineering & Structural Dynamics* **14**, 573–593.

El Marsafawi, H., Han, Y. C. & Novak, M. (1992), 'Dynamic experiments on two pile groups', *Journal of Geotechnical Engineering* **118**(4), 576–592.

El Marsafawi, H., Kaynia, A. M. & Novak, M. (1992), Superposition approach to pile group dynamics, *in* 'Proceedings of the Conference on Piles Under Dynamic Loads', ASCE, New York, NY, USA., pp. 114–135. Geotechnical Special Publication 34.

El Sharnouby, B. & Novak, M. (1985), 'Static and low frequency response of pile groups', *Canadian Geotechnical Journal* **22**(1), 79–94.

El Sharnouby, B. & Novak, M. (1986), 'Flexibility coefficient and interaction factors for pile group analysis', *Canadian Geotechnical Journal* **23**, 441–450.

El Sharnouby, B. & Novak, M. (1990), 'Stiffness constants and interaction factors for vertical response of pile groups', *Canadian Geotechnical Journal* **27**(6), 813–822.

Ensoft Inc. (1991), *LPILE: A Program for the Analysis of Piles and Drilled Shafts Under Lateral Load*, Ensoft Inc., Austin, Texas.

Fan, K., Gazetas, G., Kaynia, A., Kausel, E. & Ahmad, S. (1991), 'Kinematic seismic response of single piles and pile groups', *Journal of Geotechnical Engineering* **117**(12), 1860–1879.

Faruque, M. O. & Desai, C. S. (1982), 3-d material and gemetric non-linear analysis of a piles, *in* '2nd International Conference on Numerical Methods in Offshore Piling', Austin, TX, pp. 509–532.

Finn, W. D. L., Bransby, P. L. & Pickering, D. J. (1970), 'Effect of strain history on liquefaction of sand', *Journal of Soil Mechanics and Foundation Engineering Division, ASCE* **97**(SM6), 1917–1934.

Finn, W. D. L., Pickering, D. J. & Bransby, P. L. (1971), 'Sand liquefaction in triaxial and simple shear tests', *Journal of Soil Mechanics and Foundation Engineering Division, ASCE* **97**(SM4), 639–659.

Gazetas, G. (1984), 'Seismic response of end-bearing single piles', *Soil Dynamics and Earthquake Engineering* **3**(2), 82–93.

Gazetas, G., Fan, K., Kaynia, A. & Kausel, E. (1991), 'Dynamic interaction factors for floating pile groups', *Journal of Geotechnical Engineering* **117**(10), 1531–1548.

Gazetas, G. & Makris, N. (1991), 'Dynamic pile-soil-pile interaction. Part 1. Analysis of axial vibration', *Earthquake Engineering & Structural Dynamics* **20**(2), 115–132.

Gle, D. R. (1981), The Dynamic Lateral response of Deep Foundation, PhD thesis, University of Michigan, Ann Arbor.

Gutierrez, J. A. & Chopra, A. (1978), 'A substructure method for earthquake analysis of structures including structure-soil interaction', *Earthquake Engineering and Structural Dynamics* **6**, 51–69.

Hadjian, A. H., Falgren, R. B. & Lau, L. (1990), Imperial county services building revisited: A reevaluation with pile-soil-structure interaction, *in* 'Proceedings 4th U.S. National Conference on Earthquake Engineering', Vol. 3, Palm Springs, CA, pp. 855–844.

Hadjian, A. H., Fallgren, R. B. & Tufenkjian, M. R. (1992), Dynamic soil-pile-structure interaction - the state-of-practice., *in* S. Prakash, ed., 'Proceedings of the Conference on Piles Under Dynamic Loads', Vol. Geotechnical Special Publication 34, ASCE, New York, NY, USA, pp. 1–26.

Haldar, S. S. & Bose, S. K. (1990), 'Dynamic soil stiffness in lateral vibrations of a floating pile', *Soil Dynamics and Earthquake Engineering* **9**(1), 51–56.

Hardin, B. O. & Black, W. L. (1966), 'Sand stiffness under various triaxial stresses', *Journal of the Soil Mechanics and Foundation Division, ASCE* **92**(SM2), 22–42.

Hardin, B. O. & Black, W. L. (1968), 'Vibration modulus of normally consolidated clays', *Journal of the Soil Mechanics and Foundation Division, ASCE* **94**(SM2), 353–369.

Hardin, B. O. & Black, W. L. (1969), '(Closure to) vibration modulus of normally consolidated clays', *Journal of the Soil Mechanics and Foundation Division, ASCE* **95**(SM2), 1531–1537.

Hardin, B. O. & Drnevich, V. P. (1972), 'Shear modulus and damping of soils: Measurement and parameter effects', *Journal of the Soil Mechanics and Foundation Division, ASCE* **98**(SM6), 603–624.

Hassini, S. (1990), Static and Dynamic Behavior of Pile Groups, PhD thesis, Civil Engineering, University of Michigan, Ann Arbor, Michigan.

He, Y.-A. (1990), 'The mixed boundary problem of soil-pile interaction', *Soil Dynamics & Earthquake Engineering* **9**(1), 20–24.

Hirai, H. (1987), 'An elasto-plastic constitutive model for cyclic behavior of sands', *International Journal for Numerical and Analytical Methods in Geomechanics* **11**, 503–520.

Hofstetter, G., Simo, J. C. & Taylor, R. L. (1993), 'Modified cap model: closest point solution algorithms', *Computers and Structures* **46**(2), 203–214.

Huang, T. K. & Chen, W. F. (1990), 'Simple procedure for determining plasticity model parameters', *Journal of Geotecnical Engineering* **116**(3), 492–513.

Humphrey, D. N. (1986), Design of reinforced embankment, Technical Report FHWA/IN/JHRP-86/16, Indiana Department of Transportation, JHRP.

Idriss, I. M. & Sadigh, K. (1976), 'Seismic SSI of nuclear power plant structures', *Journal of the Geotechnical Engineering Division, ASCE* **102**(GT7), 663–682.

Idriss, I. M., Seed, H. B. & Serff, N. (1974), 'Seismic response by variable damping finite elements', *Journal of the Geotechnical Engineering ASCE* **100**(GT1), 1–3.

International Conference of Building Officials (1991), *Uniform Building Code*, Whittier, California.

Isenberg, J. (1970), Interaction between soil and nuclear reactor foundation, Report to the Reasearch Foundation, University of Toledo, Toledo, OH, Agbabian-Jacobsen Associates, Los Angeles, CA.

Kagawa, T. (1991), 'Dynamic soil reaction to axially loaded piles', *Journal of Geotechnical Engineering* **117**(7), 1001–1020.

Kagawa, T. (1992), Effects of liquefaction on lateral pile responses, *in* 'Proceedings of the Conference on Piles Under Dynamic Loads', ASCE, New York, NY, USA., pp. 207–223. Geotechnical Special Publication 34.

Kana, D. D., Bouyce, L. & Blaney, G. W. (1986), 'Development of a scale model for dynamic interaction of a pile in clay', *Journal of Energy Resource Technology* **108**, 254–261.

Kausel, E. (1988), 'Local transmitting boundaries', *Journal of the Engineering Mechanics Division, ASCE* **114**(6), 1011–1027.

Kausel, E., Roesset, J. M. & Waas, G. W. (1975), 'Dynamic analysis of footings on layered media', *Journal of the Engineering Mechanics Division, ASCE* **101**(EM5), 679–693.

Kaynia, A. M. (1982), Dynamic stiffness and seismic response of pile groups, PhD thesis, MIT, Cambridge, MA.

Kaynia, A. M. & Kausel, E. (1982), Dynamics stiffness and seismic response of pile groups, Technical Report R82-03, MIT, Cambridge, MA.

Kaynia, A. M. & Kausel, E. (1991), 'Dynamics of piles and pile groups in layered soil media', *Soil Dynamics and Earthquake Engineering* **10**(8), 386–401.

Kobori, T., Minai, R. & Baba, K. (1977), Dynamic behavior of a laterally loaded pile, *in* 'Proceedings of Specialty Session 10, 9th ICMFE', Tokyo, pp. 175–180.

Kobori, T., Nakazawa, M., Hijikata, K., Kobayashi, Y., Miura, K., Miyamoto, Y. & Moroi, T. (1991), Study on dynamic characteristics of a pile group foundation, *in* 'Proceedings of the 2nd International Conference on Recent Advances in Geotechnical Earthquake Engineering and Soil Dynamics', St. Louis, Missouri.

Krishnan, R., Gazetas, G. & Veliz, A. (1983), 'Static and dynamic lateral deflection of piles in non-homogeneous soil stratum', *Geotechique* **33**(3), 307–325.

Kuhlemeyer, R. L. (1976), Static and dynamic laterally loaded piles, Research Report CE 76-09, Department of Civil Engineering, University of Calgary, Canada.

Kuhlemeyer, R. L. (1979*a*), 'Static and dynamic laterally loaded floating piles', *Journal of Geotechnical Engineering Division, ASCE* **105**, 289–304.

Kuhlemeyer, R. L. (1979*b*), 'Vertical vibration of piles', *Journal of Geotechnical Engineering Division, ASCE* **105**, 273–287.

Kuhlemeyer, R. L. & Lysmer, J. (1973), 'Finite Element Method: Accuracy for Wave Propagation Problems', *Journal of Soil Mechanics and Foundation Division, ASCE* **99**(SM5), 421–427.

Lakshmanan, N. & Minai, R. (1981), 'Dynamic soil reactions in radially non-homogeneous soil media', *Bulletin Disaster Prevention Research Institute, Kyoto University* **31**, 79–114.

Lee, C. Y. & Small, J. C. (1991*a*), 'Finite-layer analysis of axially loaded piles', *Journal of Geotechnical Engineering* **117**(11), 1706–1722.

Lee, C. Y. & Small, J. C. (1991*b*), 'Finite layer analysis of laterally loaded piles in cross-anisotropic soils', *International Journal for Numerical and Analytical Methods in Geomechanics* **15**(11), 785–808.

Lubliner, J. (1990), *Plasticity theory*, Macmillan, New York, NY.

Luco, J. E. (1974), 'Impedence functions for a rigid foundation on a layered medium', *Nuclear Engineering and Design* **31**, 204–217.

Lysmer, J. (1978), Analytical precedures in soil dynamics, *in* 'Earthquake Engineering and Soil Dynamics, Proceedings of the ASCE Geotechnical Engineering Division Specialty Conference (Pasadena,California)', Vol. III, ASCE, New York, NY.

Lysmer, J. & Drake, L. A. (1971), *A Finite Element Method for Seismology*, Vol. 11 of *Methods in Computational Physics*, Academic Press, New York, NY, chapter Seismology.

Lysmer, J. & Kuhlemeyer, R. L. (1969), 'Finite dynamic model for infinite media', *Journal of the Engineering Mechanics Division, ASCE* **95**(EM4), 859–877.

Lysmer, J., Udaka, T., Tsai, C. F. & Seed, H. B. (1977), FLUSH — a computer program for approximate 3D analysis of soil-structure interaction problems, Research Report EERC 75-30, Earthquake Engineering Research Center, University of California, Berkeley, CA.

Makris, N. & Gazetas, G. (1991), Phase wave velocities and displacement phase differences in a harmonically oscillating pile, Technical Report NCEER 91-0010, National Center for Earthquake Engineering Research, Department of Civil Engineering, SUNY at Buffalo, Buffalo, NY.

Makris, N. & Gazetas, G. (1992), 'Dynamic Pile-Soil-Pile Interaction. Part II: Lateral and Seismic Response', *Earthquake Engineering & Structural Dynamics* **21**(2), 145–162.

Malkus, D. S. & Plesha, M. E. (1986), 'Zero and negative masses in finite element vibration and transient analysis', *Computer Methods in Applied Mechanics and Engineering* **59**(3), 281–306.

Malkus, D. S., Plesha, M. E. & Liu, M.-R. (1988), 'Reversed stability conditions in transient finite element analysis', *Computer Methods in Applied Mechanics and Engineering* **68**(1), 97–114.

Mamoon, S. M. (1990), Dynamic and Seismic Behavior of Deep Fundations, PhD thesis, Civil Engineering, SUNY at Buffalo, Buffalo, NY.

Mamoon, S. M., Banerjee, P. K. & Ahmed, S. (1988), Seismic response of pile foundations, Technical Report NCEER-88-0034, National Center for Earthquake Engineering Research, SUNY, Buffalo.

Mamoon, S. M. & Ahmed, S. (1990), 'Seismic response of piles to obliquely incident SH, SV and P waves', *Journal of Geotechnical Engineering Division, ASCE* **116**(2), 186–204.

Mamoon, S. M. & Banerjee, P. K. (1990), 'Response of piles and pile-groups to traveling SH-waves', *Journal of Earthquake Engineering and Structural Dynamics* **19**(4), 597–610.

Mamoon, S. M. & Banerjee, P. K. (1992), 'Time-domain analysis of dynamically loaded single piles', *Journal of Engineering Mechanics, ASCE* **118**(11), 140–159.

Masuda, K., Saseki, F., Urao, K., Veno, K. & Miyamoto, Y. (1986), Simulation analysis of forced vibration test of actual pile foundation by thin layer method, *in* 'Proceedings Annual Meeting of Architectural Institute of Japan'.

Matlock, H. (1970), Correlations for design of laterally loaded piles in soft clay, *in* 'Proceedings 2nd Offshore Tech. Conf.', Vol. 1, Houston, TX, pp. 577–594.

Matlock, H., Fooand, H. C. & Brayant, L. M. (1978), Simulation of lateral pile behavior under earthquake motion, *in* 'Proceedings Am. Society Civ. Engrs. Specialty Conference on Earthquake Engineering & Soil Dynamics', Vol. II, Pasadana, CA, pp. 600–619.

Matlock, H. & Foo, S. H. C. (1980), Axial analysis of pile using a hysteretic degrading soil model, *in* 'Proceedings International Symposium Numerical Methods of Offshore Piling', Institution of Civil Engineers, London, pp. 127–133.

McCarron, W. O. & Chen, W. F. (1986), Documentation for cap model subroutine, Technical Report CE-STR-86-5, Purdue University.

McCarron, W. O. & Chen, W. F. (1987), 'A capped plasticity model applied to boston blue clay', *Canadian Geotechnical Journal* **24**, 630–644.

McGuire, J. W. (1993), Analytical modeling of spread footing foundations for seismic analysis of bridges, Master's thesis, Department of Civil & Environmental Engineering, Washington State University.

McGuire, J. W., Cofer, W. F., Marsh, M. L. & McLean, D. I. (1994), 'Analytical modeling of spread footing foundations for seismic analysis of bridges', *Transportation Research Record* **1447**, 80–92.

Mitwally, H. & Novak, M. (1988), Pile driving analysis using shaft models and fem, *in* 'Proceedings 3rd International Conference on Application of Stress-Wave Theory to Piles', Ottawa, Canada, pp. 455–466.

Mizuhata, K. & Kusakabe, K. (1984), Comparision of experimental and analytical results of vibration of a full scale pile, *in* 'Proceedings 8th WCEE', Vol. III, San Francisco, CA, pp. 633–640.

Mizuno, E. & Chen, W. F. (1982), Plasticity modelling for geologic media, Technical Report CE-STR-82-15, Purdue University.

Mizuno, H. (1987), Pile damage during earthquake in Japan (1923-1983), *in* T. Nogami, ed., 'Dynamic response of Pile Foundation', ASCE, pp. 53–78. Geotechnical Special Publication 11.

Mizuno, H., Iiba, M. & Kitagawa, Y. (1984), Shaking table testing of seismic building-pile-two-layered-soil interaction, *in* '8th WCEE', Vol. III, San Francisco, pp. 649–656.

Morrison, C. S. & Reese, L. C. (1988), A lateral-load test of a full scale pile-group in sand, Geotechnical Engineering Report GR 86-1, Geotechnical Engineering Center, University of Texas at Austin, TX.

Muqtadir, A. & Desai, C. S. (1986), 'Three-dimensional analysis of a pile-group foundation', *International Journal for Numerical and Analytical Methods in Geomechanics* **10**, 41–58.

NEHRP (1991), Recommended provisions for the developement of seismic regulations for new buildings, 1991 edition, part 1: Provisions part 2: Commentary, Technical report, National Earthquake Hazards Reduction Program, Building Seismic Safety Council and Federal Emergency Management Agency, Washington, D. C.

Nogami, T. (1980), Dynamic stiffness and damping of pile-groups in inhomogeneus soil, *in* 'Proceedings Session Dynamics response Pile Foundation: Analytical Aspects ASCE', pp. 31–52.

Nogami, T. (1985), 'Flexural responses of grouped piles under dynamic loading', *Earthquake Engineering and Structural Dynamics* **13**, 321–336.

Nogami, T., ed. (1987), *Dynamic Response of Pile Foundations-Experiment, Analysis and Observation : proceedings of a session of the Geotechnical Engineering Division of the ASCE Society of Civil Engineers in conjunction with the ASCE Convention*, ASCE, New York, NY, USA. Geotechnical Special Publication 11.

Nogami, T. & Konagai, K. (1986), 'Time domain axial response of dynamically loaded single piles', *Journal of Engineering Mechanics* **112**(11), 1241–1252.

Nogami, T. & Konagai, K. (1987), 'Dynamic response of vertically loaded nonlinear pile foundations', *Journal of Geotechnical Engineering* **113**(2), 147–160.

Nogami, T. & Konagai, K. (1988), 'Time domain flexural response of dynamically loaded single piles', *Journal of Engineering Mechanics Division, ASCE* **114**(9), 1512–1525.

Nogami, T. & Novak, M. (1976), 'Soil-pile interaction in vertical vibration', *Journal of Earthquake Engineering & Structural Dynamics* **4**, 277–293.

Nogami, T. & Novak, M. (1980), 'Coefficients of soil reaction to pile vibration', *Journal of the Geotechnical Engineering Division, ASCE* **106**(GT5), 565–570.

Nogami, T., Otani, J., Konagai, K. & Chen, H. L. (1992), 'Nonlinear soil-pile interaction model for dynamic lateral motion', *Journal of Geotechnical Engineering Division ASCE* **118**(1), 89–106.

Nomura, S., Tokimatsu, K. & Shamoto, Y. (1991), Soil-structure-interaction during liquefaction, *in* 'Proceedings of the 2nd International Conference on Recent Advances in Geotechnical Earthquake Engineering and Soil Dynamics', St. Louis, Missouri.

Novak, M. (1974), 'Dynamic stiffness and damping of piles', *Canadian Geotechnical Journal* **11**(4), 574–598.

Novak, M. (1977), 'Vertical vibration of floating piles', *Journal of the Engineering Mechanics Division, ASCE* **103**(EM1), 153–168.

Novak, M. (1980), Soil-pile interaction under dynamic loads, *in* 'Proceedings Numerical Methods in Offshore Piling', ICE, London, pp. 59–68.

Novak, M. (1991), Piles under dynamic loads, *in* 'Proceedings of the 2nd International Conference on Recent Advances in Geotechnical Earthquake Engineering and Soil Dynamics', St. Louis, Missouri., pp. 250–273.

Novak, M. & Aboul-Ella, F. (1978*a*), 'Impedance functions of piles in layered media', *Journal of Engineering Mechanics Division, ASCE* **104**(EM3), 643–661.

Novak, M. & Aboul-Ella, F. (1978*b*), Stiffness and damping of piles in layered media, *in* 'Proceedings Earthquake Engineering & Soil Dynamics', ASCE Specialty Conference, Pasadena, CA, pp. 704–719.

Novak, M. & El Hifnawy, L. (1984), Effect of foundation flexibility on dynamic behavior of buildings, *in* '8th WCEE', Vol. III, San Francisco, pp. 721–728.

Novak, M. & El Sharnouby, B. (1983), 'Stiffness constants on single piles', *Journal of Geotechnical Engineering Division ASCE* **109**(7), 961–974.

Novak, M. & El Sharnouby, B. (1984), 'Evaluation of dynamic experiments on pile groups', *Journal of Geotechnical Engineering* **110**(6), 738–756.

Novak, M. & Grigg, R. F. (1976), 'Dynamic experiments with small pile foundations', *Canadian Geotechnical Journal* **13**(4), 372–385.

Novak, M. & Howell, J. F. (1977), 'Torsional vibration of pile foundations', *Journal of Geotechnical Engineering Division ASCE* **103**(GT4), 271–285.

Novak, M. & Howell, J. F. (1978), 'Dynamic response of pile foundations in torsion', *Journal of Geotechnical Engineering Division ASCE* **104**(GT5), 535–552.

Novak, M. & Mitwally, H. (1990), 'Random response of offshore towers with pile-soil-pile interaction', *Journal of Offshore Mechanics and Arctic Engineering* **112**(1), 35–41.

Novak, M. & Nogami, T. (1977), 'Soil-pile interaction in horizontal vibration', *Earthquake Engineering and Structural Dynamics* **5**, 263–282.

Novak, M. & Sheta, M. (1980), Approximate approach to contact problems of piles, *in* 'Proceedings Dynamic Response of Pile Foundation: Analytical Aspects', Florida, pp. 53–79.

Novak, M. & Sheta, M. (1982), Dynamic response of piles and pile groups, *in* 'Proceedings 2nd International Conference on Numerical Methods in Offshore Piling', Texas, pp. 487–507.

Novak, M., Nogami, T. & Aboul-Ella, F. (1978), 'Dynamic soil reactions for plane strain case', *Journal of the Engineering Mechanics Division, ASCE* **104**(EM4), 953–959. Technical note.

Novak, M., Sheta, M., El Sharnouby, B. & El Hifnawy, L. (1985), *DYNA: A Computer Program for Calculation of Response of Rigid Foundations to Dynamic Loads. The Systems Analysis, Control and Design Activity*, Canada.

O'Neill, M. W. & Dobry, R., eds (1980), *Dynamic Response of Pile Foundations, Analytical Aspects: Proceedings of a Session*, ASCE, New York, N.Y.

Ostadan, F. (1983), Dynamic Analysis of Soil-Pile-Structure Systems, PhD thesis, University of California, Berkeley, CA.

Ottaviani, M. (1975), 'Three-dimensional finite element analysis of vertically loaded pile-groups', *Geotechnique* **25**(2), 159–174.

Pak, R. Y. S. & Jennings, P. C. (1987), 'Elastodynamic response of pile under traverse excitations', *Journal of the Engineering Mechanics Division, ASCE* **113**, 1101–1116.

Parmelee, R. A., Penzien, J., Scheffey, C. F., Seed, H. B. & Thiers, G. R. (1964), Seismic effects on structures supported on piles extending through deep sensitive clays, Rearch Report SESM 64-2, Institute Engineering Research, University of California, Berkeley.

Penzien, J. (1970), Soil-pile foundation interaction, *in* R. L. Weigel, ed., 'Earthquake Engineering', Prentice-Hall Inc., Englewood Cliffs, New Jersey, pp. 349–381.

Poulos, H. G. (1968), 'Analysis of settlement of pile-groups', *Geotechnique* **18**, 449–471.

Poulos, H. G. (1971), 'Behavior of laterally loaded piles. II — pile groups', *Journal of Soil Mechanics & Foundations Division ASCE* **97**(SM5), 733–751.

Poulos, H. G. (1979), 'Group factors for pile-deflection estimation', *Journal of Geotechnical Engineering Division ASCE* **105**(GT12), 1489–1509.

Poulos, H. G. (1980), An approach for the analysis of offshore pile-groups, *in* 'Proceedings Numerical Methods in Offshore Piling', ICE, London, pp. 119–126.

Poulos, H. G. & Davis, E. H. (1980), *Pile Foundations Analysis and Design*, John Wiley & Sons.

Prakash, S. & Sharma, H. D. (1990), *Pile Foundation in Engineering Practice*, Wiley, chapter 7.

Pressley, J. S. & Poulos, H. G. (1986), 'Technical notes on practical applications: Finite element analysis of mechanism of pile group behavior', *International Journal for Numerical and Analytical Methods in Geomechanics* **10**, 213–221.

Rajapakse, R. K. N. D. & Shah, A. H. (1987*a*), 'On the lateral harmonic motion of an elastic bar embedded in an elastic half-space', *International Journal of Solids and Structures* **23**, 287–303.

Rajapakse, R. K. N. D. & Shah, A. H. (1987*b*), 'On the longitudinal harmonic motion of an elastic bar embedded in an elastic half space', *International Journal of Solids and Structures* **23**, 267–285.

Rajapakse, R. K. N. D. & Shah, A. H. (1989), 'Impedence curves for elastic piles', *Soil Dynamics and Earthquake Engineering* **8**(3), 145–152.

Reese, L. C., Cox, W. R. & Koop, R. D. (1975), Field testing and analysis of laterally loaded piles in stiff clay, *in* 'Proceedings 7th Offshore Tech. Conf.', Vol. 2, Houston, TX, pp. 473–483.

Reese, L. C. & Matlock, H. (1956), Non-dimensional solution for laterally loaded piles with soil modulus proportional to depth, *in* 'Proceedings 8th Texas Conf. Soil Mech. Found. Engg.', Houston, TX, pp. 1–41.

Reese, L. C. & Sullivan, W. R. (1984), *Analysis of Stress and Deflections for Laterally Loaded Piles Including Generation of p-y Curves*, Geotechnical Engineering Center, Bureau of Engineering Research, The University of Texas at Austin, Austin, Texas. Documentation of Computer Program COM624.

Roesset, J. M. (1980), Stiffness and damping coefficient of foundations, *in* 'Proceedings of Session on Dynamics Response of Pile Found: Analytical Aspects, ASCE National Convention', Florida, pp. 1–30.

Roesset, J. M. & Angelides, D. (1979), 'Dynamic stiffness of piles: Numerical methods in offshore piling', pp. 75–82.

Roesset, J. M. & Tassoulas, J. L. (1982), Nonlinear soil-structure interaction: An overview, *in* S. K. Datta, ed., 'Earthquake Ground Motion and Its Effects on Structues', Vol. 53, Applied Mechanics Division, ASME, New York, N.Y, pp. 59–76.

Roesset, J. M., Stokoe, K. H., Baka, J. E. & Kwok, S. T. (1986), Dynamic response of vertically loaded small-scale pile in sand, *in* 'Proceedings 8th European Conference Earthquake Engineering', Vol. 2 (5.6), Lisbon, pp. 65–72.

Roscoe, K. H. & Burland, J. B. (1968), On the generalized stress-strain behavior of "wet" clays, *in* J. Heyman & F. A. Leckie, eds, 'Engineering Plasticity', Cambridge University Press, pp. 535–609.

Sanchez-Salinero, I. (1982), Static and dynamic stiffnesses of single piles, Geotechnical Engineering Report GR 82-31, Civil Engineering Department, University of Texas at Austin.

Sandler, I. S., DiMaggio, F. L. & Baladi, G. Y. (1976), 'Generalized cap model for geologic material', *Journal of Geotechnical Engineering Division, ASCE* **102 (GT7)**, 683–699.

Sandler, I. S. & Rubin, D. (1979), 'An algorithm and a modular subroutine for the cap model', *International Journal for Numerical and Analytical Methods in Geomechanics* **3**, 173–186.

Sayegh, A. F. & Tso, F. K. (1988), 'Finite element analysis of 3-d beam-columns on a nonlinear foundation', *Computers and Structures* **28**(6 1988), 699–715.

Schnabel, P. B., J., L. & Seed, H. B. (1972), SHAKE: A computer program for earthquake response analysis of horizontally layered soil, Research Report EERC 72-12, Earthquake Engineering Research Center, University of California, Berkeley, California.

Schofield, A. N. & Wroth, P. (1968), *Critical State Soil Mechanics*, McGraw-Hill, New York, NY.

Seed, H. B. & Idriss, I. M. (1969*a*), 'Analysis of soil liquefaction: Niigata earthquake', *Journal of the Soil Mechanics and Foundation Division, ASCE* **93**(SM3), 83–108.

Seed, H. B. & Idriss, I. M. (1969*b*), 'Influence of soil conditions on ground motions during earthquake', *Journal of the Soil Mechanics and Foundation Division, ASCE* **95**(SM1), 99–137.

Seed, H. B. & Idriss, I. M. (1975), Soil moduli and damping factors for dynamic response analysis, Research Report EERC 70-10, Earthquake Engineering Research Center, University of California, Berkeley, California.

Seed, H. B. & Lysmer, J. (1977), Soil-structure interaction analysis by finite element methods, state-of-the-art, *in* 'Transaction of the 4th International Conference on Structural Mechanics in Reactor Technology, SmiRT4', San Francisco, pp. 1–11. K(a) K2/1.

Seed, H. B., Lysmer, J. & Hwang, R. (1975), 'Soil-structure interaction analyses for seismic response', *Journal of the Geotechnical Engineering Division, ASCE* **101**(GT5), 439–457.

Seed, H. B., Whiteman, R. V. & Lysmer, J. (1977), Soil-structure interaction effects in the design of nuclear power plant, *in* W. J. Hall, ed., 'Structural and Geotechnical Mechanics', Prentice-Hall, Englewood Cliffs, New Jersey, pp. 220–239.

Selby, A. R. & Arta, M. R. (1991), 'Three-dimensional finite element analysis of pile groups under lateral loading', *Computers and Structures* **40**(5), 1329–1336. First International Conference on Computational Structures Technology and Edinburgh, Scotland.

Sen, R., Davis, T. G. & Banerjee, P. K. (1985), 'Dynamic analysis of pile and pile-groups embedded in homogeneous soils', *Earthquake Engineering and Structural Dynamics* **13**, 53–65.

Sheta, M. & Novak, M. (1982), 'Vertical vibration of pile groups', *Journal of Geotechnical Engineering Division ASCE* **108**(GT4), 570–590.

Shimizu, N., Yamamoto, S. & Koori, Y. (1977), 'Three-dimensional dynamic analysis of soil-structure system by thin layer element method', *Transaction Architecture Institute of Japan* **253**, 31–41.

Simo, J. C., Ju, J.-W., Pister, K. S. & Taylor, R. L. (1988), 'Assessment of CAP model: Consistent return mapping algorithms and rate dependent extension', *Journal of the Engineering Mechanics, ASCE* **114**(2), 191–218.

Singh, A. K., Hsu, T., Khatua, T. P. & Chu, S. (1980), Evaluation of soil-strucure interaction methods, *in* G. Hart, ed., 'Dynamic Response of Structures', ASCE, New York, NY, pp. 580–599.

Sooysmith, C. (1896), "'Concerning Foundations for Heavy Buildings in New York City"', *Transaction ASCE* **35**, 459–469.

Swane, I. C. & Poulos, H. G. (1982), A theoretical study of the cyclic shakedown of laterally loaded piles, Research Report R415, University of Sydney, School of Civil and Mining Engineering.

Tajimi, H. (1966), Earthquake response of foundation structures, Report of Faculty Science Engineering 3, Nithon University.

Tajimi, H. (1977), Seismic effects on piles, *in* 'Proceedings of Specialty Session 10, State-of-the-Art Report, 9th ICSMFE', Tokyo, pp. 15–26.

Takemiya, H. & Yamada, Y. (1981), 'Layered soil-pile-structure dynamic interaction', *Earthquake Engineering and Structural Dynamics* **9**, 437–458.

Terzaghi, K. & Peck, R. B. (1967), *Soil Mechanics in Engineering Practice*, 2nd edn, Wiley, New York.

Toki, K., Sato, T., Kiyono, J., Garmroudi, N. K., Emi, S. & Yoshikawa, M. (1991), 'Seismic behaviour of pile groups by hybrid experiments', *Earthquake Engineering & Structural Dynamics* **20**(10), 895–909.

Trbojevic, V. M., Marti, J., Danisch, R. & Delinic, K. (1981), 'Pile-soil-pile interaction analysis for pile groups', 6th SMIRT, Paris, France.

Trochanis, A. M., Bielak, J. & Christano, P. (1988), A three-dimensional non-linear study of piles leading to the development of a simplified model, Research Report R-88-176, Department of Civil Engineering, Carnegie Mellon University, Pittsburgh, Pennsylvania.

Trochanis, A. M., Bielak, J. & Christiano, P. (1991*a*), 'Simplified model for analysis of one or two piles', *Journal of Geotechnical Engineering* **117**(3), 448–466.

Trochanis, A. M., Bielak, J. & Christiano, P. (1991*b*), 'Three-dimensional nonlinear study of piles', *Journal of Geotechnical Engineering* **117**(3), 429–447.

Valsangkar, A. J. & Pradhanang, R. B. (1987), 'Free vibration of partially supported piles', **113**(8), 1244–1247.

Veletsos, A. S. (1977), Dynamics of structure-foundation system, *in* W. J. Hall, ed., 'Structural and Geotechnical Mechanics', Prentice Hall, Englewood Cliffs, New Jersey, pp. 333–361.

Waas, G. & Hartmann, H. G. (1981), Pile foundation subjected to dynamic horizontal loads, *in* 'Modeling and simulation of large scale structural systems', SMIRT, Paris.

Waas, G. & Hartmann, H. G. (1984), Seismic analysis of pile foundations including pile-soil-pile interaction, *in* 'Proceedings 8th WCEE, San Francisco', Vol. V, San Francisco, pp. 55–62.

Wang, H. C. (1989), A General Purpose Development of BEM for Axisymmetric Solids, PhD thesis, Civil Engineering, SUNY at Buffalo, Buffalo, NY.

Wang, H. C. & Banerjee, P. K. (1990), 'Axisymmetric transient elastodynamic analysis by BEM', *International Journal of Solids and Structures* **26**(March), 401–415.

Whirley, R. G. & Hallquist, J. O. (1991), "DYNA3D: A nonlinear, Explicit, Three-Dimensional Finite Element Code for Solid and Structural Mechanics – User Manual", Technical report, Methods Development Group, UC, LLNL.

Wolf, J. P. (1985), *Dynamic Soil-Structure Interaction*, Prentice-Hall, Inc, Englewood Cliffs, New Jersey.

Wolf, J. P. (1988), Soil-structure-interaction analysis in time domain, *in* W. J. Hall, ed., 'Prentice Hall International Series in Civil Engineering and Mechanics', Prentice-Hall, Inc, Englewood Cliffs, New Jersey.

Wolf, J. P. & von Arx, G. A. (1978), Impedence functions of a group of vertical piles, *in* 'Proceedings ASCE Specialty Conference on Earthquake Engineering & Soil Dynamics', Vol. II, Pasadena, CA, pp. 1024–1041.

Wolf, J. P. & von Arx, G. A. (1982), 'Horizontally travelling waves in a group of piles taking pile-soil-pile into account', *Earthquake Engineering & Structural Dynamics* **10**(2), 225–237.

Wolf, J. P. & Weber, B. (1986), Approximate dynamic stiffness of embedded foundation based on independent thin layers with separation of soil, *in* 'Proceedings 8th European Conference on Earthquake Engineering', Vol. 2, Lisbon, pp. 33–40. 5.6.

Woods, R. D. (1984), Lateral interaction between pile and soil, *in* 'Proceedings of the International Symposium on Dynamic Soil-Strunture Interaction', Minneapolis, MN, pp. 47–54.

Yan, L. (1990), Hydraulic Gradient Similitude Method for Geotechnical Modelling Tests with Emphasis on Laterally Loaded Piles, PhD thesis, Civil Engineering, University of British Columbia, Canada.

Zienkiewicz, O. C. (1985*a*), Coupled problems of soil-pore fluid-external fluid interaction - basis for a general geomechanics code, *in* 'Proceedings of the Fifth International Conference on Numerical Methods in Geomechanics.; Nagoya, Jpn;', Vol. 4, pp. 1731–1740.

Zienkiewicz, O. C. (1985*b*), 'Numerical modelling and geomechanics (soil-rock-concrete)', pp. 471– 499.

Zienkiewicz, O. C., Chang, C. T. & Hinton, E. (1978), 'Nonlinear seismic response and liquefaction', *"International Journal for Numerical and Analytical Methods in Geomechanics"* **2**, 381–404.

Zienkiewicz, O. C. & Shiomi, T. (1984), 'Dynamic behavior of saturated porous media: The generalized biot formulation and its numerical solution', *International Journal for Numerical and Analytical Methods in Geomechanics* **8**, 71–96.

Zienkiewicz, O. C., Pastor, M. & Xie, Y. M. (1991), Constitutive modelling of soils and computation of earthquake damage and liquefaction - state of the art paper, *in* 'Pro c. of Second Int. Conf. on Recent Advances in Geo. Earthq. Eng. and Soil Dynamics', Missouri, pp. 1743–1752.

APPENDICES

Appendix A: Soil-Pile Interaction Model for Lateral Vibration of a Single Pile

A.1 Introduction

The subgrade medium around the pile shaft is modeled within the frame of Winkler's hypothesis; i.e., the soil response at a given depth is related to the force intensity applied only at the depth considered. Figure A.1 shows a schematic view of such a soil model proposed for the nonlinear subgrade behavior. The model is completely described in Figure 2.3. The near-field element in the model can account for the nonlinear soil behavior in the vicinity of the pile shaft, and the far-field element reproduces the elastic behavior of the soil outside the region of strong nonlinear behavior (Nogami et al. 1992). The arrangement of near-field and far-field elements with masses, springs, and dashpots are shown in Figure 2.4. This arrangement enables the model to logically reproduce the nonlinear effects in the dynamic response by transferring the motion through the area of strong nonlinear behavior to the far-field. In time-domain analysis, the interface model is placed in between the pile shaft and the soil model in order to reproduce precisely the formation and behavior of a gap at the soil-pile interface.

A.2 Soil Model

Soil behavior is assumed to be more or less elastic in the area beyond some distance from the loaded pile shaft. Such a distance is artificially taken to be r_1 from the center of the pile shaft, and uniform displacements in the direction of the applied force are assumed along this artificial circle. The far-field element is defined by the behavior of the medium at the artificial circle assuming an empty hole inside of the circle. The system, as shown in Figure 2.4 with the following parameters, can reproduce the far-field element behavior very well for $0.02 < a_0 < 2.0$ (Nogami & Konagai 1988).

$$\begin{Bmatrix} K_1 \\ K_2 \\ K_3 \end{Bmatrix} = G\,\xi_k(\nu) \begin{Bmatrix} 3.518 \\ 3.518 \\ 5.529 \end{Bmatrix}, \qquad \text{[A.1]}$$

$$\begin{Bmatrix} C_1 \\ C_2 \\ C_3 \end{Bmatrix} = \left[\frac{G\,r_1}{V_s}\,\xi_k(\nu)\right] \begin{Bmatrix} 113.0973 \\ 25.133 \\ 9.362 \end{Bmatrix}, \text{and} \qquad \text{[A.2]}$$

$$m = \pi \rho_s\, r_1^2\, \xi_m(\nu) \qquad \text{[A.3]}$$

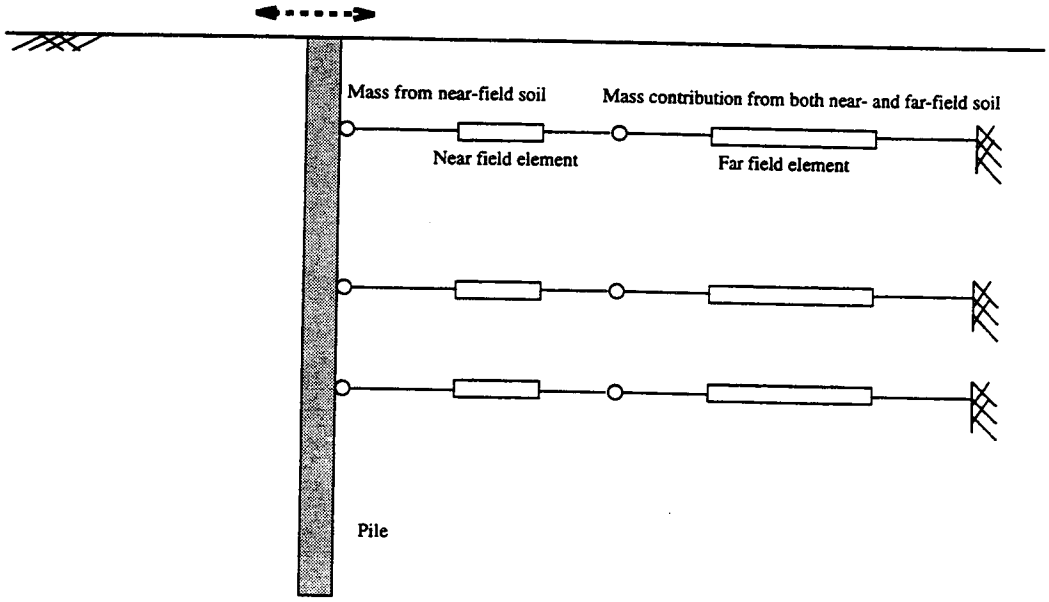

Figure A.1 Schematic representation of a soil model for subgrade behavior. Near-field elements account for the local non-linearity, and the far-field elements represent an infinite boundary. (Redrawn after Nogami 1992)

where G, ν, and V_s, are shear modulus, Poisson's ratio, and shear wave velocity of soil, respectively. $\xi_k(\upsilon)$ and $\xi_m(\upsilon)$ are parameters dependent on υ, provided in Table 2.3 and Figure 2.9. The near-field element represents the soil in the immediate vicinity of the pile, and they are strongly affected by the nonlinearity of the soil. It is modeled by the nonlinear spring and consistent mass matrix, $\mathbf{M}_n$, as shown in Equation A.4. Assuming a linear variation of the soil displacement with the radial distance from the pile, this consistent mass is defined by

$$[\mathbf{M}_n] = \left\{\frac{\pi\rho_s r_0^{\,2}}{6}\left(\frac{r_1}{r_0}-1\right)\right\}\begin{bmatrix}\frac{r_1}{r_0}+3 & 3\frac{r_1}{r_0}+1\\ 3\frac{r_1}{r_0}+1 & \frac{r_1}{r_0}+1\end{bmatrix} \qquad [A.4]$$

where ρ_s is the mass of unit volume of soil, r_0 is the radius of the pile, and r_1 is the radius of near-field zone. The degree of freedom numbers at the pile side and far-field element side are designated as 1 and 2, respectively. The nonlinear spring stiffness, k_n, is independent of frequency but dependent on the amount of its elongation.

A.3 Interface Model

Because only the amplitude and damping are needed in frequency domain analysis, the effects of the soil-pile separation can be conveniently accommodated in the complex soil stiffness, K_n. On the other hand, time domain analysis requires the response at each time step following the response process and, therefore, soil-pile separation must be treated precisely by using the interface model, as shown in Figure A.1. It is assumed that the soil displacement at the front side,

$$u_f = u^e + u^p, \qquad [A.5]$$

accompanies the soil displacement at the back side,

$$u_b = u^e + (1 - \gamma)u^p. \qquad [A.6]$$

where u^e is the elastic displacement, u^p is the plastic soil displacement, and γ is an empirical parameter between 0 and 1. Therefore, when the plastic displacement develops, the gap is formed according to $u_{gap} = \gamma u^p$. If $\gamma = 0$, no gap is formed, if $\gamma = 1$, the gap is equal to the full plastic displacement at the front side. A reasonable agreement was obtained by Nogami assuming $\gamma = 0.8$ for the particular site and pile conditions that were analyzed (Nogami et al. 1992). It is also seen that negligence of the gap effects results in overestimation of the hysteretic damping.

Appendix B: Soil-Pile Interaction Model for Axial Vibration of a Single Pile

The pile-soil interaction model for axial vibration of single piles is adopted from Nogami and Konagai (1986, 1987, 1988). This model is similar to that described in Appendix A for lateral vibration of single pile. Similar to the model for lateral vibration, this model also includes two nodes for each layer: a pile node and an auxiliary node, two lumped masses, a nonlinear near-field spring, a linear near-field viscous damper, three linear far-field springs and three linear far-field viscous dampers. The far-field spring constants, damping coefficients, and mass contribution from far-field to the auxiliary node can be obtained from the same equations given for lateral vibration, Equations A.1, A.2, and A.3, respectively. But the difference is that the functions $\xi_k(\nu) = 1$ and $\xi_m(\nu) = 1$ for all values of ν in this mode of vibration. Also, it should be obvious that all the elements would provide resistance to axial response, rather than lateral response. The complete model is shown in Figure 2.10.

Appendix C: Laboratory Test Results of Soil from Snohomish River Site

C.1 Introduction

The rheological parameters of the piles for dynamic analysis were computed for a site-specific soil at the Snohomish river site. For use in the finite element model, the constitutive properties of soils were needed. However, these properties of soil are based on the conventional soil properties. These conventional soil properties were measured in the laboratory. The tests that were performed included the moisture content test, the specific gravity test, the hydrometer test, the triaxial consolidation test, the permeability test, and the triaxial test. For the last three tests, undisturbed cylindrical samples were needed, which were made from the soil sample provided by WSDOT. The trimmed soil was used for the first three tests. In the following subsections the tests are described in brief. The results are summarized in Tables C.1 through C.6 and Figures C.1 through C.4. The laboratory measured quantities are used to compute some other properties which are given in Table C.7.

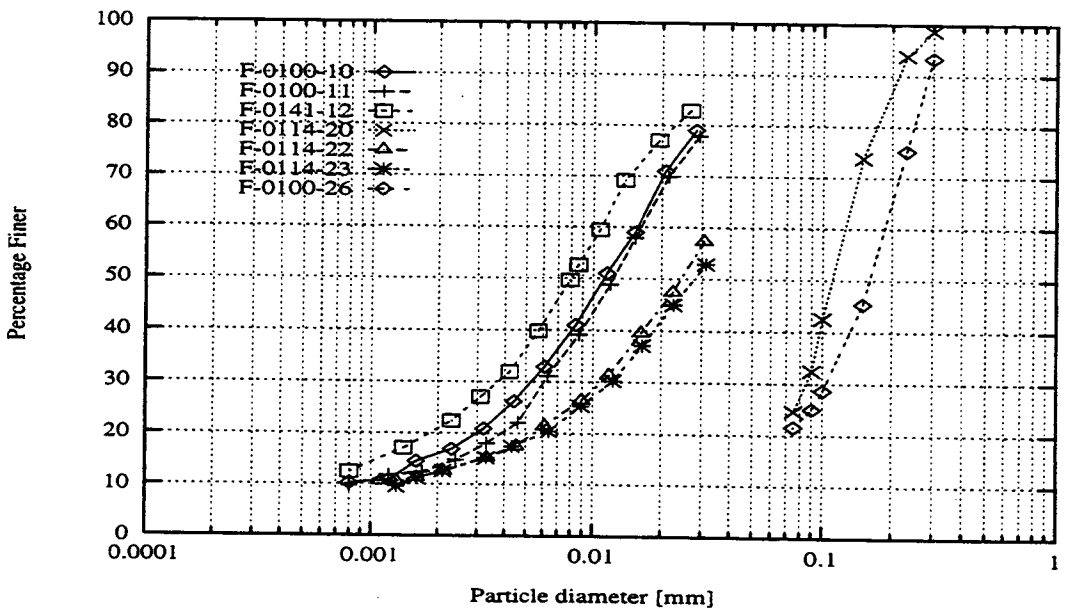

Figure C.1 Grain size distribution.

The isotropic consolidation and the triaxial tests were done on samples of diameters 3.7 cm and with an approximate length/diameter ratio of 2.5. Comprehensive and

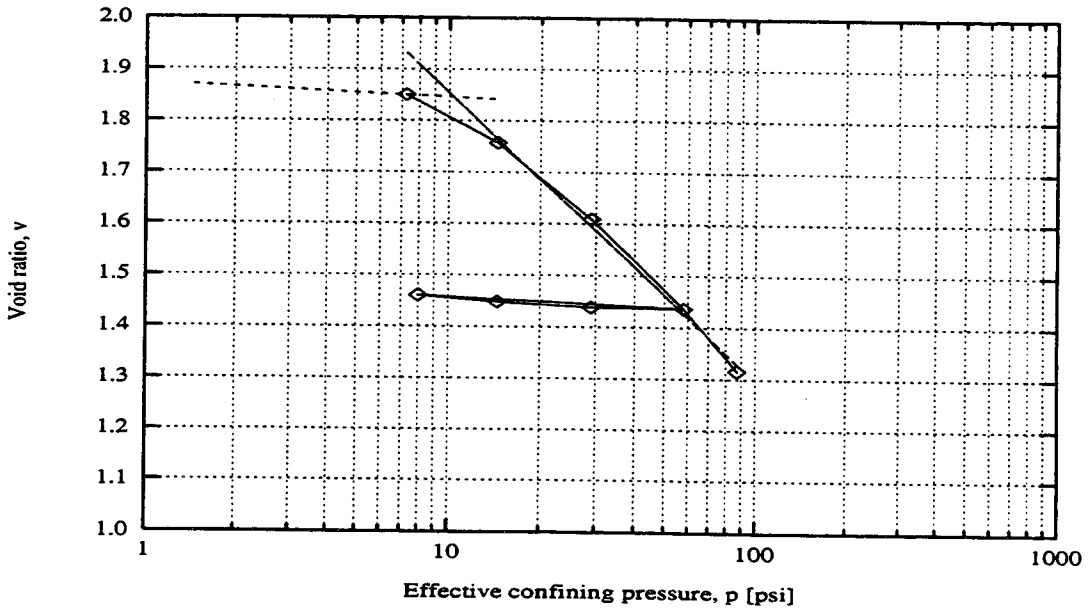

Figure C.2 Void ratio-effective mean stress relationship.

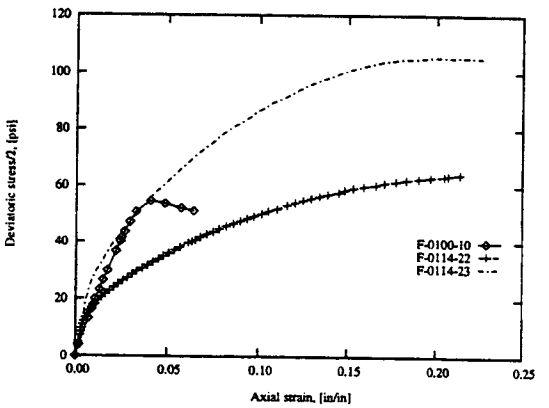

(a)

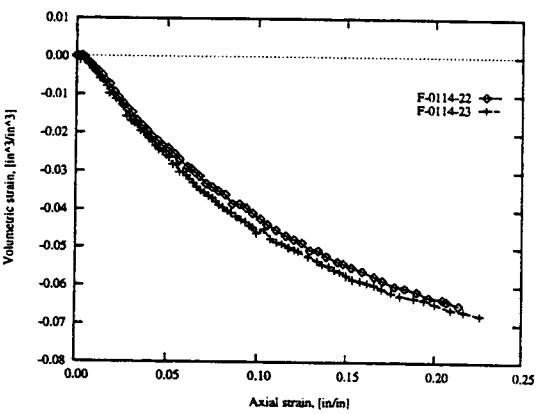

(b)

Figure C.3 Drained triaxial test results.

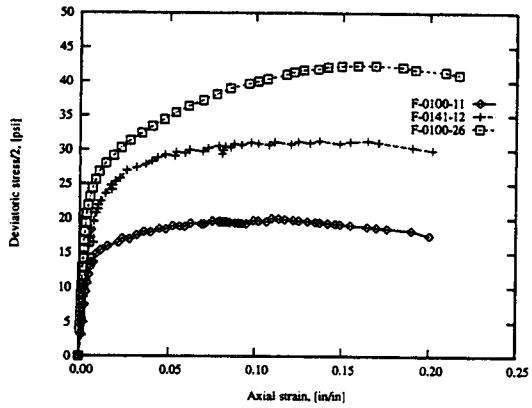

(a)

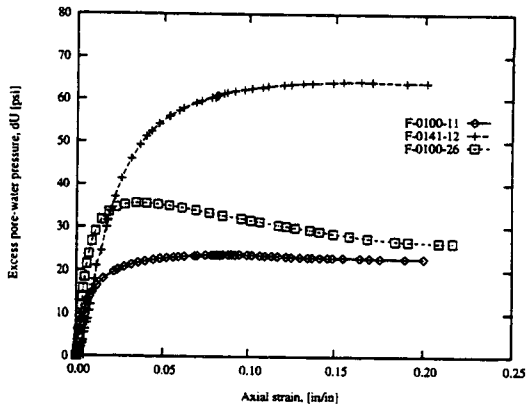

(b)

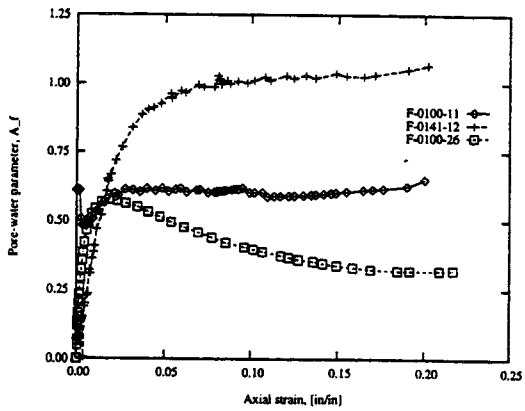

(c)

Figure C.4 Undrained triaxial test results.

Table C.1 Description and identification of soil samples from Snohomish river site.

Bore hole location		Hole	Dr.	Tube	Depth	Sample	SPT	WSDOT
Station	Offset	No.	No.	posn.		ID		Unit
LE 65+62	15′ RT	T-H-9-92	U4	B	22′04″–22′08″	F-0100-10	2-4	2-4A
LE 65+62	15′ RT	T-H-9-92	U4	B	22′08″–23′00″	F-0100-11	2-4	2-4A
LE 65+62	15′ RT	T-H-9-92	U8	E	48′04″–48′08″	F-0100-26	6-8	5
LE 65+62	15′ RT	T-H-9-92	U8	F	48′08″–49′00″	F-0100-27	6-8	5
LE 80+44	18′ RT	T-H-12-92	U3	B	19′08″–20′00″	F0141-11	0-2	2
LE 80+44	18′ RT	T-H-12-92	U3	C	19′08″–20′00″	F0141-12	0-2	2
LE 83+22	18′ OC	T-H-11-92	U9	B	25′08″–26′00″	F-0114-20	0-4	2-3
LE 83+22	15′ OC	T-H-11-92	U9	B	30′00″–30′04″	F-0114-22	0-4	3
LE 83+22	15′ OC	T-H-11-92	U9	B	30′04″–30′08″	F-0114-23	0-4	3

Notes:

1. Snohomish river to Ebey Slough east bound replacement
2. Contact number L-0666
3. WSDOT soil descriptor
   - Unit 1A: Fill – sand and gravel.
   - Unit 1B: Fill – gravelly sand, silty sand, and sand.
   - Unit 2: Very soft to soft, clayey silt, sandy silt, organic silt, and silty clay with thin to thick layers of peat. Fibrous organic material is present.
   - Unit 3: Very loose to loose sand and silty sand.
   - Unit 4: Medium dense to very dense slightly silty sand.
   - Unit 4A: Medium dense to dense sand, gravelly sand and sandy gravel with variable amount of silt and inter-bed of sandy silt. Cobbles might be encountered.
   - Unit 5: Inter-bedded medium stiff to stiff clayey silt and sandy silt, and medium dense to very dense silty sand.

Table C.2 The physical properties of soils from Snohomish river site.

Sample designator	Depth (ft)	Moisture content	Degree of saturation	Sp. Gr. of solid	Bulk den.	LL	PL	PI
F-0100-10	20.50	62.1	91.2	2.63	1.528	40.4	36.4	4.0
F-0100-11	22.83	56.8	91.7	2.64	1.571	40.4	34.9	4.5
F-0100-26	48.50	28.0	85.0	2.71	1.833	22.3	xxxx	xxxx
F-0114-22	30.17	43.2	89.5	2.71	1.681	31.2	26.7	4.5
F-0114-23	30.41	34.5	89.0	2.73	1.784	27.1	23.5	3.5
F-0141-12	19.50	56.3	79.1	2.75	1.453	54.9	40.9	14.0

xxxx data not available

Table C.3 The grain size distribution and classification.

Sample designator	Grain sizes in mm					Coefficient		Classification	
	D_{10}	D_{20}	D_{30}	D_{60}	D_{70}	C_u	Cc	*USGS*	*WSDOT*
F-0100-10	0.0008	0.004	0.011	0.016	0.020	20.0	1.25	ML	Unit 2
F-0100-11	0.0008	0.005	0.012	0.016	0.020	20.0	1.95	ML	Unit 2
F-0100-26	0.0300	0.100	0.160	0.170	0.210	5.67	2.10	SM	Unit 3
F-0114-20	0.0300	0.085	0.110	0.130	0.140	4.33	1.65	SM	Unit 2
F-0114-22	0.0010	0.011	0.024	0.032	0.046	32.0	4.18	ML	Unit 3
F-0114-23	0.0013	0.028	0.040	0.040	0.070	30.8	2.50	ML	Unit 3
F-0141-12	0.0006	0.004	0.008	0.010	0.014	16.7	2.67	MH	Unit 2

Table C.4 The isotropic-consolidation test results of soil from Snohomish river site.

Sample designator	Depth ft	e_0	C_c	C_r	p_{precon} psi	σ''_v psi	OCR
F-0100-10	20.50	1.79	0.51	0.042	21.18	14.91	2.20
F-0100-11	22.83	1.37	0.40	0.036	11.60	15.56	1.15
F-0100-26	48.50	0.89	0.14	0.031	22.63	38.54	1.00
F-0114-22	30.17	1.29	0.48	0.084	11.60	22.00	1.00
F-0114-23	30.41	1.05	0.46	0.023	22.77	23.53	1.50
F-0141-12	19.50	2.01	0.51	0.028	12.33	12.29	1.55

Note: OCR is based on $\gamma = 102.44$ pcf and $K_0 = 0.47$.

Table C.5 The drained triaxial test results of soil from Snohomish river site.

Sample designator	Depth ft	E' psi	K' psi	$\sigma'_{v0} = \sigma'_{h0}$ psi	σ'_v psi	$\frac{\sigma_{vf}-\sigma_{hf}}{2}$ psi	ϵ_{vf} in/in	$epsilon_{af}$ in/in
F-0100-10	20.50	36600	37900	24.8	140.8	58.0		0.20
F-0114-22	30.17	54600	36500	58.2	184.2	63.0	-0.063	0.04
F-0114-23	30.41	63100	63100	86.6	298.6	106.0	-0.065	0.20

Table C.6 The undrained triaxial test results of soil from snohomish river site.

Sample designator	Depth ft	E psi	K psi	$\sigma'_{v0} = \sigma'_{h0}$ psi	Δu_f psi	σ'_{hf} psi	σ'_{vf} psi	S_u psi	$\frac{S_u}{\sigma'_{v0}}$
F-0100-11	22.83	5200	553900	36.3	23.5	12.8	52.8	20.0	0.551
F-0100-26	48.50	14820	679500	57.2	24.3	32.9	117.5	42.3	0.740
F-0141-22	19.50	5780	47979	87.0	65.0	22.0	84.6	31.3	0.360

Table C.7 Some computed soil properties of soil from Snohomish river site.

Sample no.	**Depth ft**	ν'	G' **psi**	ν_u	G_u **psi**	c' **psi**	ϕ' **degree**	c **psi**	ϕ **degree**
F-0100-10	20.50	0.34	1367			2.344	32.05		
F-0114-22	30.17	0.25	2183			2.344	32.05		
F-0114-23	30.41	0.44	2190			2.344	32.05		
F-0100-11	22.83			0.498	1735	2.344	32.05	9.892	10.5
F-0100-26	48.50			0.496	4951	2.344	32.05	9.892	10.5
F-0141-12	19.50			0.4498	1929	2.344	32.05	9.892	10.5

successful tests were done on six samples out of nine samples provided by WSDOT. Consolidation tests were performed isotropically to obtain pressure volume change behavior. Subsequently, triaxial tests were performed on these six samples. Undrained triaxial tests were performed on three, and drained triaxial tests were performed on the remaining three samples. For all the tests, standard procedures were followed.

Consolidation was initiated after saturation was completed. The confining pressure was increased with an increment factor of 2. The change in void ratio was calculated using the change in volume that was measured, and the volume of the solid was calculated from the initial conditions of the soil. After performing the test, the void ratio was plotted with the effective confining pressure as an e-$\log_{10} p$ plot. The compression index, C_c, was calculated from the steepest slope by regression analysis, and the recompression index, C_r, was calculated from unloading data or, in some cases, from the first load increment. The results are summarized in Table C.4 and in Figure C.2.

The triaxial tests were performed on the consolidated soil samples after performing the isotropic-consolidation tests. The consolidated drained (CD) test was performed at a strain rate of 0.08%/min. The consolidated undrained (CU) test was performed at a much faster rate. In the CD test, the volume change was measured using the water flowing in or out of the sample. The tangent modulus was obtained by regression analysis on the initial portion of the stress-strain curves. Ultimate stress was obtained either from the peak value or the value at 20% strain. Using regression analysis, the values of the intercept and the slope in the p-q diagram were obtained and the Mohr circle parameters were obtained from those data. The same procedure was followed to obtain the Mohr circle parameters for the undrained condition. Since pore water pressure was measured in undrained tests, the effective stress properties obtained from undrained tests were also used in addition to those obtained from the drained triaxial tests to compute effective strength parameters. The results are summarized in Tables C.5 through C.7 and in Figures C.3 and C.4.

Appendix D: Geologic Cap Model for Soil

The Cap model is a nonlinear elastic-plastic isotropic work hardening plasticity model. Originally, it was developed from the classical incremental theory of work-hardening plasticity for materials which have time and temperature independent properties. In general, cap models describe the yielding behavior of soil with an ultimate yield surface that is fitted with a movable end cap. Both the ultimate yield and cap surfaces are symmetric about the hydrostatic axis. The movement of the cap is controlled by the hardening and softening behavior of the soil, which is expressed as a hardening law and rate of strain. For some versions of the cap model, the ultimate failure surface is also allowed to move as controlled by a hardening law. Strains are elastic for stress changes that fall within the region defined by the ultimate yield and cap surface, but are elastic-plastic for stress changes on the surfaces.

The first such model for use in soil mechanics was proposed by Drucker, et al. (Drucker et al. 1957). It consisted of a cone shaped extended von-Mises or Drucker-Prager ultimate yield surface (Drucker & Prager 1952) fitted with a spherical end cap. Both the cone and cap expand as the soil strain hardens. The current soil density was used in the hardening law to control the position of successive yielding surfaces. The concept of isotropic hardening plasticity was incorporated into the Cam-Clay model (Schofield & Wroth 1968) for triaxial behavior of clay. It was extended to the general three dimensional stress state by Roscoe and Burland (1968). The model uses the concept of a critical state line on which failure of an initially isotropically consolidated sample will occur regardless of the stress path (Atkinson & Bransby 1978). A generalized cap model was proposed by DiMaggio and Sandler (1971) and developed further by others (Sandler et al. 1976, Sandler & Rubin 1979, Simo et al. 1988, Hofstetter et al. 1993, Whirley & Hallquist 1991). The yield function consists of a fixed ultimate yield surface fitted with a movable elliptical strain-hardening cap. Movement of the cap was controlled by

the plastic volumetric strain. The cap controls plastic dilation once the failure stress is reached.

Several models based on work hardening theory are available for modeling porous media. The model which was used in this study was developed at Purdue University (Mizuno & Chen 1982, Chen & Baladi 1985, McCarron & Chen 1986, McCarron & Chen 1987, Huang & Chen 1990). This model was used for its simplicity and immediate availability.

With the underlying assumption that soil behavior is independent of the orientation of the principal axes (isotropic), the model is formulated in terms of the stresses using the first invariant of the stress tensor, I_1', and the second invariant of the stress tensor or stress deviator tensor J_2', given by

$$I_1' = \sigma_1' + \sigma_2' + \sigma_3', \qquad [D.1]$$

$$J_2' = \frac{1}{6}\left[(\sigma_1' - \sigma_2')^2 + (\sigma_2' - \sigma_3')^2 + (\sigma_3' - \sigma_1')^2\right], \qquad [D.2]$$

where σ_1' = Major effective principal stress,
σ_2' = Intermediate effective principal stress, and
σ_3' = Minor effective principal stress.

The first invariant of the stress tensor, I_1', is simply the sum of the effective normal stresses, or equivalently three times the effective pressure. The square root of the second invariant of the deviatoric stress tensor, $\sqrt{J_2'}$, is an objective scalar measure of the distortional or shearing stress.

The cap model consists of three surfaces in space, as shown in Figure D.1. First, there is a failure envelope surface denoted by f_1:

$$f_1 = \sqrt{J_2} - F_e(I_1') = 0, \qquad [D.3]$$

where F_e is given by

$$F_e(I_1') = \kappa - \alpha I_1', \qquad [D.4]$$

This failure envelope surface is fixed in space and therefore does not harden. Next, there is a cap surface denoted by f_2:

$$f_2 = \sqrt{J_2} - F_c(I_1, \kappa) = 0, \qquad [D.5]$$

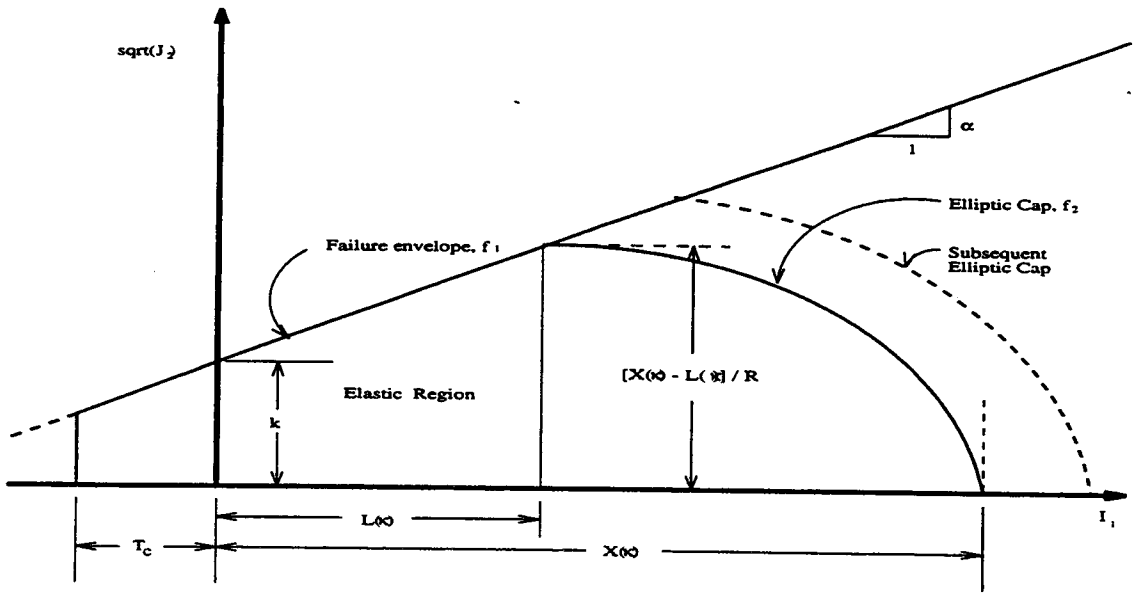

Figure D.1 Cap model in I_1'–J_2 space. (After Chen 1985)

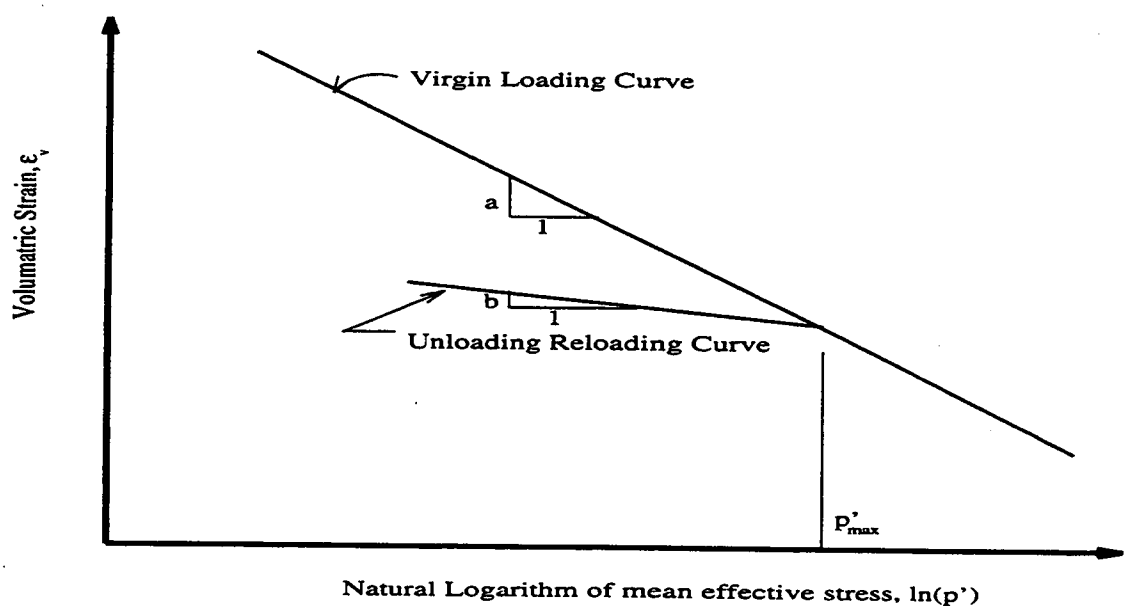

Figure D.2 Relation between ϵ, b, and $\ln p$. (After Humphrey 1986)

where F_c is defined by

$$F_c(I_1', \kappa) = \frac{1}{R}\sqrt{[X(\kappa) - L(\kappa)]^2 - [I_1' - L(\kappa)]^2}, \qquad [D.6]$$

$X(\kappa)$ is the intersection of the cap surface with the I_1' axis,

$$X(\kappa) = L(\kappa) + R\,F_e(\kappa), \qquad [D.7]$$

and the value of R is the ratio of major to minor axes of the quarter ellipse defining the cap surface. R is defined by

$$R = \frac{X(\kappa) - L(\kappa)}{F_c(L(\kappa), \kappa)}, \qquad [D.8]$$

and $L(\kappa)$ is defined by

$$L(\kappa) = \begin{cases} l(\kappa) & \text{if } \kappa > 0 \\ 0 & \text{if } \kappa \leq 0 \end{cases}. \qquad [D.9]$$

The hardening parameter, κ, is related to the plastic volume changes, ϵ_v^p, through the hardening law.

$$\epsilon_v^p = W\,\{exp[DX(\kappa)] - 1\}. \qquad [D.10]$$

The value of W represents the void fraction of the uncompressed sample, and D governs the slope of the initial loading curve in hydrostatic compression. Finally, there is the tension cutoff surface, denoted by f_3. The function f_3 is given by

$$f_3 = T - I_1' = 0, \qquad [D.11]$$

where T is an input material parameter which specifies the maximum hydrostatic tension sustainable by the material. The elastic domain in $I_1' - J_2^{1/2}$ space is then bounded by the failure envelope surface above, the tension cutoff surface on the left, and the cap surface on the right.

The yield condition may be written as

$$f_1(\sigma) \leq 0 \qquad [D.12]$$

$$f_2(\sigma, \kappa) \leq 0 \qquad [D.13]$$

$$f_3(\sigma) \leq 0 \qquad [D.14]$$

and the plastic continuity condition requires that

$$\lambda_\kappa f_\kappa = 0 \qquad [D.15]$$

$$\lambda_\kappa \geq 0 \qquad [D.16]$$

where $\kappa = 1$, 2, and 3; and λ_k is the plastic consistency parameter for surface k. If $f_k < 0$, then $\lambda_k = 0$ and the response is elastic. If $f_k > 0$, then surface k is active and λ_k is found from the requirement that $f_k = 0$.

An additive decomposition of the strain into elastic and plastic parts is assumed:

$$\epsilon_{ij} = \epsilon^e_{ij} + \epsilon^p_{ij} \qquad [D.17]$$

where ϵ^e_{ij} is the elastic strain, and ϵ^p_{ij} is the plastic strain. Stress is found from the elastic strain using Hooke's law,

$$\sigma_{ij} = C_{ijkl} (\epsilon_{kl} - \epsilon^p_{kl}), \qquad [D.18]$$

where σ is the stress, and C is the elastic constitutive tensor.

Associated plastic flow is assumed so, using Koiter's flow rule, the plastic strain rate is given as the sum of contributions from all of the active surfaces,

$$\epsilon_{ij} = \sum_{k=1}^{3} \lambda_k \frac{\partial f_k}{\partial \sigma_{ij}} \qquad [D.19]$$

D.1 Elasto-Plastic Constitutive Relationship

The constitutive matrix depends on the current state of stress. If the stress point is such that it falls within the yield surface, then the stiffness matrix is the same as that for elastic stiffness. If the stress point falls on the specific yield surface, elasto-plastic stiffness should be used. The elasto-plastic stiffness depends on the yield surface.

A general formulation of the elasto-plastic stiffness matrix computation for the cap model described in the previous section was presented by Chen and McCaron (1983) and McCarron & Chen (1986). Detailed derivation is also given by others (Mizuno & Chen 1982, Humphrey 1986). This formulation has been used in this work.

The formulation presented in those references is based on the tangent stiffness approach. However, it has been found that the tangent stiffness operator consistent with "continuum" elasto-plastic equations performs much better than the tangent stiffness operator. The reasons lie in the consistency of state determination and stiffness computation. It is expected that the consistent tangent stiffness will improve the convergence.

D.2 State Determination

In finite element analysis it is necessary to compute the stresses and the internal variables for a strain increment starting with a known state. The algorithm for this determination is given in Sandler and Rubin (1979), Chen and Baladi (1985), and Chen and Han (Chen & Han 1988). This involves numerical integration of the rate form of the constitutive equations. The details of the procedure of this integration depend on the stress path. Also, subintegration with forward or backward integration is needed. For every increment, it is necessary to keep the stress point on the yield surface if elasto-plastic strain is involved.

The algorithm described by Chen and Baladi (1985) was adopted with the modification (Simo et al. 1988) in the "corner coding".

D.3 Procedure for Determination of Cap Parameters

There are 16 parameters used to describe soil behavior in the current version of the cap model. They can be conveniently grouped into parameters for the ultimate failure surface, elastic behavior, strain hardening cap, initial stress, and pore pressure response. They are generally based on experimental data. The parameters κ and α are usually evaluated by fitting a curve through failure data taken from a set of triaxial compression tests. The parameters W, D, and X_0 define the cap hardening law. Additional details and guidelines for fitting the cap model to experimental data may be found in the book by Chen and Baladi (1985).

Traditionally, the model parameters, for example, R, X_0, D, and W, were obtained by using a trial and error procedure or using an optimization procedure (Simo et al. 1988). These procedures are tedious for routine applications. New procedures were developed (Chen & McCarron 1983, Humphrey 1986, Huang & Chen 1990) to determine the bulk modulus, hardening parameters, cap aspect ratio, and initial cap position which eliminate the need for a trial and error solution. The parameters can be determined from commonly available soil properties such as results from consolidation tests and consolidated undrained triaxial tests on normally consolidated samples. The procedures are described in the following sections.

D.3.1 Ultimate Failure Surface

The Drucker-Prager criterion is used to describe the ultimate failure surface. Its circular cross-section is an approximation of the Mohr-Coulomb criterion which has a hexagonal shape in stress (Chen & Saleeb 1982). For triaxial compression ($\sigma_2 = \sigma_3$) the criteria can be matched on the compressive meridian to obtain the material constants α and κ from shear strength parameters c' and ϕ' by

$$\alpha = \frac{2\sin\phi'}{\sqrt{3}(3-\sin\phi')}, \qquad [D.20]$$

and,

$$\kappa = \frac{6c'\cos\phi'}{\sqrt{3}(3-\sin\phi')}. \qquad [D.21]$$

The tension cut-off, T_c, specifies a limiting value of tensile stress for soils with non-zero cohesion. Since most soils can not support significant tensile stress, the value of T_c can be taken close to but greater than zero.

D.3.2 Elastic Behavior

Elastic behavior is governed by the bulk modulus, K, and shear modulus, G. In the model, K is assumed to be a function of I_1'.

$$K = K_1 A_p \left[I_1' / (3A_p) \right]^{K_2} \qquad [D.22]$$

where A_p is atmospheric pressure, which non-dimensionalizes the formulation. The bulk modulus parameters, K_1 and K_2, are determined from the unloading/reloading portion of a hydrostatic consolidation test. This curve is assumed to be linear on an $\epsilon_v - ln(p')$ plot where p' is the mean effective stress.

$$p' = I_1'/3. \qquad \text{[D.23]}$$

Furthermore, curves for unloading from different maximum values of p' are assumed to be parallel, all having a slope of b, given by

$$b = \frac{\epsilon_{v2} - \epsilon_{v1}}{ln(p_2') - ln(p_1')} \qquad \text{[D.24]}$$

where ϵ_{v2}, ϵ_{v2}, p_1' are shown in Figure D.2. A similar approach is used in the modified Cam-clay soil model (Wroth and Houslby 1985) . In the limit, as point 1 approaches point 2, Equation D.24 becomes

$$b = \frac{d\epsilon_v}{d(ln\ p')} = \frac{d\epsilon_v}{dp'}\ p'. \qquad \text{[D.25]}$$

Rearranging and using the definition of K,

$$K = \frac{dp'}{d\epsilon_v} = \frac{p'}{b}. \qquad \text{[D.26]}$$

For linear unloading/reloading curves

$$K_2 = 1, \qquad \text{[D.27]}$$

$$K_1 = 1/b, \ and \qquad \text{[D.28]}$$

$$K = p'/b. \qquad \text{[D.29]}$$

In many cases, only results of one-dimensional consolidation tests are available. For this test, the average slope of the unloading/reloading curve on a e-log(σ_v') scale is the recompression index, C_r. If the unloading /reloading curves from hydrostatic and one-dimensional consolidation tests are assumed to be parallel, b and C_r are related by

$$b = \frac{C_r}{\ln(10)\ (1 + e_0)}, \qquad \text{[D.30]}$$

where e_0 is the initial void ratio. Wroth and Houlsby (1985) noted that the curves are not parallel since the coefficient of lateral earth pressure, K_0', is not constant during unloading/reloading, and that the above equation will underestimate b; however, the approximation is adequate for most purposes.

The shear modulus is known to increase with I_1' and with consolidation ratio OCR (Wroth and Houslby 1985). However, test data on the relationship is limited. In this work, it is assumed that G is either constant or proportional to the bulk modulus. The latter assumption allows G to increase with I_1', but the effect of OCR is not considered. Accordingly, the following relation is used:

$$G = G_2 + G_1 K, \qquad \text{[D.31]}$$

where G is a constant equal to G_2 when G_1 is 0. For G_2 equals 0, G is a multiple of K, which implies that Poisson's ratio, v', is constant. Young's modulus, E, can be evaluated from the slope of an unloading/reloading cycle of a triaxial test and then G is given by Chen and Saleeb (1982)

$$G = \frac{3KE}{9K - E}. \qquad \text{[D.32]}$$

If test data is not available, a reasonable value of Poisson's ratio for effective stress ν can be assumed (Wroth and Houslby 1985), and G is computed from

$$G = \frac{3K\ (1 - 2\nu)}{2\ (1 + \nu)}, \text{ or} \qquad \text{[D.33]}$$

$$G = \frac{E}{2\ (1 + \nu)}, \text{ if } \nu = 0. \qquad \text{[D.34]}$$

It should be noted that taking G as a function of K can lead to the generation of energy on some loading/unloading paths.

D.3.3 Cap Surface Parameters

The derivation of the formulae needed here is quite complicated. The formulae are presented here only. The reader is referred to (Humphrey 1986) for details.

1. The ratio of $J_2^{1/2}$ at failure and the initial vertical stress for a consolidated undrained test is given by

$$\frac{{J_{2f}}^{1/2}}{\sigma_{vo}\prime} = -\frac{2}{\sqrt{3}}\frac{S_u}{\sigma'_{vo}} \qquad [D.35]$$

2. The equation for the X parameter at the time of failure and the initial X parameter is given by

$$\frac{X_f}{X_0} = \exp\left\{-\frac{b}{a+b}\ln\left[\frac{\kappa/\sigma'_{vo} - {J_{2f}}^{1/2}/\sigma'_{vo}}{\alpha\,(1+2K_0)}\right]\right\}, where \qquad [D.36]$$

$$a = \frac{C_c}{\ln(10)\,(1+e_0)}, \text{ and} \qquad [D.37]$$

$$b = \frac{C_r}{\ln(10)\,(1+e_0)}. \qquad [D.38]$$

3. The value of DX_0 can be found from

$$DX_0 = 2\,\frac{\ln[(1-P)/P]}{(X_f/X_0 - 1)}, \text{where} \qquad [D.39]$$

$$P = \frac{\ln[(1+X_f/X_0)/2]}{\ln(X_f/X_0)} \qquad [D.40]$$

The value of D can be found as soon as X_0 is known. X_0 can not be found until R is known.

4. The value of W can be found from the following equation.

$$W = \frac{\ln(X_f/X_0)}{\exp[(DX_0)(X_f/X_0)] - \exp[DX_0]}\,(b-a). \qquad [D.41]$$

5. The value of R can be found from the implicit equation stated below by trial and error or some other procedure.

$$\frac{X_f}{X_0} = \frac{[\,(\kappa/\sigma'_{v0})(1-\alpha R) - ({J_{2f}}^{1/2}/\sigma'_{v0})(1-\alpha^2R^2)]}{\alpha\,[-R\,(\kappa/\sigma'_{v0}) + (1+2K_0) - RH^{1/2}]}, \text{where} \qquad [D.42]$$

$$H = (1-K_0)^2(\alpha^2R^2-1)/3 + \alpha^2(1+2K_0)^2 + (\kappa/\sigma'_{v0}) - 2\alpha(\kappa/\sigma'_{v0})(1+2K_0) \qquad [D.43]$$

6. The initial cap position, X_0, for normally consolidated soil can be found from the following equation.

$$X_0 = \left[(1+2K_0) - R(\kappa/\sigma'_{v0}) - RH^{1/2}\right] \left\{\frac{\sigma'_{v0}}{1-\alpha R}\right\}. \qquad [D.44]$$

For overconsolidated soil the equation becomes

$$X_0 = \kappa/\alpha - (R+1/\alpha)\, {J_2}_f{}^{1/2}. \qquad [D.45]$$

D.4 Advantages of the Cap Model

One of the major advantages of the cap model over other classical pressure-dependent plasticity models is its ability to control the amount of dilatancy produced under shear loading. Dilatancy is produced under shear loading as a result of the yield surface having a positive slope in I'_1 - $\sqrt{J'_2}$ space, so that the assumption of plastic flow in the direction normal to the yield surface produces a plastic strain rate vector that has a component in the volumetric (hydrostatic) direction. In models such as those of Drucker-Prager (1952) and Mohr-Coulomb, this dilatancy continues as long as shear loads are applied, and in many cases produces far more dilatancy than is experimentally observed in material tests. In the cap model, when the failure surface is active, dilatancy is produced just as with the Drucker-Prager and Mohr-Coulomb models. However, the hardening law permits the cap surface to contract until the cap interacts with the failure envelope at the stress point, and the cap remains at that point. The local normal to the yield surface is now vertical, and therefore, the normality rule assures that no further plastic volumetric strain (dilatancy) is created. Adjustment of the parameters that control the rate of cap contraction permits experimentally observed amounts of dilatancy to be incorporated into the model, thus producing a constitutive law which better represents the physics to be modeled.

Another advantage of the cap model over other models, such as those of Drucker-Prager and Mohr-Coulomb, is the ability to model plastic compaction. In these models, all purely volumetric response is elastic. In the cap model, volumetric response is elastic

until the stress point hits the cap surface. Thereafter, plastic volumetric strain (compaction) is generated at a rate controlled by the hardening law. Thus, in addition to controlling the amount of dilatancy, the introduction of the cap surface adds another experimentally observed response characteristic of geological materials into the model.

D.5 Limitations of the Cap Model

The cap model has at least the following limitations (Humphrey 1986).

- The prediction of pore water pressure changes due to change in strain in an undrained condition is not satisfactory. This is particularly true when stress reversal is observed. The reason is that that effective stress path is obtained from the total stress path. This limitation is not expected to affect the solution of deformable porous media significantly, because in this case the pore water pressure is already known before. This makes the computational stress path equivalent to an undrained path.
- The model does not properly account for the strain softening behavior. Strain softening was not considered in this work.
- It is very difficult to compute the initial value of X_0 for the initial insitu state of an overconsolidated clay. Moreover, the error involved here deteriorates the pore water prediction. The effect of OCR was considered in the determination of the cap parameters in this work.

D.6 Soil Parameter Computation

For computing all these parameters, a computer program was written in FORTRAN which is presented at the end of this appendix. The basic parameters used in this computation are presented in Tables D.1 through D.2. The resulting cap parameters for those soils at different layers are presented in Table D.3. In Table D.1, some averaging

was used to obtain a set of uniform values throughout the depths. In Table D.2, the following formulas were used. The mean stress was computed as

$$p' = \frac{1 + 2K_0'}{3}\sigma_v'. \qquad [D.46]$$

The value of the depth was computed assuming the GWT would be much below such that drained condition would be maintained. In that case

$$h = \frac{\sigma_v'}{\gamma}. \qquad [D.47]$$

The OCR was estimated for the laboratory test result of the soil sample of the same depth. The value of e_0 was estimated for that specific depth from soils of nearby depth. The E' was found linearly varying with confining pressure, p'. From the laboratory test, it was found to be

$$E' = 2702 + 43.24p', \text{ psi}. \qquad [D.48]$$

The bulk modulus, K' was computed as

$$K' = \frac{p'}{b} = \frac{2.303(1 + e_0)}{C_r}p'. \qquad [D.49]$$

The Poisson's ratio, ν', was obtained from the following formula

$$\nu' = 0.5 - \frac{E'}{6K'}. \qquad [D.50]$$

If ν' was found to be negative, the E' was adjusted such that, ν' becomes 0.10. This means that ν' was limited as, $0.10 \leq \nu' \leq 0.5$. The shear modulus, G', was computed from the following relation.

$$G' = \frac{E'}{2(1 + \nu')}. \qquad [D.51]$$

Table D.1 Depth independent basic soil parameters used to compute cap parameters

Parameters		Average values	
C_c	=	0.476	
C_r	=	0.0337	
c'	=	2.340	psi
ϕ'	=	32.05^0	
$(K_0)_{consolidation}$	=	1.0	(isotropic consolidation)
$(K_0)_{field}$	=	0.50	(estimated)
γ	=	102.4	pcf

Table D.2 Depth dependent basic soil parameters used to compute cap parameters

σ'_v	h	OCR	p'	E'	Strength		
					e_0	$\sigma'_{v0,con}$	$\frac{S_u}{\sigma'_{v0,con}}$
psi	**ft**		**psi**	**psi**		**psi**	
0.5	00.5	3.50	0.33	85.2	1.191	11.67	0.668
1.0	1.41	3.50	0.66	240.2	1.191	11.67	0.668
2.5	3.51	3.00	1.67	606.0	1.221	11.67	0.668
5.0	7.03	2.50	3.33	1233.0	1.256	11.67	0.668
10.0	14.1	2.00	6.67	2456.8	1.241	15.42	0.612
20.0	28.1	1.00	13.3	3278.0	1.198	36.26	0.551
40.0	56.25	1.00	26.7	3855.1	1.198	36.26	0.551
80.0	112.5	1.00	53.3	5008.1	1.198	36.26	0.551
160.0	225.0	1.00	106.7	7314.3	1.198	36.26	0.551

Table D.3 The cap parameters obtained from the basic soil properties.

σ'_v psi	E psi	ν	K psi	G psi	κ psi	α	R	W	D	X_0 psi
0.5	85.2	0.10	35.5	38.7	2.782	0.248	0.269	0.238	1.377	491.6
1.0	240.2	0.10	100.1	109.2	2.782	0.248	0.269	0.238	0.488	240.2
2.5	606.0	0.10	252.5	275.5	2.782	0.248	0.269	0.235	0.196	114.5
5.0	1233.0	0.10	513.7	560.4	2.782	0.248	0.269	0.231	0.098	51.6
10.0	2456.8	0.10	1023.7	1116.7	2.782	0.248	0.584	0.233	0.046	21.5
20.0	3278.0	0.23	2000.4	1335.9	2.782	0.248	0.910	0.238	0.019	10.1
40.0	3855.1	0.34	4004.3	1438.9	2.782	0.248	0.910	0.238	0.009	5.0
80.0	5008.1	0.40	8008.6	1794.0	2.782	0.248	0.910	0.238	0.004	2.0
160.0	7314.3	0.42	16017.2	2568.4	2.782	0.248	0.910	0.238	0.002	0.7

Computer Program to Compute Cap Model Parameters from Conventional Laboratory Test Results and Field Condition of Soil

```
PROGRAM CAP_MODEL

IMPLICIT DOUBLEPRECISION (A-H, O-Z)
DOUBLEPRECISION K, K0, K1, K2, I1
CHARACTER INFILE*27, OUTFIL*27, OUTFL*27, INF*5, INFF*23

PARAMETER (SLOP=43.24, CONST=2702.00)
YM(A,B,P)=A*P+B

PI   = 4.0*ATAN(1.0)
SRT3 = SQRT(3.0)
TOL  = 0.000001

PRINT*
PRINT*, 'PLEASE TYPE INPUT FILE NAME.....................'
READ(*,'(A)')INF
PRINT*

INFF  =INF
INFILE=INFF//'.dat'
OUTFIL=INFF//'.out'
OUTFL =INFF

OPEN(1,FILE=INFILE,FORM='FORMATTED',STATUS='OLD')
OPEN(2,FILE=OUTFIL,FORM='FORMATTED',STATUS='UNKNOWN')
OPEN(3,FILE=OUTFL ,FORM='FORMATTED',STATUS='UNKNOWN')

READ(1,'(F15.5)') PHI, CPRIME, CC, CR, PR, E0, SUDSV, SIGMAV, K0

SIGMAV = -SIGMAV

WRITE(2,*)
WRITE(2,'(A)')'******************** TEST DATA ******************'
WRITE(2,*)

WRITE(2,'(A15,F10.3)')'PHI (DEGREE) =', PHI
WRITE(2,'(A15,F10.3)')'CPRIME       =', CPRIME
WRITE(2,'(A15,F10.3)')'CC           =', CC
WRITE(2,'(A15,F10.3)')'CR           =', CR
```

```
      WRITE(2,'(A15,F10.3)')'PR          =', PR
      WRITE(2,'(A15,F10.3)')'E0          =', E0
      WRITE(2,'(A15,F10.3)')'SUDSV       =', SUDSV
      WRITE(2,'(A15,F10.3)')'SIGMAV      =', SIGMAV
      WRITE(2,'(A15,F10.3)')'K0          =', K0

      PHIP = PHI*PI/180.0
      SINP = DSIN(PHIP)
      COSP = DCOS(PHIP)
      TANP = DTAN(PHIP)

1000  PRINT*,'TYPE OF TEST DONE:'
      PRINT*
      PRINT*,'     TRIAXIAL COMPRESSION :     1'
      PRINT*,'     TRIAXIAL EXTENSION   :     2'
      PRINT*,'     PLANE STRAIN         :     3'
      PRINT*,'     OTHER CONDITIONS     :     4'
c     READ(*,*)I
      I=1


      IF (I.EQ.1) THEN
         ALPHA= 2.0*SINP/((3.0-SINP)*SRT3)
         CAPA = 6.0*CPRIME*COSP/((3.0-SINP)*SRT3)
         WRITE(2,'(A)')'TRIAXIAL COMPRESSION TEST DATA'
      ELSEIF (I.EQ.2) THEN
         ALPHA= 2.0*SINP/((3.0+SINP)*SRT3)
         CAPA = 6.0*CPRIME*COSP/((3.0+SINP)*SRT3)
         WRITE(2,'(A)')'TRIAXIAL EXTENSION TEST DATA'
      ELSEIF (I.EQ.3) THEN
         ALPHA= TANP/ SQRT(9.0+12*TANP)
         CAPA = 3.0*CPRIME/ SQRT(9.0+12*TANP)
         WRITE(2,'(A)')'PLANE STRAIN TEST DATA'
      ELSEIF (I.EQ.4) THEN
         READ(1,'(F15.5)')SIGMA1, SIGMA2, SIGMA3
         ETA=DABS((SIGMA3-SIGMA2)/(SIGMA3-SIGMA1))
         THETA= (1.0/3.0)*DACOS(0.5*(2.0*ETA**3-3.0*ETA**2-3.0*ETA+2)/
     +           (ETA**2-ETA+1.0)**1.5)
         ALPHA= (1.0/3.0)*SINP/(DSIN(THETA+PI/3.0)-
     +          DCOS(THETA+PI/3.0)*SINP/SRT3)
         CAPA = CPRIME*COSP/(DSIN(THETA+PI/3.0)-
     +          DCOS(THETA+PI/3.0)*SINP/SRT3)
         WRITE(2,'(A)')'GENERAL TRIAXIAL COMPRESSION TEST DATA'
      ELSE
         PRINT*,'ERROR'
         WRITE(2,'(A)')'TYPE OF TEST DOES NOT MAKE SENSE'
         GOTO 1000
```

```
      ENDIF

      A=CC/((1.0+E0)* LOG(10.0))
      B=CR/((1.0+E0)* LOG(10.0))

      ITER=1

      R1 =-(2.0/SRT3)*SUDSV
      R2 = CAPA/SIGMAV
      R3 = ((R2-R1)/(ALPHA*(1.0+2.0*K0)))**(B/(B-A))

      P   =  LOG((1.0+R3)/2.0)/ LOG(R3)
      DX0 = 2.0* LOG(1.0/P-1.0)/(R3-1.0)
      W   = (B-A)* LOG(R3)/(DEXP(DX0*R3)-DEXP(DX0))

      DELR = 999999999.0
      R    =-3.0*R3/R1-1.0/ALPHA

2000  H    = (1.0-K0)**2*(ALPHA**2*R**2-1.0)/3.0
      H    = H+(ALPHA**2)*(1.0+2.0*K0)**2+R2**2
      H    = H-2.0*ALPHA*R2*(1.0+2.0*K0)

      IF (H.LT.0.0) THEN
         H=0.0
         PRINT*,'CAUTION >>> NEGATIVE VALUE OF H. ERROR LEVEL 1:'
         PRINT*,'IT IS MADE ZERO, BUT ACTUAL VALUE OF H IS ',H
      ENDIF


      R4   =  SQRT(H)

      RNEW=(1.0+2.0*K0)
      RNEW=RNEW-(R2*(1.0-ALPHA*R)-R1*(1.0-(ALPHA*R)**2)/ALPHA)/R3
      RNEW=RNEW/(R2+R4)

      PRINT*,'ITERATION = ', ITER,'  R  = ',RNEW

      DR   = DABS(RNEW-R)
      DELR = DR
      R    = RNEW
      ITER = ITER+1

      IF (DELR.GT.TOL) GOTO 2000

      IF(DABS((1.0-K0)/SRT3).GE.DABS(R1))PRINT*,'ERROR : LEVEL 1'
      IF(DABS(R1/(R2-ALPHA*(1.+2.*K0))).GE.1.0)PRINT*,'ERROR : LEVEL 2'
```

```
H=(1.0-K0)**2*(ALPHA**2*R**2-1.0)/3.0
H=H+(ALPHA**2)*(1.0+2.0*K0)**2+R2**2
H=H-2.0*ALPHA*R2*(1.0+2.0*K0)

IF (H.LT.0.0) THEN
   H=0.0
   PRINT*,'CAUTION >>> NEGATIVE VALUE OF H. ERROR LEVEL 1:'
   PRINT*,'IT IS MADE ZERO, BUT ACTUAL VALUE OF H IS ',H
ENDIF

X0 = (SIGMAV/(1.0-ALPHA*R))*((1.0+2.0*K0)-R*R2-R* SQRT(H))
D  = DX0/X0

WRITE(2,*)
WRITE(2,'(A)')'******************** PARAMETERS ******************'
WRITE(2,*)

WRITE(2,'(A15,F10.3)')'ALPHA          =', ALPHA
WRITE(2,'(A15,F10.3)')'CAPA           =', CAPA
WRITE(2,'(A15,F10.3)')'D              =', D
WRITE(2,'(A15,F10.3)')'W              =', W
WRITE(2,'(A15,F10.3)')'R              =', R
WRITE(2,'(A15,F10.3)')'X0             =', X0
WRITE(2,'(A15,F10.3)')'DX0            =', DX0

X0 = CAPA/ALPHA+(2.0/SRT3)*SUDSV*SIGMAV*(R+1.0/ALPHA)
D  = DX0/X0

WRITE(2,*)
WRITE(2,'(A15,F10.3)')'D              =', D
WRITE(2,'(A15,F10.3)')'X0             =', X0

READ(1,'(F15.5)') SIGMAV, K0
SIGMAV=-SIGMAV

WRITE(2,*)
WRITE(2,'(A)')'******************** FIELD DATA ******************'
WRITE(2,*)

WRITE(2,'(A15,F10.3)')'PHI (DEGREE) =', PHI
WRITE(2,'(A15,F10.3)')'CPRIME       =', CPRIME
WRITE(2,'(A15,F10.3)')'CC           =', CC
WRITE(2,'(A15,F10.3)')'CR           =', CR
WRITE(2,'(A15,F10.3)')'PR           =', PR
WRITE(2,'(A15,F10.3)')'E0           =', E0
WRITE(2,'(A15,F10.3)')'SUDSV        =', SUDSV
WRITE(2,'(A15,F10.3)')'SIGMAV       =', SIGMAV
```

```
      WRITE(2,'(A15,F10.3)')'K0          =', K0

      H=(1.0-K0)**2*(ALPHA**2*R**2-1.0)/3.0
      H=H+(ALPHA**2)*(1.0+2.0*K0)**2+R2**2
      H=H-2.0*ALPHA*R2*(1.0+2.0*K0)

      IF (H.LT.0.0) THEN
         H=0.0
         PRINT*,'CAUTION >>> NEGATIVE VALUE OF H. ERROR LEVEL 2:'
         PRINT*,'IT IS MADE ZERO, BUT ACTUAL VALUE OF H IS ',H
      ENDIF

      X0=(SIGMAV/(1.0-ALPHA*R))*((1.0+2.0*K0)-R*R2-R* SQRT(H))
      D=DX0/X0
      X0NC=X0

      I1 = SIGMAV*(1.0+2.0*K0)
      K1 = 1.0/B
      K2 = 1.0
      AP = 1.0
      K  = K1*AP*(ABS(I1/(3.0*AP)))**K2

      CONP=-I1/3.0
      YMOD=YM(SLOP,CONST,CONP)
      PR  =0.5-YMOD/(6.0*K)

c     G2 = 0.0
c     G1 = 1.5*(1.0-2.0*PR)/(1.0+PR)
c     G  = G2+G1*K

      G=YMOD/(2.0*(1.0+PR))

      WRITE(2,*)
      WRITE(2,'(A)')'******************** PARAMETERS ******************'
      WRITE(2,*)

      WRITE(2,'(A15,F10.3)')'ALPHA       =', ALPHA
      WRITE(2,'(A15,F10.3)')'CAPA        =', CAPA
      WRITE(2,'(A15,F10.3)')'D           =', D
      WRITE(2,'(A15,F10.3)')'W           =', W
      WRITE(2,'(A15,F10.3)')'R           =', R
      WRITE(2,'(A15,F10.3)')'X0          =', X0
      WRITE(2,'(A15,F10.3)')'DX0         =', DX0

      WRITE(2,'(A15,F10.3)')'K           =', K
      WRITE(2,'(A15,F10.3)')'G           =', G
```

```
X0 = CAPA/ALPHA+(2.0/SRT3)*SUDSV*SIGMAV*(R+1.0/ALPHA)
D  = DX0/X0
X00C = X0

IF(ABS(X0NC).GT.ABS(X00C)) X0=X0NC
D=DX0/X0

WRITE(2,*)

WRITE(2,'(A15,F10.3)')'D              =', D
WRITE(2,'(A15,F10.3)')'X0             =', X0

WRITE(3,'(A)')'material type # 25  (cap model)'

WRITE(3,'(8E10.4)')    K,     G, 0.0, 0.0, 0.0, 0.0, 0.0, 0.0
WRITE(3,'(8E10.4)') CAPA, ALPHA, 0.0, 0.0,   R, 0.0, 0.0, 0.0
WRITE(3,'(8E10.4)')    D,     W, -X0, 0.0, 0.0, 0.0, 0.0, 0.0
WRITE(3,'(8E10.4)')  3.0,   0.0, 0.0, 0.0, 0.0, 0.0, 0.0, 0.0
WRITE(3,'(8E10.4)')  1.0,   0.0, 0.0, 0.0, 0.0, 0.0, 0.0, 0.0
WRITE(3,'(8E10.4)')-0.01,   0.0, 0.0, 0.0, 0.0, 0.0, 0.0, 0.0

STOP
END
```

Appendix E: Force-Displacement Curves for Single Piles, Two-Pile Groups, and Pile Caps

E.1 Introduction

For time domain nonlinear analysis, a rational, dynamic, nonlinear soil-pile interaction model has been developed for a single pile, a pile group, and a pile group with cap for axial and lateral vibrations. These are formulated as simple combinations of frequency independent masses, springs, and dashpots. Explicit expressions have been presented for near- and far-field masses, near- and far-field dampers, and far-field springs. The p-y and t-z curves of the near-field springs for piles and pile- groups for dynamic analysis were computed using finite element analysis for a site-specific soil at the Snohomish river site. The results of these analysis have been presented in this appendix in the following order:

1. Force-displacement curves of the near-field spring of a single pile of diameters 18″ and 24″
   (a) Lateral vibration for 8 different confining pressures in plane-strain condition,
   (b) Lateral vibration for 4 different confining pressures in plane-stress condition, and
   (c) Axial vibration for 8 different confining pressures.
2. p-y and t-z curves of the pile-pile interaction of two-pile groups of diameters 18″ and 24″.
   (a) For direct-lateral vibration
      i. Near-field spring for plane-strain condition for 8 different confining pressures,
      ii. Near-field spring for plane-stress condition for 2 different confining pressures,

iii. Interaction-spring for plane-strain condition for 8 different confining pressures, and

iv. Interaction-spring for plane-stress condition for 2 different confining pressures.

(b) For shear-lateral vibration

i. Near-field spring for plane-strain condition for 8 different confining pressures,

ii. Near-field spring for plane-stress condition for 2 different confining pressures,

iii. Interaction-spring for plane-strain condition for 8 different confining pressures, and

iv. Interaction-spring for plane-stress condition for 2 different confining pressures.

(c) For axial vibration

i. Near-field spring for 8 different confining pressures, and

ii. Interaction-spring for 8 different confining pressures.

3. P_c-Y_c and T_c-Z_c curves of the cap-soil interaction-spring due to side friction

(a) For lateral vibration of four different diameters and four different squares, and

(b) For axial vibration of four different diameters and four different squares.

E.2 Characteristics of the Near-Field Springs

E.2.1 Vibration of a Single Pile

E.2.1.1 Lateral Vibration of a Single Pile

To develop the nonlinear near-field spring, the pile segment was forced to move laterally either in the plane-stress or plane-strain condition during the computer simulation of a lateral load test, and the displacement of the segment was observed. A comprehensive

determination of near-field spring constants has been made for piles with diameters of $0.457m$ (18″) and $0.610m$ (24″), respectively, using soil parameters determined from laboratory tests performed on soil samples taken from a Snohomish river site in Washington State. These thin-layer p-y curves were produced for 6.9, 17.3, 34.5, 68.9, 137.8, 275.6, 551.2, and 1102.4 kPa (1, 2.5, 5, 10, 20, 40, 80, and 160 psi) of vertical effective stress, assuming drained conditions. In all cases, the coefficient of earth pressure at rest was assumed to be 0.5 and the coefficient of friction between the pile and soil interface was assumed to be 0.4. The p-y curve for very small vertical stresses, 6.9, 17.3, 34.5, and 68.9 kPa (1, 2.5, 5, and 10 psi), was developed for the plane-stress condition. All p-y curves are presented in Figures E.1 through E.4, and the corresponding parameters for the idealized p-y curves are presented in Tables 2.1 and 2.2.

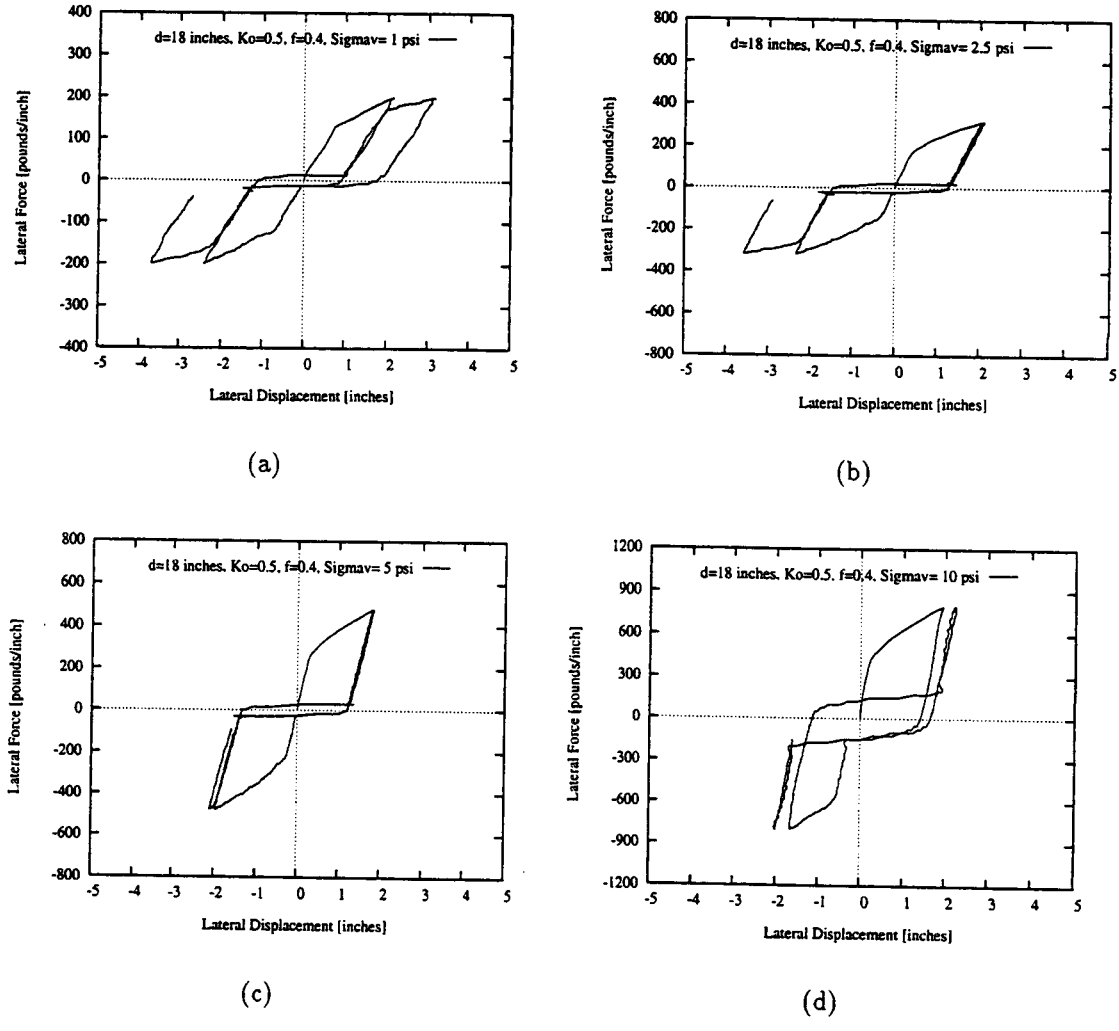

Figure E.1 p-y curves for lateral vibration of a near-field spring for single pile for different confining pressures for plane-strain condition [$d = 0.457\text{m} = 18$ in.] (continued to the next page)

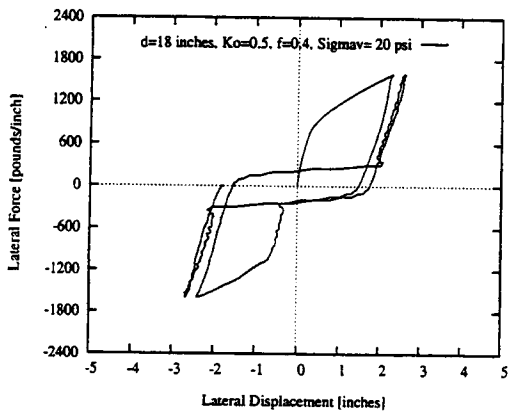

(e)

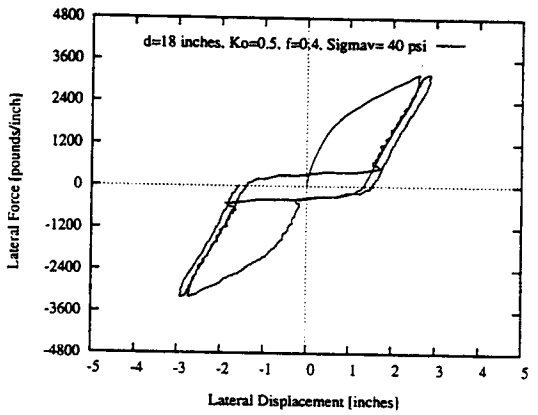

(f)

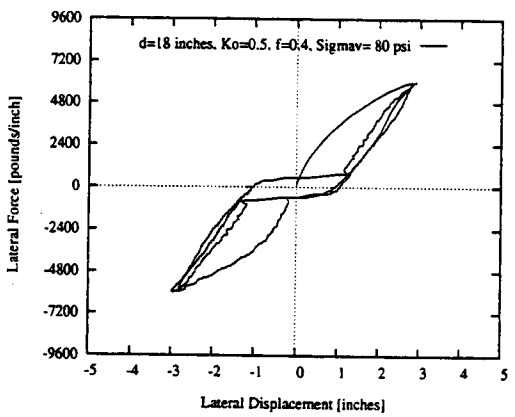

(g)

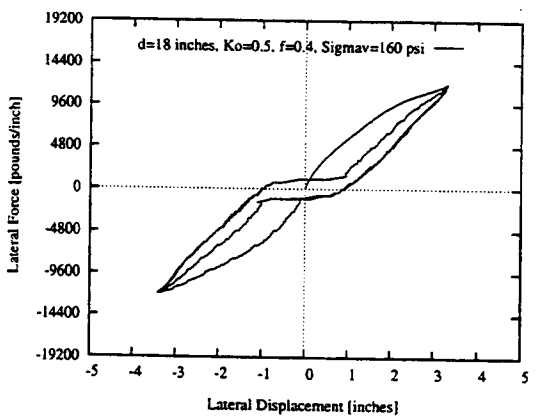

(h)

Figure E.1 p-y curves for lateral vibration of a near-field spring for single pile for different confining pressures for plane-strain condition [$d = 0.457\text{m} = 18$ in.] (continued)

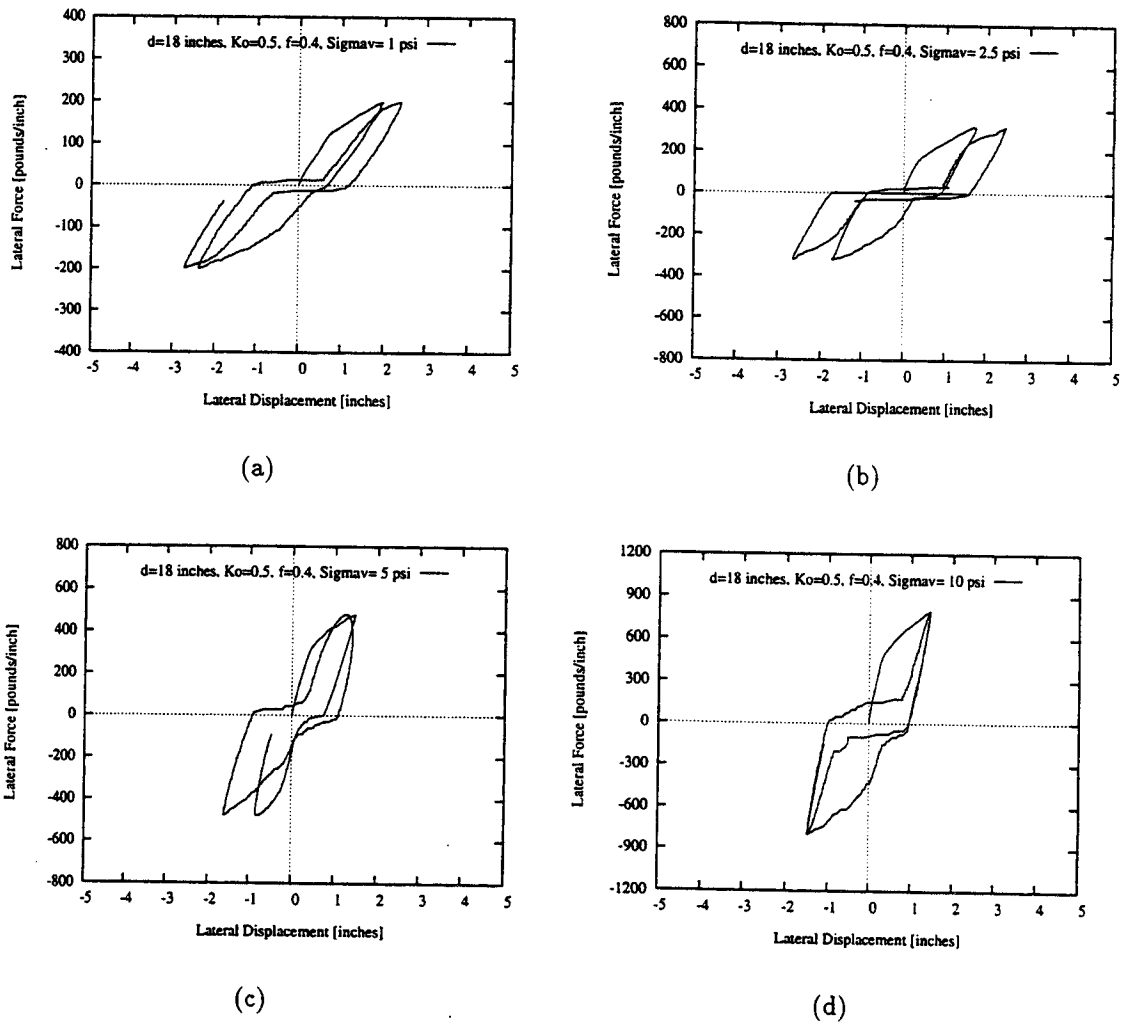

Figure E.2 p-y curves for lateral vibration of a near-field spring for single pile for different confining pressures for plane-stress condition [$d = 0.457\text{m} = 18$ in.]

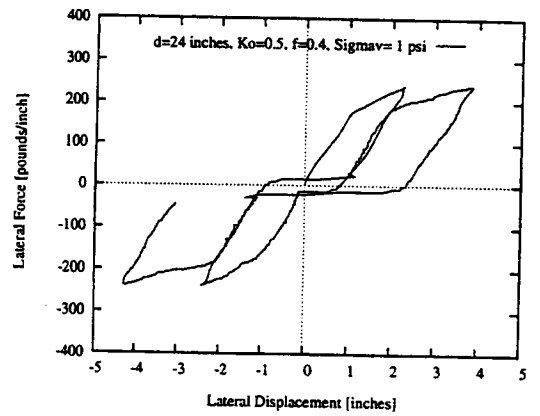

(a)

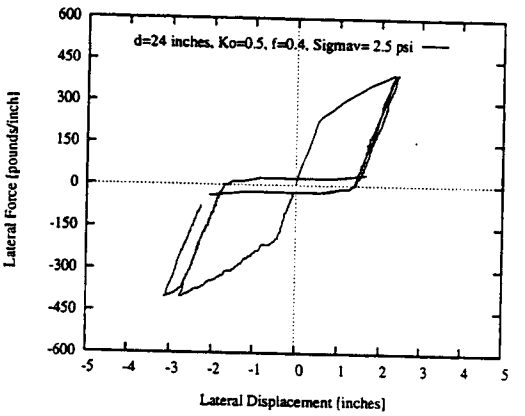

(b)

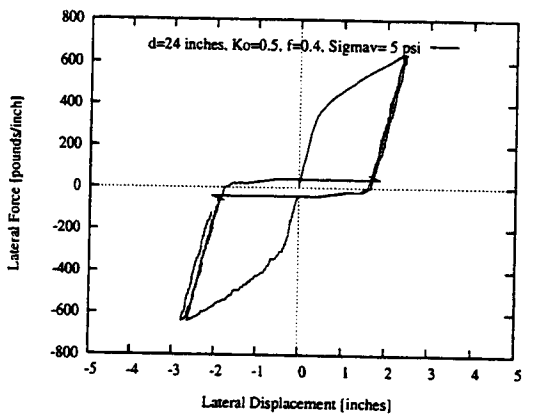

(c)

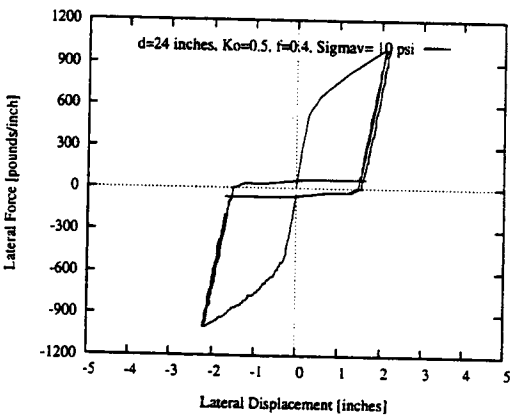

(d)

Figure E.3 p-y curves for lateral vibration of a near-field spring for single pile for different confining pressures for plane-strain condition [$d = 0.610\text{m} = 24$ in.] (continued to the next page)

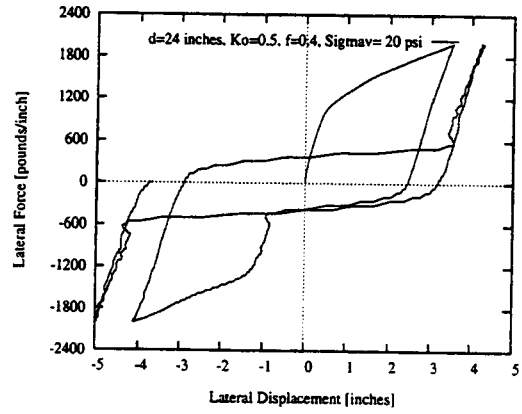

(e)

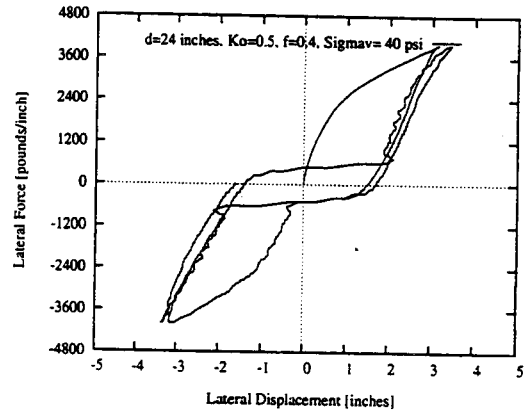

(f)

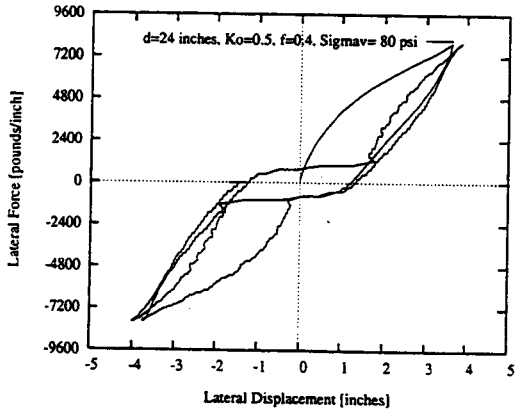

(g)

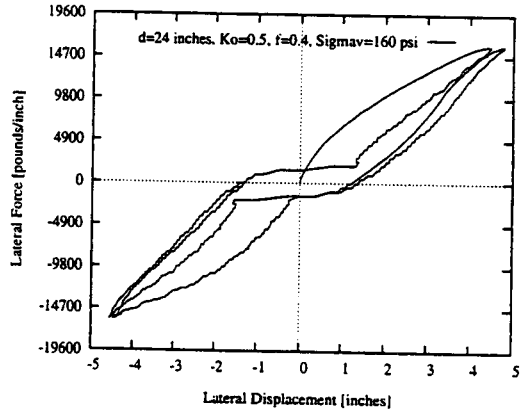

(h)

Figure E.3 p-y curves for lateral vibration of a near-field spring for single pile for different confining pressures for plane-strain condition [$d = 0.610\text{m} = 24$ in.] (continued)

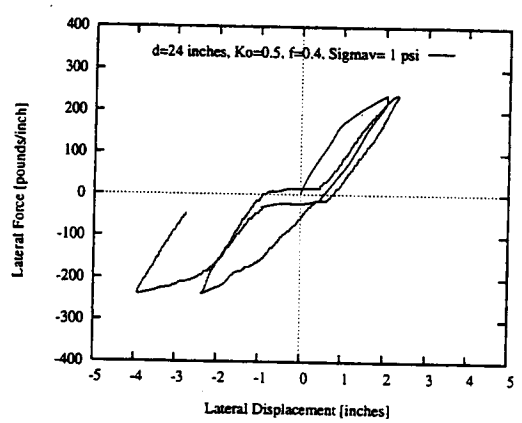

(a)

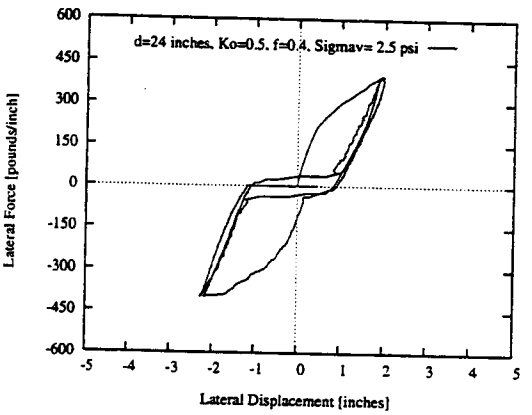

(b)

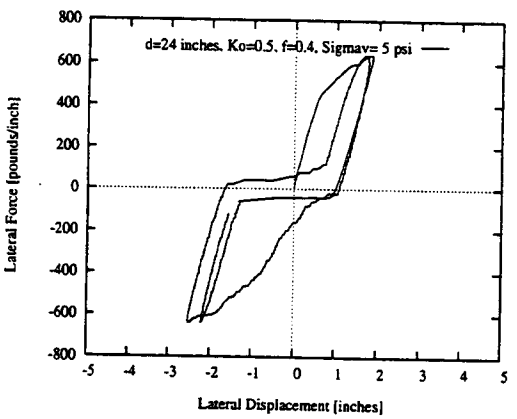

(c)

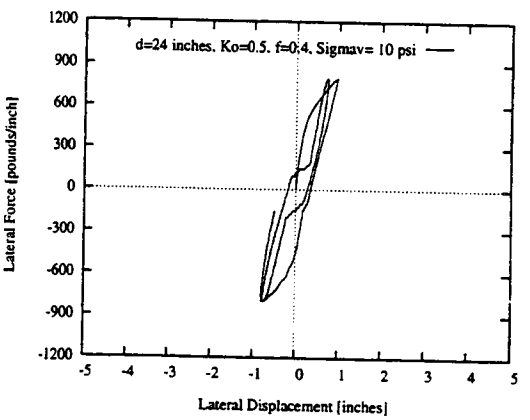

(d)

Figure E.4 *p-y* curves for lateral vibration of a near-field spring for single pile for different confining pressures for plane-stress condition [$d = 0.610\text{m} = 24$ in.]

E.2.1.2 Axial Vibration of a Single Pile

To develop the nonlinear spring characteristics, a finite element model was developed for a thin layer elasto-plastic soil and a rigid pile segment. Soil within $4d$ of the pile was modeled with the geologic cap model. It was observed that soil displacement at a large distance (20 diameters) from the pile center was negligibly small and, therefore, an artificial, no displacement boundary was placed there. A pseudo-static load was applied along the pile axis to observe the resulting displacement. No sliding interface was assumed to exist between the pile and soil because initial observations showed that it induces instability. The initial K_0-state of stress was assumed as the initial condition. The overburden pressure was always maintained to ensure the confining effect.

All nodes along the boundary were assumed to be fixed, and the rest of the nodes were allowed to move only vertically. The resulting force (per unit thickness)- displacement behavior, represented by t-z curves, were produced with 8 different confining pressures for soil of the Snohomish river site. These curves are presented in Figures E.5 and E.6 for piles of 18″ ($0.457m$) and 24″ ($0.610m$) diameters respectively. The corresponding bilinear parameters are presented in Tables 2.4 and 2.5.

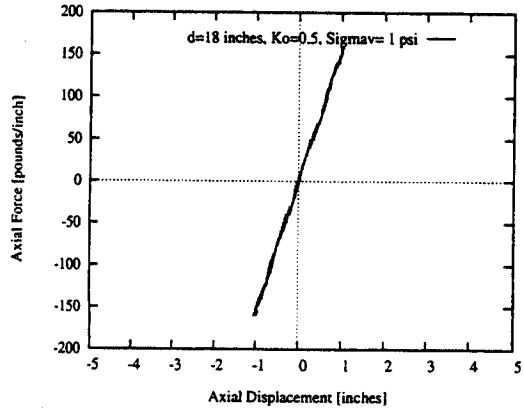

(a)

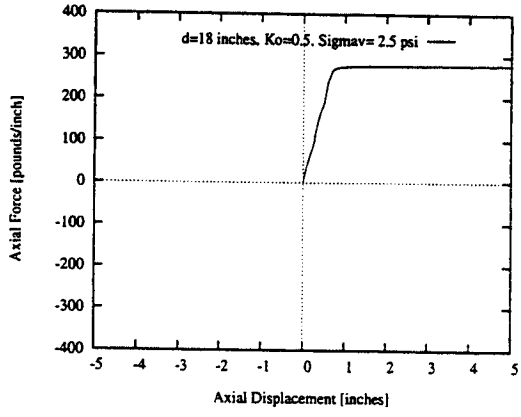

(b)

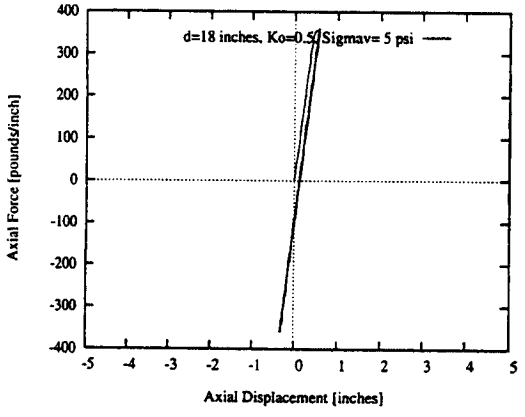

(c)

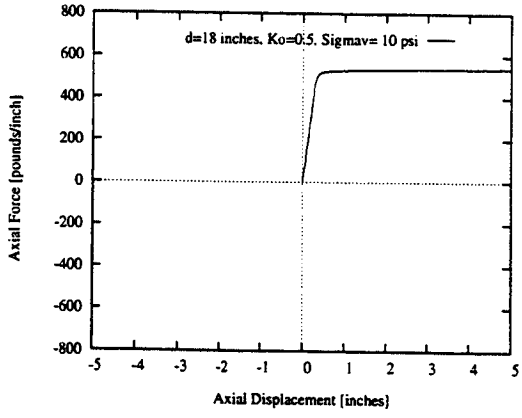

(d)

Figure E.5 t-z curves for axial vibration of a near-field spring for single pile for different confining pressures. [$d = 0.457\text{m} = 18$ in.] (continued to the next page)

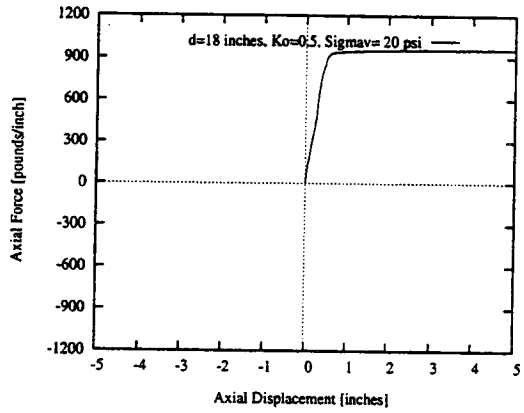

(e)

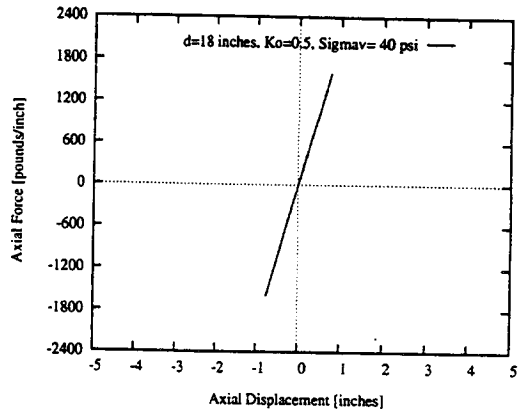

(f)

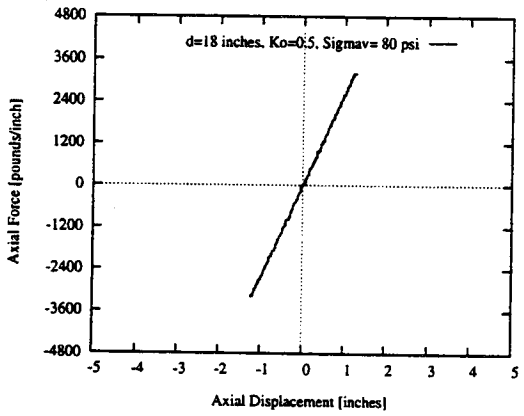

(g)

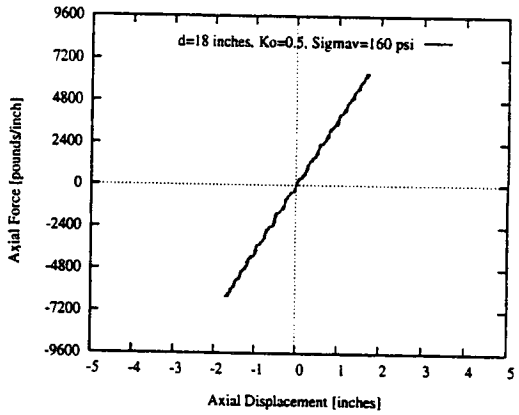

(h)

Figure E.5 t-z curves for axial vibration of a near-field spring for single pile for different confining pressures. [$d = 0.457\text{m} = 18$ in.] (continued)

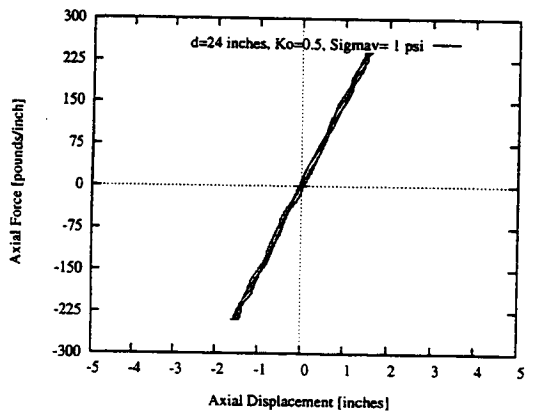

(a)

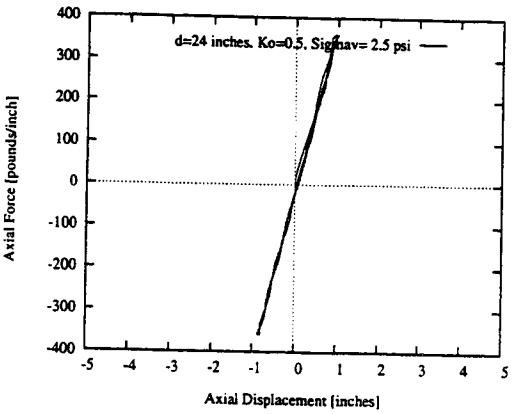

(b)

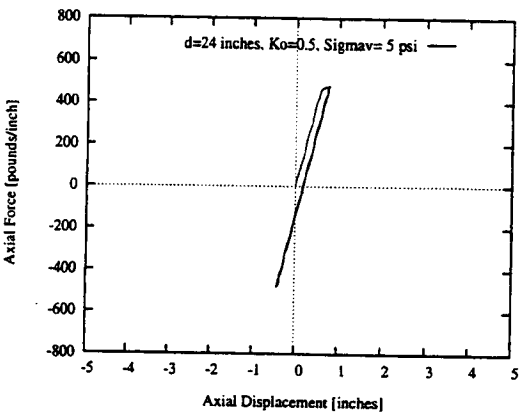

(c)

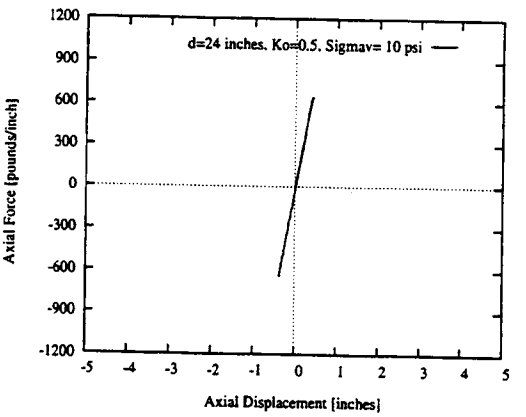

(d)

Figure E.6 t-z curves for axial vibration of a near-field spring for single pile for different confining pressures. [$d = 0.610\text{m} = 24$ in.] (continued to the next page)

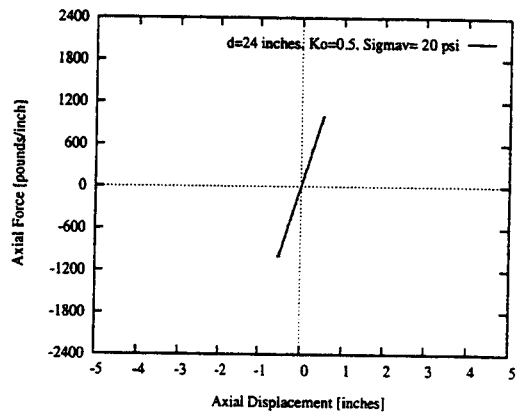

(e)

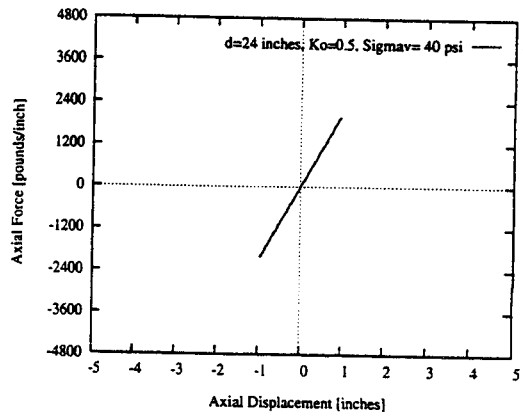

(f)

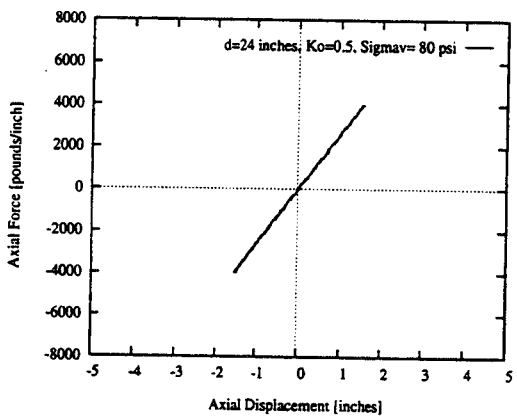

(g)

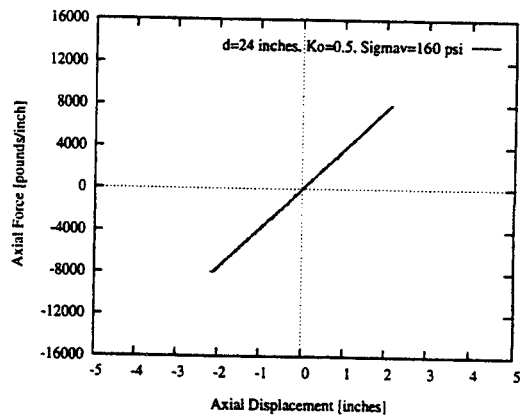

(h)

Figure E.6 t-z curves for axial vibration of a near-field spring for single pile for different confining pressures. [$d = 0.610\text{m} = 24$ in.] (continued)

E.2.2 Vibration of a Two-Pile Group

All pile segments were assumed to be interconnected to neighboring pile-segments by interacting nonlinear springs and dashpots. All pile segments were connected to the soil by near-field nonlinear springs and dampers, while all external pile segments were connected to far-field discrete elements through near-field elements. The spring constants which represent interaction between piles, i.e. the springs connecting the pile segments with each other, can be obtained by introducing a displacement into a segment in a pile group while keeping all others fixed. The force generated in each pile-segment as an active or reactive force can be analyzed to characterize the interacting spring parameters.

E.2.2.1 Direct-Lateral Vibration of a Two-Pile Group

There are three basic types of springs in pile group models. These include nonlinear near-field springs, nonlinear interacting springs, and linear far-field springs. Nonlinear springs are required for those connecting piles with surrounding soil, and for those connecting the piles themselves, i.e., interaction-springs. The characteristics of the interaction-springs between two piles and the near-field spring which connects a pile to soil have been computed for different confining pressures and for the drained condition for soil taken from the Snohomish river site. For the determination of the direct interaction-spring constants for lateral vibration, plane-strain conditions were assumed for all the depths other than zero. At or near the surface, plane-stress conditions were assumed. A pseudo-static load was applied to one rigid segment of the pile either toward the other pile or in the reverse direction, varying sinusoidally with a very small frequency, keeping the other pile fixed. The resulting displacement in the first pile, and active or reactive force on both piles, were observed and analyzed to establish the p-y behavior of the two-pile group. The above procedure was followed for different depths represented by 6.9, 17.3, 34.5, 68.9, 137.8, 275.6, 551.2, and 1102.4 kPa (1, 2.5, 5, 10, 20, 40, 80, and 160 psi) vertical stresses in plane-strain condition, and 6.9 and 34.5 kPa (1 and 5 psi) for plane-stress condition, for drained behavior of the soil, and for center spacing of $2d$, $4d$,

and $8d$. The resulting p-y behavior of the interaction springs and the near-field springs are presented in Figures E.7 through E.22 for soil from the Snohomish river site. The NEABS parameters for those spring were computed, and they are presented in Tables 2.7 through 2.9.

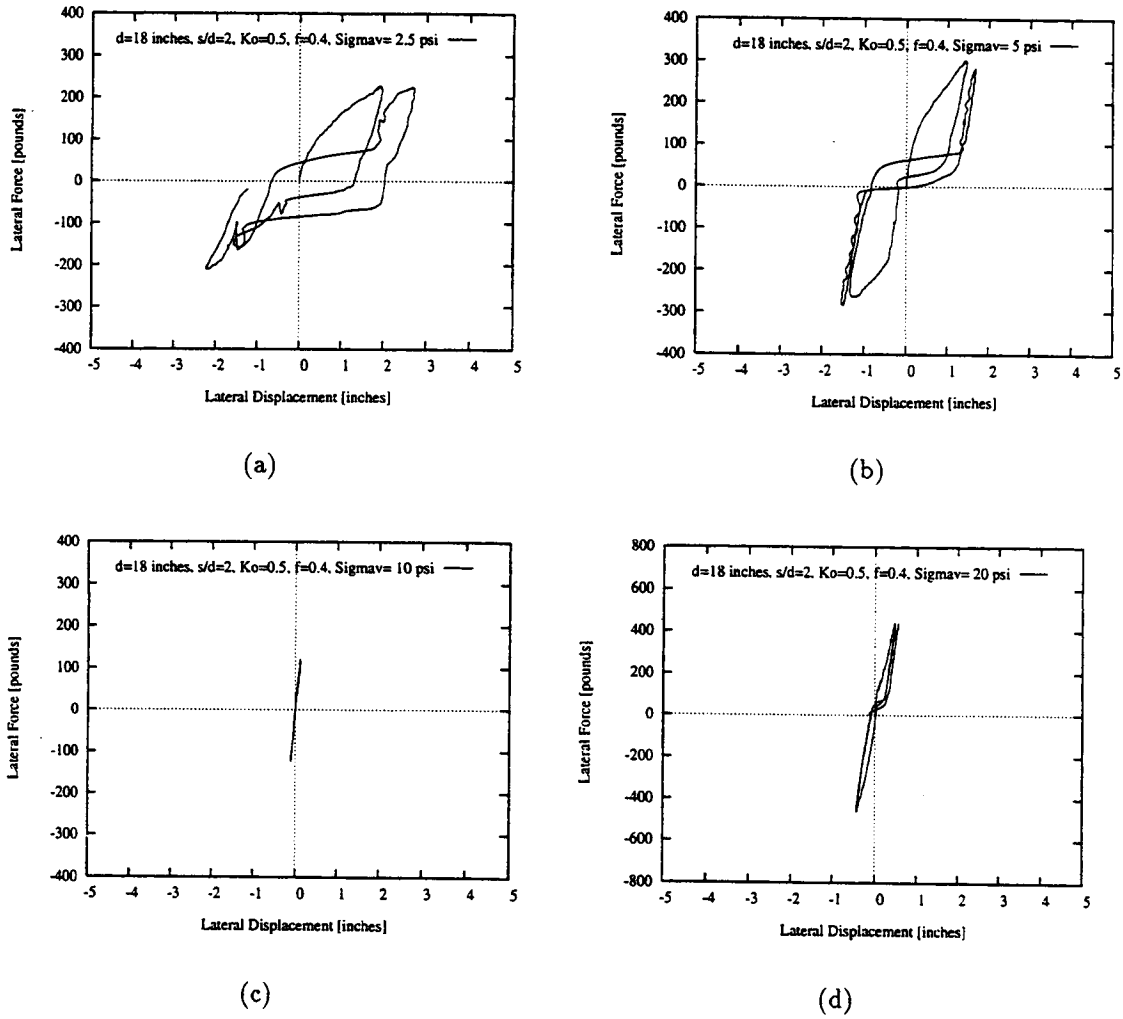

Figure E.7 p-y curves for the external near-field springs between two piles for direct-lateral vibration for different confining pressures in plane-strain condition. [d = 0.457m = 18 in.; $s = 2d$] (continued to the next page)

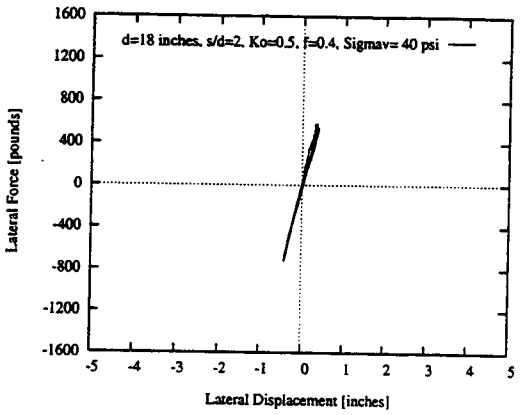

(e)

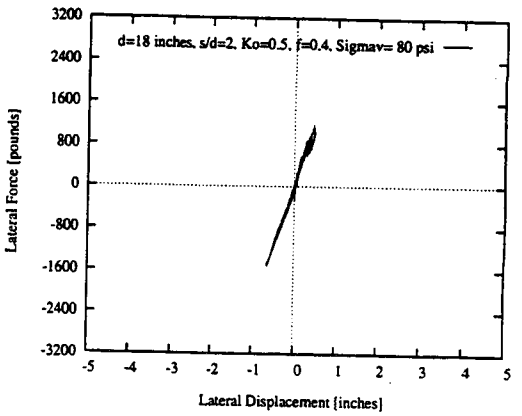

(f)

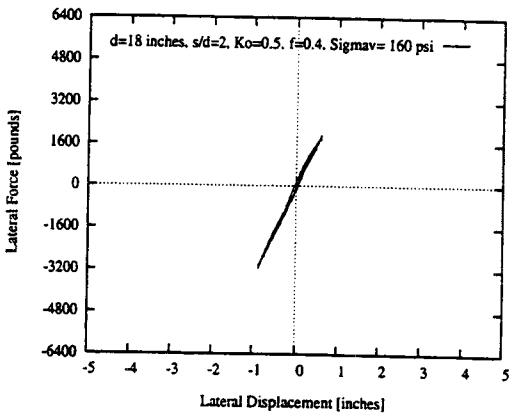

(g)

Figure E.7 p-y curves for the external near-field springs between two piles for direct-lateral vibration for different confining pressures in plane-strain condition. [d = 0.457m = 18 in.; $s = 2d$] (continued)

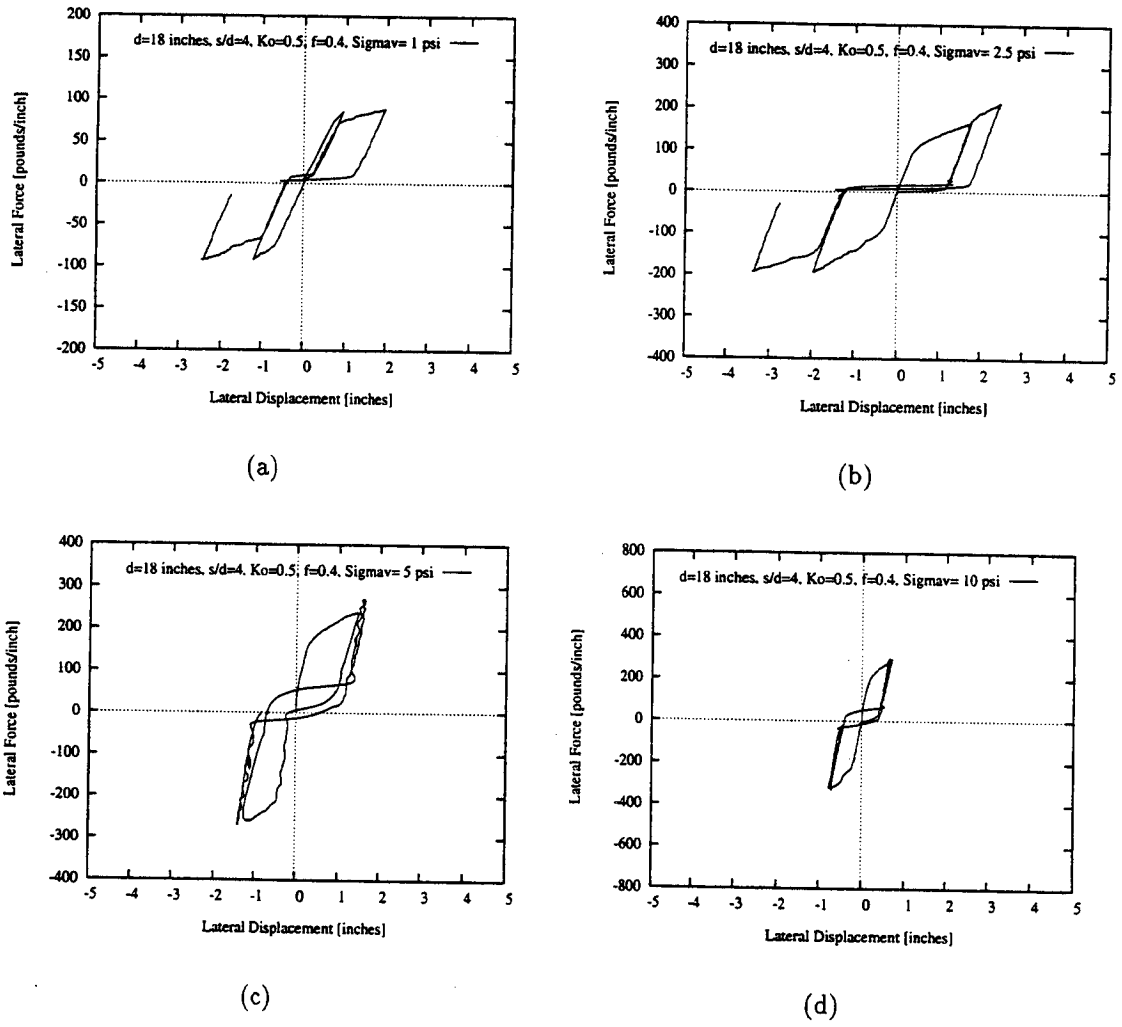

Figure E.8 p-y curves for the external near-field springs between two piles for direct-lateral vibration for different confining pressures in plane-strain condition. [d = 0.457m = 18 in.; $s = 4d$] (continued to the next page)

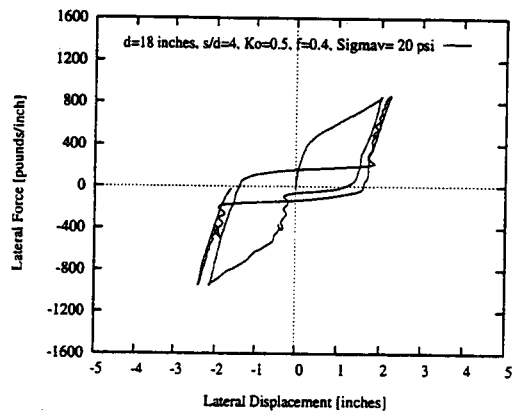

(e)

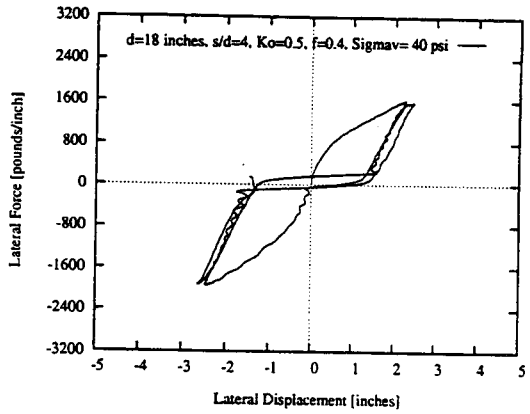

(f)

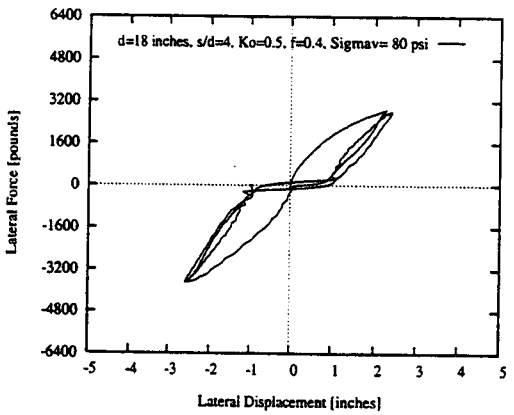

(g)

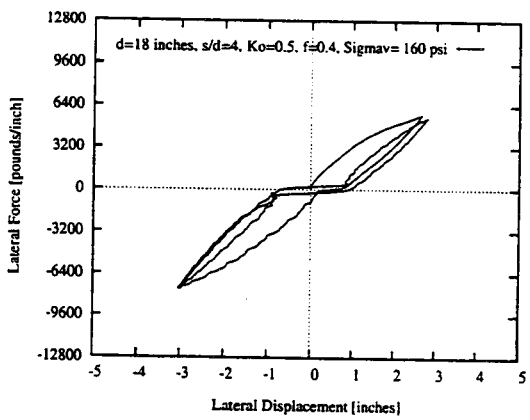

(h)

Figure E.8 p-y curves for the external near-field springs between two piles for direct-lateral vibration for different confining pressures in plane-strain condition. [d = 0.457m = 18 in.; $s = 4d$] (continued)

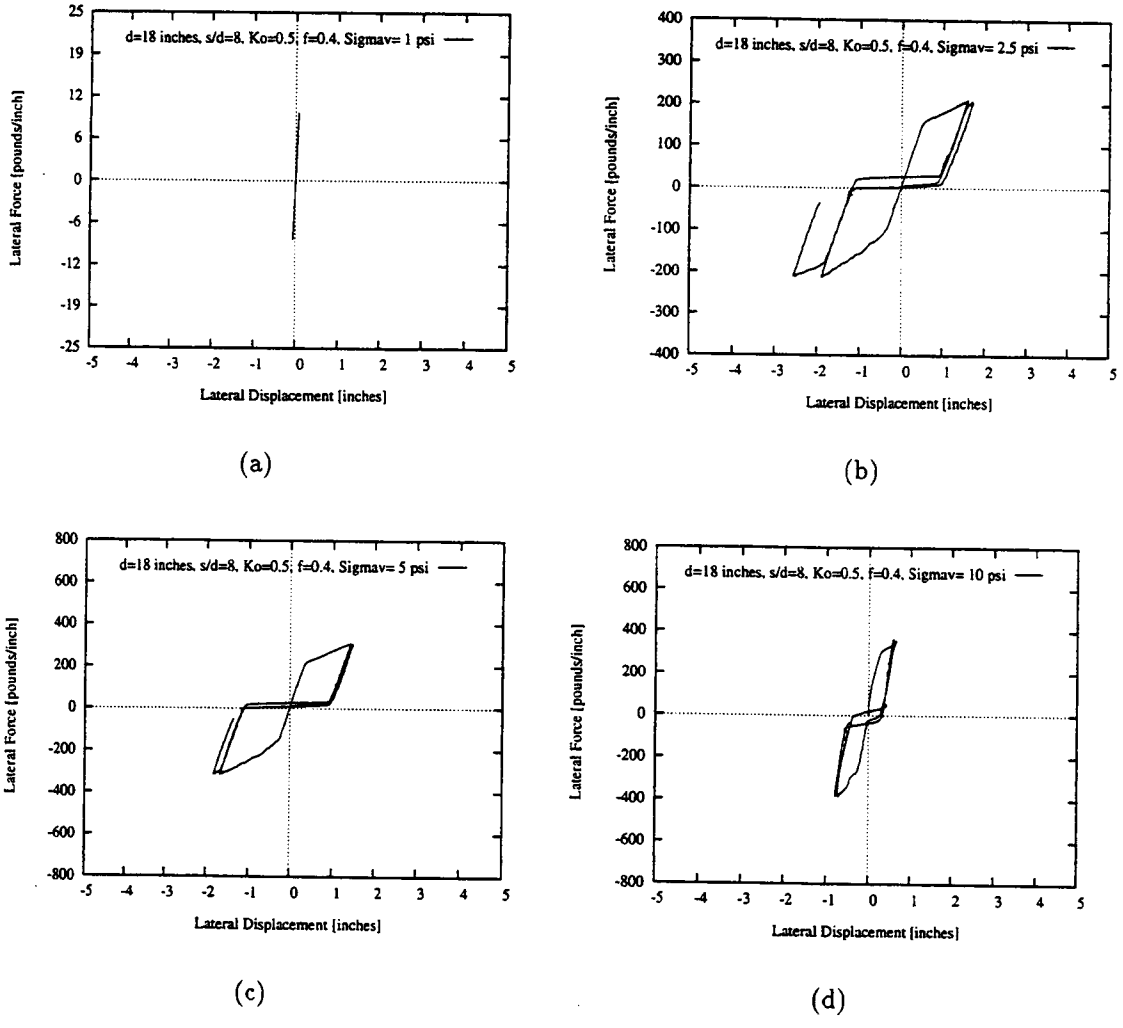

Figure E.9 p-y curves for the external near-field springs between two piles for direct-lateral vibration for different confining pressures in plane-strain condition. [d = 0.457m = 18 in.; $s = 8d$] (continued to the next page)

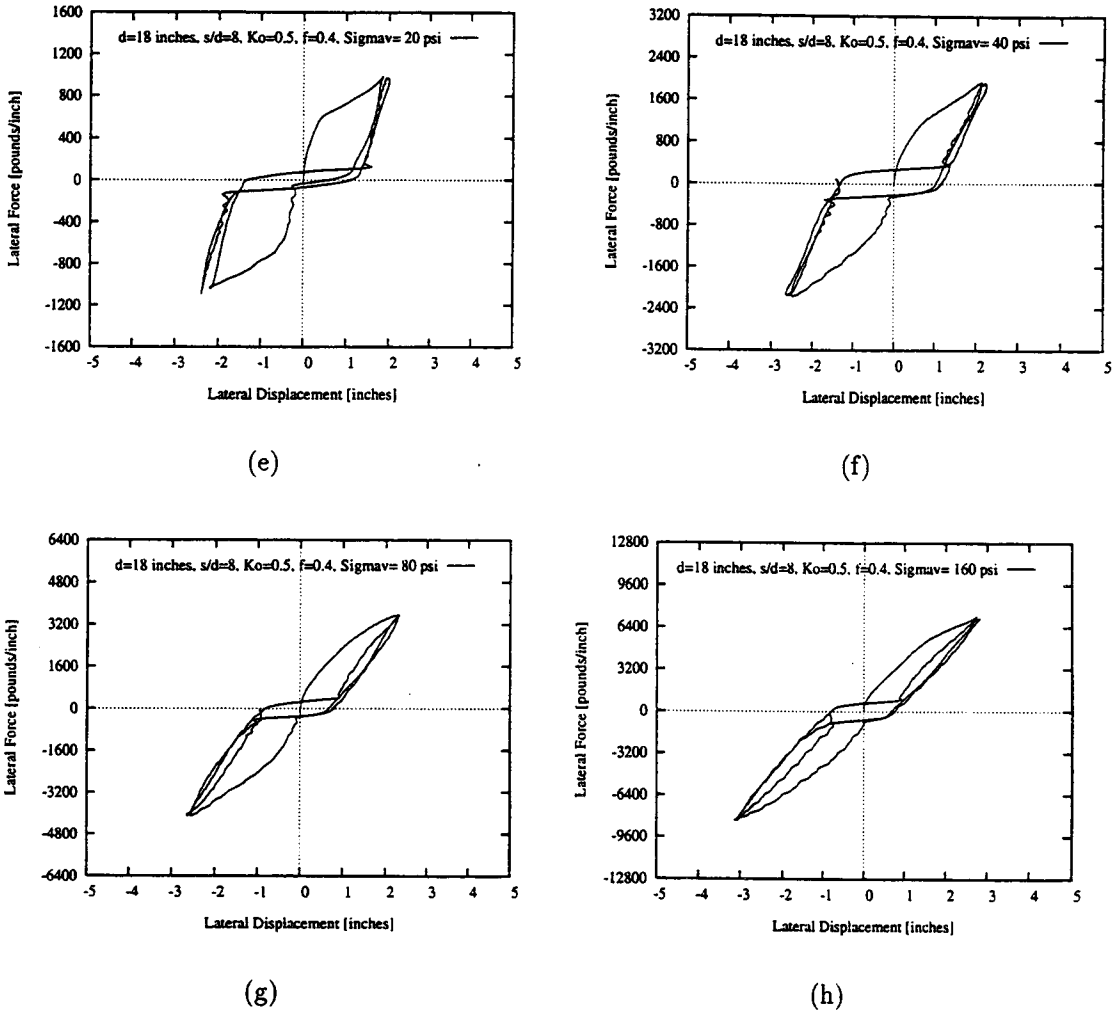

Figure E.9 p-y curves for the external near-field springs between two piles for direct-lateral vibration for different confining pressures in plane-strain condition. [d = 0.457m = 18 in.; $s = 8d$] (continued)

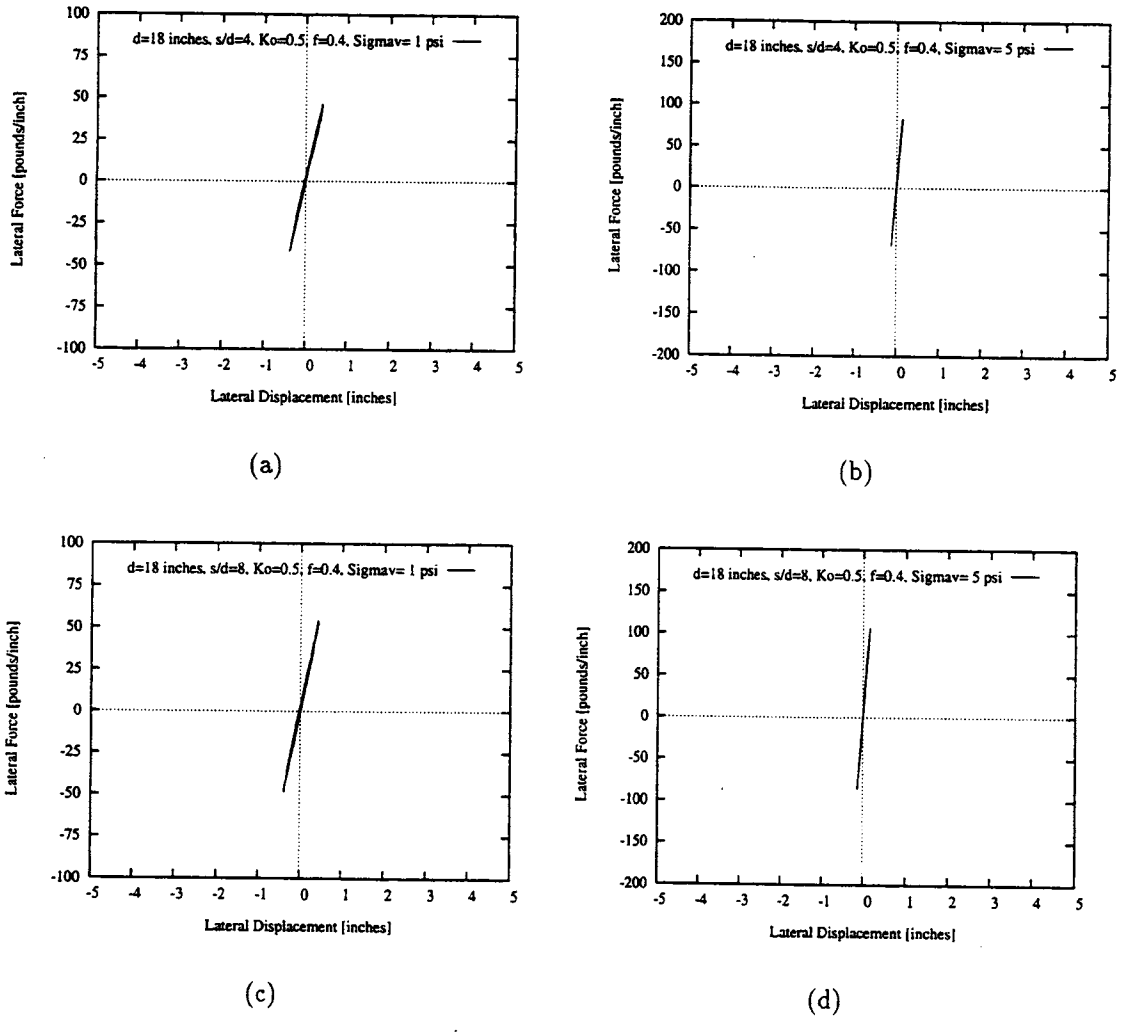

Figure E.10 p-y curves for the external near-field springs between two piles for direct-lateral vibration for different confining pressures in plane-stress condition. [d = 0.457m = 18 in.]

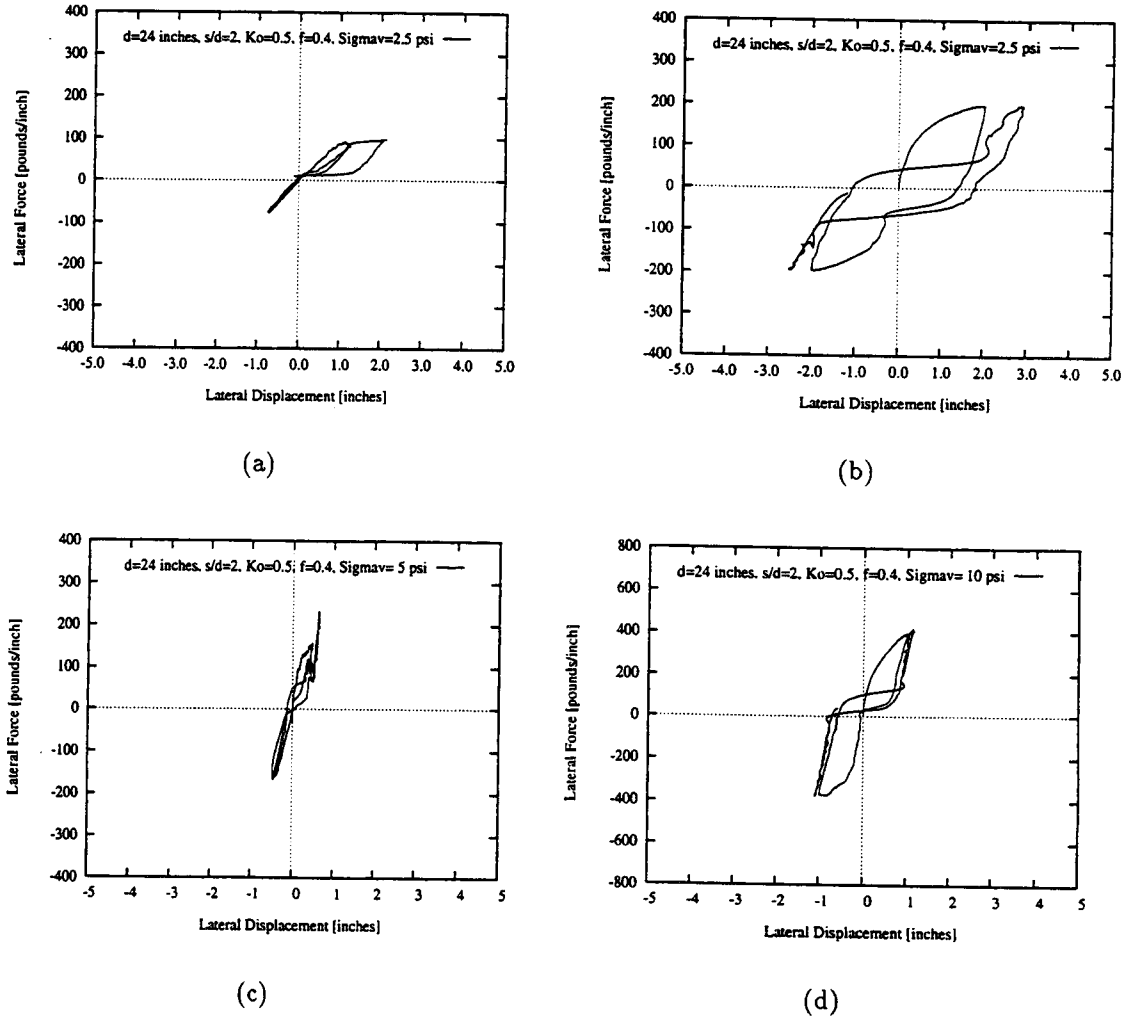

Figure E.11 p-y curves for the external near-field springs between two piles for direct-lateral vibration for different confining pressures in plane-strain condition. [d = 0.610m = 24 in.; $s = 2d$] (continued to the next page)

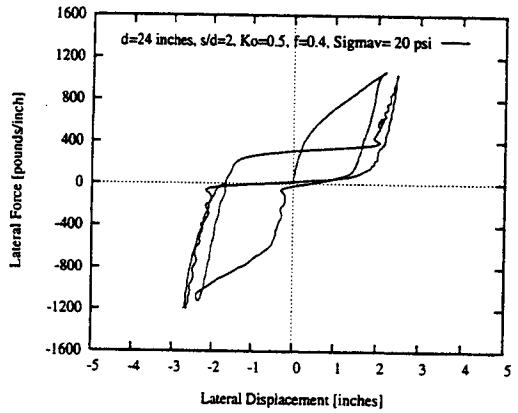

(e)

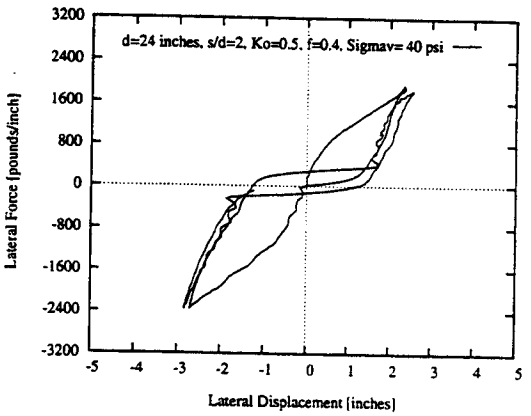

(f)

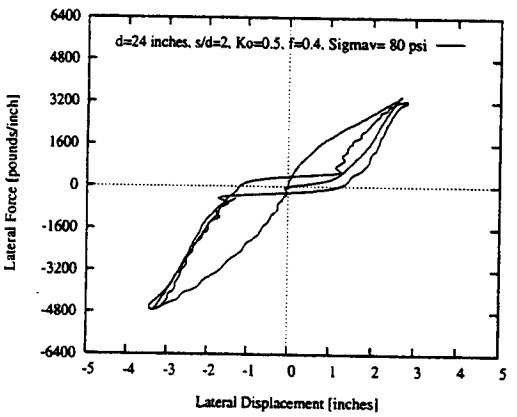

(g)

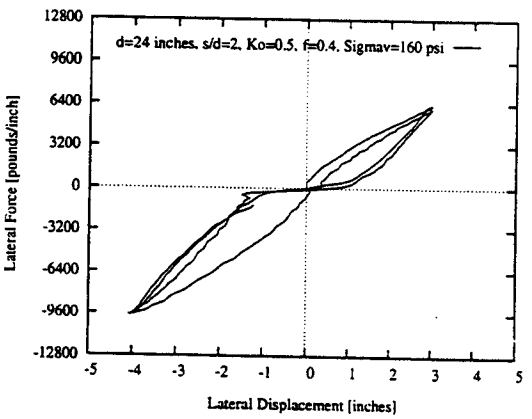

(h)

Figure E.11 p-y curves for the external near-field springs between two piles for direct-lateral vibration for different confining pressures in plane-strain condition. [d = 0.610m = 24 in.; $s = 2d$] (continued)

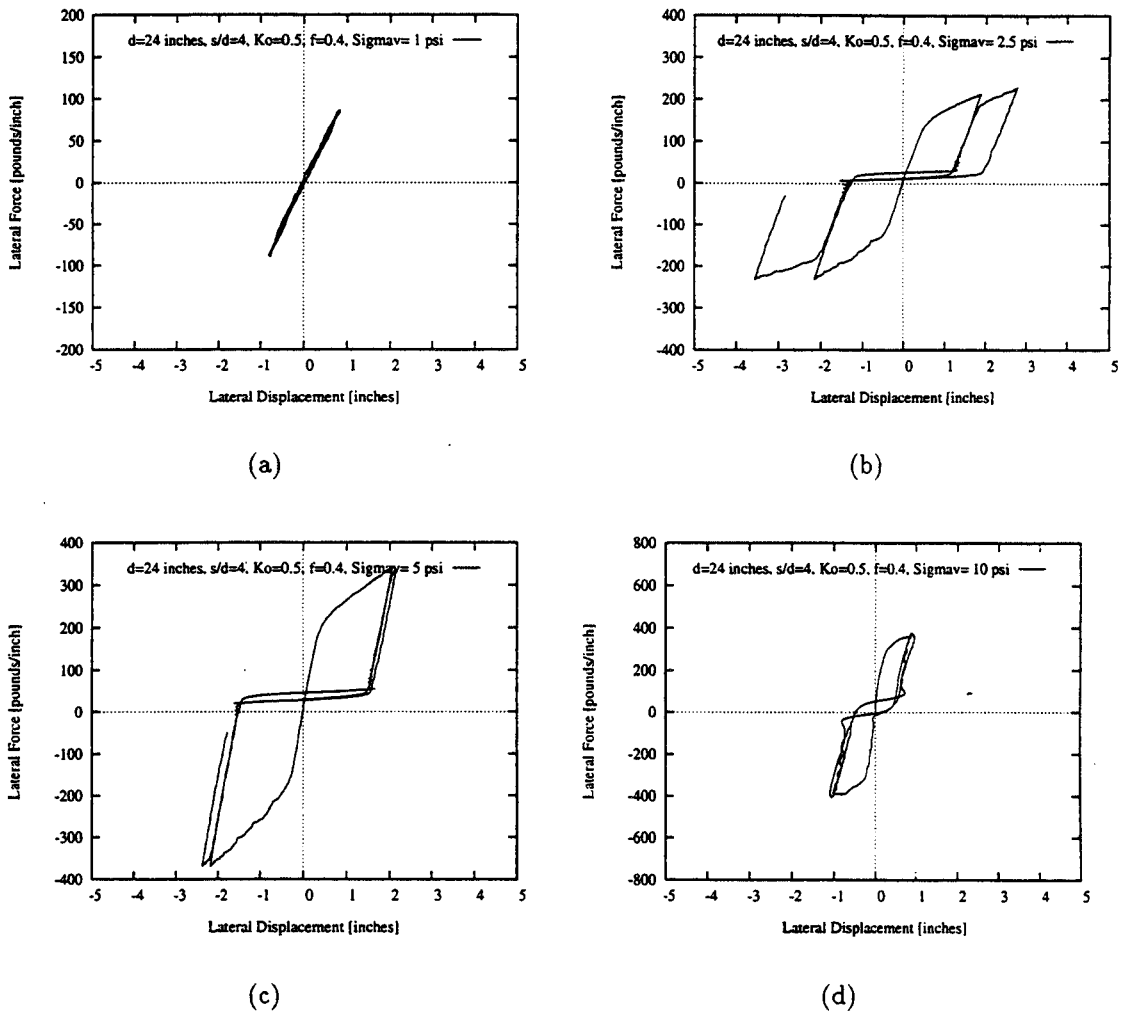

Figure E.12 p-y curves for the external near-field springs between two piles for direct-lateral vibration for different confining pressures in plane-strain condition. [d = 0.610m = 24 in.; $s = 4d$] (continued to the next page)

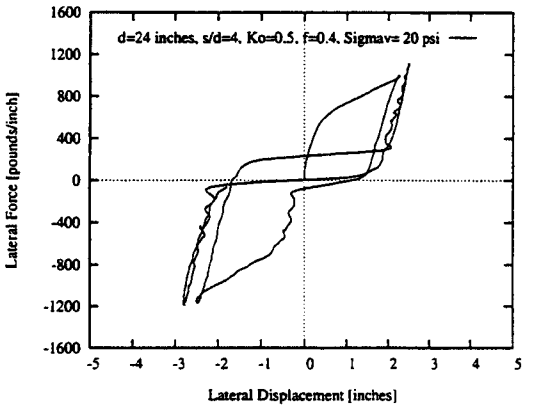

(e)

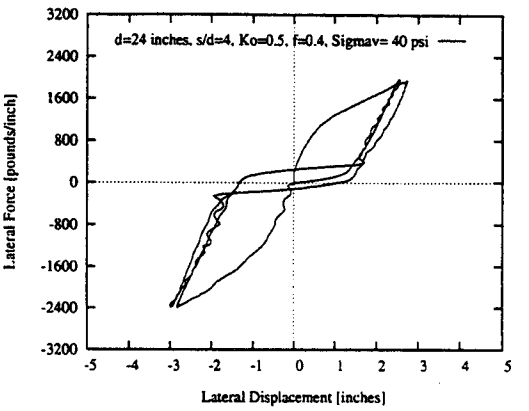

(f)

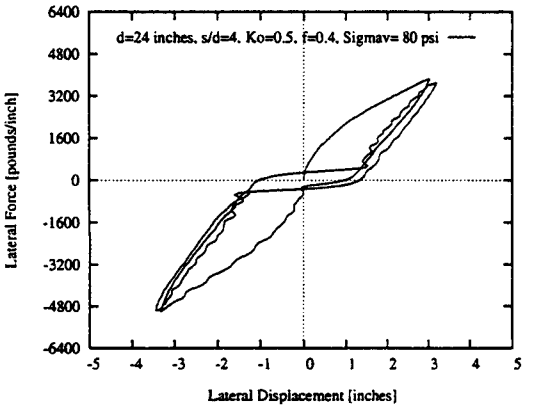

(g)

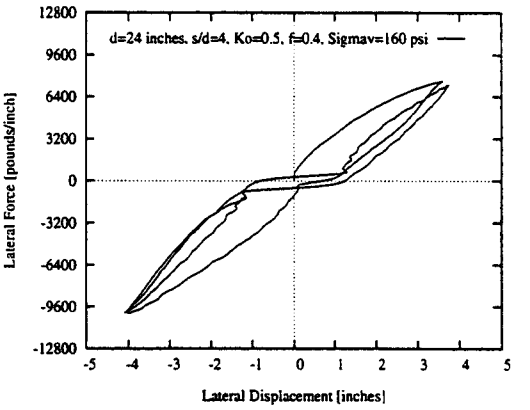

(h)

Figure E.12 p-y curves for the external near-field springs between two piles for direct-lateral vibration for different confining pressures in plane-strain condition. [d = 0.610m = 24 in.; $s = 4d$] (continued)

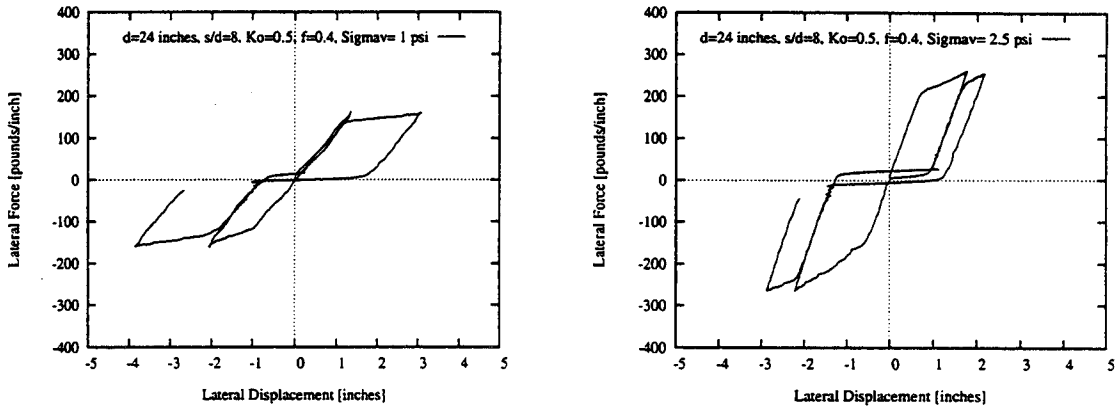

(a)

(b)

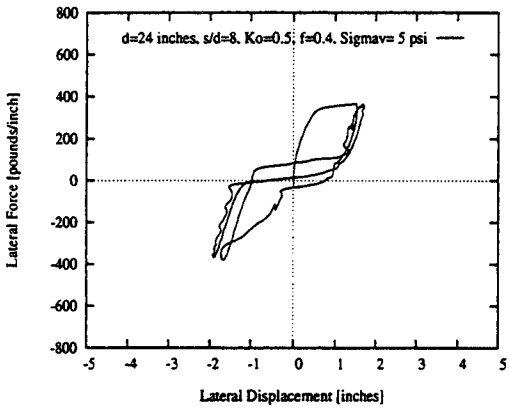

(c)

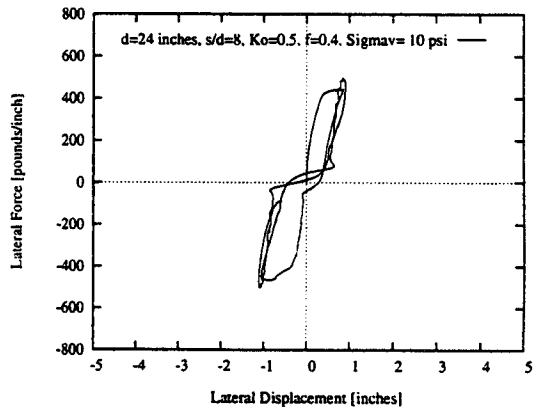

(d)

Figure E.13 p-y curves for the external near-field springs between two piles for direct-lateral vibration for different confining pressures in plane-strain condition. [d = 0.610m = 24 in.; $s = 8d$] (continued to the next page)

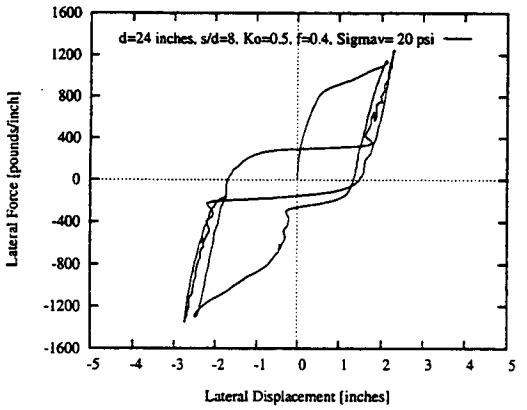

(e)

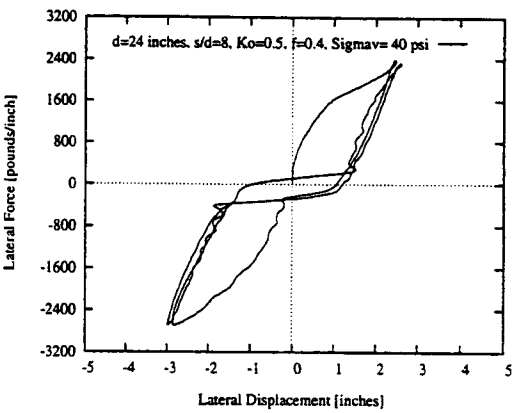

(f)

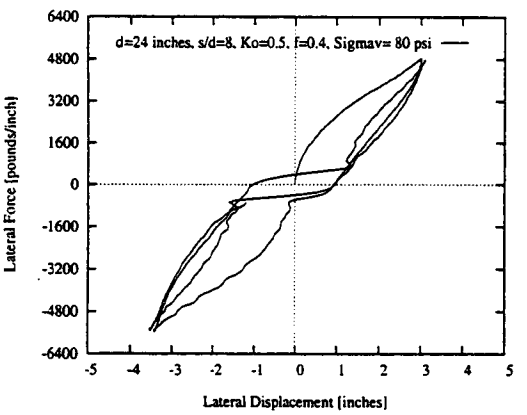

(g)

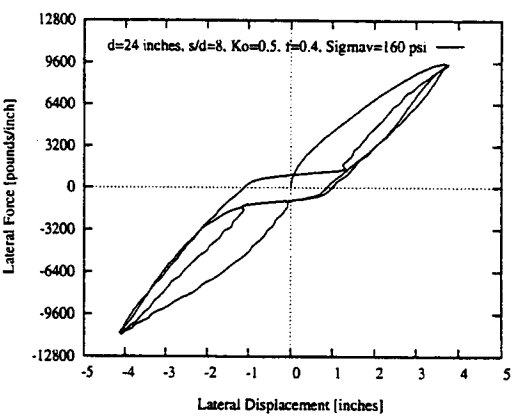

(h)

Figure E.13 p-y curves for the external near-field springs between two piles for direct-lateral vibration for different confining pressures in plane-strain condition. [d = 0.610m = 24 in.; $s = 8d$] (continued)

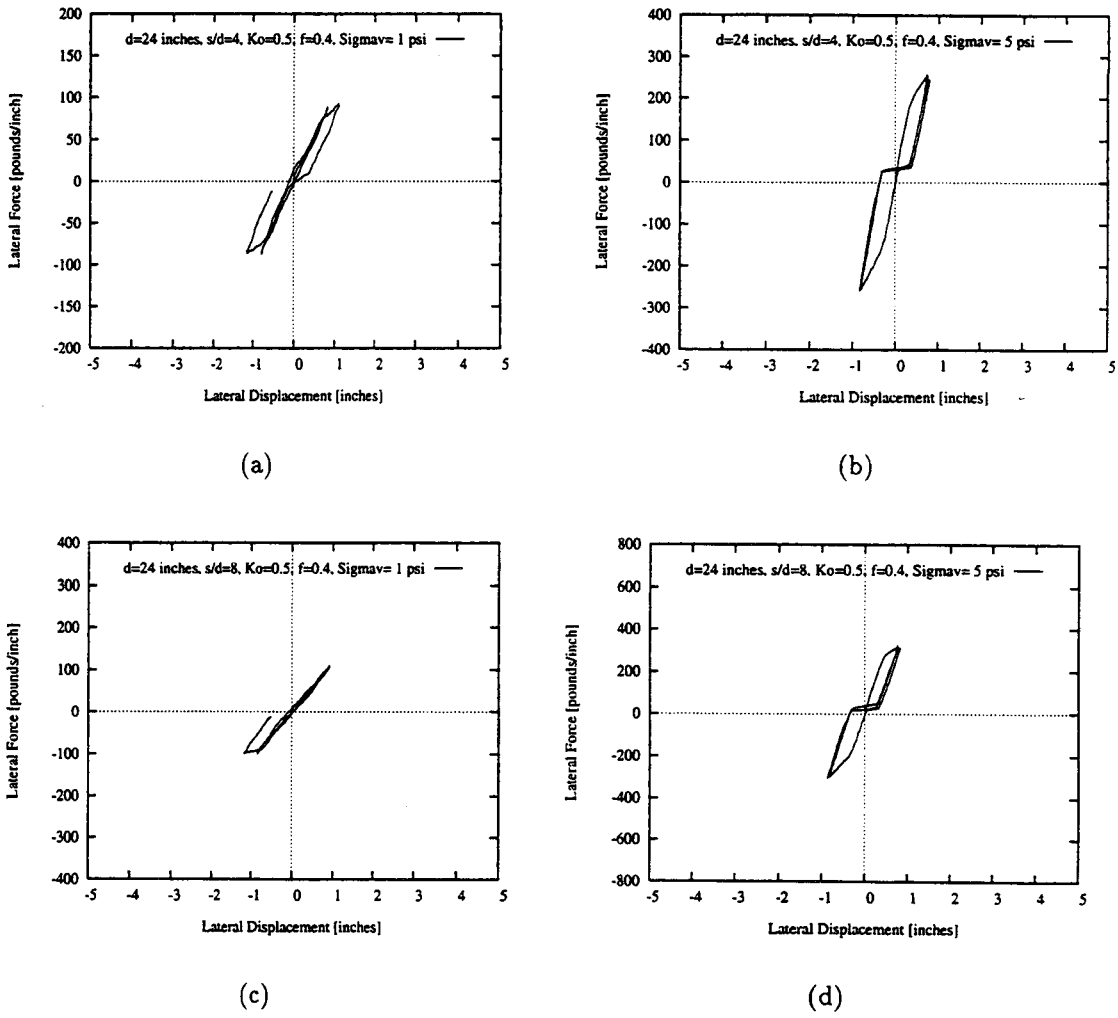

Figure E.14 p-y curves for the external near-field springs between two piles for direct-lateral vibration for different confining pressures in plane-stress condition. [d = 0.610m = 24 in.]

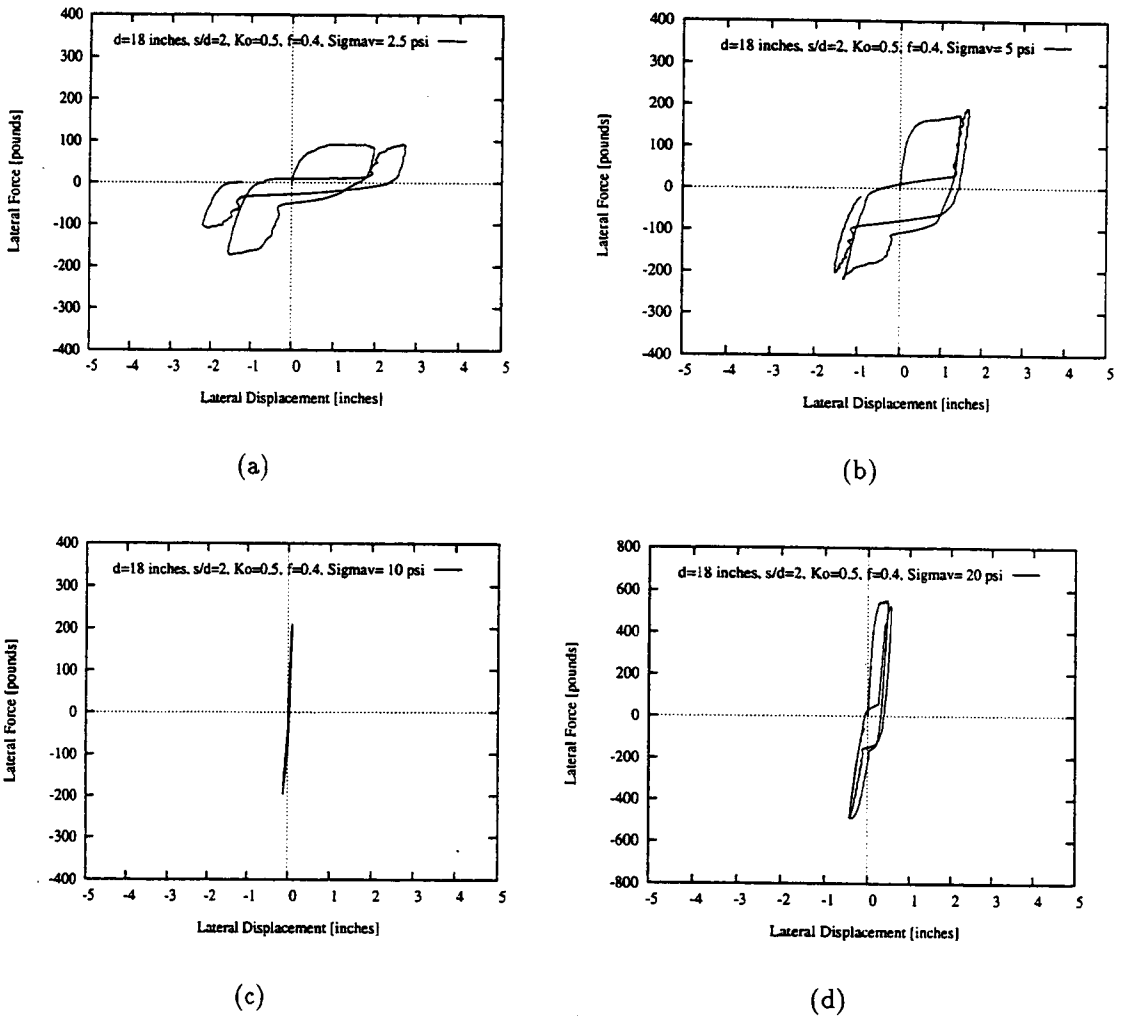

Figure E.15 p-y curves for the interaction-springs between two piles for direct-lateral vibration for different confining pressures in plane-strain condition. [$d = 0.457\text{m} = 18$ in.; $s = 2d$] (continued to the next page)

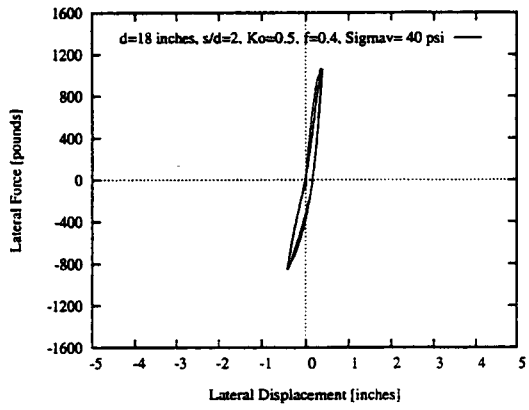

(e)

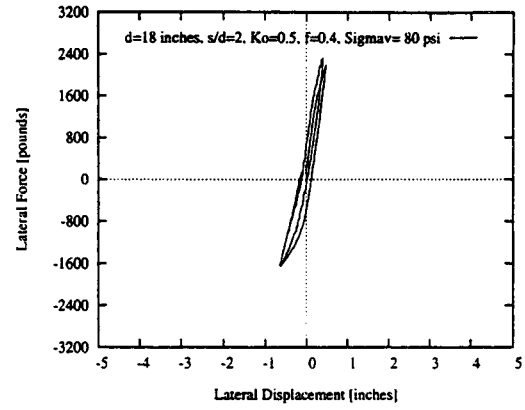

(f)

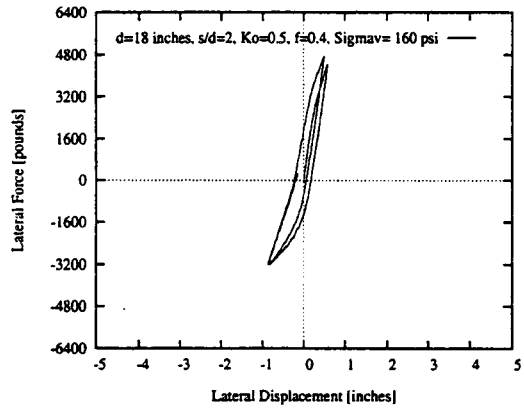

(g)

Figure E.15 p-y curves for the interaction-springs between two piles for direct-lateral vibration for different confining pressures in plane-strain condition. [$d = 0.457\text{m} = 18$ in.; $s = 2d$] (continued)

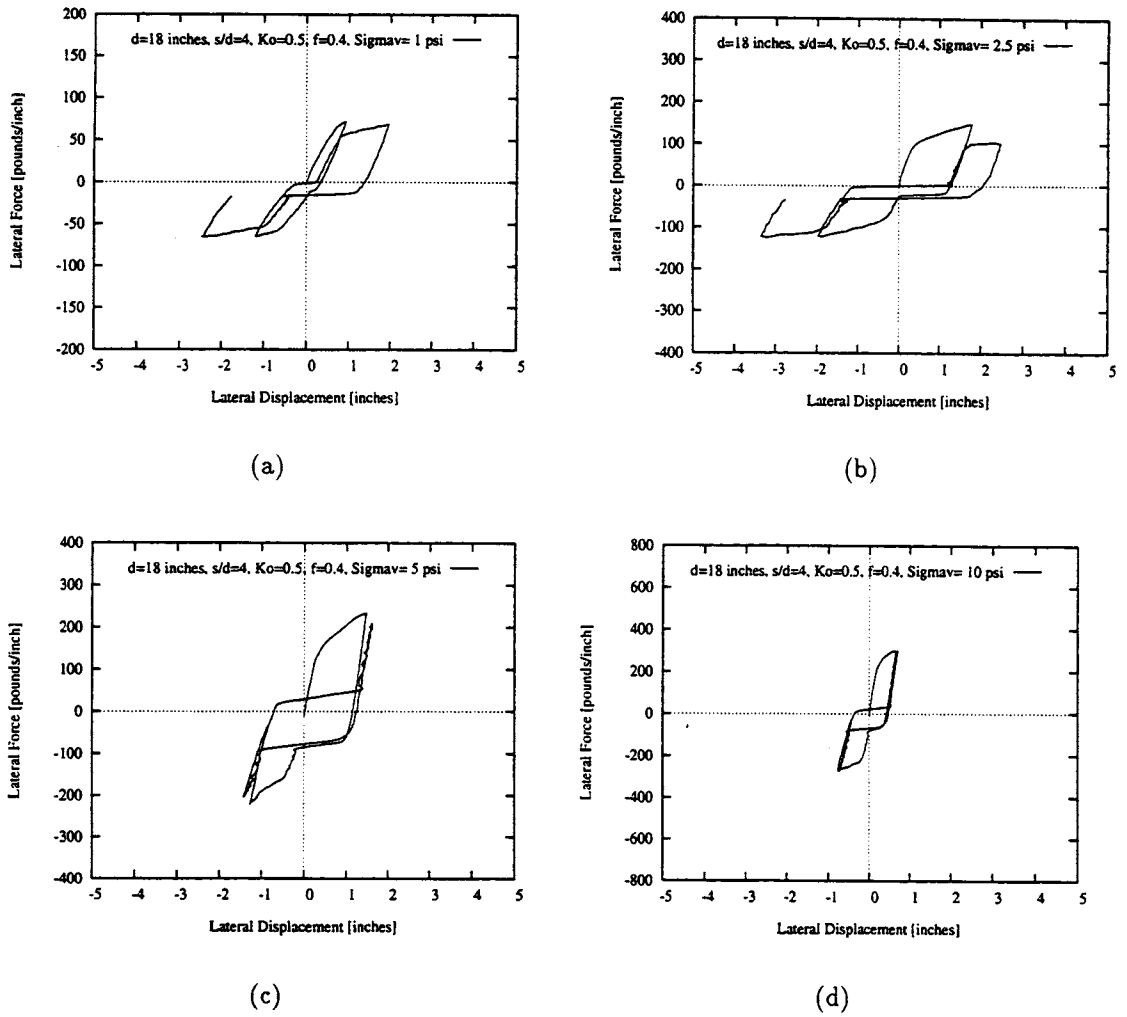

Figure E.16 p-y curves for the interaction-springs between two piles for direct-lateral vibration for different confining pressures in plane-strain condition. [$d = 0.457\text{m} = 18$ in.; $s = 4d$] (continued to the next page)

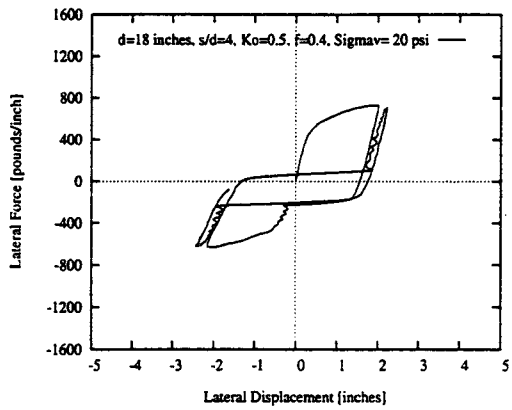

(e)

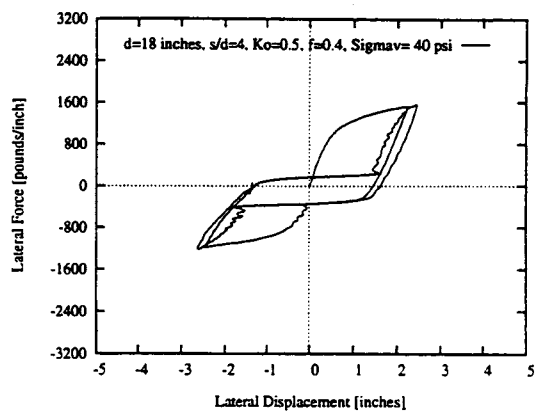

(f)

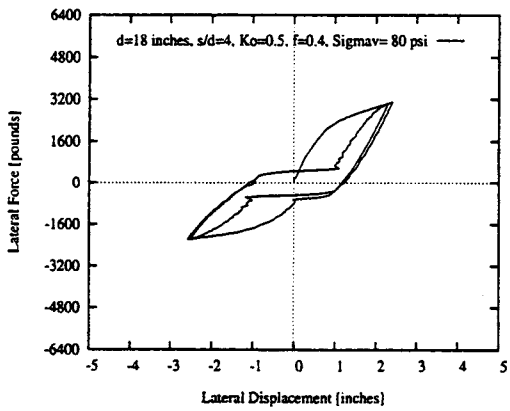

(g)

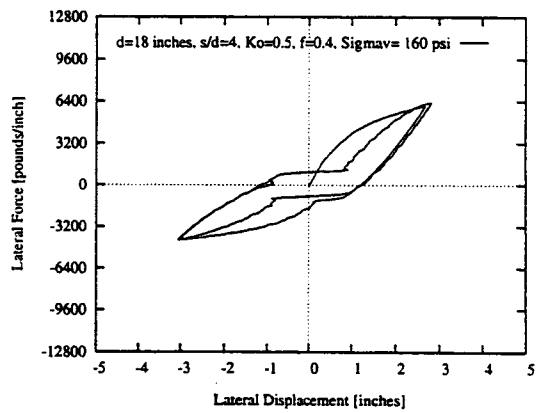

(h)

Figure E.16 p-y curves for the interaction-springs between two piles for direct-lateral vibration for different confining pressures in plane-strain condition. [$d = 0.457\text{m} = 18$ in.; $s = 4d$] (continued)

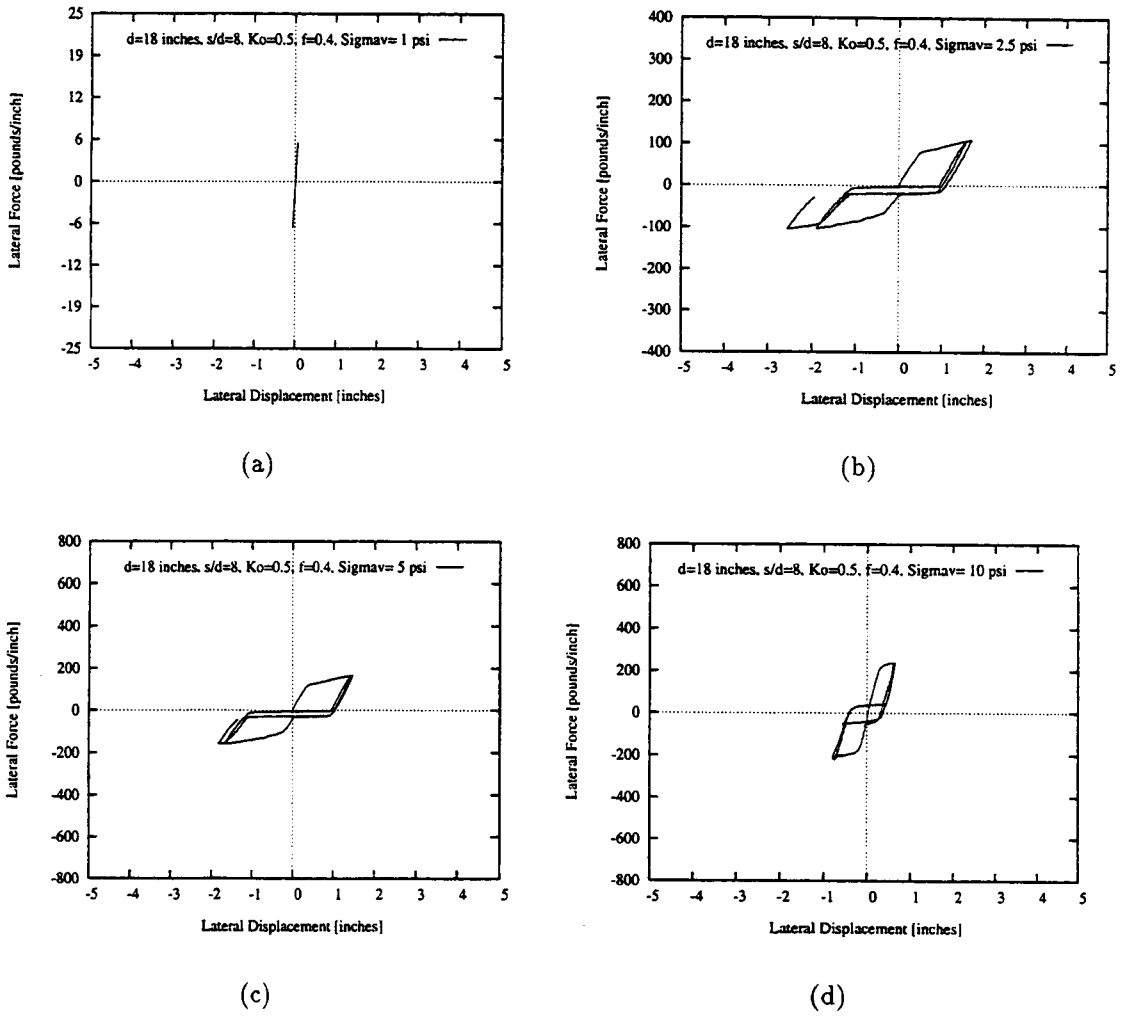

Figure E.17 p-y curves for the interaction-springs between two piles for direct-lateral vibration for different confining pressures in plane-strain condition. [$d = 0.457\text{m} = 18$ in.; $s = 8d$] (continued to the next page)

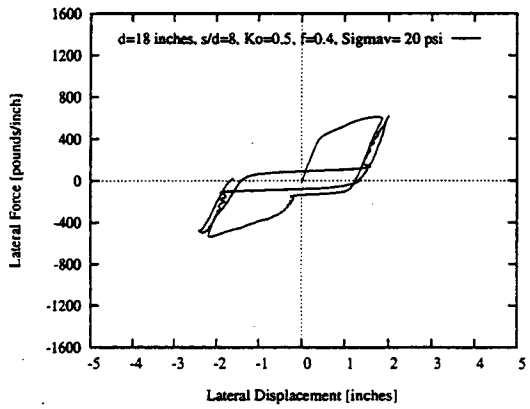

(e)

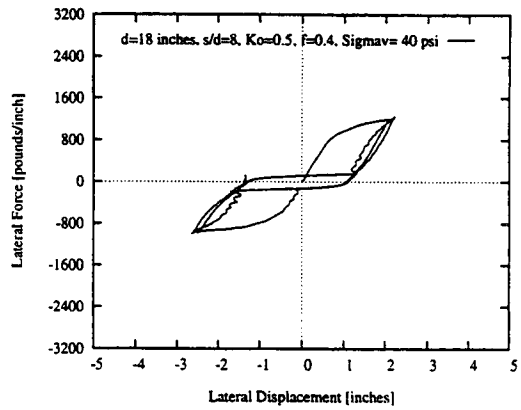

(f)

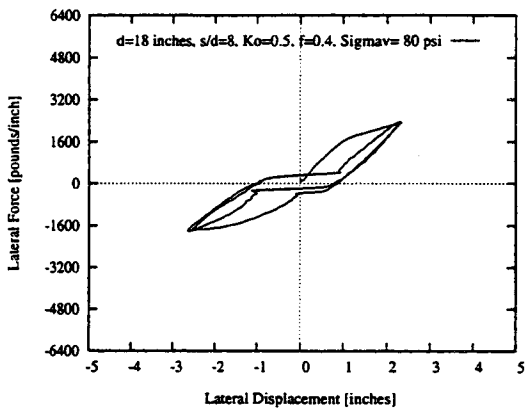

(g)

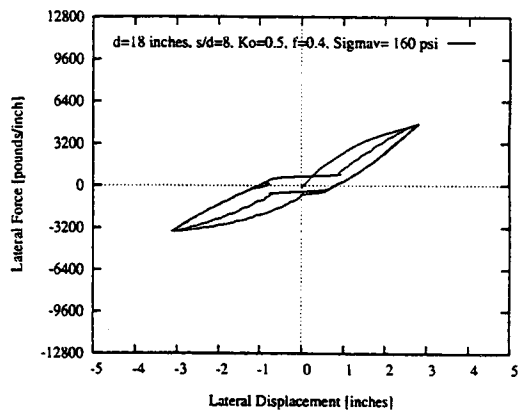

(h)

Figure E.17 p-y curves for the interaction-springs between two piles for direct-lateral vibration for different confining pressures in plane-strain condition. [$d = 0.457\text{m} = 18$ in.; $s = 8d$] (continued)

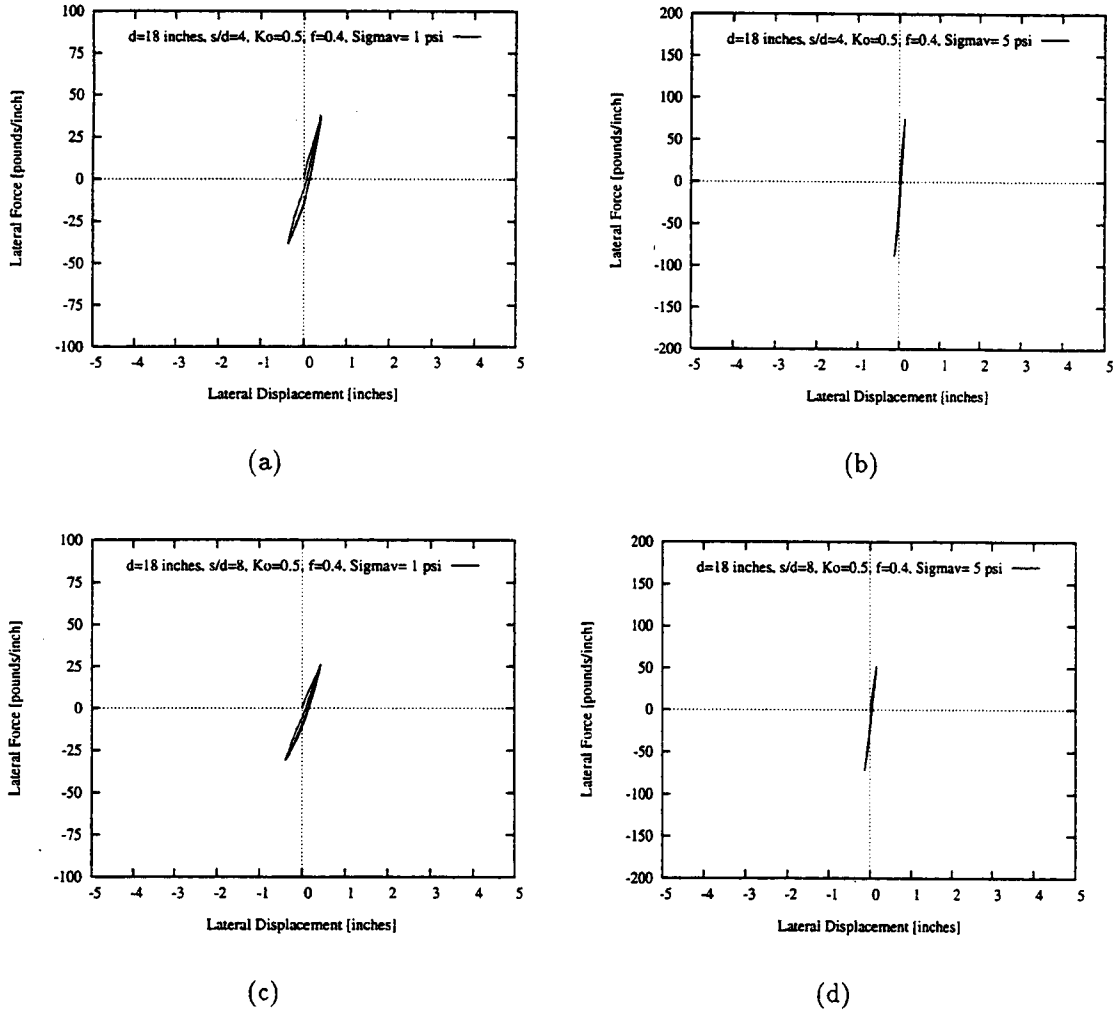

Figure E.18 p-y curves for the interaction-springs between two piles for direct-lateral vibration for different confining pressures in plane-stress condition. [$d = 0.457\text{m} = 18$ in.]

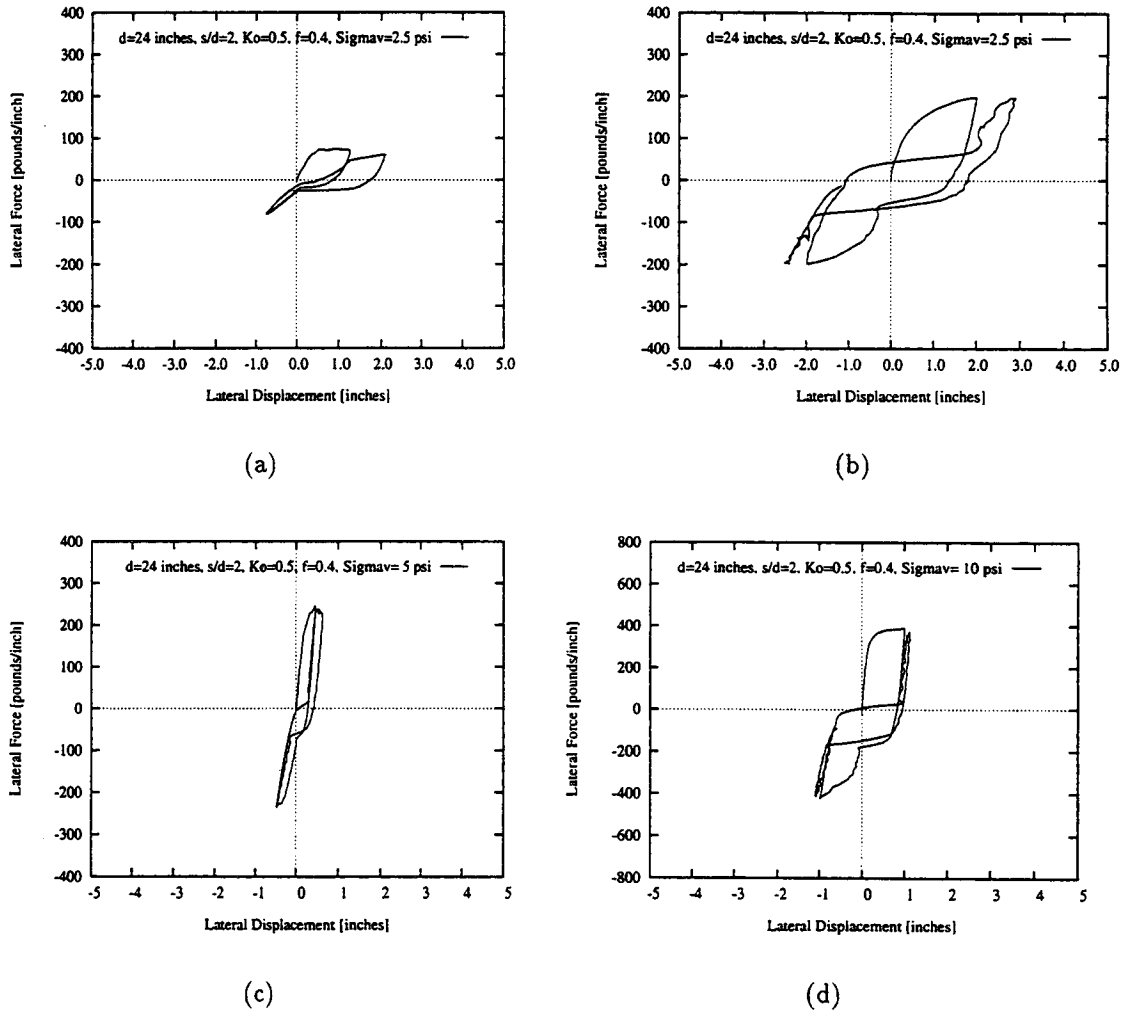

Figure E.19 p-y curves for the interaction-springs between two piles for direct-lateral vibration for different confining pressures in plane-strain condition. [$d = 0.610\text{m} = 24$ in.; $s = 2d$] (continued to the next page)

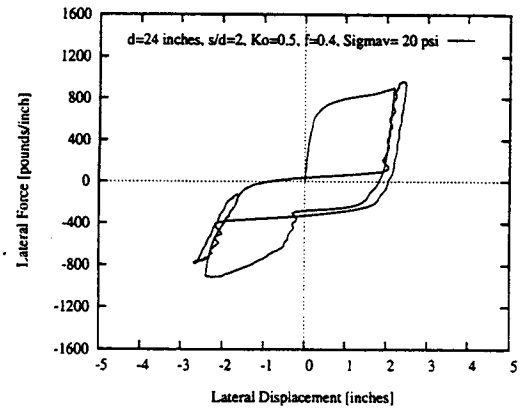

(e)

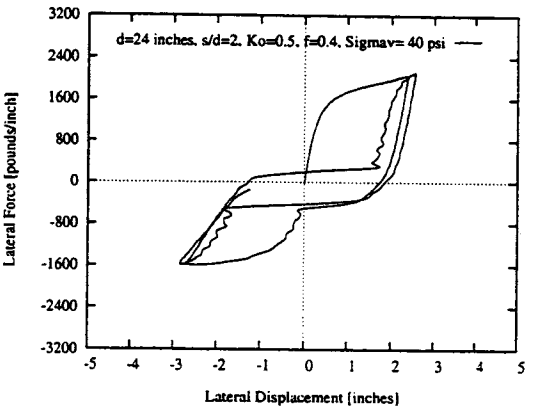

(f)

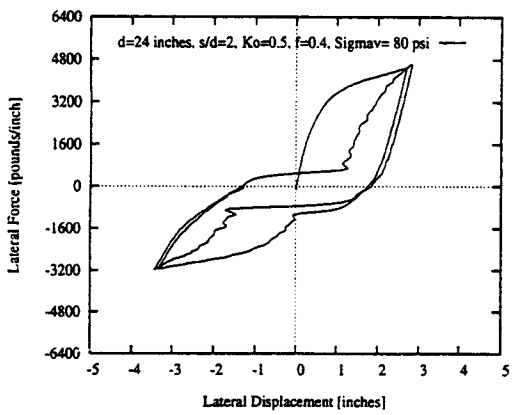

(g)

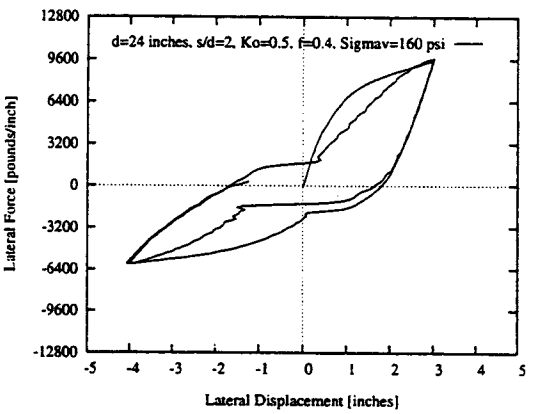

(h)

Figure E.19 p-y curves for the interaction-springs between two piles for direct-lateral vibration for different confining pressures in plane-strain condition. [d = 0.610m = 24 in.; $s = 2d$] (continued)

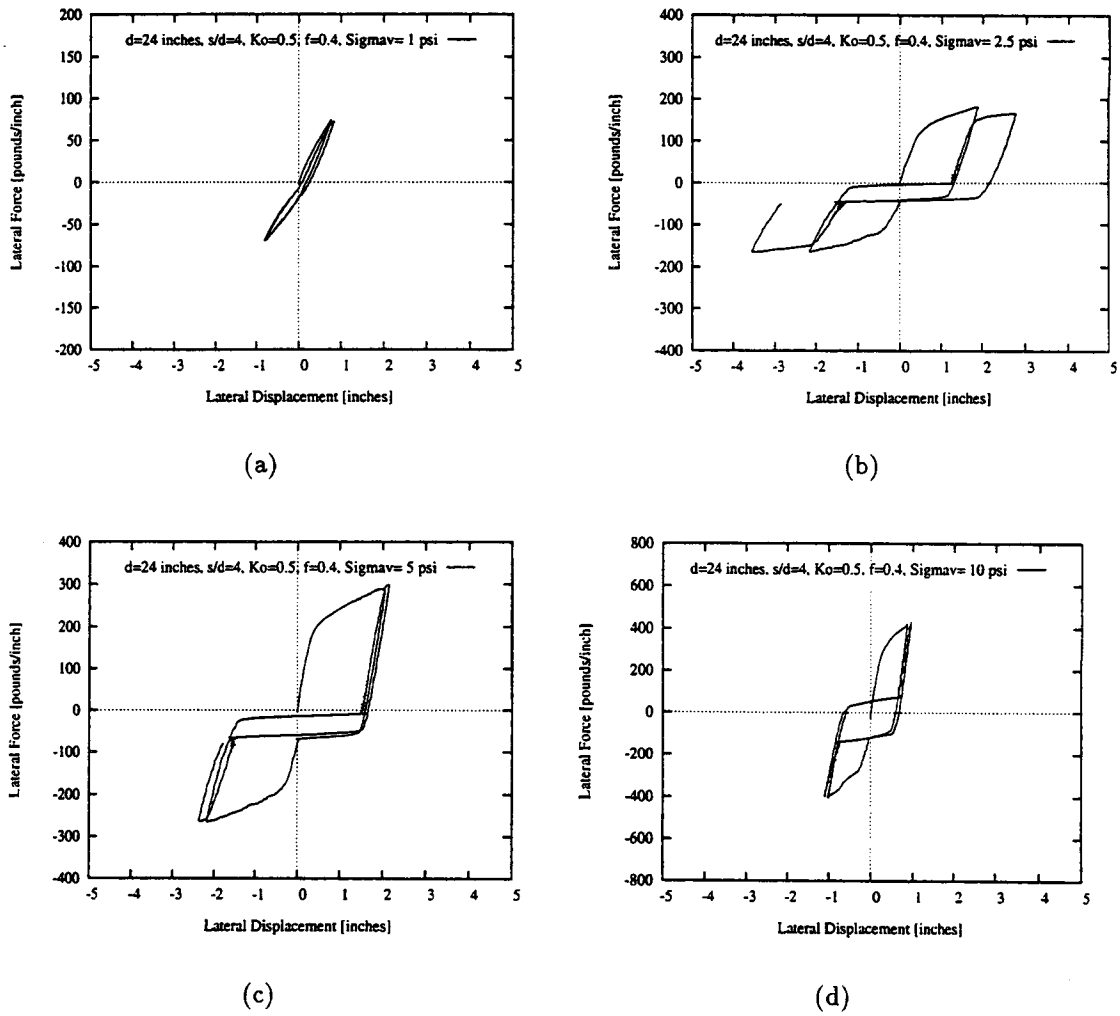

Figure E.20 p-y curves for the interaction-springs between two piles for direct-lateral vibration for different confining pressures in plane-strain condition. [$d = 0.610\text{m} = 24$ in.; $s = 4d$] (continued to the next page)

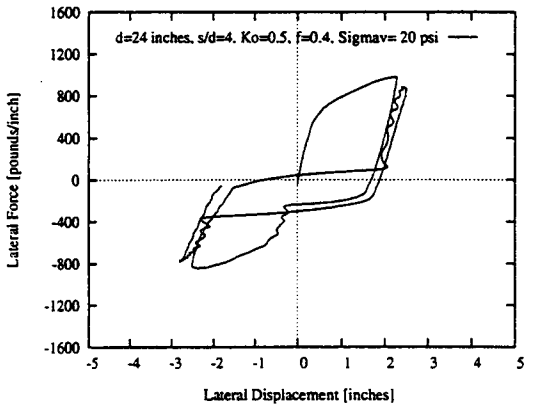

(e)

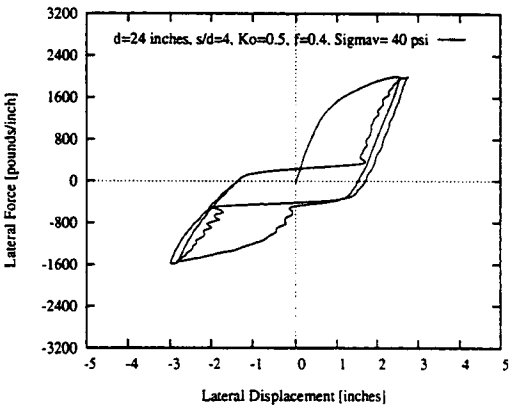

(f)

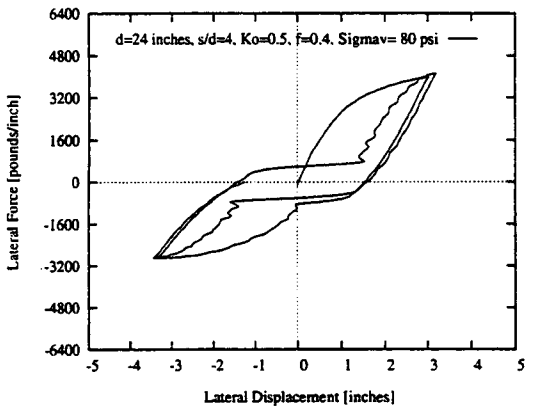

(g)

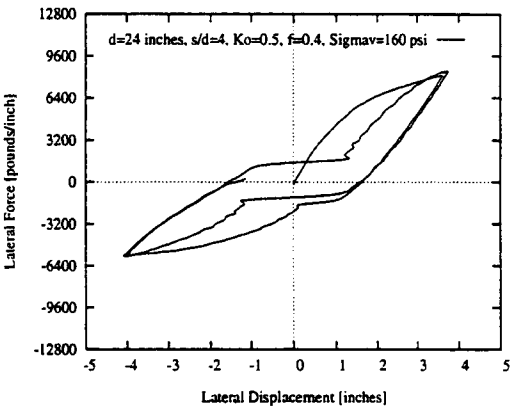

(h)

Figure E.20 p-y curves for the interaction-springs between two piles for direct-lateral vibration for different confining pressures in plane-strain condition. [$d = 0.610\text{m} = 24$ in.; $s = 4d$] (continued)

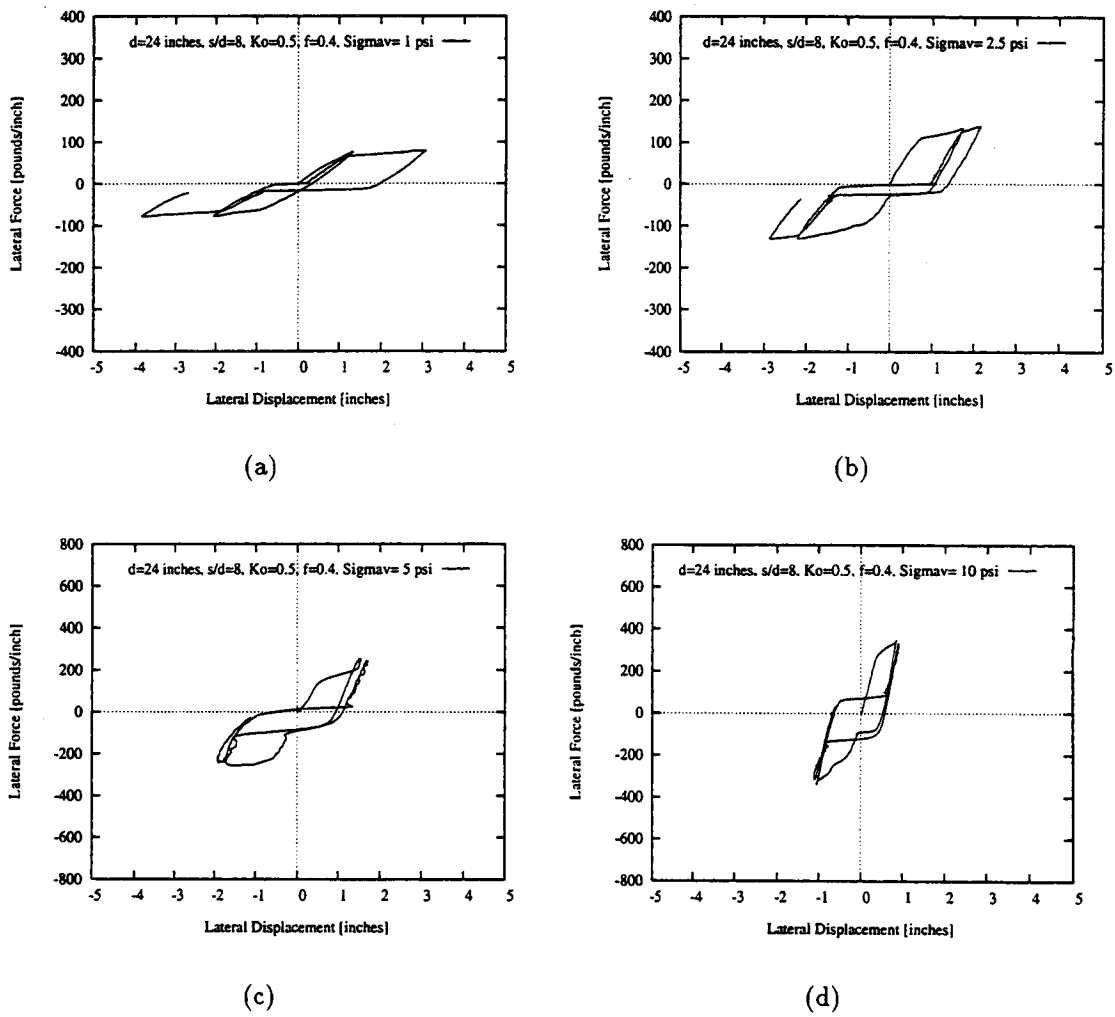

Figure E.21 p-y curves for the interaction-springs between two piles for direct-lateral vibration for different confining pressures in plane-strain condition. [$d = 0.610\text{m} = 24$ in.; $s = 8d$] (continued to the next page)

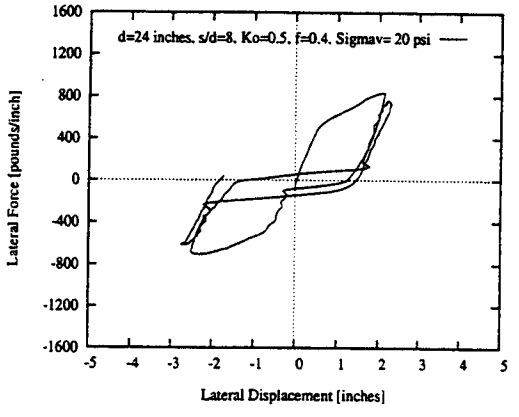

(e)

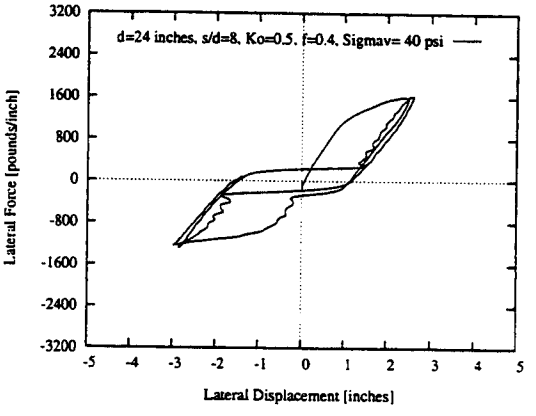

(f)

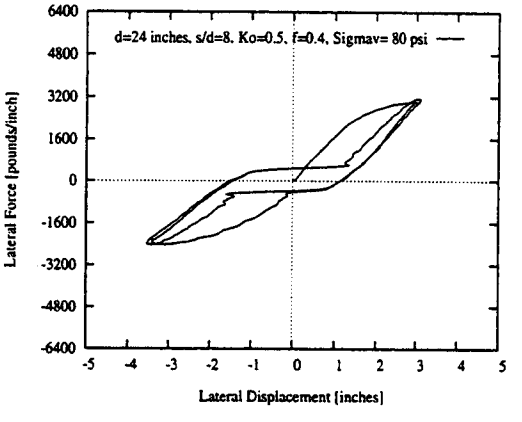

(g)

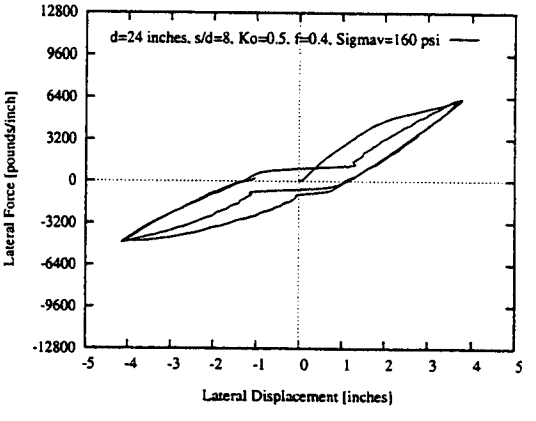

(h)

Figure E.21 p-y curves for the interaction-springs between two piles for direct-lateral vibration for different confining pressures in plane-strain condition. [$d = 0.610\text{m} = 24$ in.; $s = 8d$] (continued)

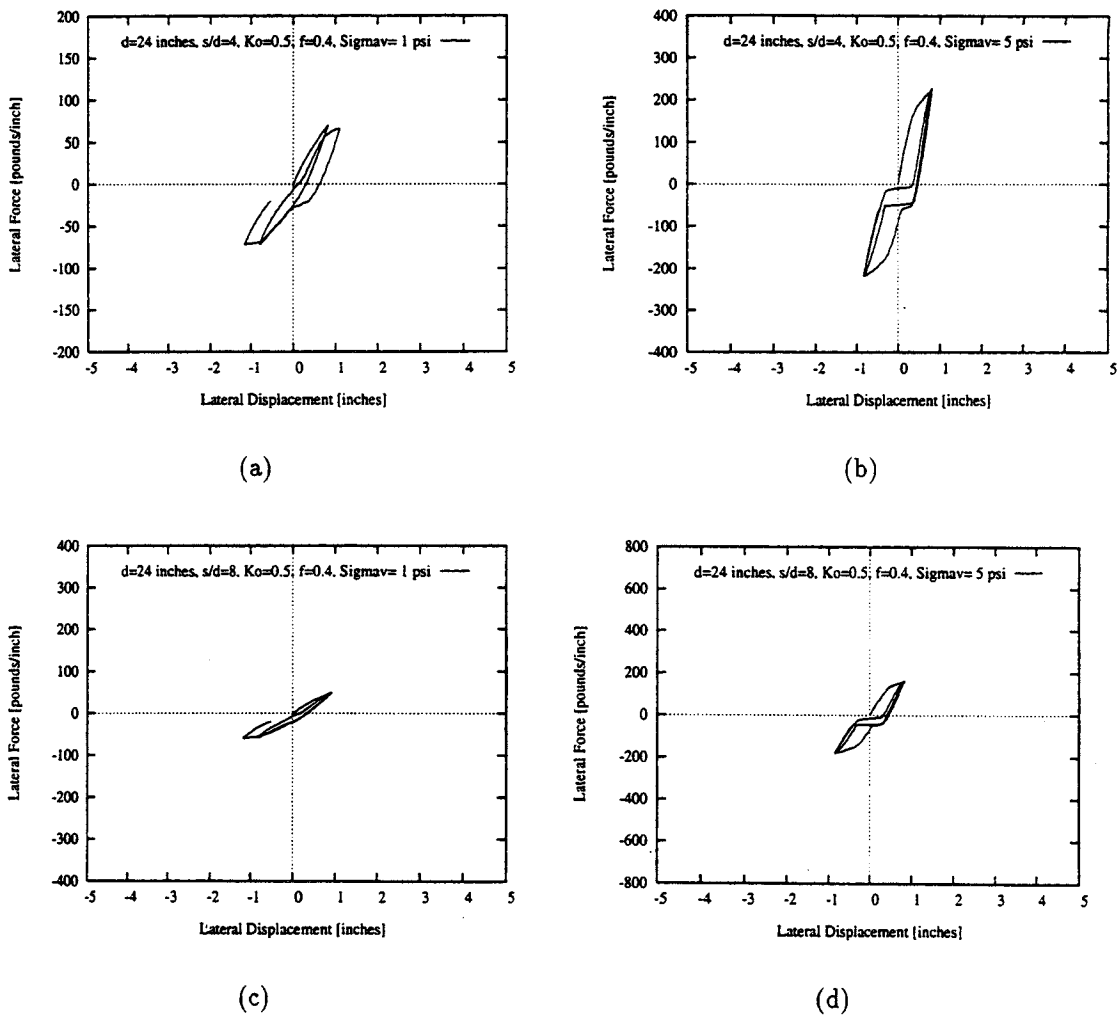

Figure E.22 p-y curves for the interaction-springs between two piles for direct-lateral vibration for different confining pressures in plane-stress condition. [$d = 0.610\text{m} = 24$ in.]

E.2.2.2 Shear-Lateral Vibration of Two-Pile Group

For the two-pile groups with vibration in both lateral directions, two types of additional springs are required. One is an interaction shear-spring and the other is for connecting pile-segments with the surrounding soil. For the computation of shear-interaction-spring behavior, the two piles with soil were modeled within the finite element framework. From this thin layer finite element model, the interaction behavior was obtained using the same procedure as that used for direct interaction-springs. The above procedure was followed for different depths represented by 6.9, 17.3, 34.5, 68.9, 137.8, 275.6, 551.2, and 1102.4 kPa (1, 2.5, 5, 10, 20, 40, 80, and 160 psi) vertical stresses in plane-strain condition, and 6.9 and 34.5 kPa (1 and 5 psi) in plane-stress condition, for drained behavior of the soil, and for center spacing of $2d$, $4d$, and $8d$. The resulting p-y behavior of the interaction-springs and the near-field springs is presented in Figures E.23 through E.38 for soil from the Snohomish river site. The NEABS parameters for those spring were computed, and they are presented in Tables 2.11 through 2.14.

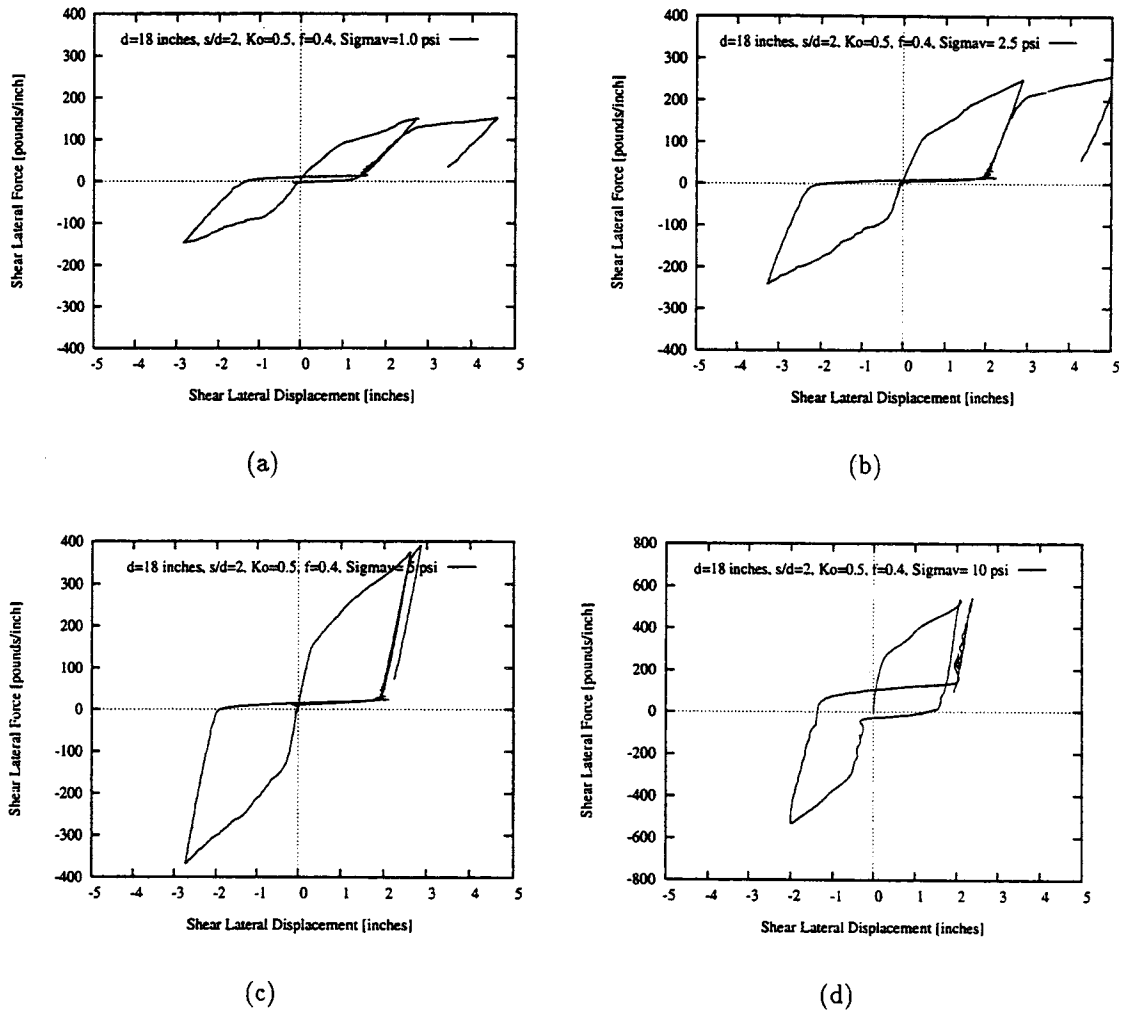

Figure E.23 p-y curves for the near-field springs between two piles in a two-pile group for shear-lateral vibration for different confining pressures for plane-strain condition. [d = 0.457m = 18 in.; $s = 2d$] (continued to the next page)

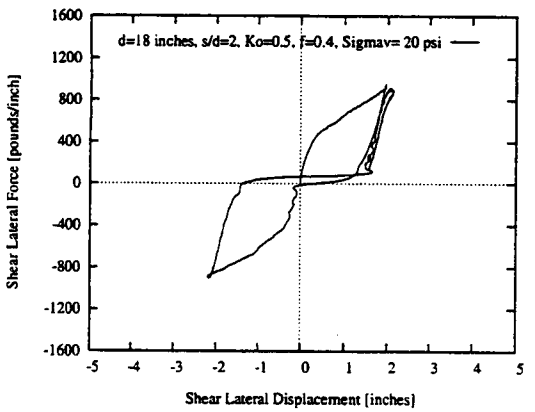

(e)

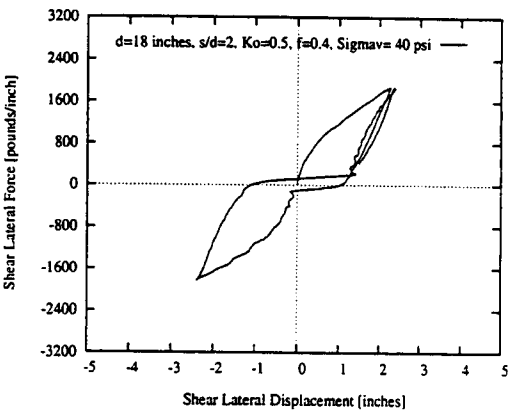

(f)

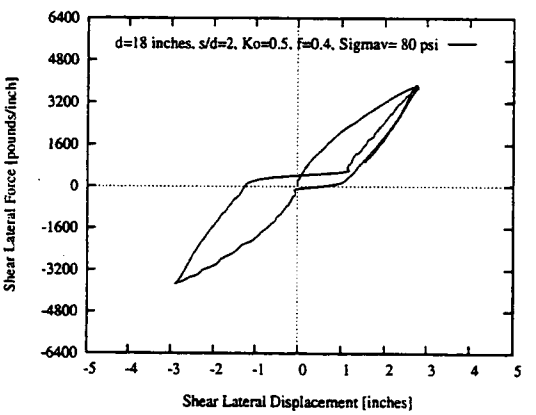

(g)

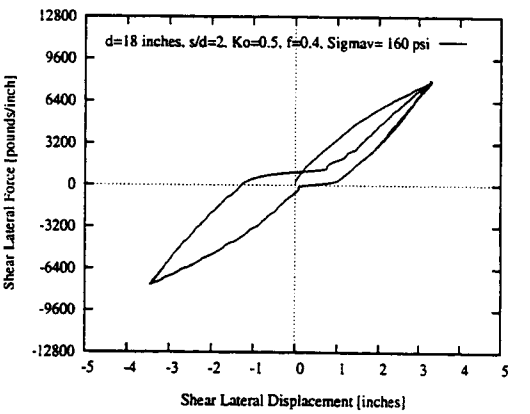

(h)

Figure E.23 p-y curves for the near-field springs between two piles in a two-pile group for shear-lateral vibration for different confining pressures for plane-strain condition. [d = 0.457m = 18 in.; $s = 2d$] (continued)

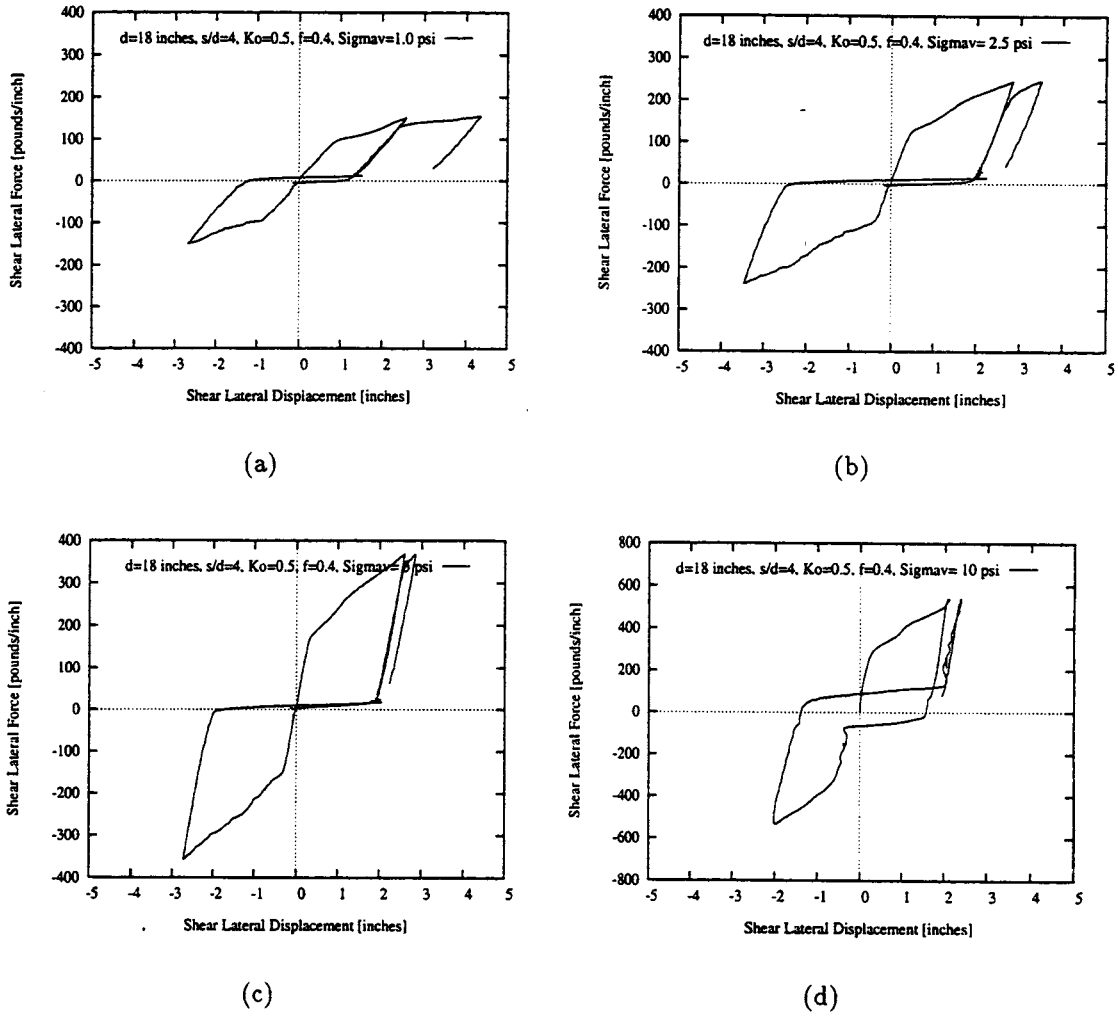

Figure E.24 p-y curves for the near-field springs between two piles in a two-pile group for shear-lateral vibration for different confining pressures for plane-strain condition. [d = 0.457m = 18 in.; $s = 4d$] (continued to the next page)

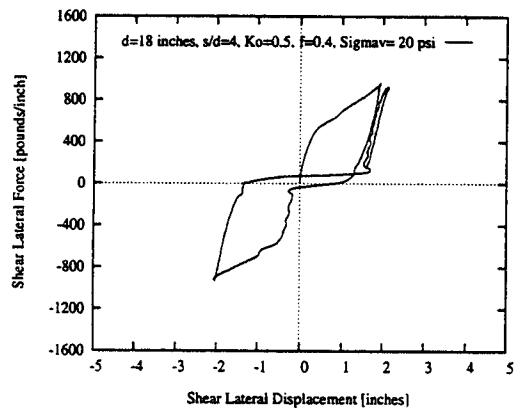

(e)

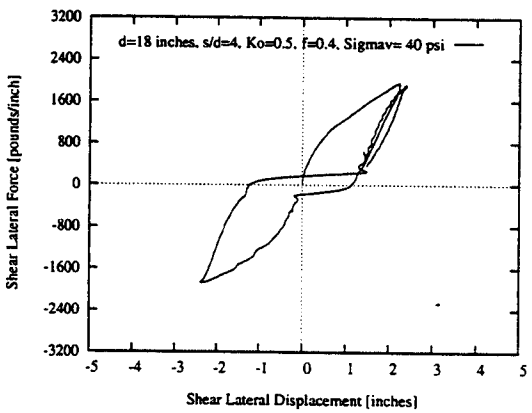

(f)

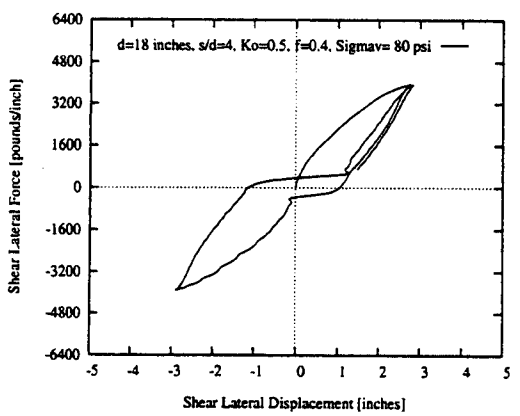

(g)

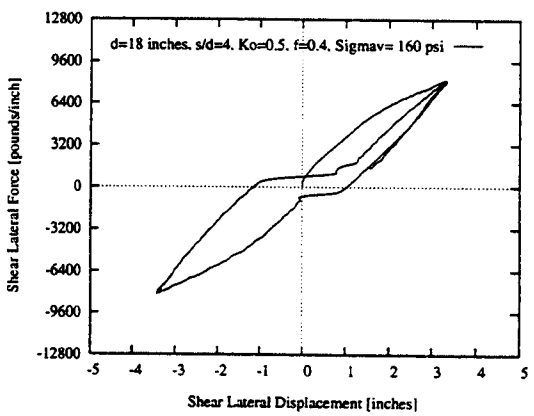

(h)

Figure E.24 *p-y* curves for the near-field springs between two piles in a two-pile group for shear-lateral vibration for different confining pressures for plane-strain condition. [d = 0.457m = 18 in.; $s = 4d$] (continued)

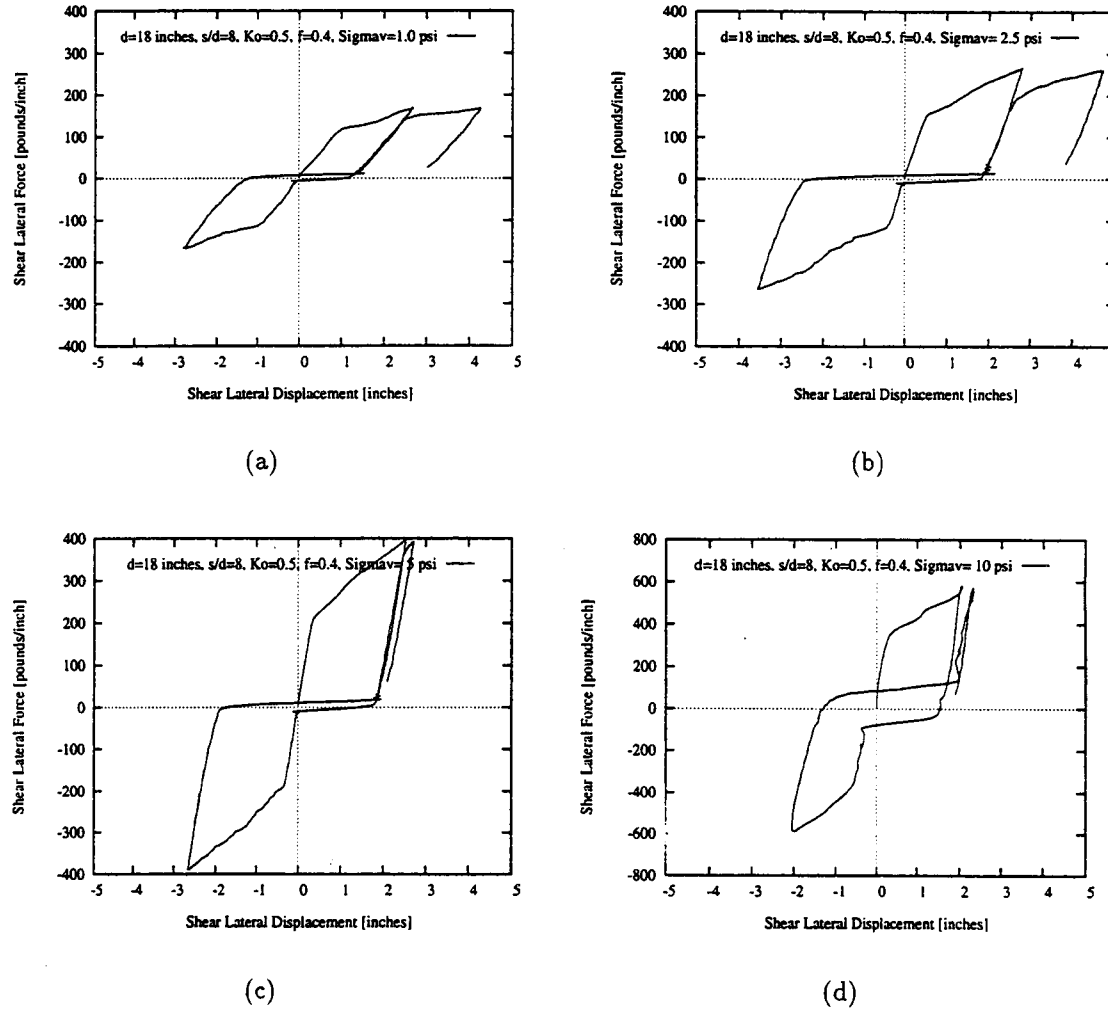

Figure E.25 p-y curves for the near-field springs between two piles in a two-pile group for shear-lateral vibration for different confining pressures for plane-strain condition. [d = 0.457m = 18 in.; $s = 8d$] (continued to the next page)

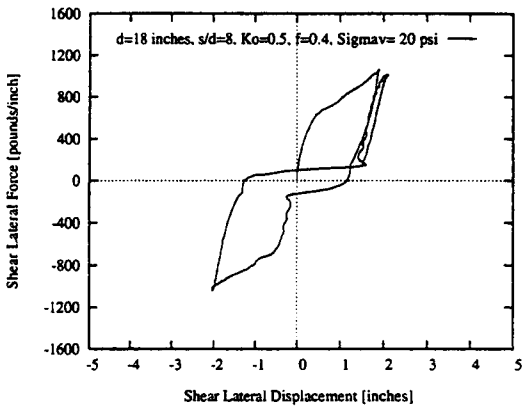

(e)

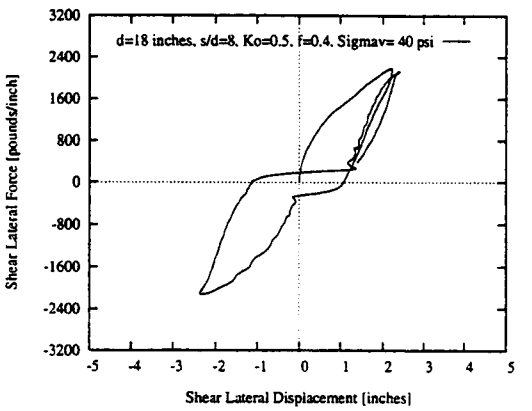

(f)

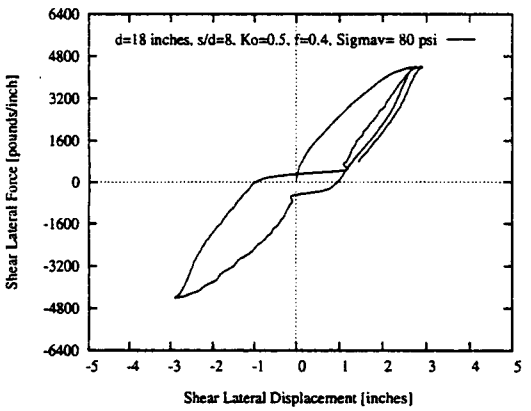

(g)

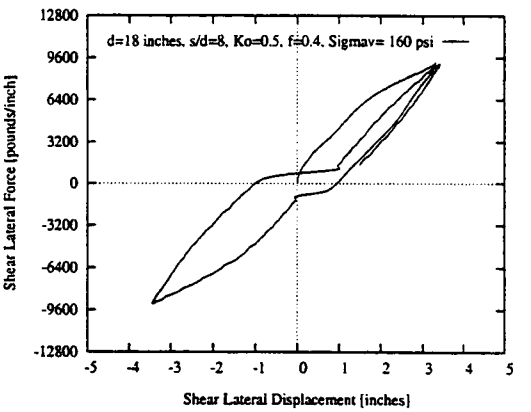

(h)

Figure E.25 p-y curves for the near-field springs between two piles in a two-pile group for shear-lateral vibration for different confining pressures for plane-strain condition. [d = 0.457m = 18 in.; $s = 8d$] (continued)

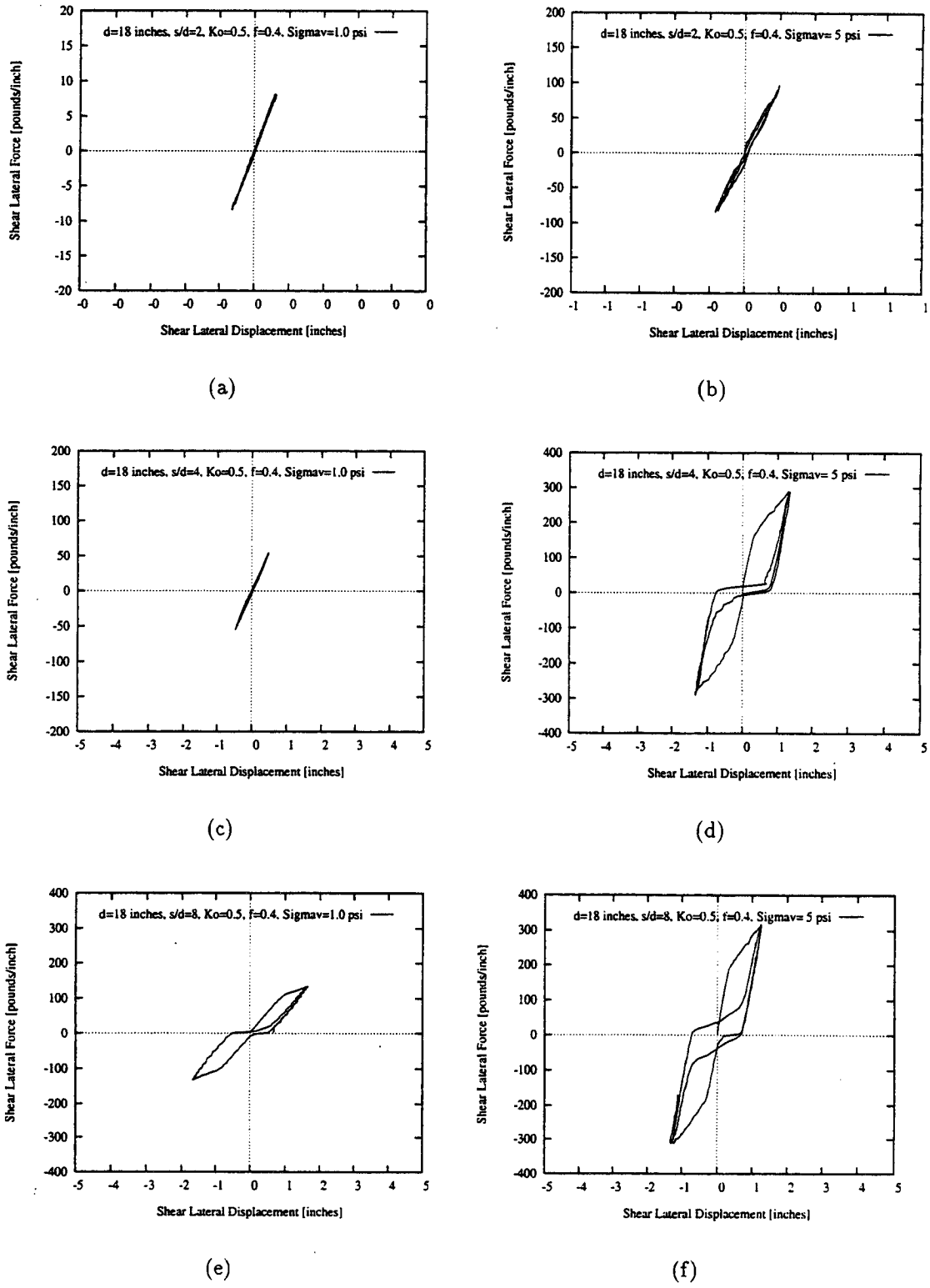

Figure E.26 p-y curves for the near-field springs between two piles in a two-pile group for shear-lateral vibration for different confining pressures for plane-stress condition. [d = 0.457m = 18 in.]

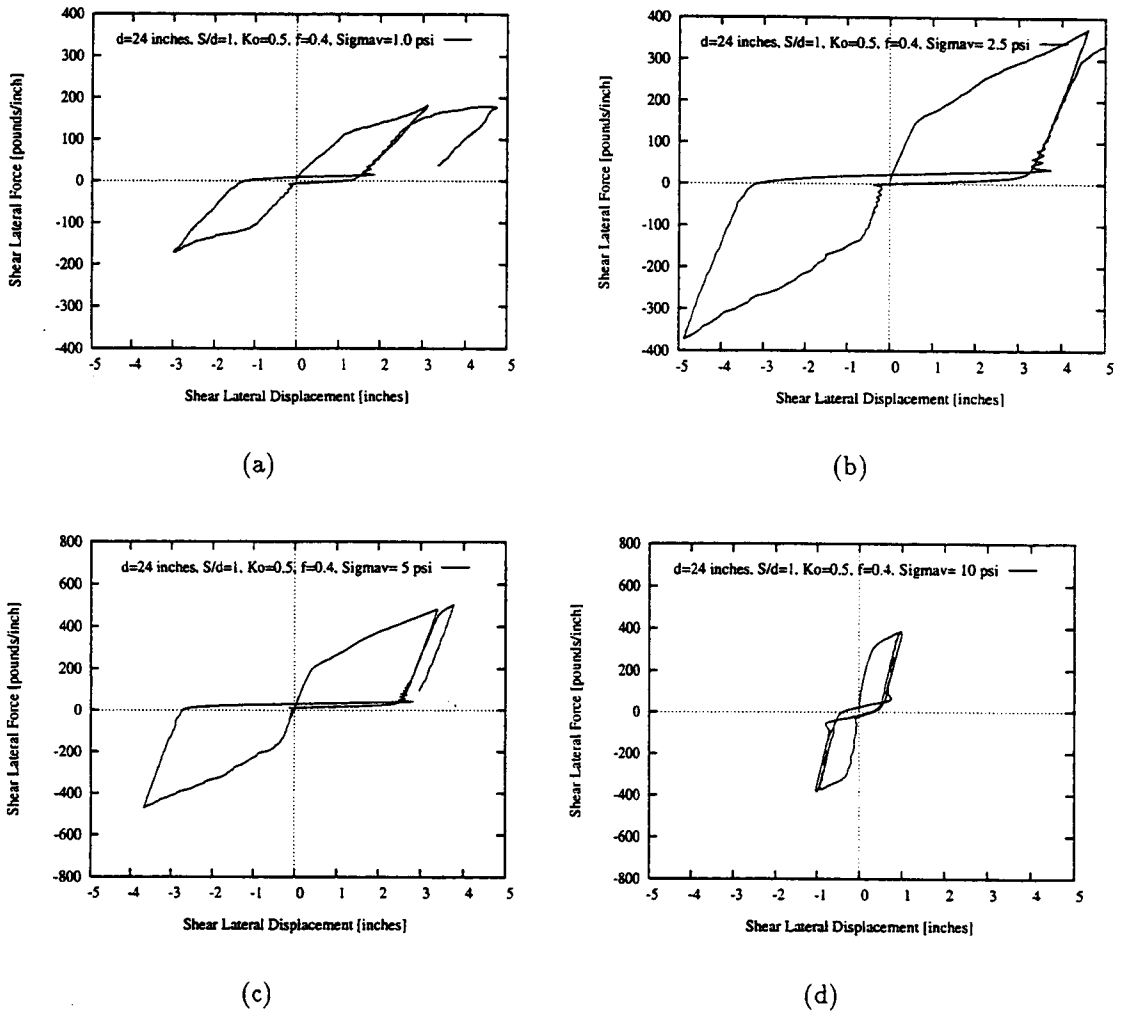

Figure E.27 p-y curves for the near-field springs between two piles in a two-pile group for shear-lateral vibration for different confining pressures for plane-strain condition. [d = 0.610m = 24 in.; $s = 2d$] (continued to the next page)

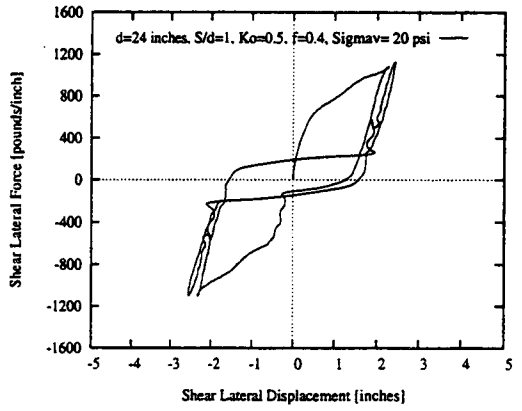

(e)

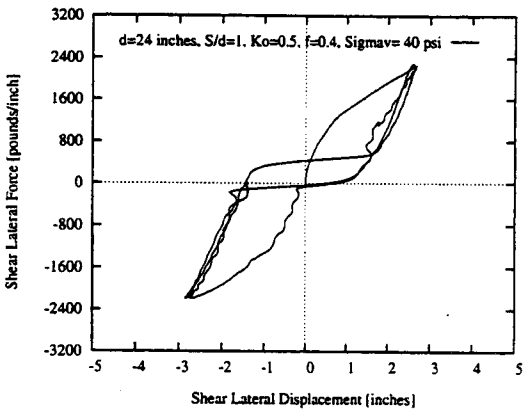

(f)

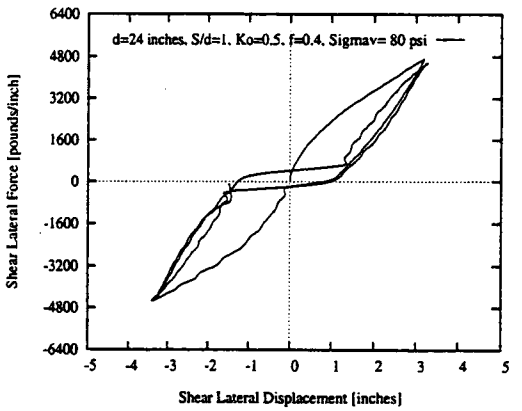

(g)

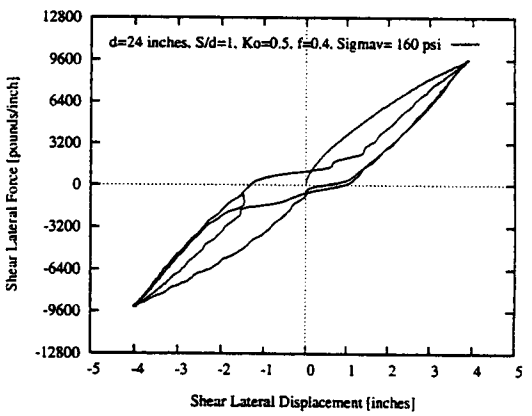

(h)

Figure E.27 p-y curves for the near-field springs between two piles in a two-pile group for shear-lateral vibration for different confining pressures for plane-strain condition. [d = 0.610m = 24 in.; $s = 2d$] (continued)

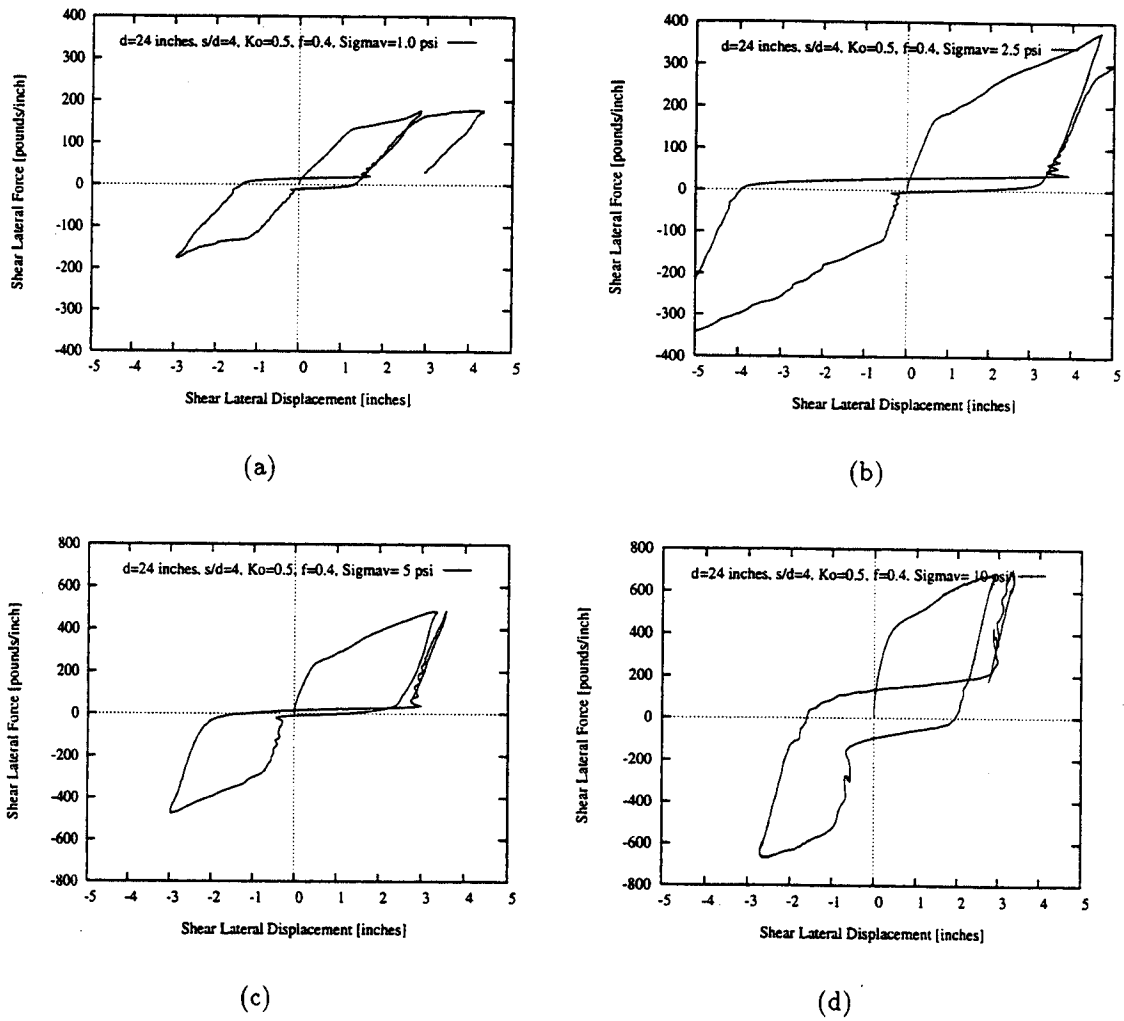

Figure E.28 p-y curves for the near-field springs between two piles in a two-pile group for shear-lateral vibration for different confining pressures for plane-strain condition. [d = 0.610m = 24 in.; $s = 4d$] (continued to the next page)

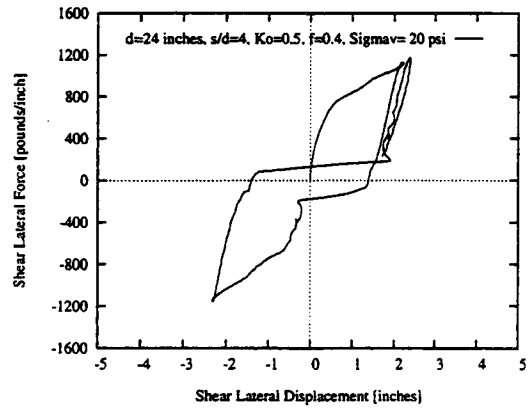

(e)

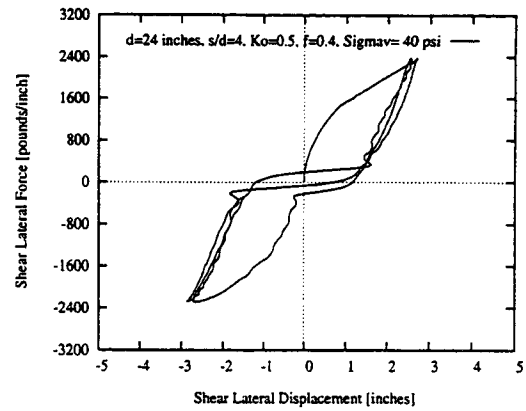

(f)

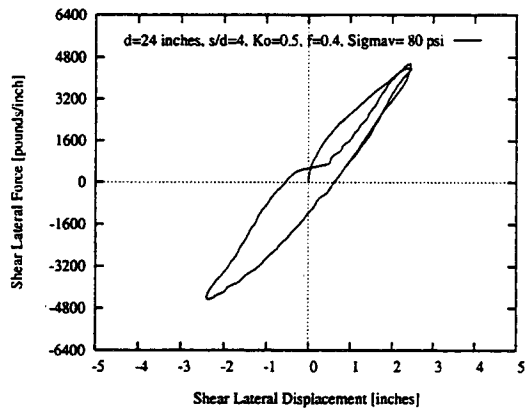

(g)

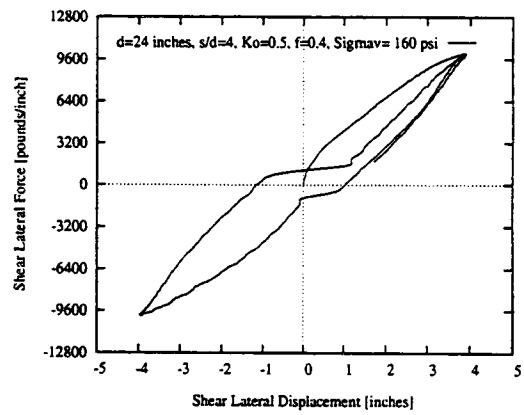

(h)

Figure E.28 p-y curves for the near-field springs between two piles in a two-pile group for shear-lateral vibration for different confining pressures for plane-strain condition. [d = 0.610m = 24 in.; $s = 4d$] (continued)

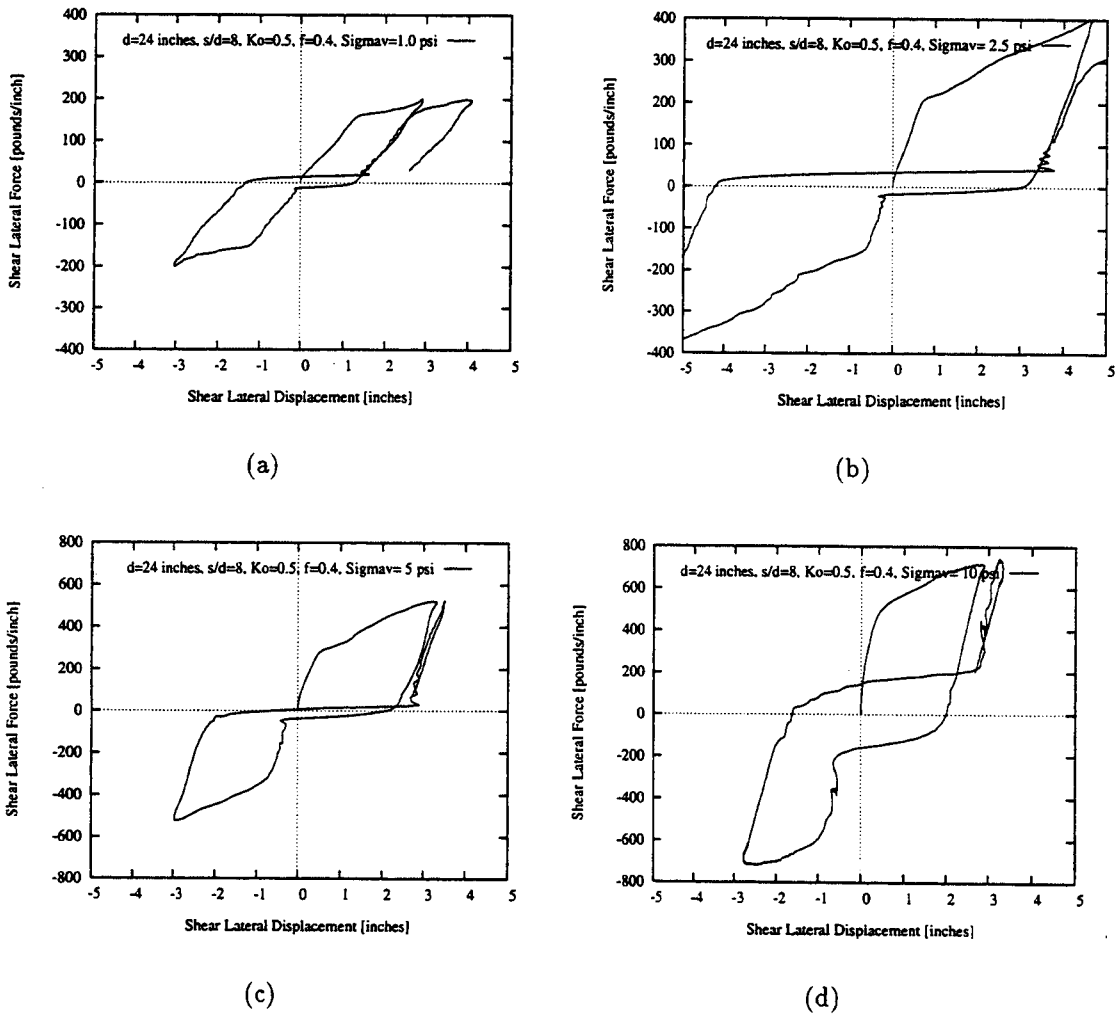

Figure E.29 p-y curves for the near-field springs between two piles in a two-pile group for shear-lateral vibration for different confining pressures for plane-strain condition. [d = 0.610m = 24 in.; $s = 8d$] (continued to the next page)

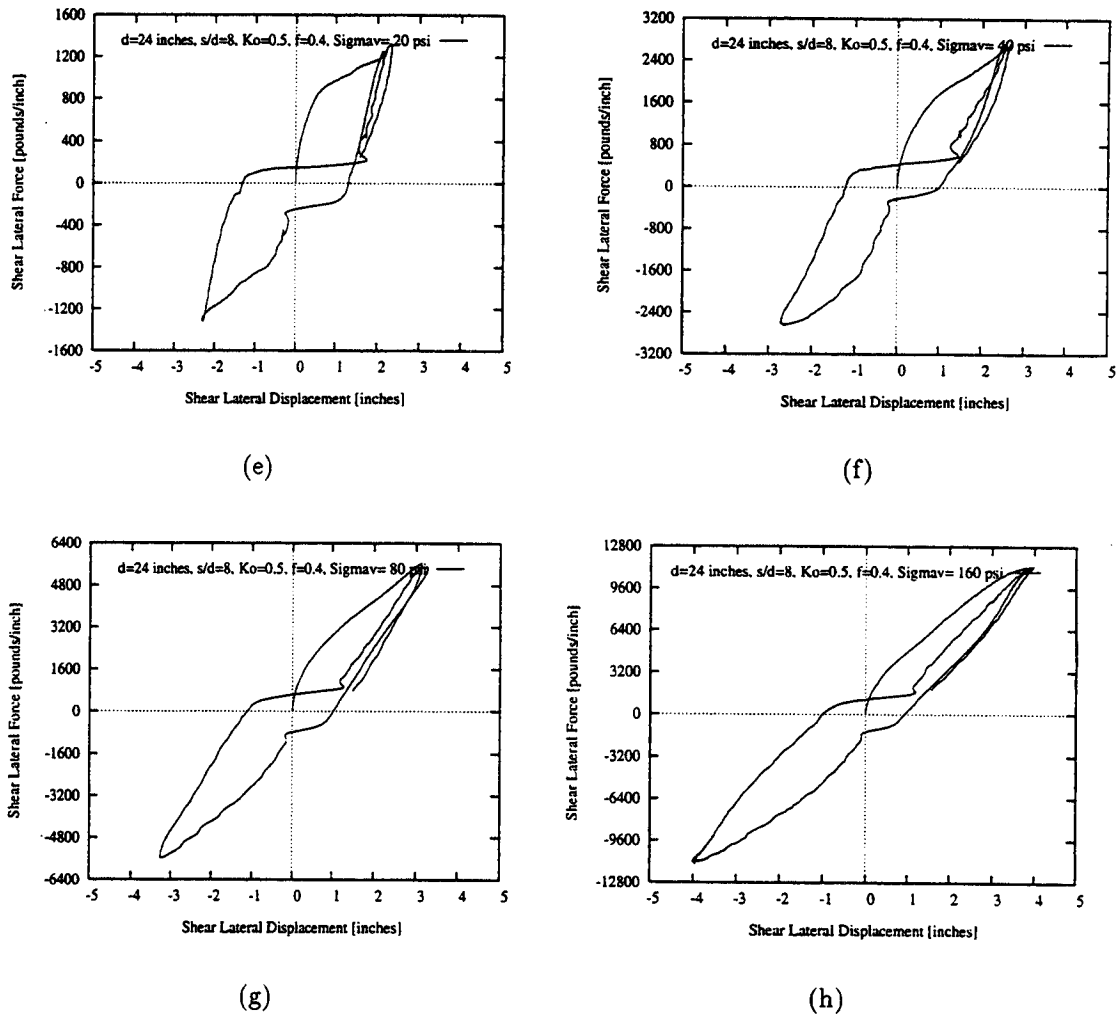

Figure E.29 p-y curves for the near-field springs between two piles in a two-pile group for shear-lateral vibration for different confining pressures for plane-strain condition. [d = 0.610m = 24 in.; $s = 8d$] (continued)

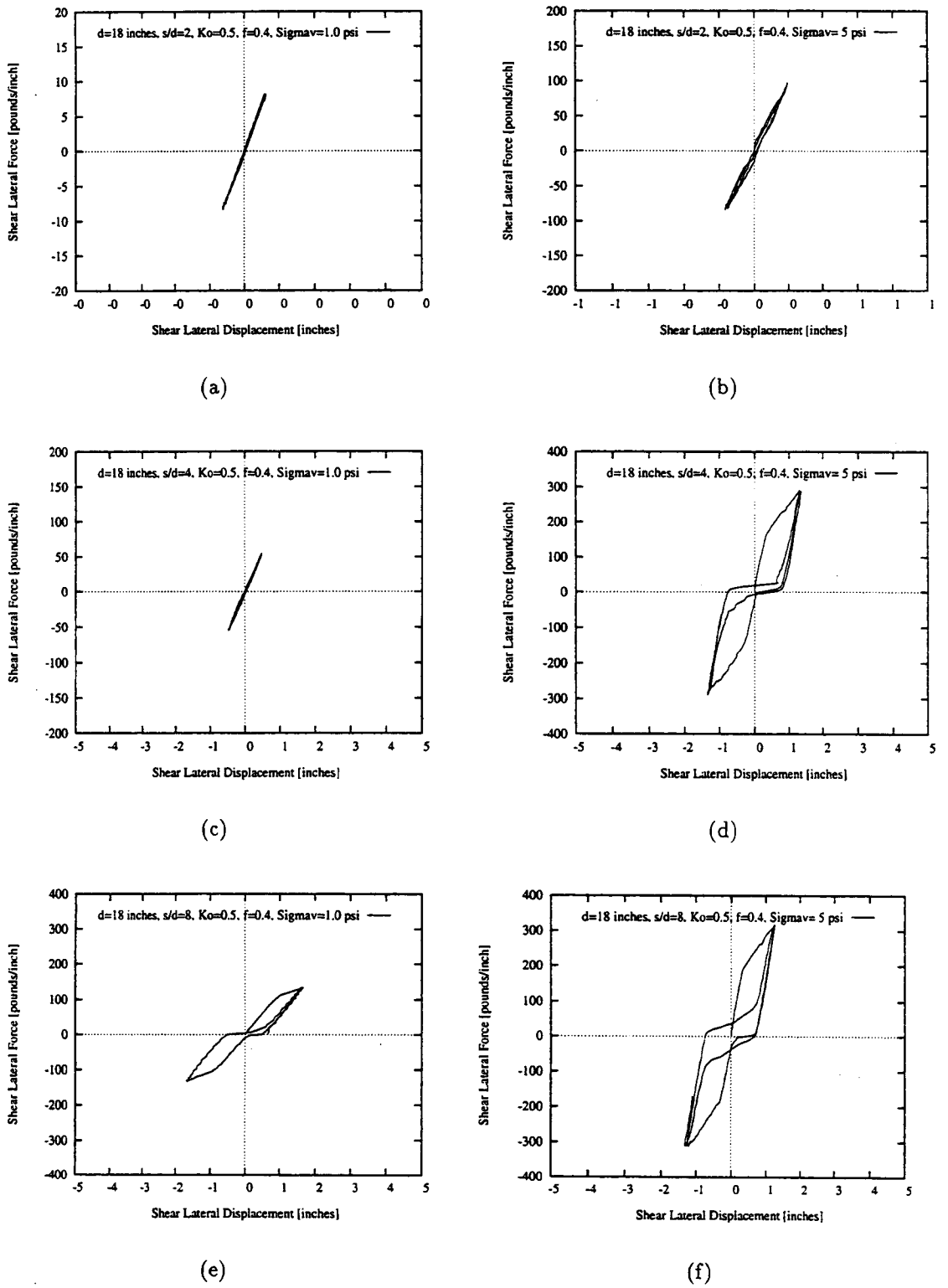

Figure E.30 *p-y* curves for the near-field springs between two piles in a two-pile group for shear-lateral vibration for different confining pressures for plane-stress condition. [d = 0.610m = 24 in.]

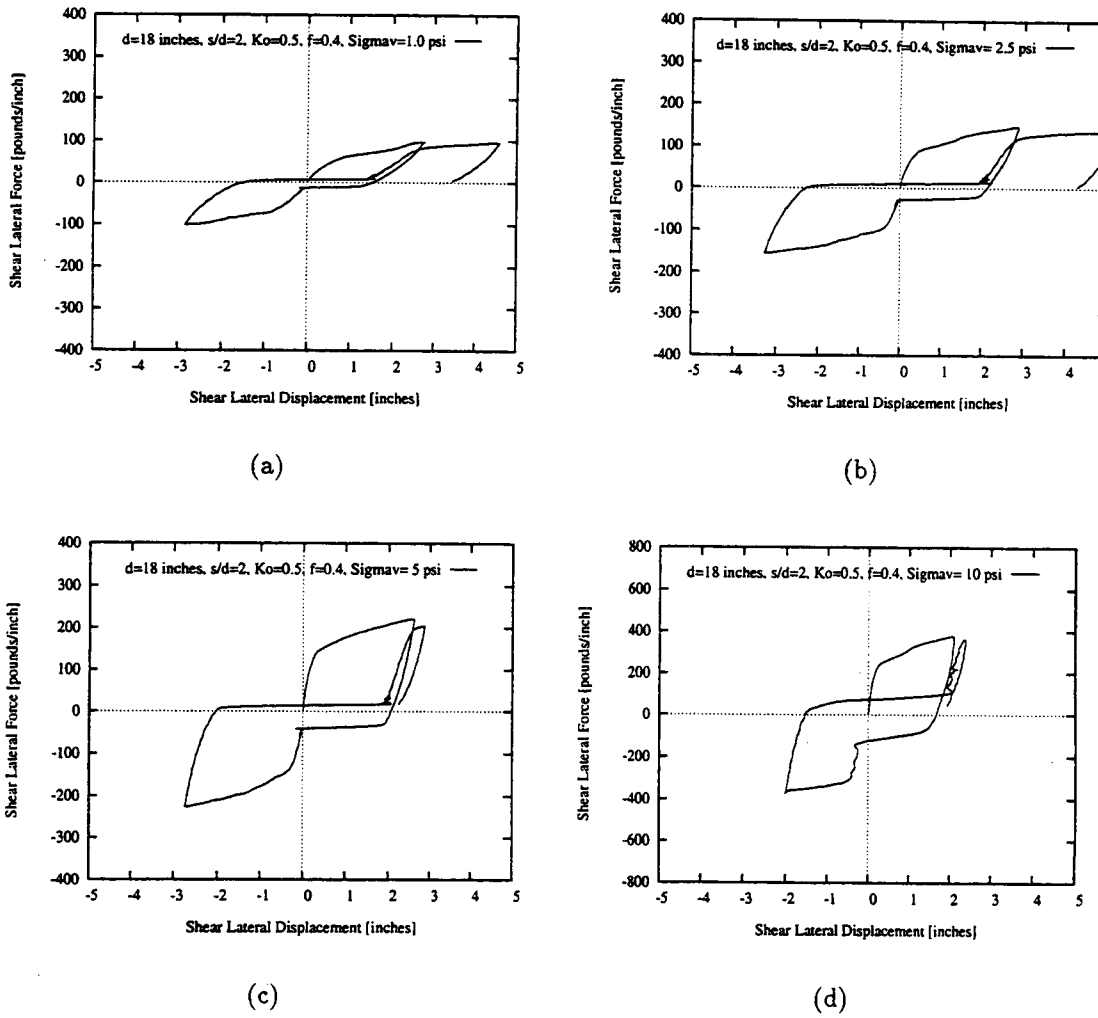

Figure E.31 p-y curves for the interaction-springs between two piles in a two-pile group for shear-lateral vibration for different confining pressures for plane-strain condition. [d = 0.457m = 18 in.; $s = 2d$] (continued to the next page)

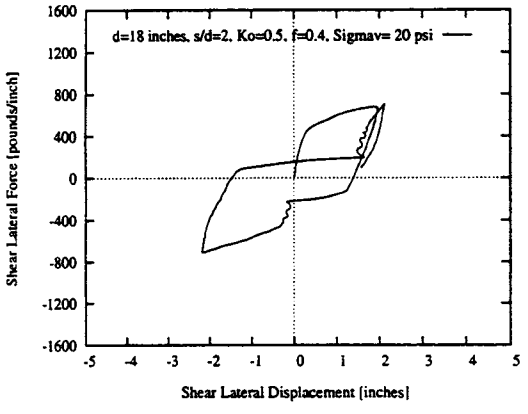

(e)

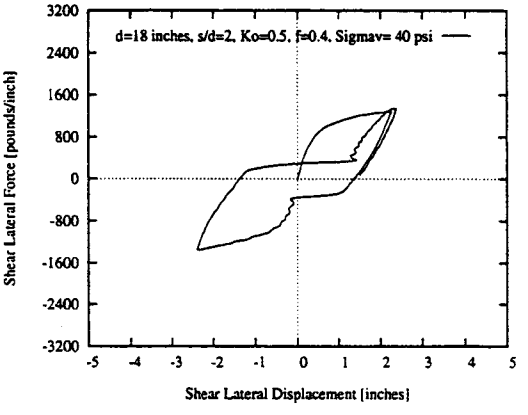

(f)

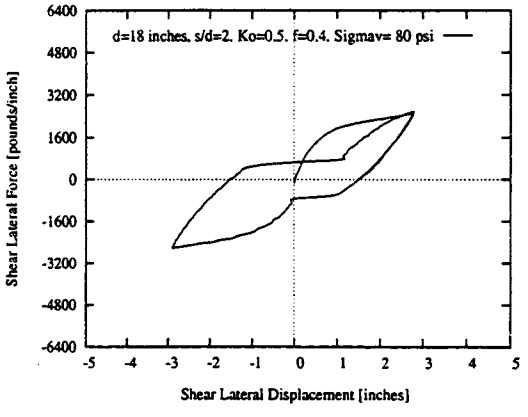

(g)

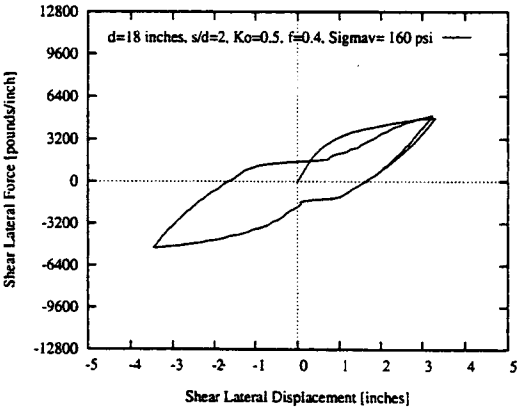

(h)

Figure E.31 p-y curves for the interaction-springs between two piles in a two-pile group for shear-lateral vibration for different confining pressures for plane-strain condition. [d = 0.457m = 18 in.; $s = 2d$] (continued)

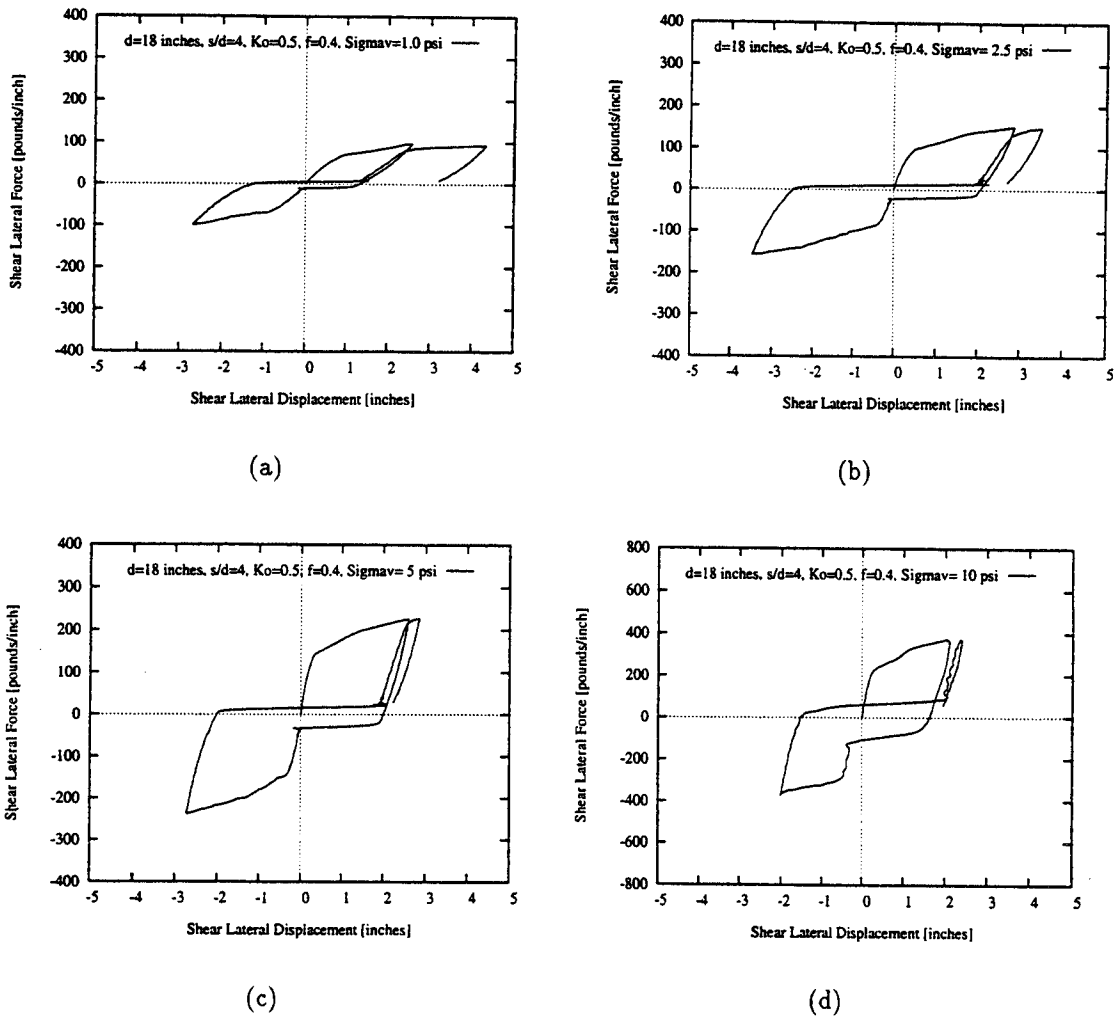

Figure E.32 p-y curves for the interaction-springs between two piles in a two-pile group for shear-lateral vibration for different confining pressures for plane-strain condition. [d = 0.457m = 18 in.; $s = 4d$] (continued to the next page)

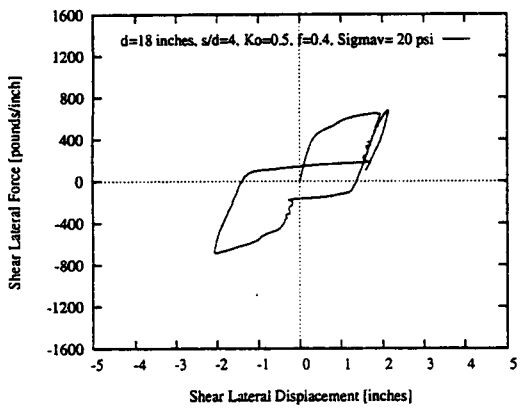

(e)

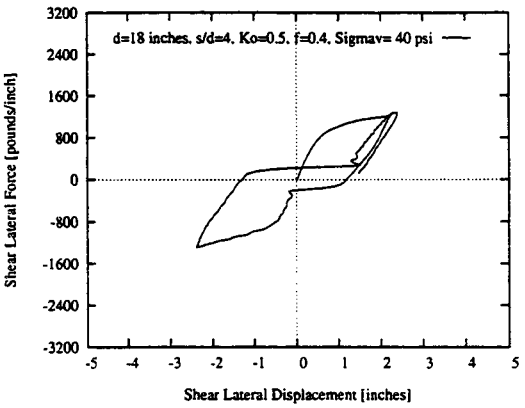

(f)

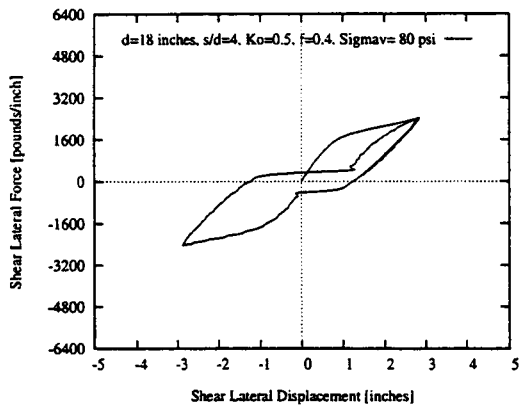

(g)

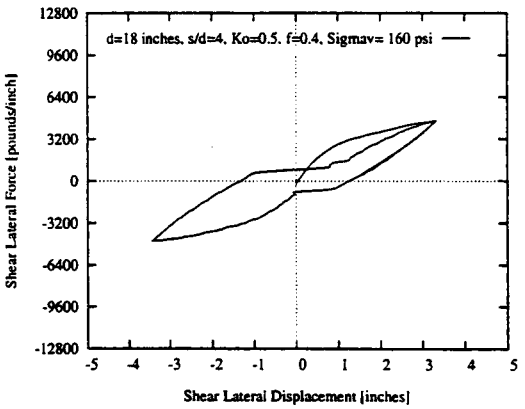

(h)

Figure E.32 p-y curves for the interaction-springs between two piles in a two-pile group for shear-lateral vibration for different confining pressures for plane-strain condition. [d = 0.457m = 18 in.; $s = 4d$] (continued)

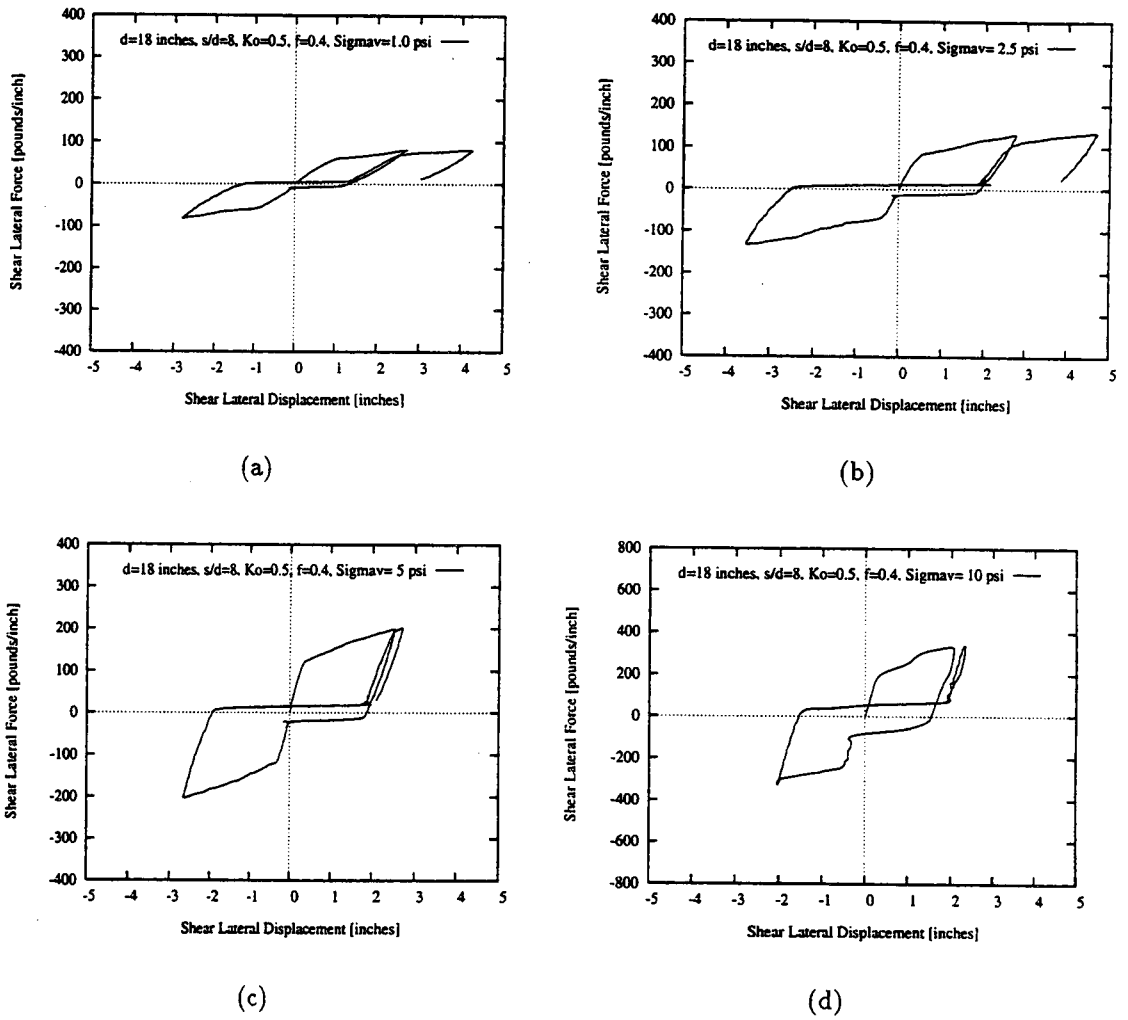

Figure E.33 p-y curves for the interaction-springs between two piles in a two-pile group for shear-lateral vibration for different confining pressures for plane-strain condition. [d = 0.457m = 18 in.; $s = 8d$] (continued to the next page)

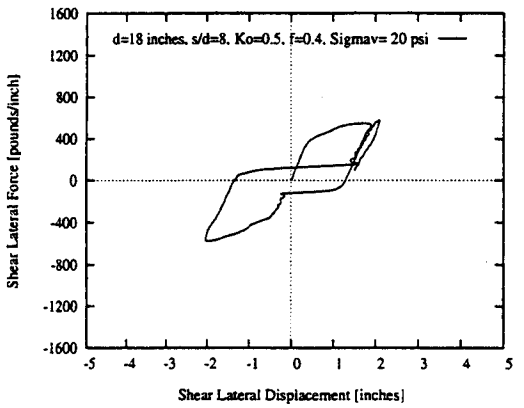

(e)

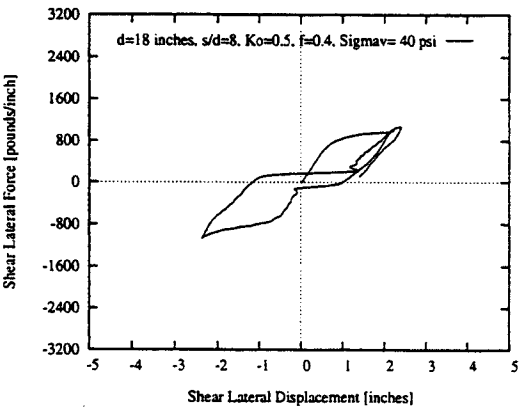

(f)

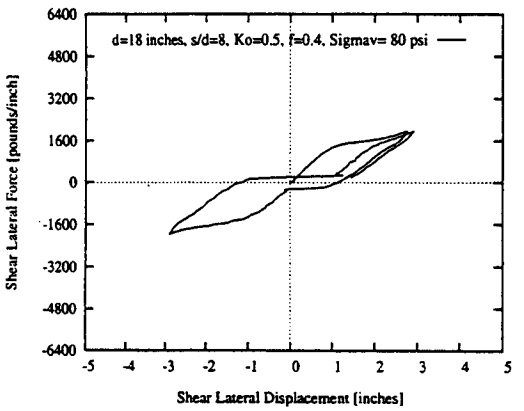

(g)

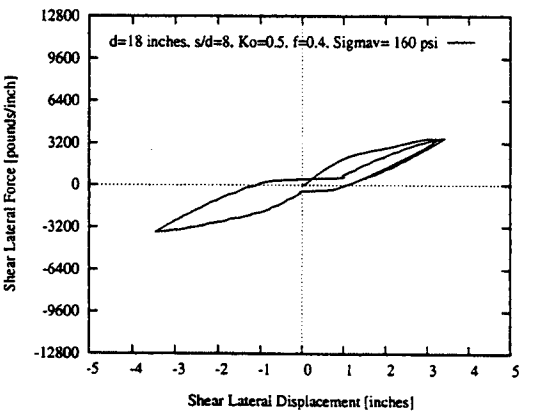

(h)

Figure E.33 p-y curves for the interaction-springs between two piles in a two-pile group for shear-lateral vibration for different confining pressures for plane-strain condition. [d = 0.457m = 18 in.; $s = 8d$] (continued)

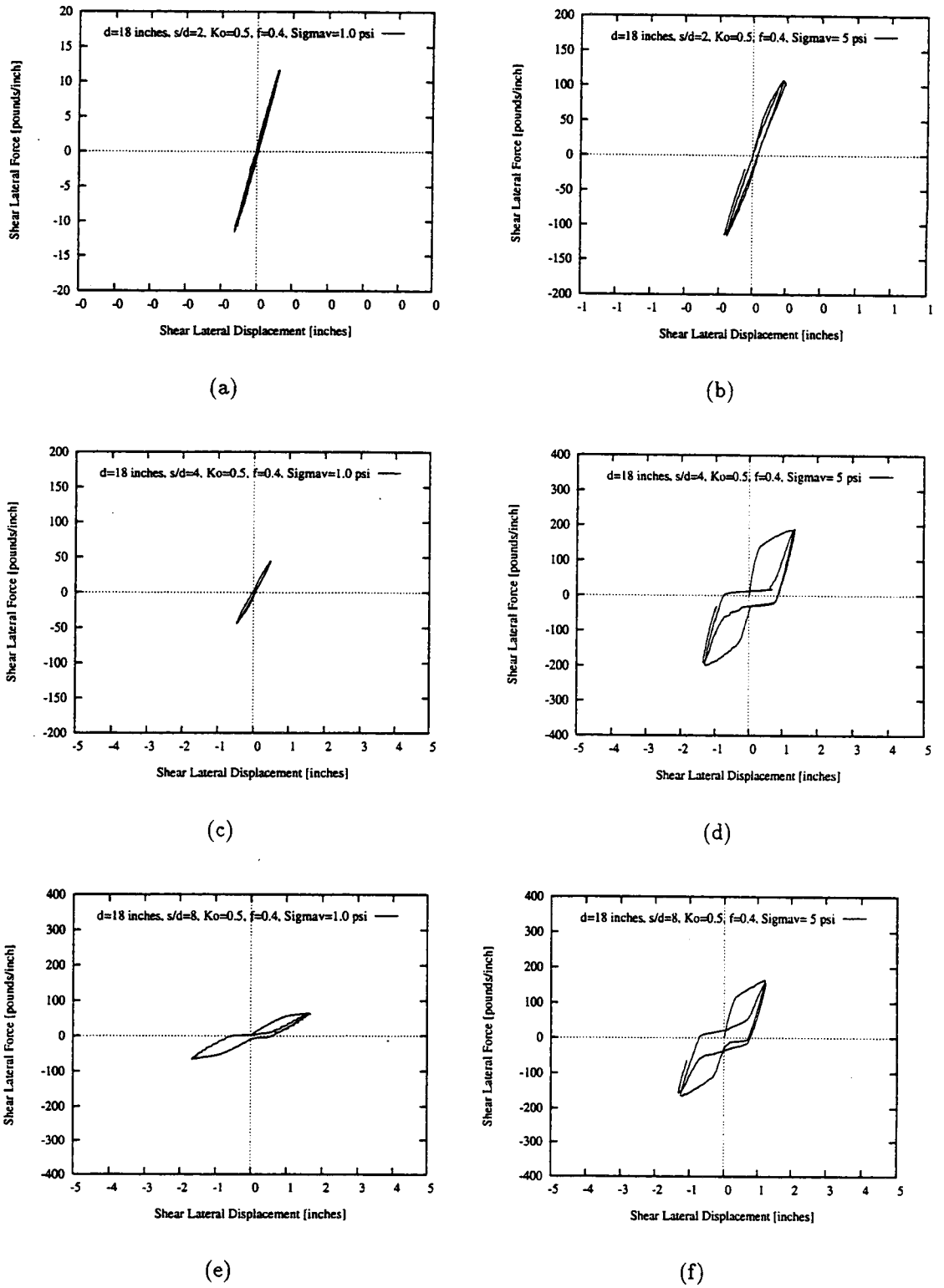

Figure E.34 p-y curves for the interaction-springs between two piles in a two-pile group for shear-lateral vibration for different confining pressures for plane-stress condition. [d = 0.457m = 18 in.]

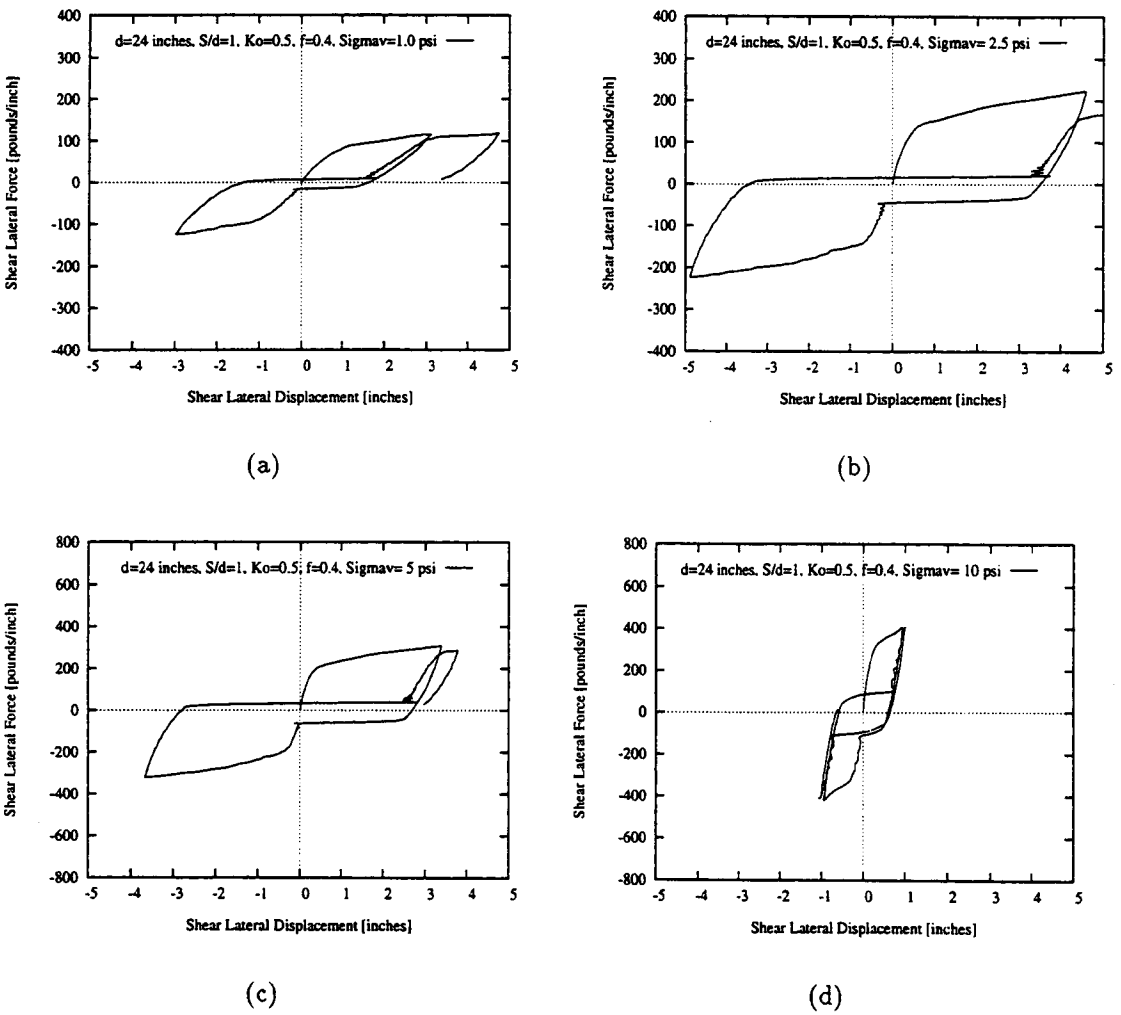

Figure E.35 p-y curves for the interaction-springs between two piles in a two-pile group for shear-lateral vibration for different confining pressures for plane-strain condition. [d = 0.610m = 24 in.; $s = 2d$] (continued to the next page)

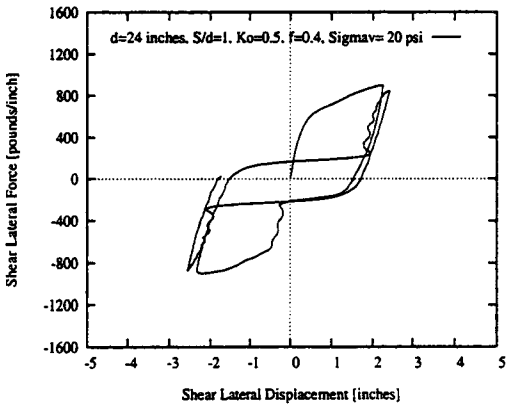

(e)

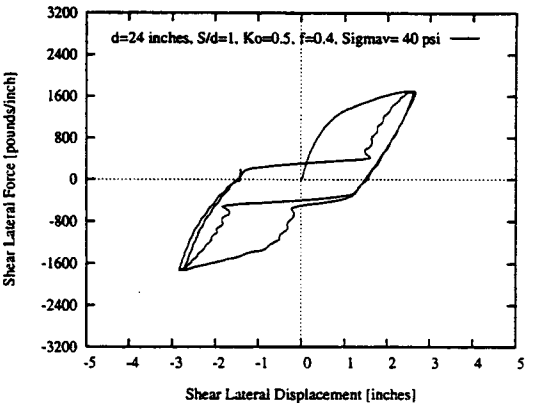

(f)

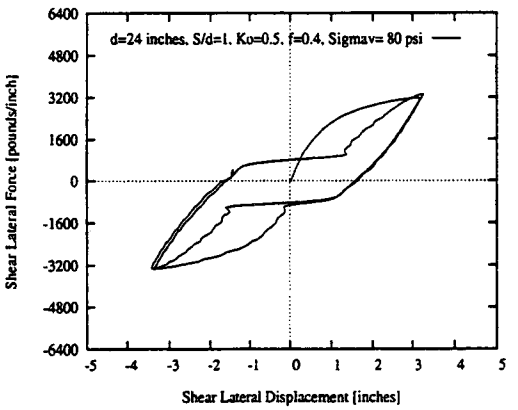

(g)

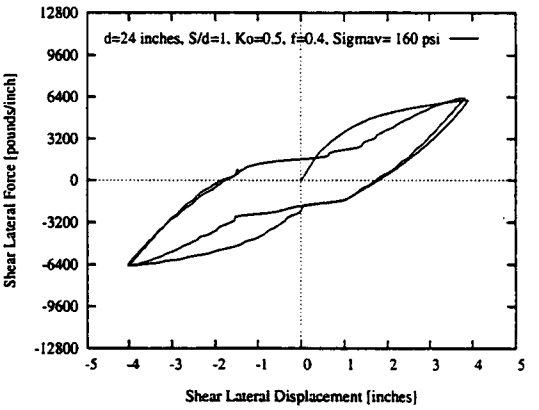

(h)

Figure E.35 p-y curves for the interaction-springs between two piles in a two-pile group for shear-lateral vibration for different confining pressures for plane-strain condition. [d = 0.610m = 24 in.; $s = 2d$] (continued)

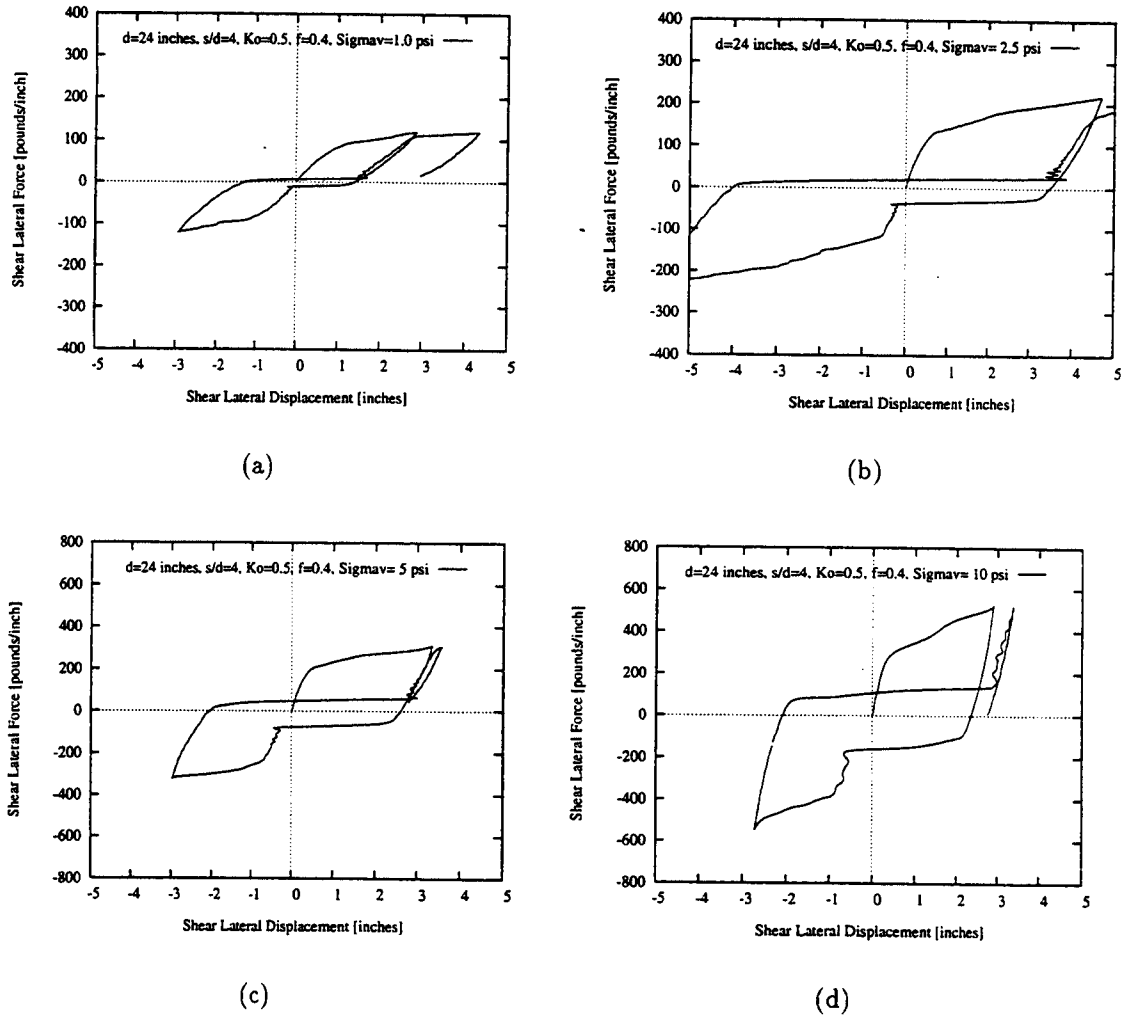

Figure E.36 p-y curves for the interaction-springs between two piles in a two-pile group for shear-lateral vibration for different confining pressures for plane-strain condition. [d = 0.610m = 24 in.; $s = 4d$] (continued to the next page)

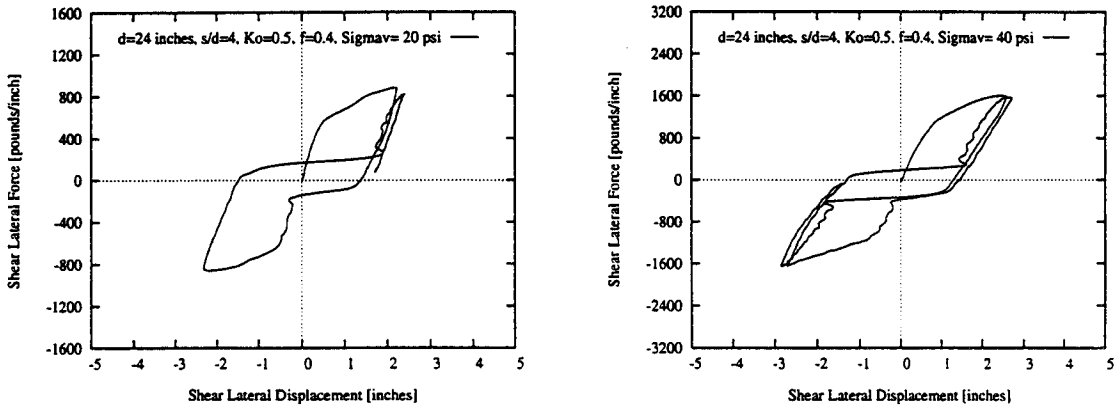

(e)

(f)

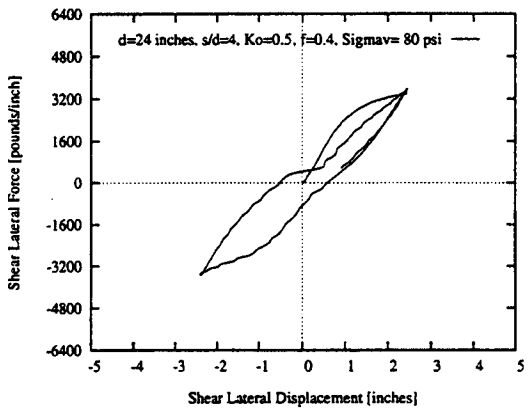

(g)

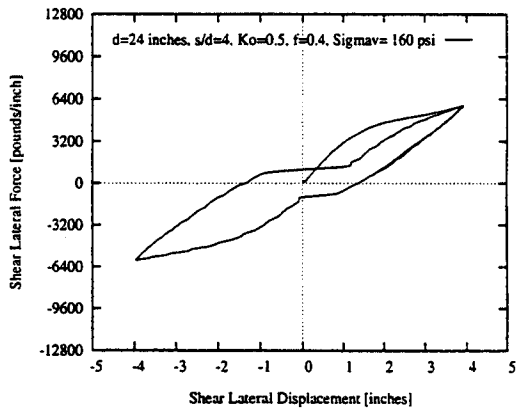

(h)

Figure E.36 p-y curves for the interaction-springs between two piles in a two-pile group for shear-lateral vibration for different confining pressures for plane-strain condition. [d = 0.610m = 24 in.; $s = 4d$] (continued)

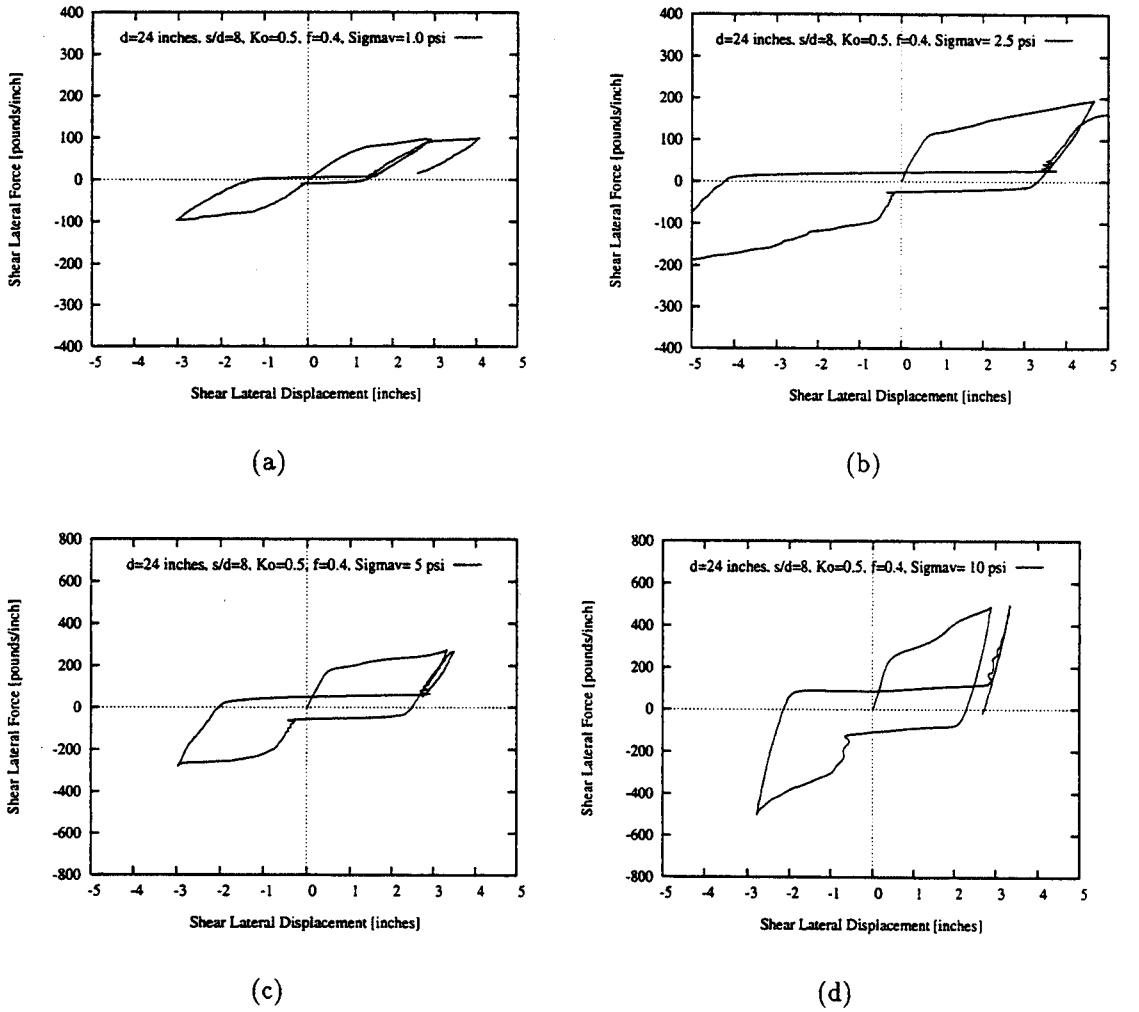

Figure E.37 p-y curves for the interaction-springs between two piles in a two-pile group for shear-lateral vibration for different confining pressures for plane-strain condition. [d = 0.610m = 24 in.; $s = 8d$] (continued to the next page)

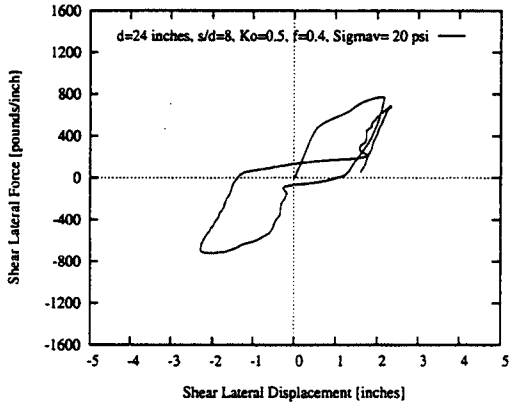

(e)

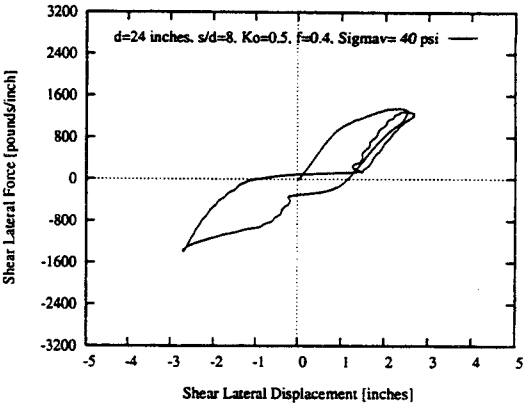

(f)

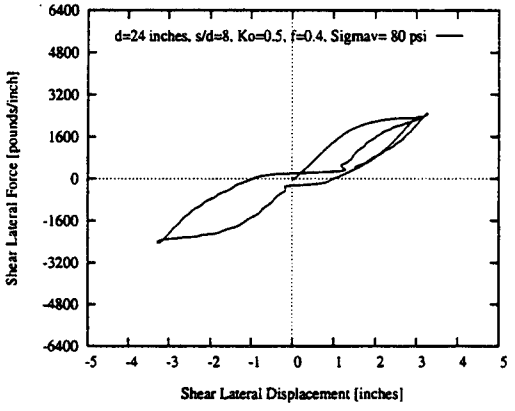

(g)

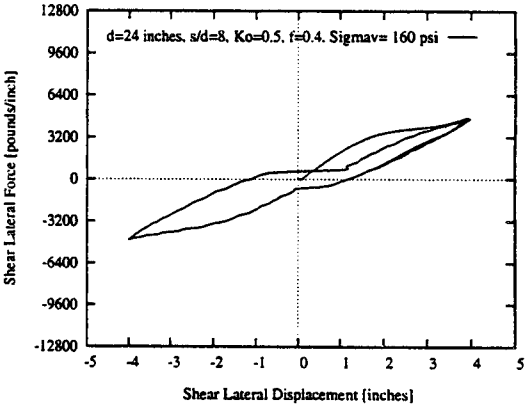

(h)

Figure E.37 p-y curves for the interaction-springs between two piles in a two-pile group for shear-lateral vibration for different confining pressures for plane-strain condition. [d = 0.610m = 24 in.; $s = 8d$] (continued)

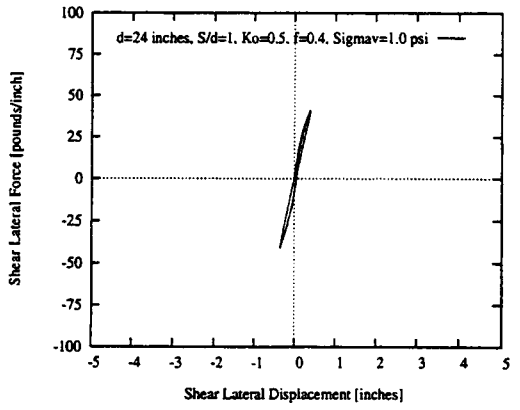

(a)

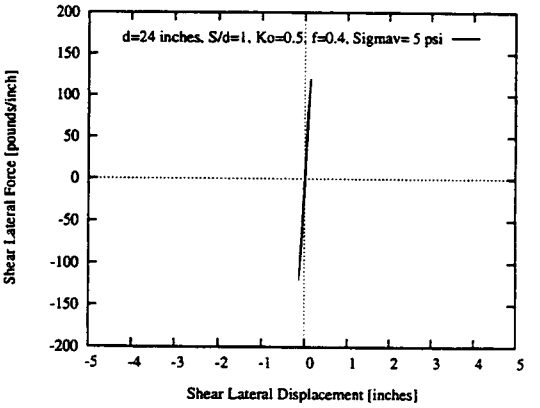

(b)

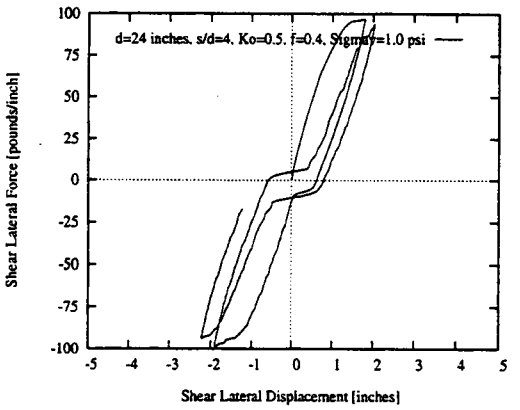

(c)

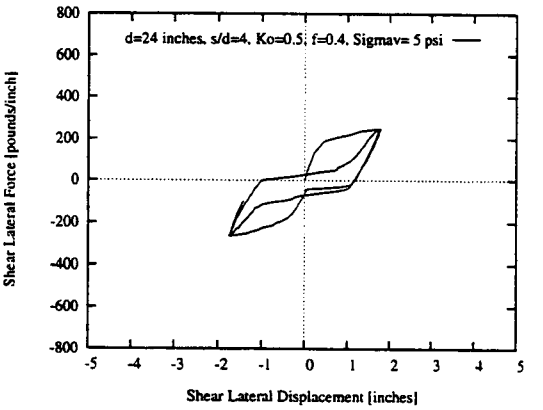

(d)

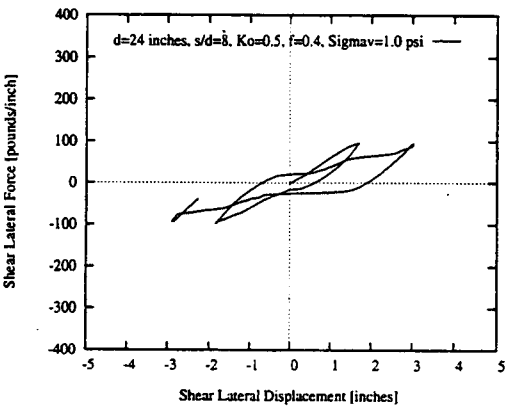

(e)

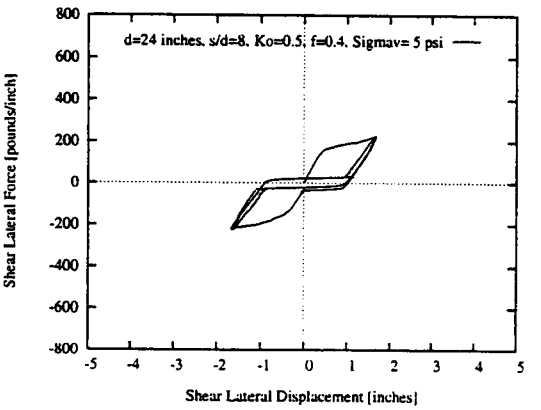

(f)

Figure E.38 *p-y* curves for the interaction-springs between two piles in a two-pile group for shear-lateral vibration for different confining pressures for plane-stress condition. [d = 0.610m = 24 in.]

E.2.2.3 Axial Vibration of Two-Pile Group

For the axial interaction-springs, two piles were modeled once again within the finite element framework. No sliding interface was assumed to exist to avoid instability and the condition of symmetry was utilized. No lateral displacement boundary condition was used. Vertical displacement of soil at a distance of $20d$ from the pile or further apart was neglected by using an artificial, no-displacement boundary. Vertical stresses were maintained to simulate confining effects. Perturbation was given only in one pile, and the resulting displacement of the pile and the reactive forces in both pile segments were observed and analyzed to obtain the interaction characteristics. The above procedure was followed for different depths represented by 6.9, 17.3, 34.5, 68.9, 137.8, 275.6, 551.2, and 1102.4 kPa (1, 2.5, 5, 10, 20, 40, 80, and 160 psi) vertical stresses, for drained behavior of the soil, and for center spacing of $2d$, $4d$, and $8d$. The resulting t-z behavior of the interaction-springs and the near-field springs is presented in Figures E.39 through E.50 for soil from the Snohomish river site. The NEABS parameters for those spring were computed, and they are presented in Tables 2.15 through 2.18.

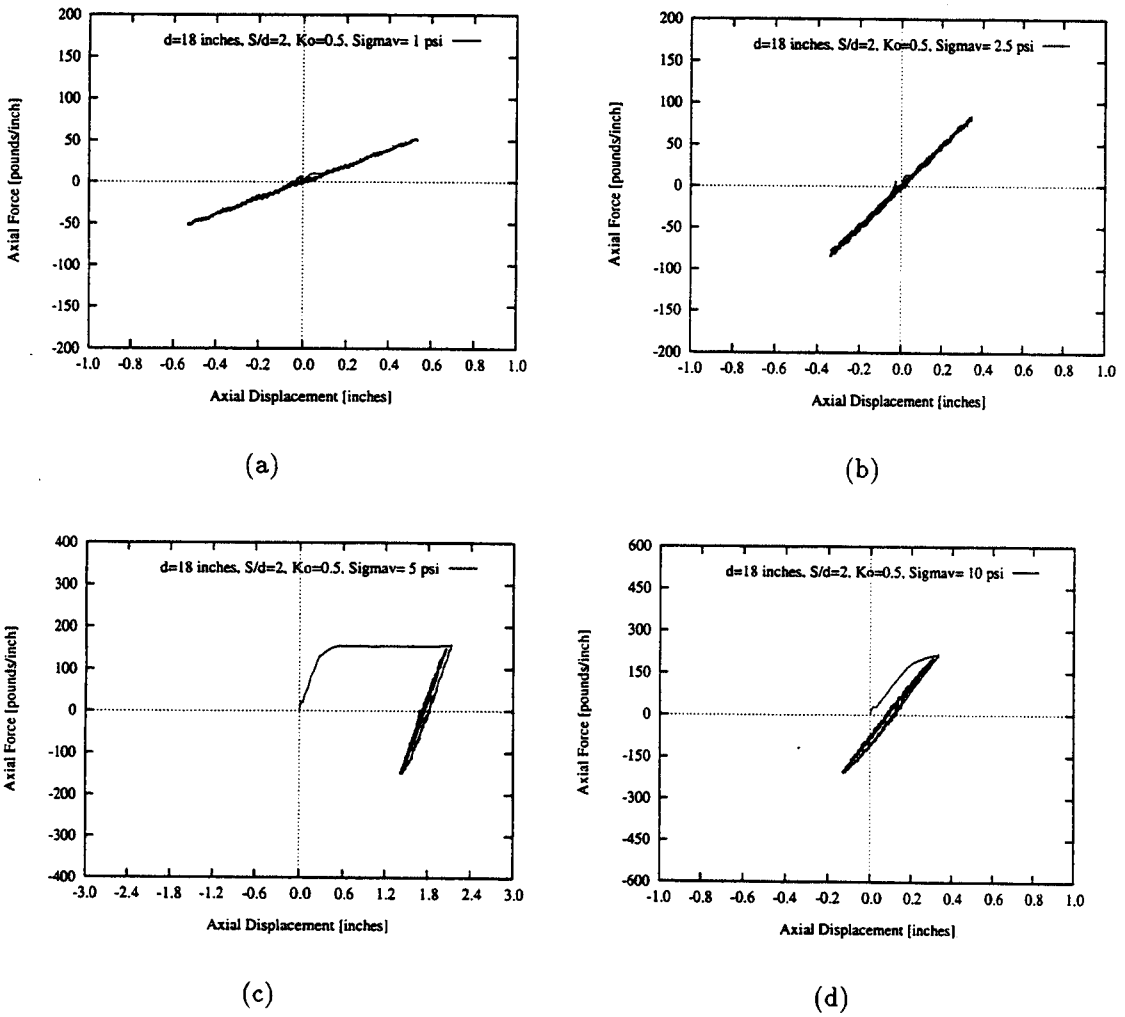

Figure E.39 p-y curves for the near-field springs between pile and soil in a two-pile group for axial vibration for different confining pressures. [$d = 0.457\text{m} = 18$ in.; $s = 2d$]
(continued to the next page)

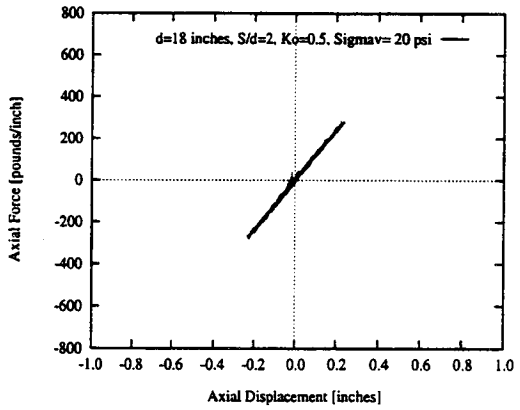

(e)

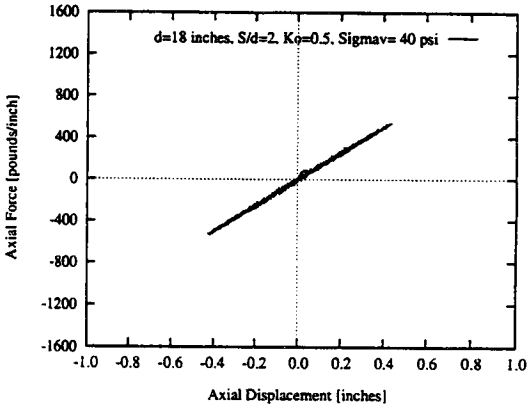

(f)

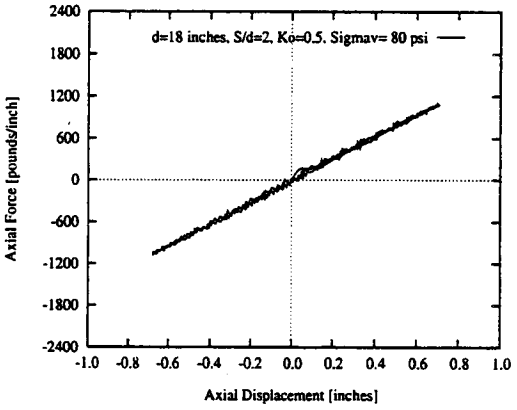

(g)

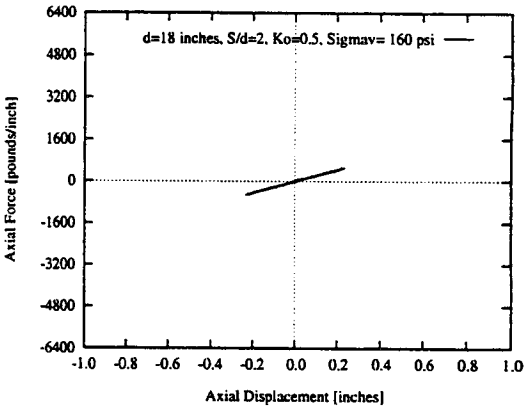

(h)

Figure E.39 p-y curves for the near-field springs between pile and soil in a two-pile group for axial vibration for different confining pressures. [$d = 0.457\text{m} = 18$ in.; $s = 2d$] (continued)

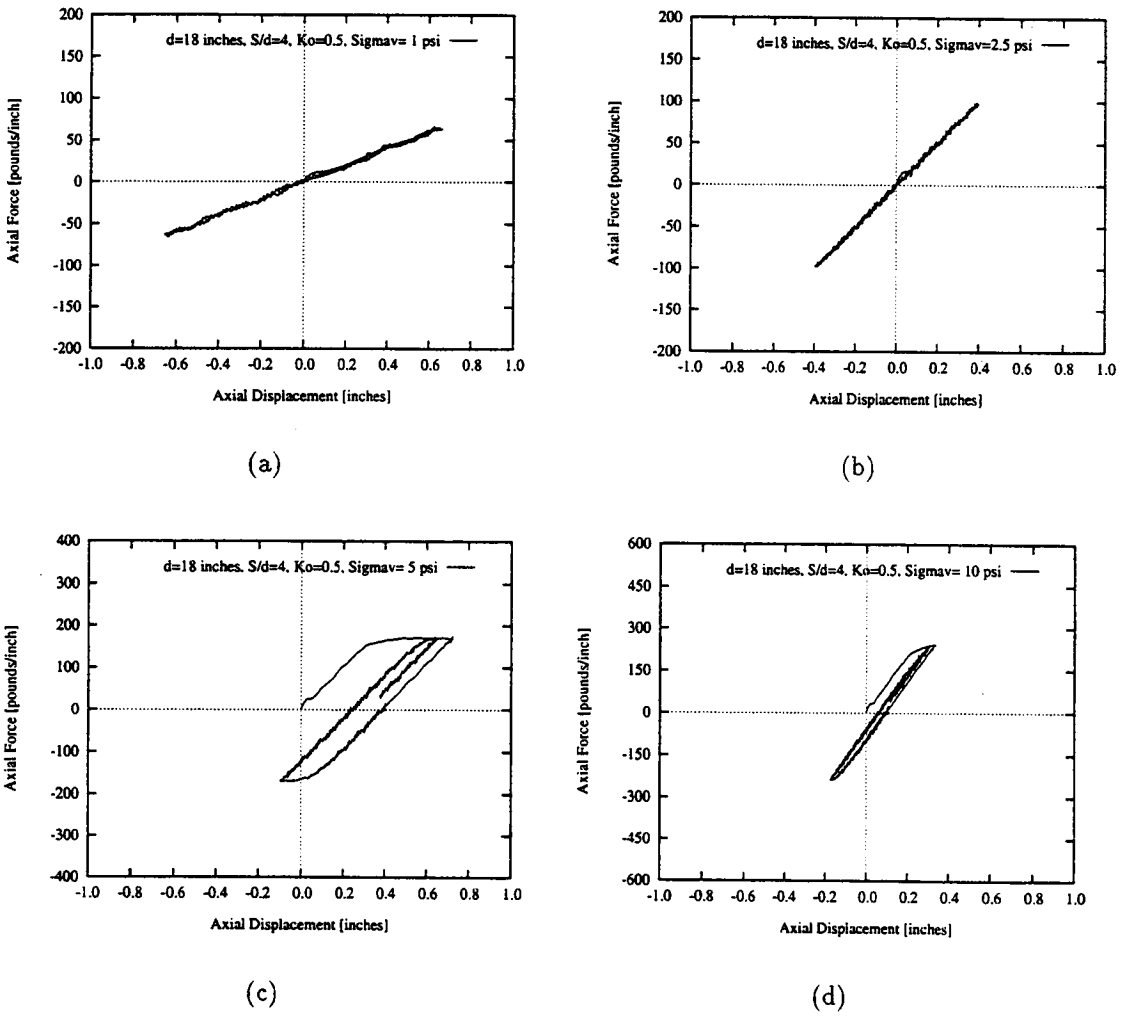

Figure E.40 p-y curves for the near-field springs between pile and soil in a two-pile group for axial vibration for different confining pressures. [$d = 0.457\text{m} = 18$ in.; $s = 4d$]
(continued to the next page)

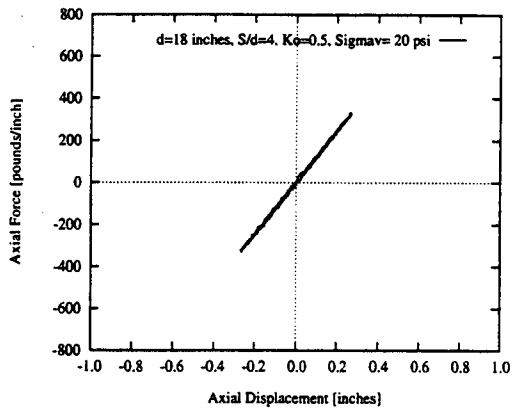

(e)

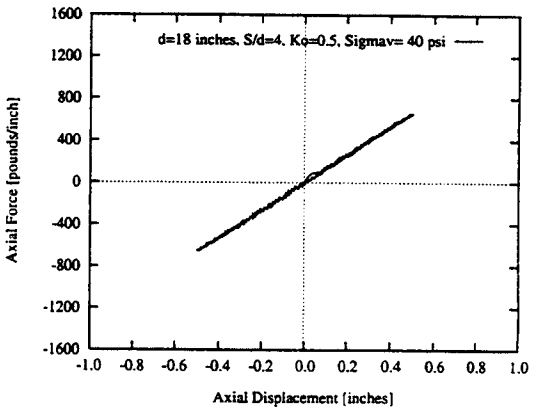

(f)

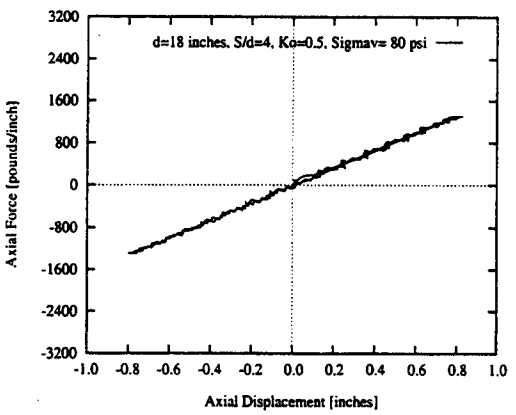

(g)

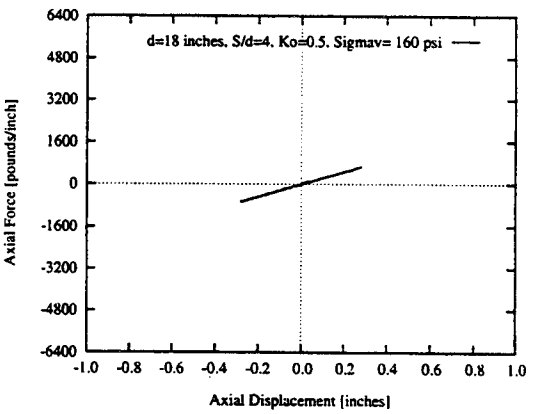

(h)

Figure E.40 p-y curves for the near-field springs between pile and soil in a two-pile group for axial vibration for different confining pressures. [$d = 0.457\text{m} = 18$ in.; $s = 4d$] (continued)

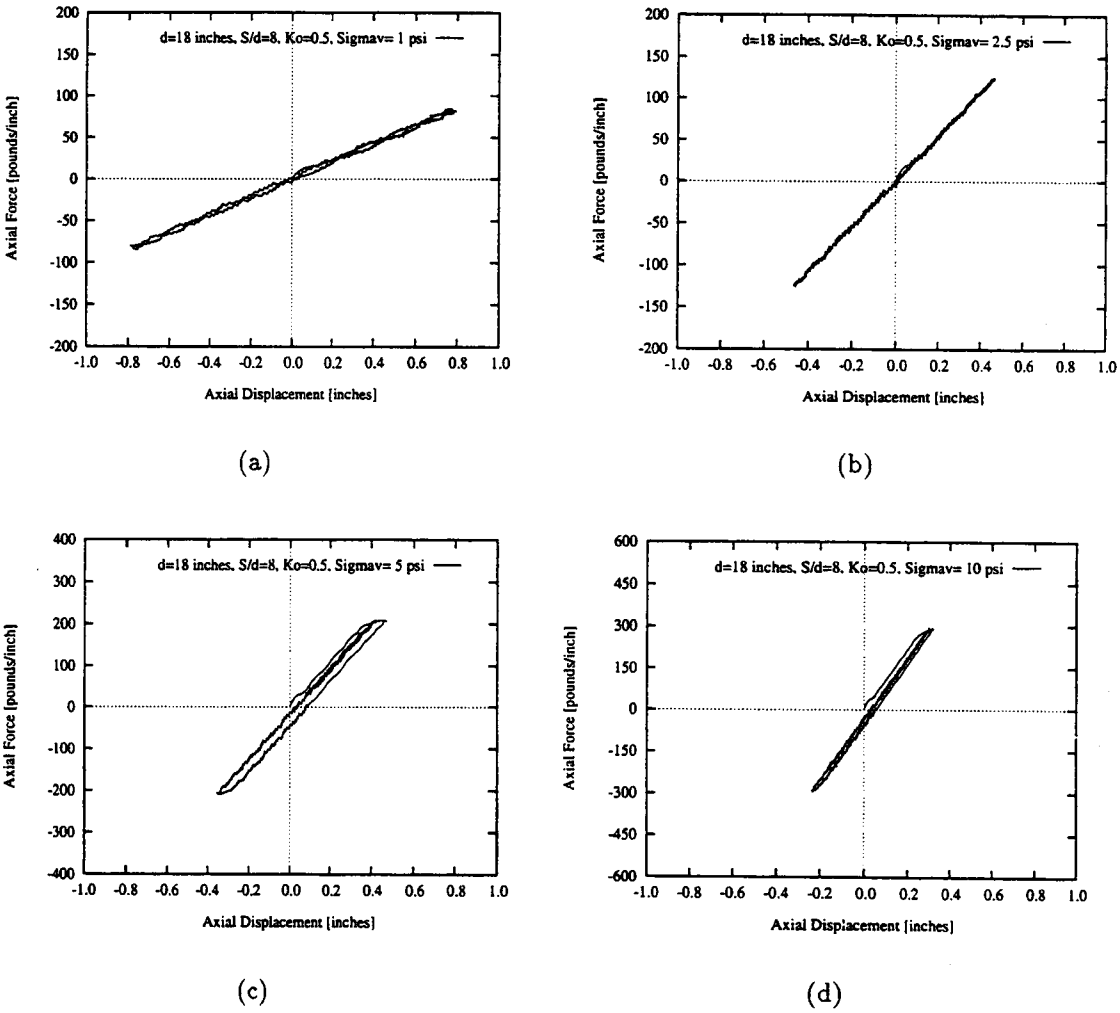

Figure E.41 p-y curves for the near-field springs between pile and soil in a two-pile group for axial vibration for different confining pressures. [$d = 0.457\text{m} = 18$ in.; $s = 8d$]
(continued to the next page)

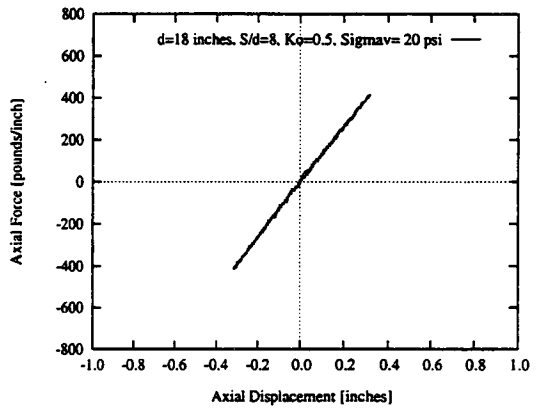

(e)

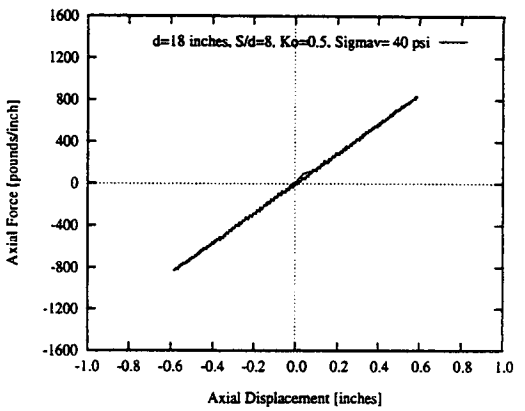

(f)

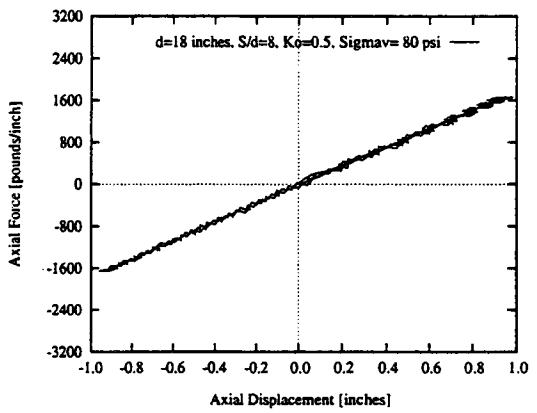

(g)

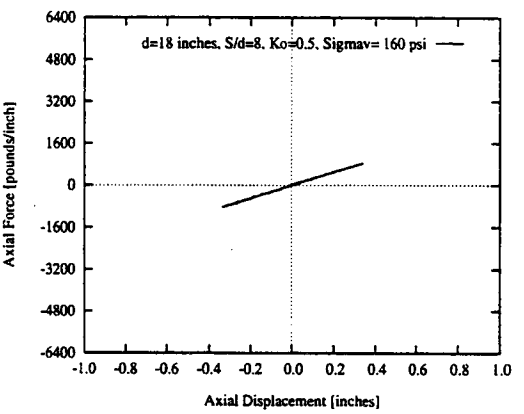

(h)

Figure E.41 p-y curves for the near-field springs between pile and soil in a two-pile group for axial vibration for different confining pressures. [$d = 0.457\text{m} = 18$ in.; $s = 8d$] (continued)

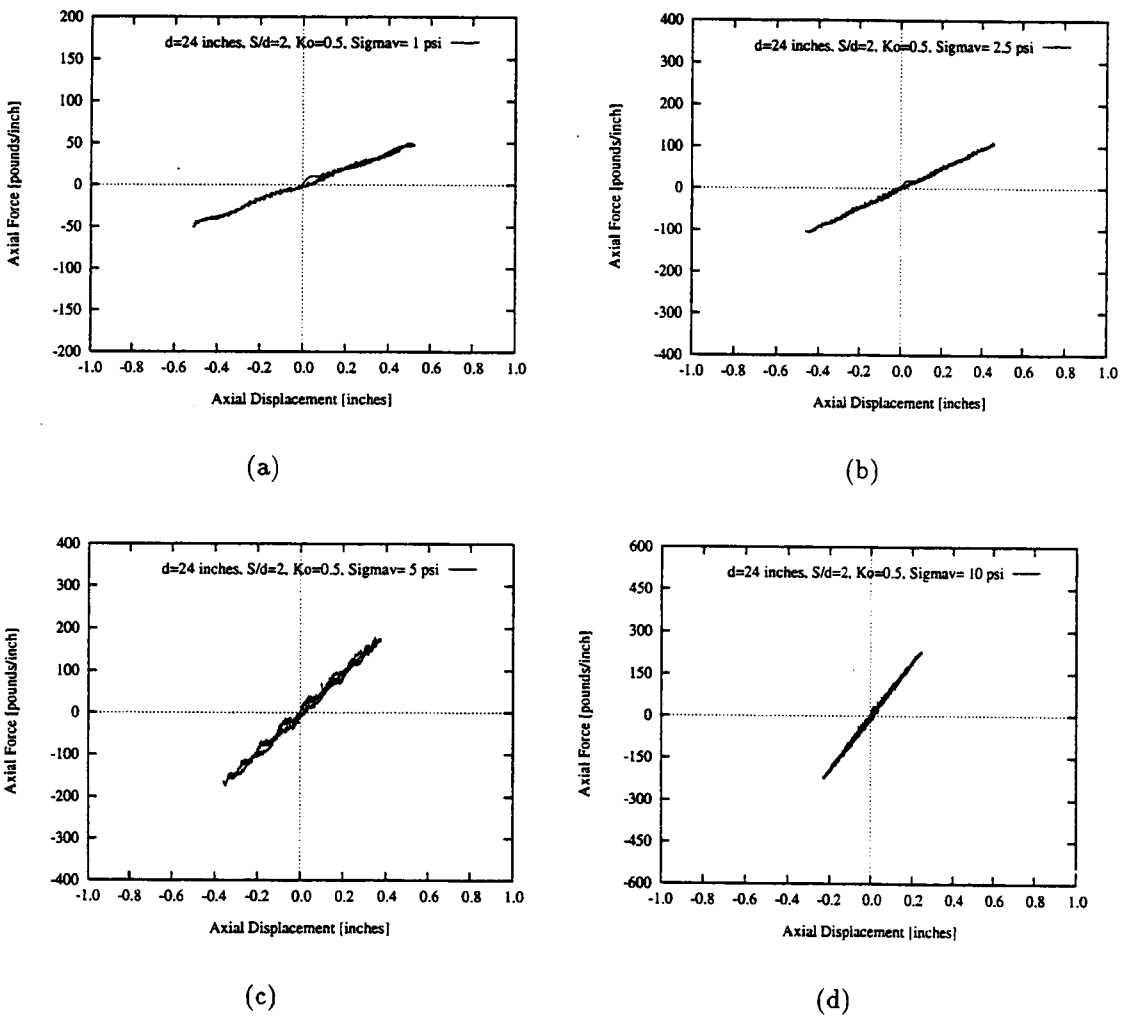

Figure E.42 p-y curves for the near-field springs between pile and soil in a two-pile group for axial vibration for different confining pressures. [$d = 0.610\text{m} = 24$ in.; $s = 2d$]
(continued to the next page)

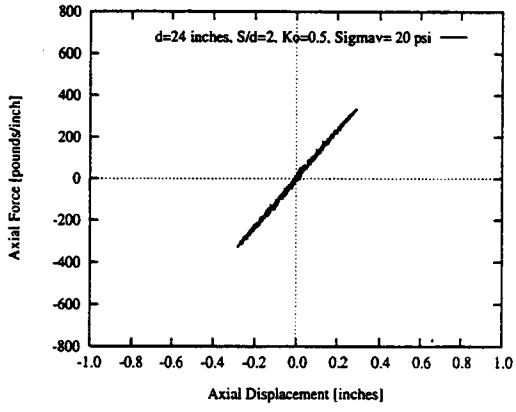

(e)

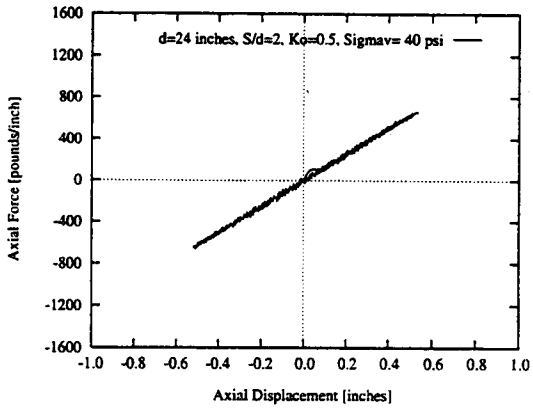

(f)

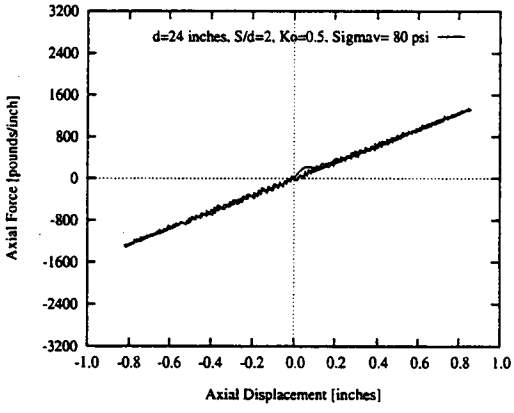

(g)

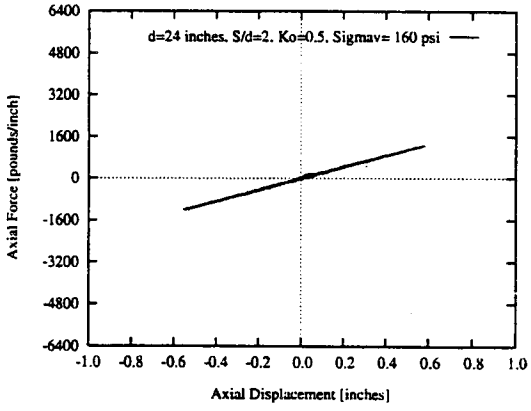

(h)

Figure E.42 p-y curves for the near-field springs between pile and soil in a two-pile group for axial vibration for different confining pressures. [$d = 0.610\text{m} = 24$ in.; $s = 2d$] (continued)

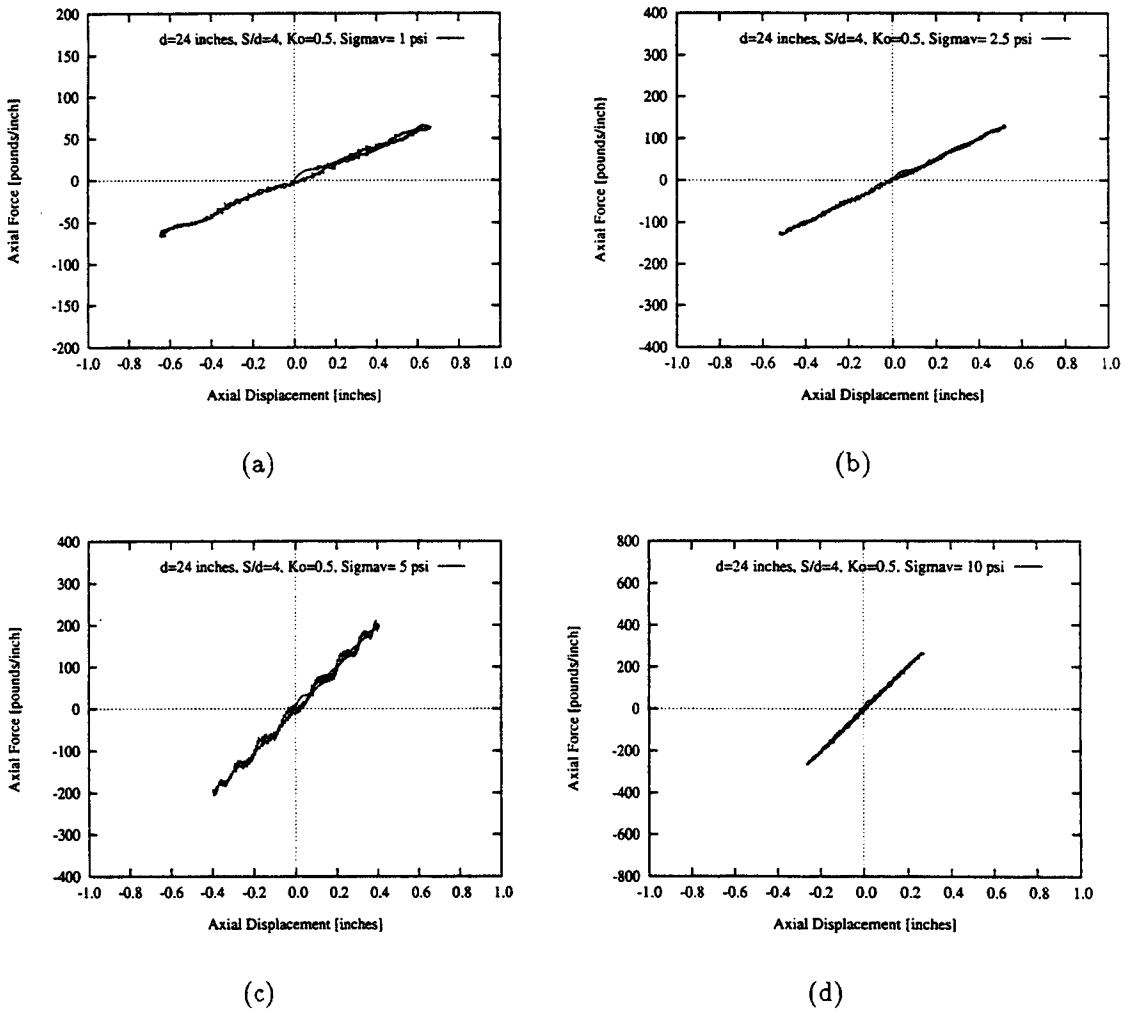

Figure E.43 p-y curves for the near-field springs between pile and soil in a two-pile group for axial vibration for different confining pressures. [$d = 0.610\text{m} = 24$ in.; $s = 4d$]
(continued to the next page)

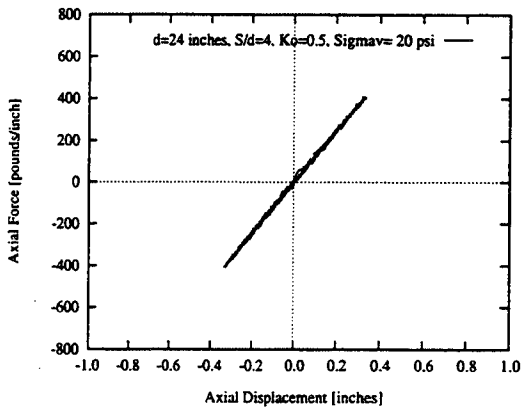

(e)

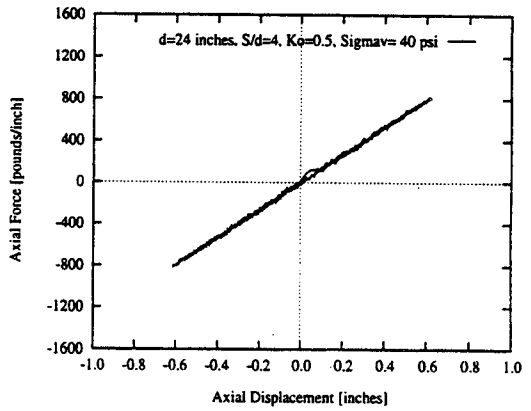

(f)

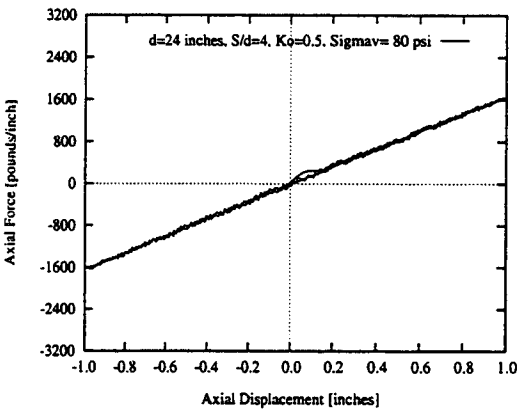

(g)

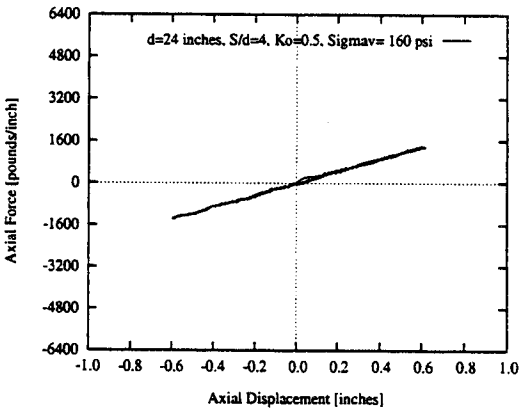

(h)

Figure E.43 p-y curves for the near-field springs between pile and soil in a two-pile group for axial vibration for different confining pressures. [$d = 0.610\text{m} = 24$ in.; $s = 4d$] (continued)

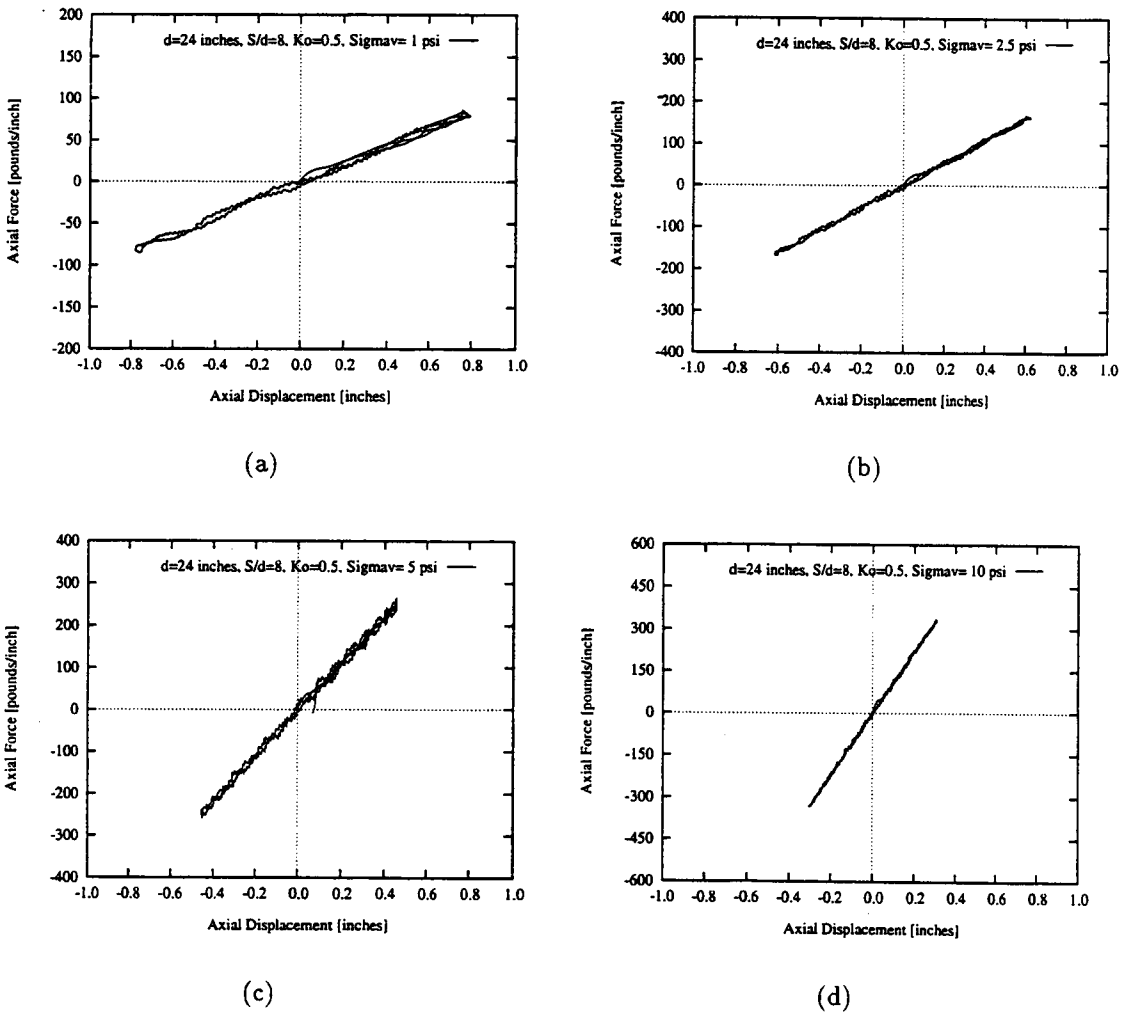

Figure E.44 p-y curves for the near-field springs between pile and soil in a two-pile group for axial vibration for different confining pressures. [$d = 0.610\text{m} = 24$ in.; $s = 8d$]
(continued to the next page)

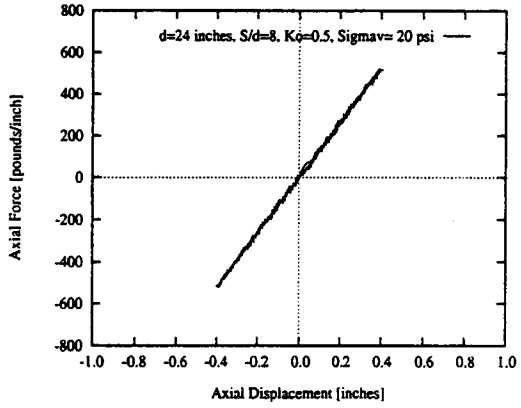

(e)

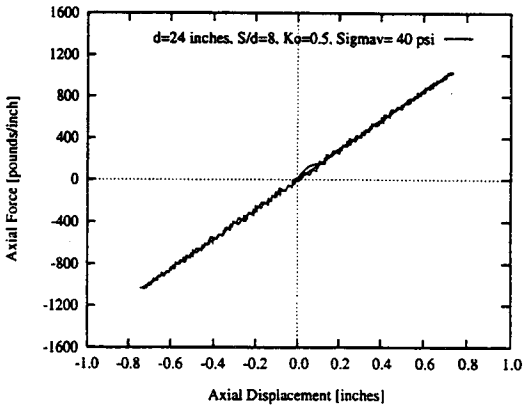

(f)

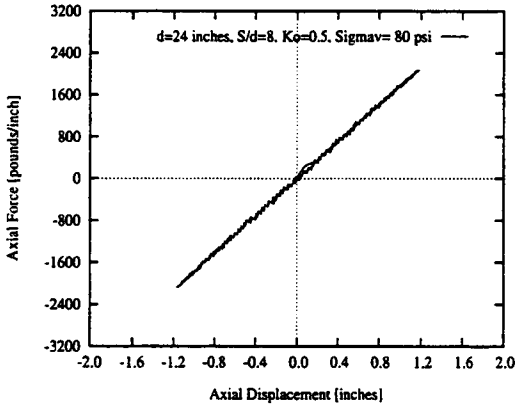

(g)

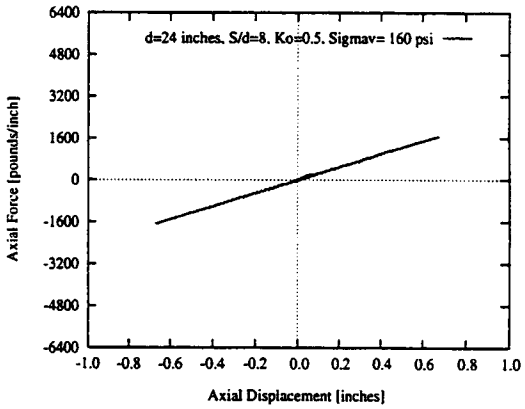

(h)

Figure E.44 p-y curves for the near-field springs between pile and soil in a two-pile group for axial vibration for different confining pressures. [$d = 0.610\text{m} = 24$ in.; $s = 8d$] (continued)

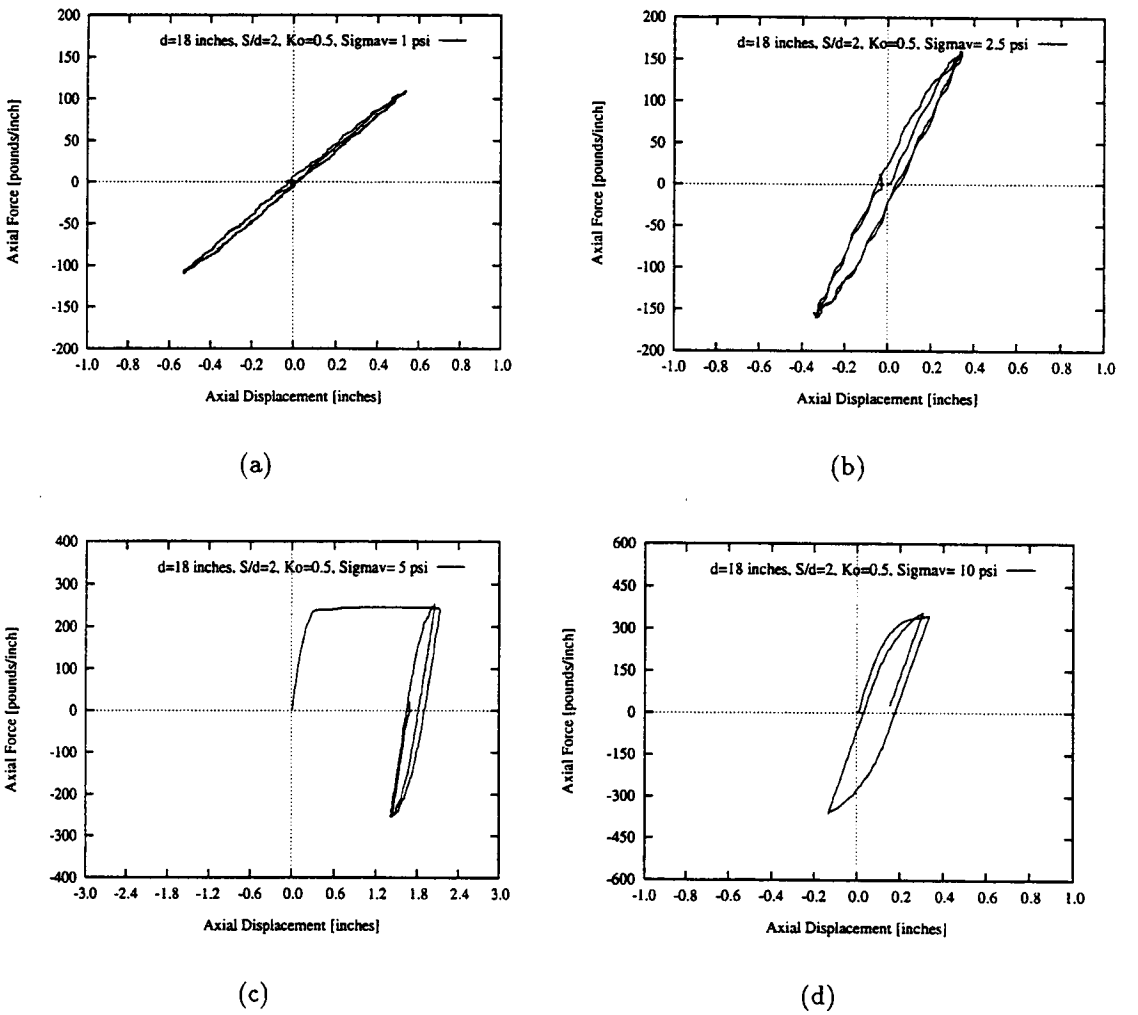

Figure E.45 p-y curves for the interaction-springs between pile and soil in a two-pile group for axial vibration for different confining pressures. [$d = 0.457\text{m} = 18$ in.; $s = 2d$]
(continued to the next page)

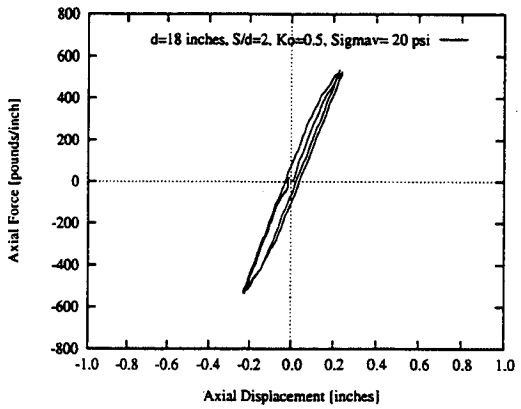

(e)

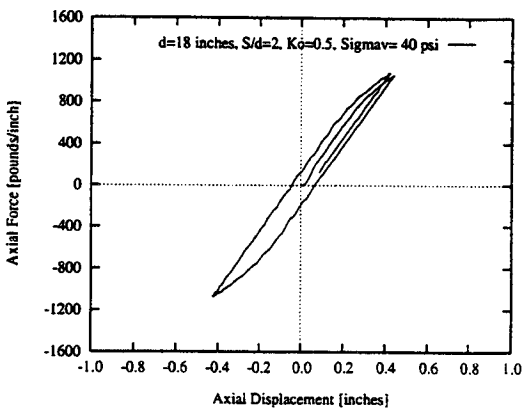

(f)

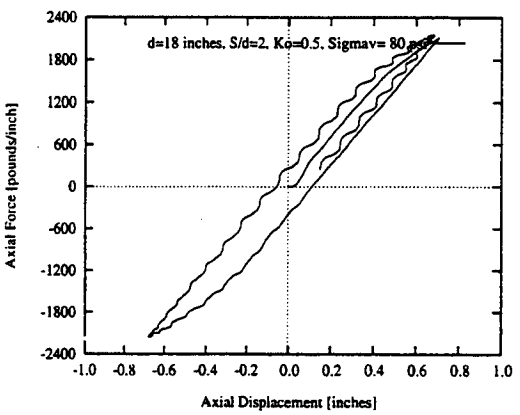

(g)

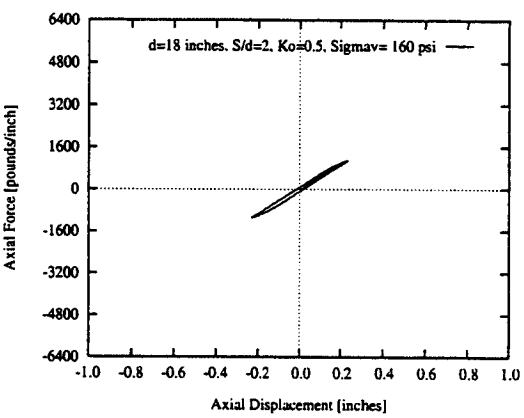

(h)

Figure E.45 p-y curves for the interaction-springs between pile and soil in a two-pile group for axial vibration for different confining pressures. [$d = 0.457\text{m} = 18$ in.; $s = 2d$] (continued)

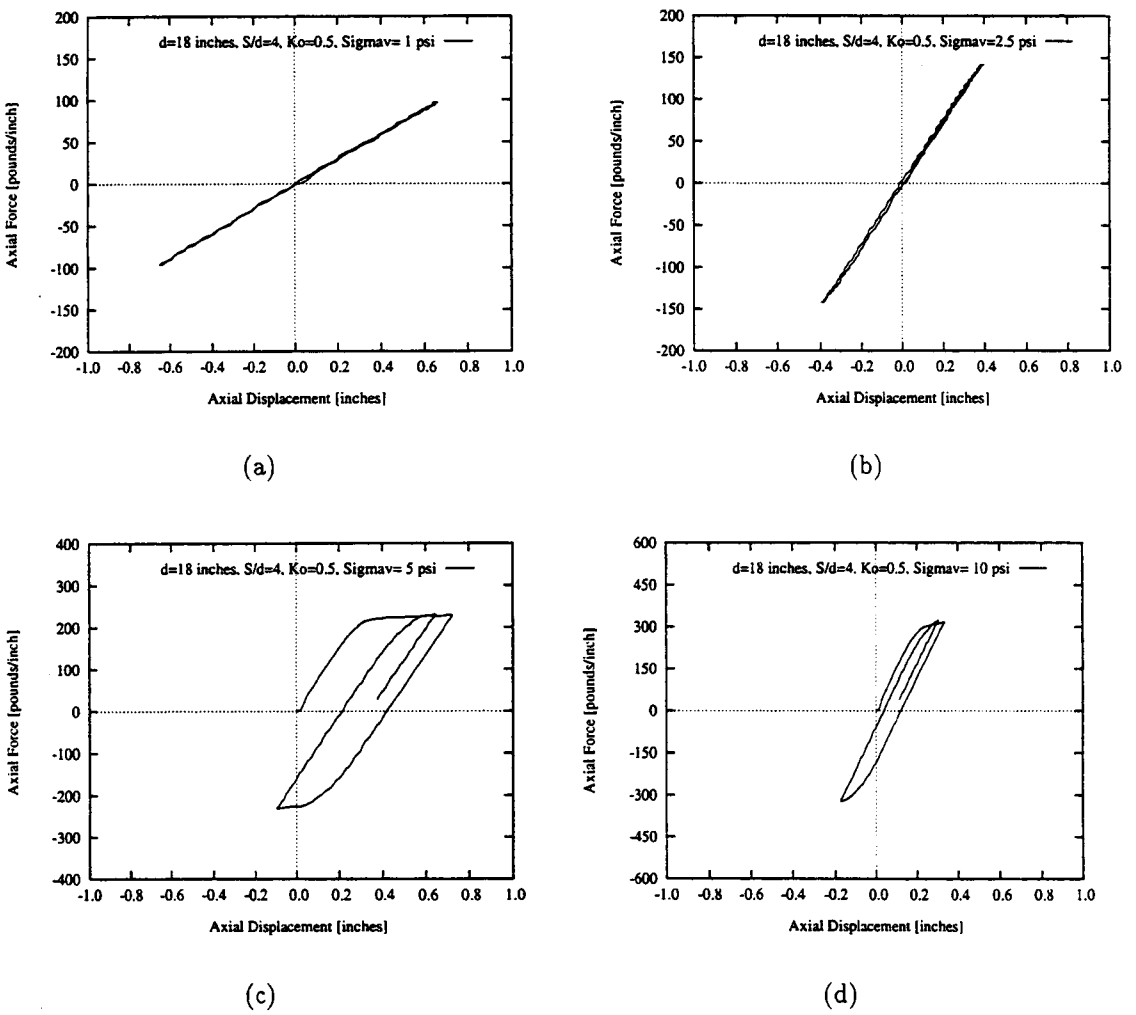

Figure E.46 p-y curves for the interaction-springs between pile and soil in a two-pile group for axial vibration for different confining pressures. [d = 0.457m = 18 in.; $s = 4d$]
(continued to the next page)

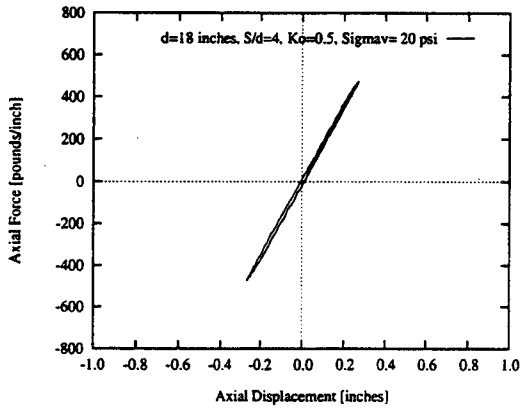

(e)

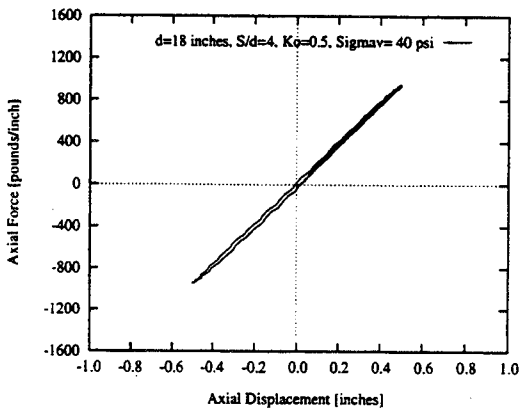

(f)

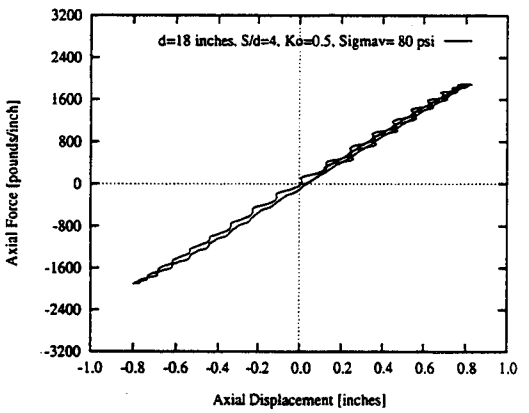

(g)

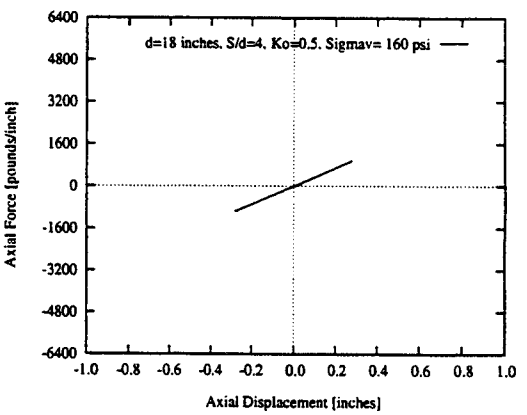

(h)

Figure E.46 p-y curves for the interaction-springs between pile and soil in a two-pile group for axial vibration for different confining pressures. [$d = 0.457\text{m} = 18$ in.; $s = 4d$] (continued)

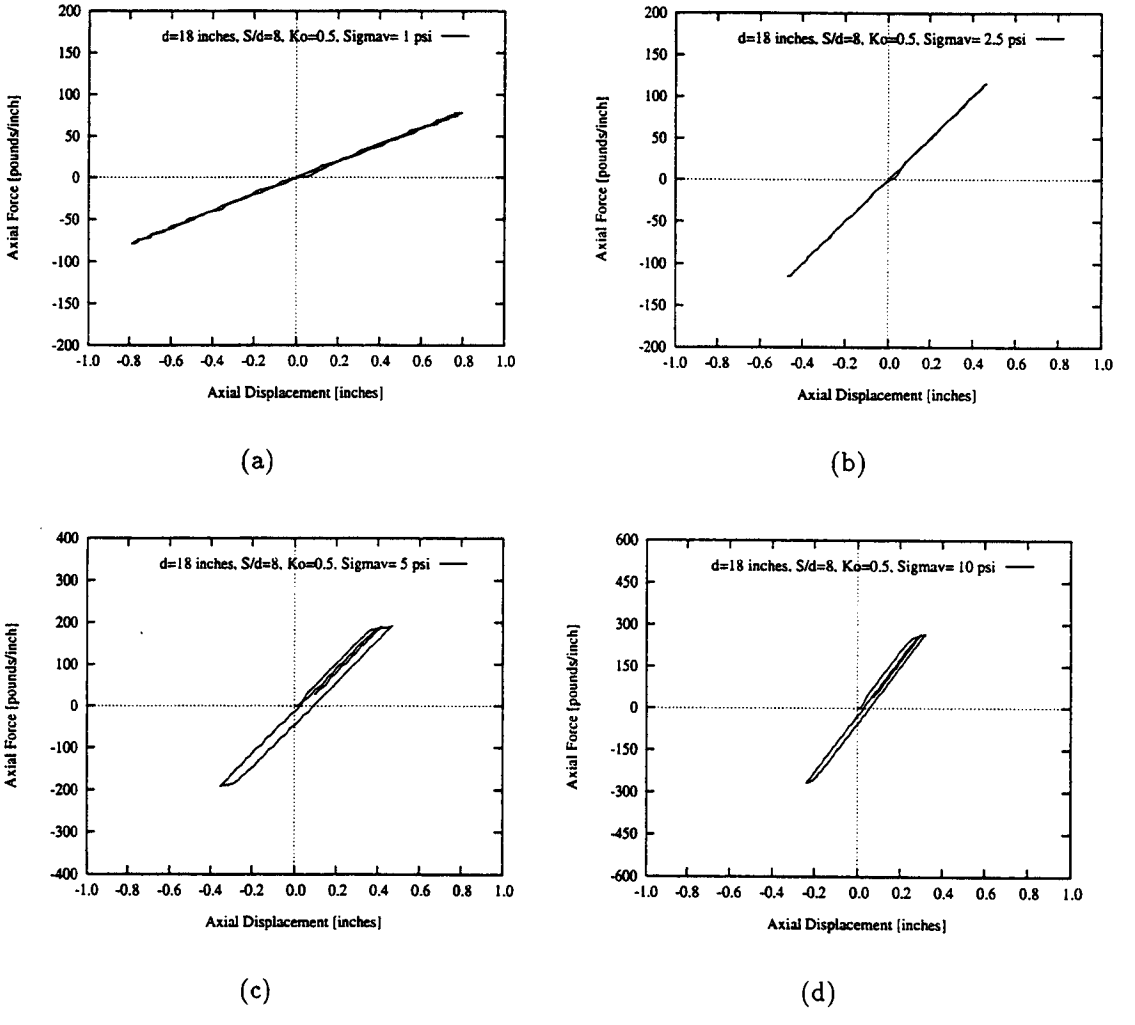

Figure E.47 *p-y* curves for the interaction-springs between pile and soil in a two-pile group for axial vibration for different confining pressures. [$d = 0.457\text{m} = 18$ in.; $s = 8d$]
(continued to the next page)

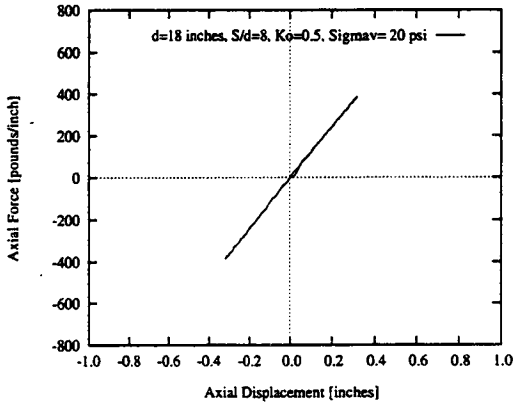

(e)

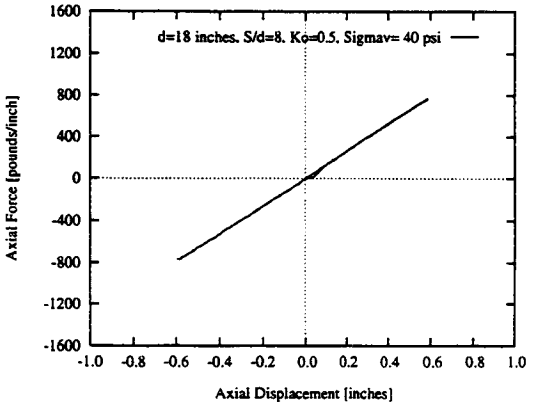

(f)

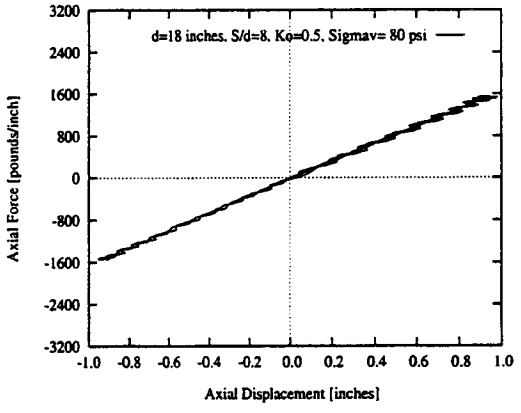

(g)

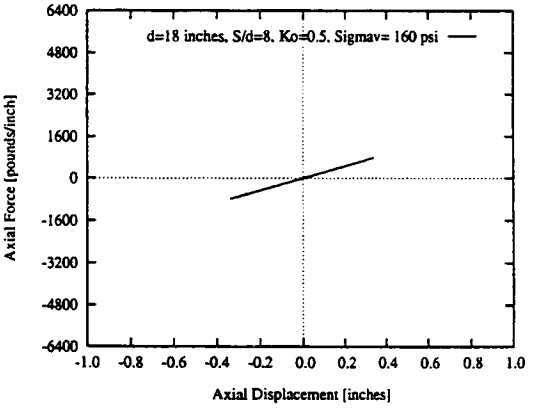

(h)

Figure E.47 p-y curves for the interaction-springs between pile and soil in a two-pile group for axial vibration for different confining pressures. [$d = 0.457\text{m} = 18$ in.; $s = 8d$] (continued)

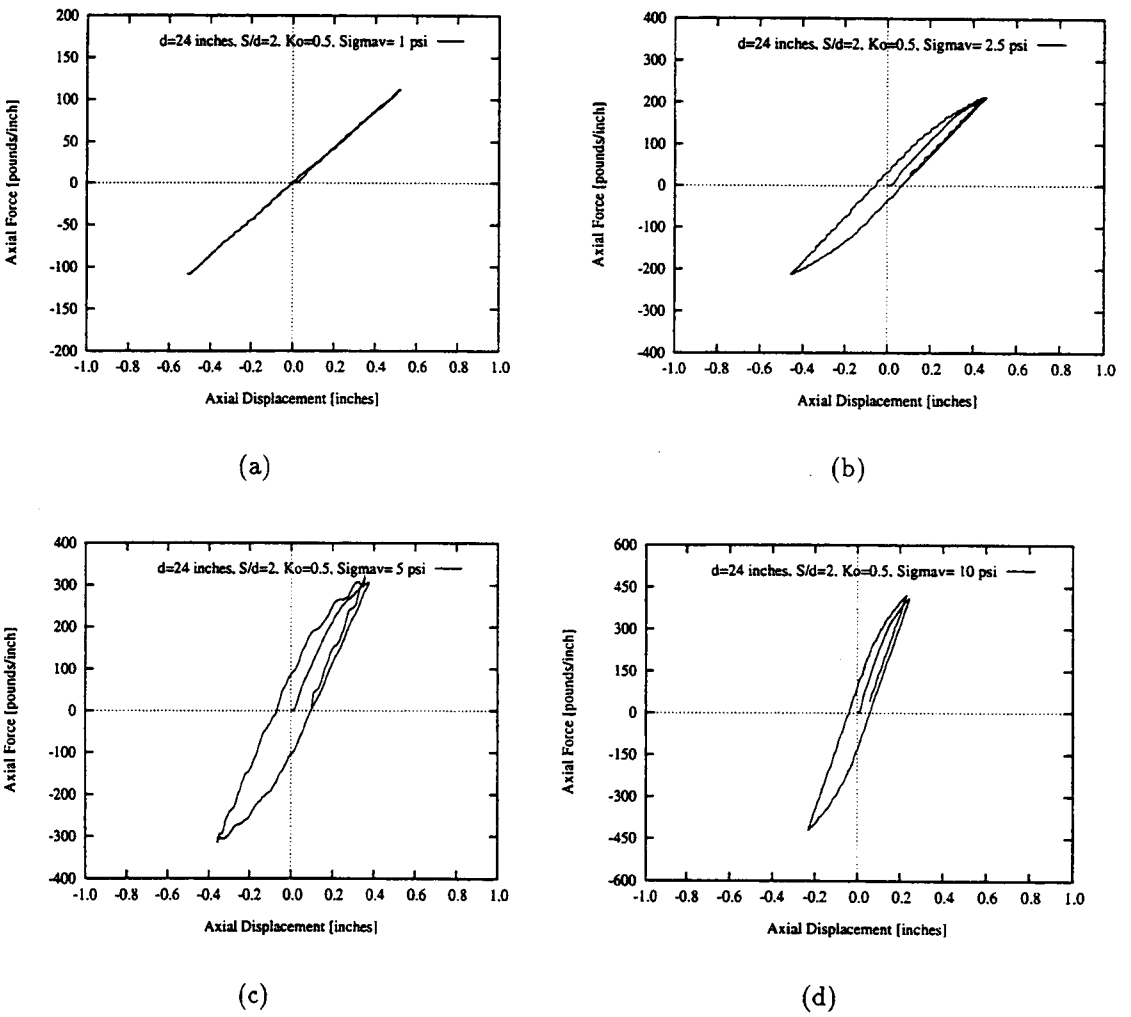

Figure E.48 p-y curves for the interaction-springs between pile and soil in a two-pile group for axial vibration for different confining pressures. [$d = 0.610\text{m} = 24$ in.; $s = 2d$]
(continued to the next page)

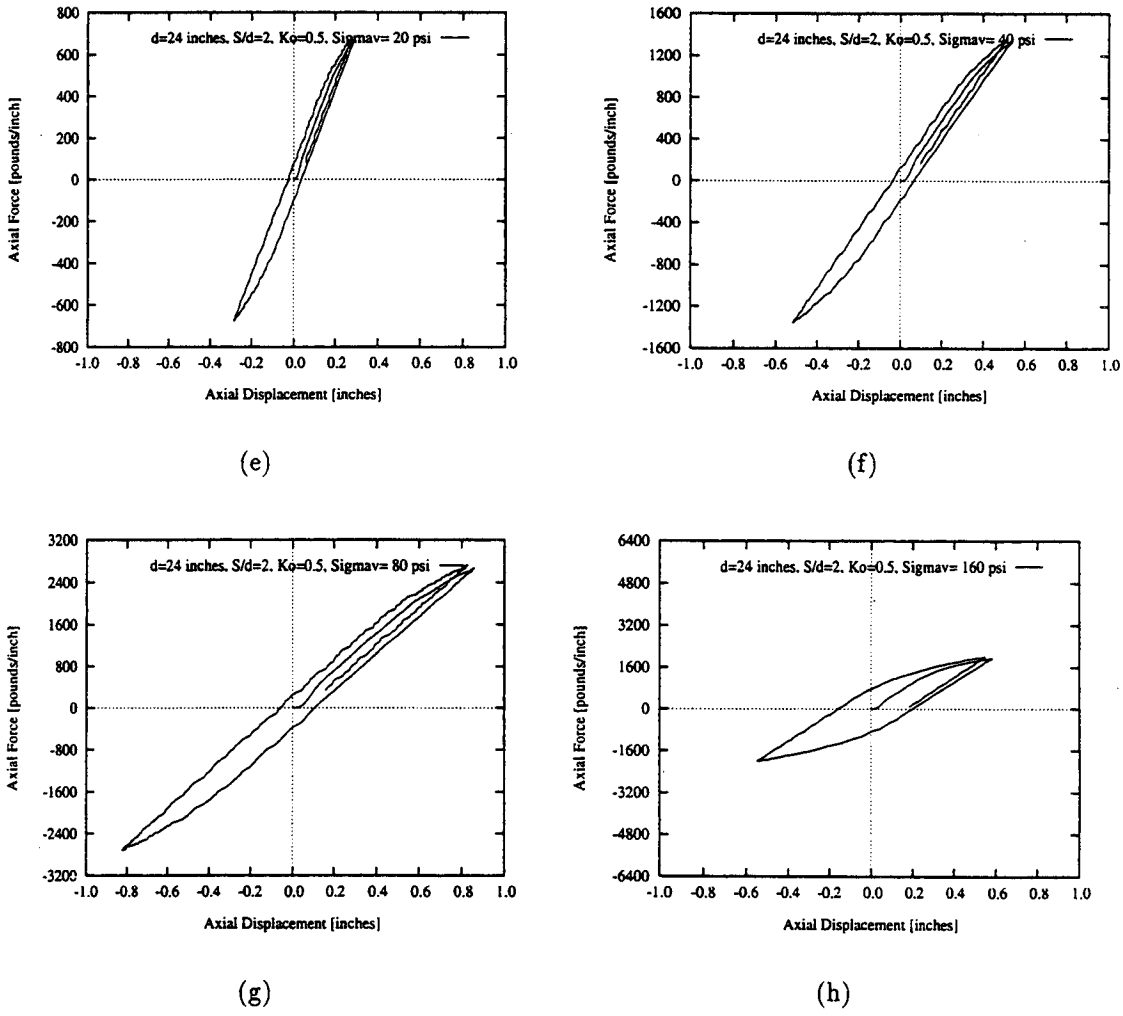

Figure E.48 p-y curves for the interaction-springs between pile and soil in a two-pile group for axial vibration for different confining pressures. [$d = 0.610\text{m} = 24$ in.; $s = 2d$] (continued)

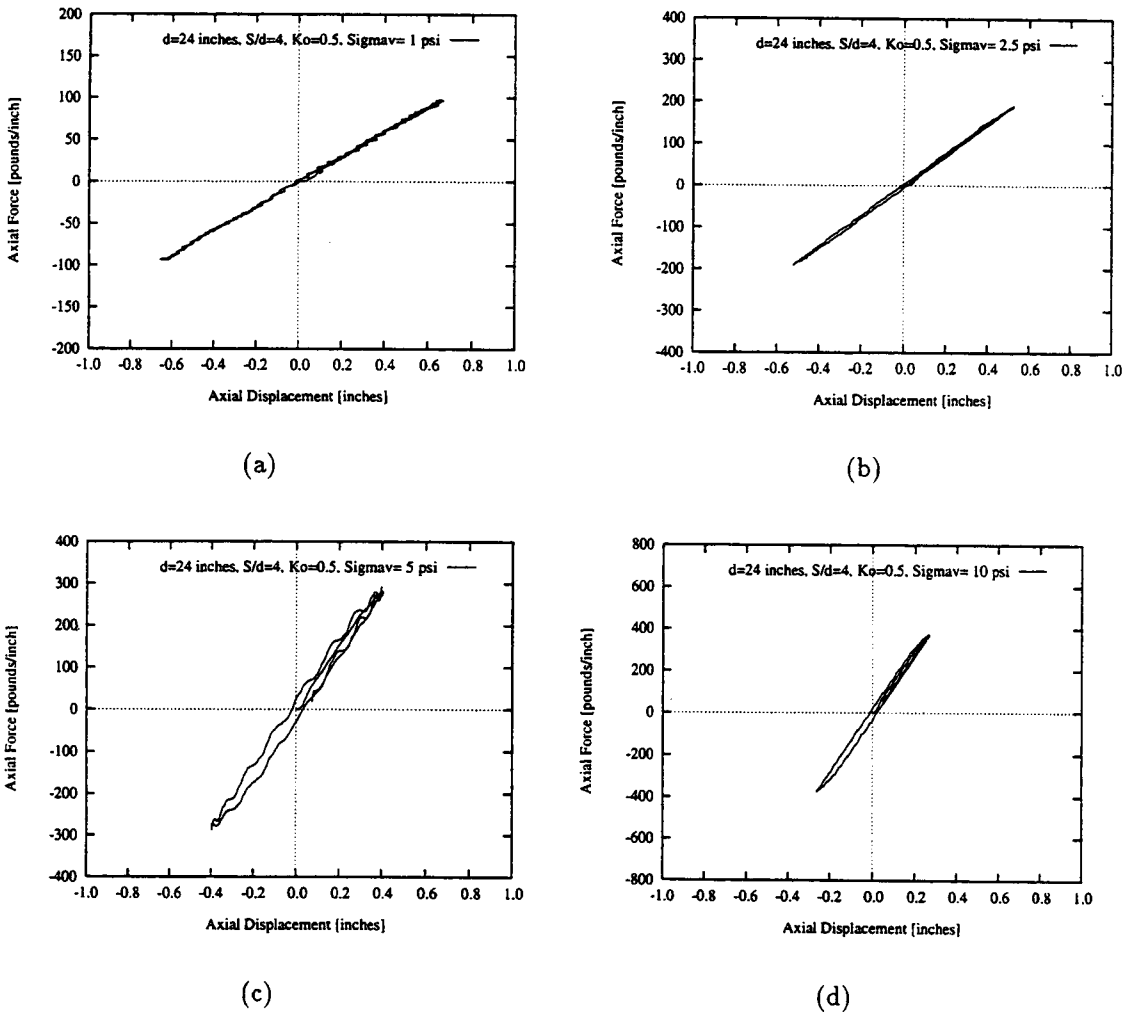

Figure E.49 p-y curves for the interaction-springs between pile and soil in a two-pile group for axial vibration for different confining pressures. [$d = 0.610\text{m} = 24$ in.; $s = 4d$]
(continued to the next page)

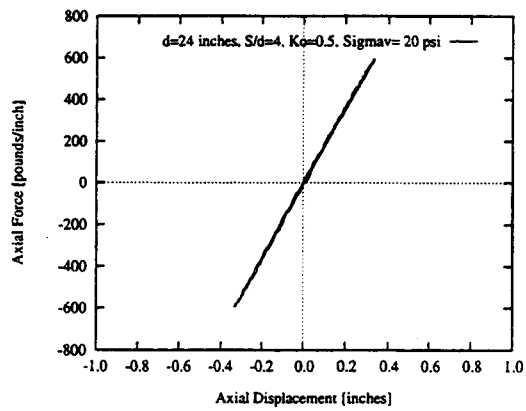

(e)

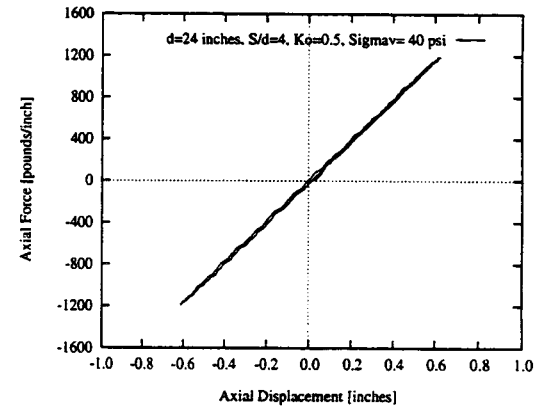

(f)

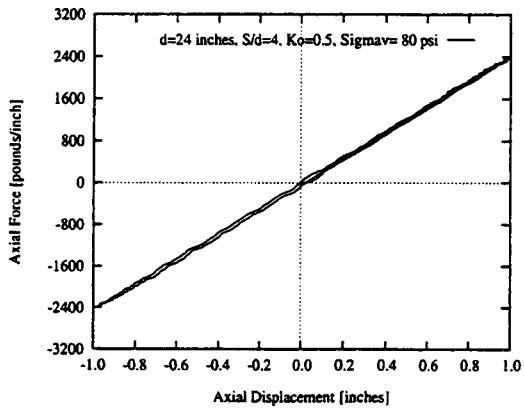

(g)

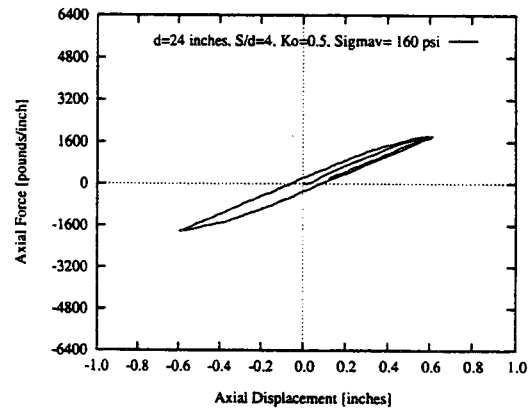

(h)

Figure E.49 p-y curves for the interaction-springs between pile and soil in a two-pile group for axial vibration for different confining pressures. [$d = 0.610\text{m} = 24$ in.; $s = 4d$] (continued)

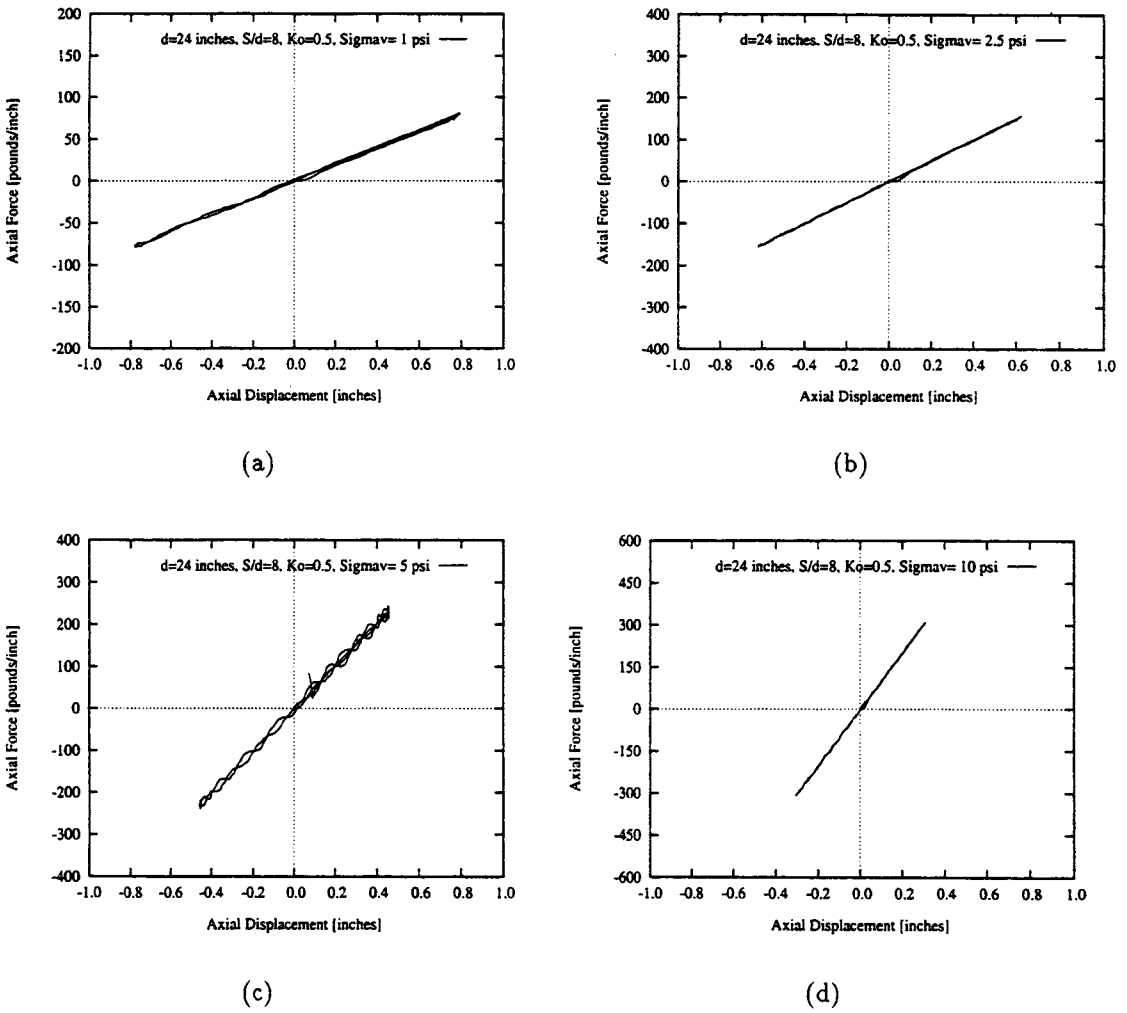

Figure E.50 p-y curves for the interaction-springs between pile and soil in a two-pile group for axial vibration for different confining pressures. [$d = 0.610\text{m} = 24$ in.; $s = 8d$]
(continued to the next page)

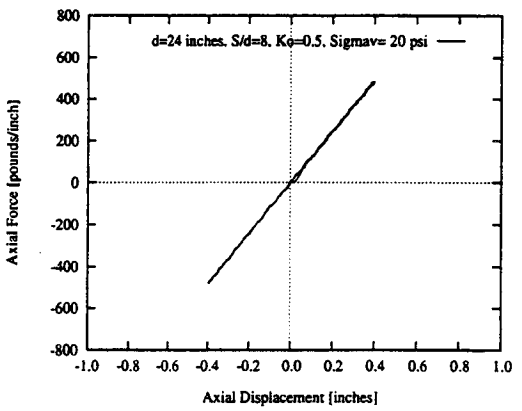

(e)

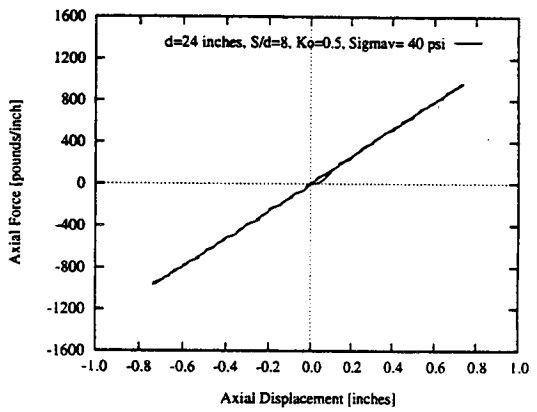

(f)

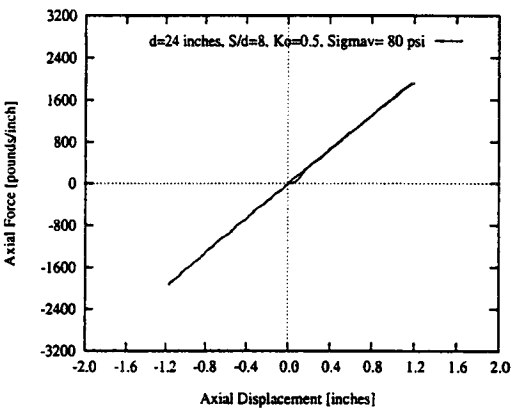

(g)

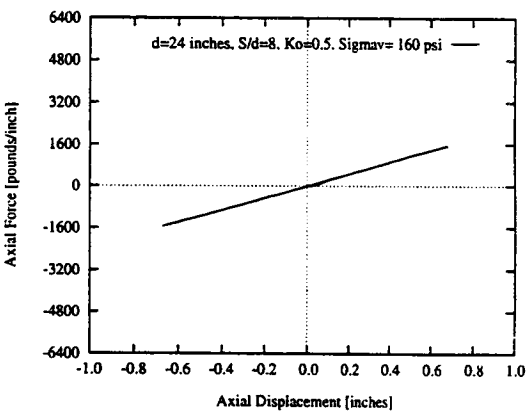

(h)

Figure E.50 p-y curves for the interaction-springs between pile and soil in a two-pile group for axial vibration for different confining pressures. [$d = 0.610\text{m} = 24$ in.; $s = 8d$] (continued)

E.2.3 Vibration of Pile Cap

E.2.3.1 Lateral Vibration of Pile Cap

For the modeling of this resistance, p-y curves were developed for circular and rectangular pile caps of different dimensions. Rigid behavior of the cap, elasto-plastic and elastic behavior of the soil in the near- and far-zones respectively, sliding interfaces, and plane-stress conditions were considered. Displacement of the soil at a distance of $20d$ or $20a$ (d, a = Dimensions of the circular and square caps, respectively) was considered to be negligible by providing an artificial, no displacement boundary. The resulting p-y behavior of the near-field springs are presented in Figures E.51 and E.52 for four different sizes of square and four different sizes of circular pile-caps for soil from the Snohomish river site. The NEABS parameters for those springs were computed, and they are presented in Table 2.19.

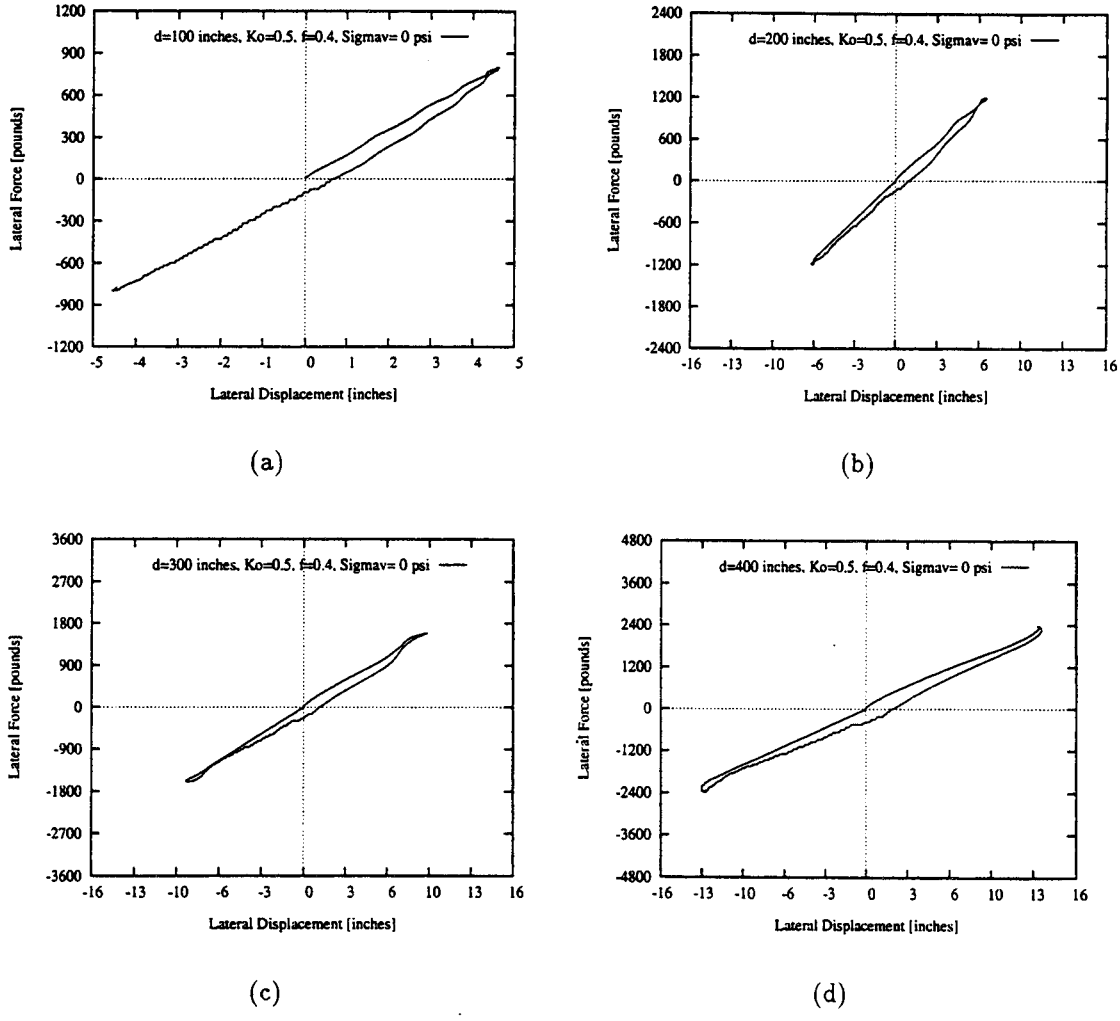

Figure E.51 P_c-Y_c curves for circular pile-caps of different sizes vibrating laterally. [K_0' = 0.50, f = 0.40, isotropic hardening, drained condition]

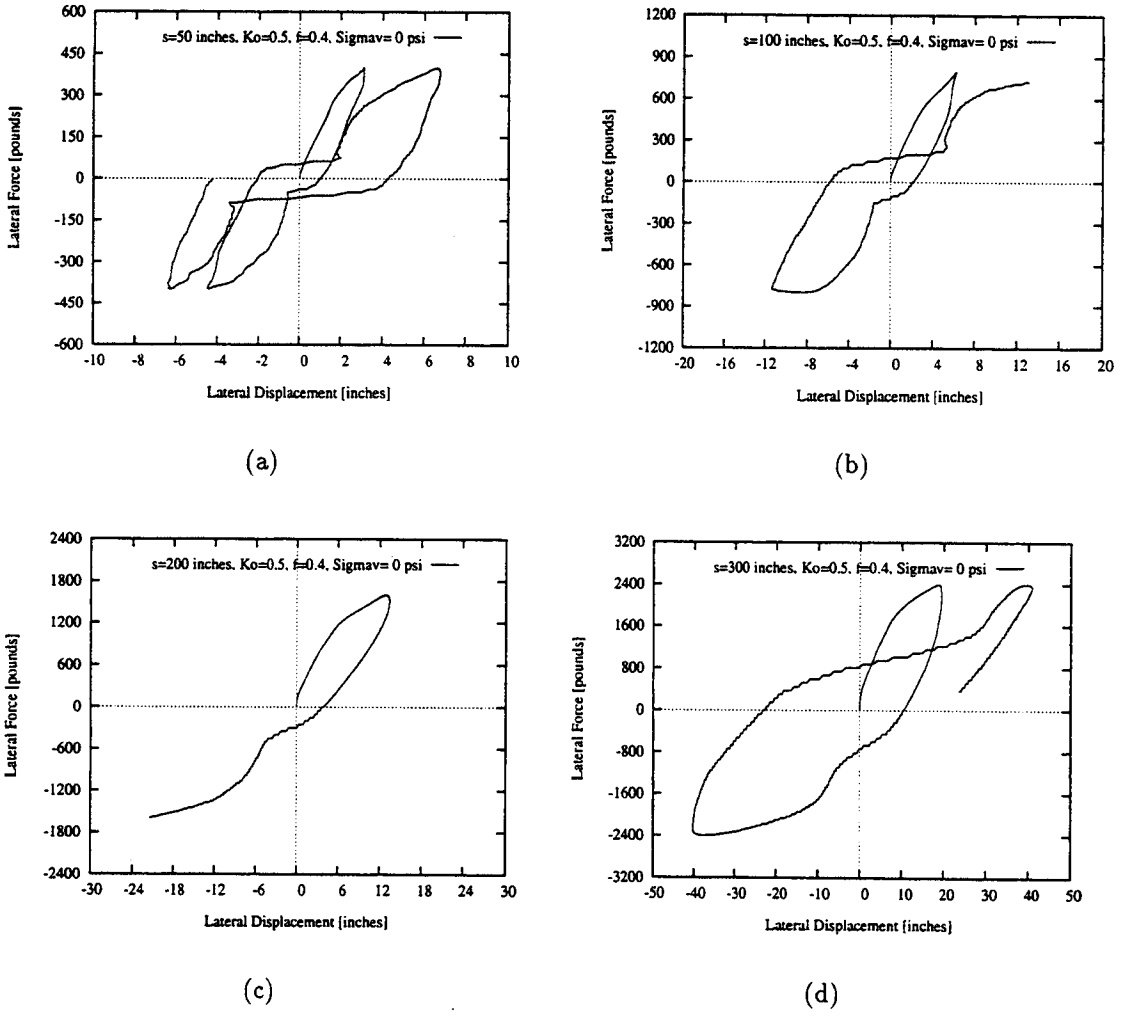

Figure E.52 P_c-Y_c curves for square pile-caps of different sizes vibrating laterally. [K_0' = 0.50, f = 0.40, isotropic hardening, drained condition]

E.2.3.2 Axial Vibration of Pile Cap

The side shear resistance to vertical movement was developed for both circular and rectangular caps in the same manner as for the single pile segment. No sliding interface was assumed to exist. Very little confining pressure, 6.9 kPa (1 psi) was considered. No lateral movement of the soil was assumed. The resulting T_c-Z_c behavior of the near-field springs are presented in Figures E.53 and E.54 for four different sizes of square and four different sizes of circular pile-caps for soil from the Snohomish river site. The NEABS parameters for those spring were computed, and they are presented in Table 2.20.

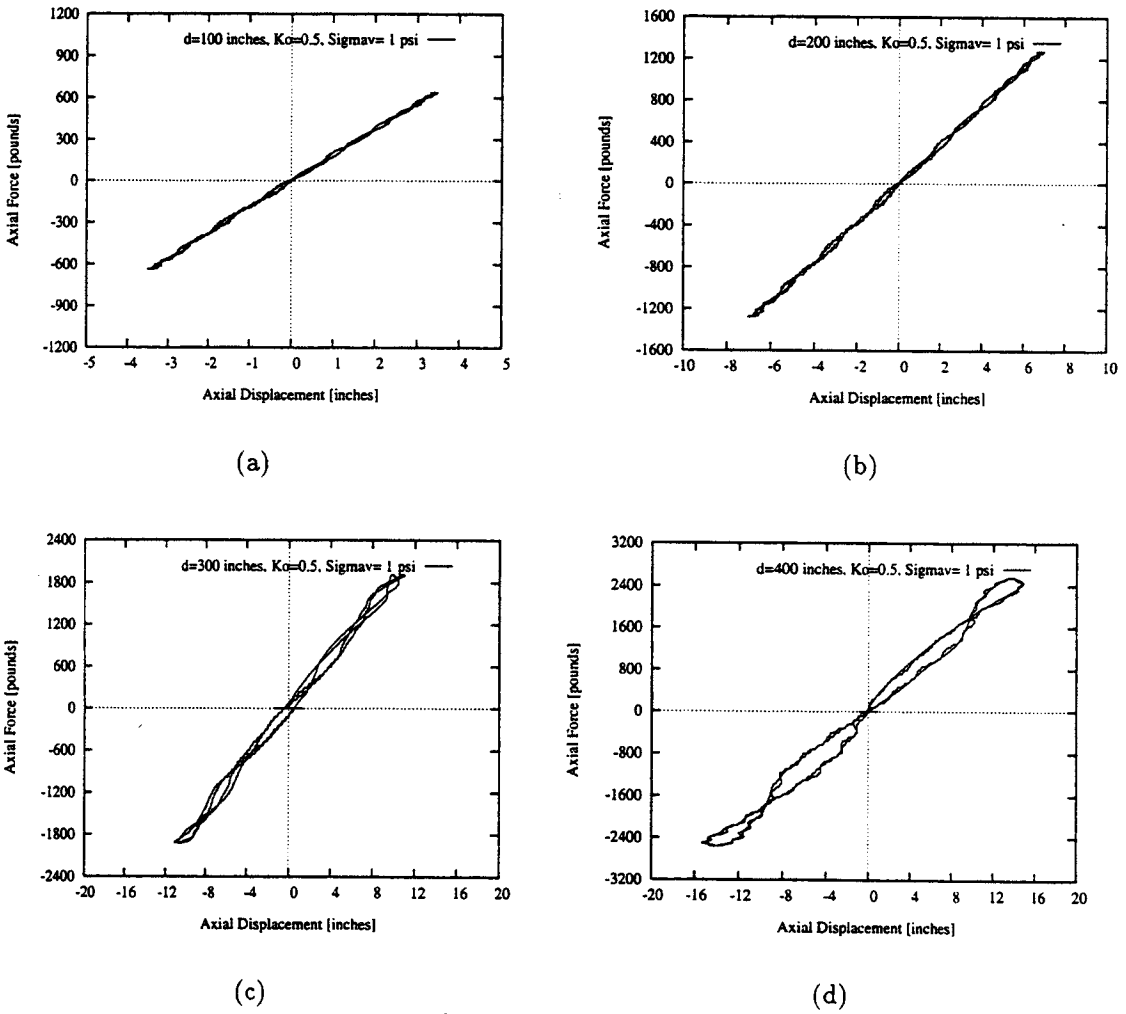

Figure E.53 T_c-Z_c curves for circular pile-caps for different sizes vibrating axially. [K_0' = 0.50, isotropic hardening, drained condition]

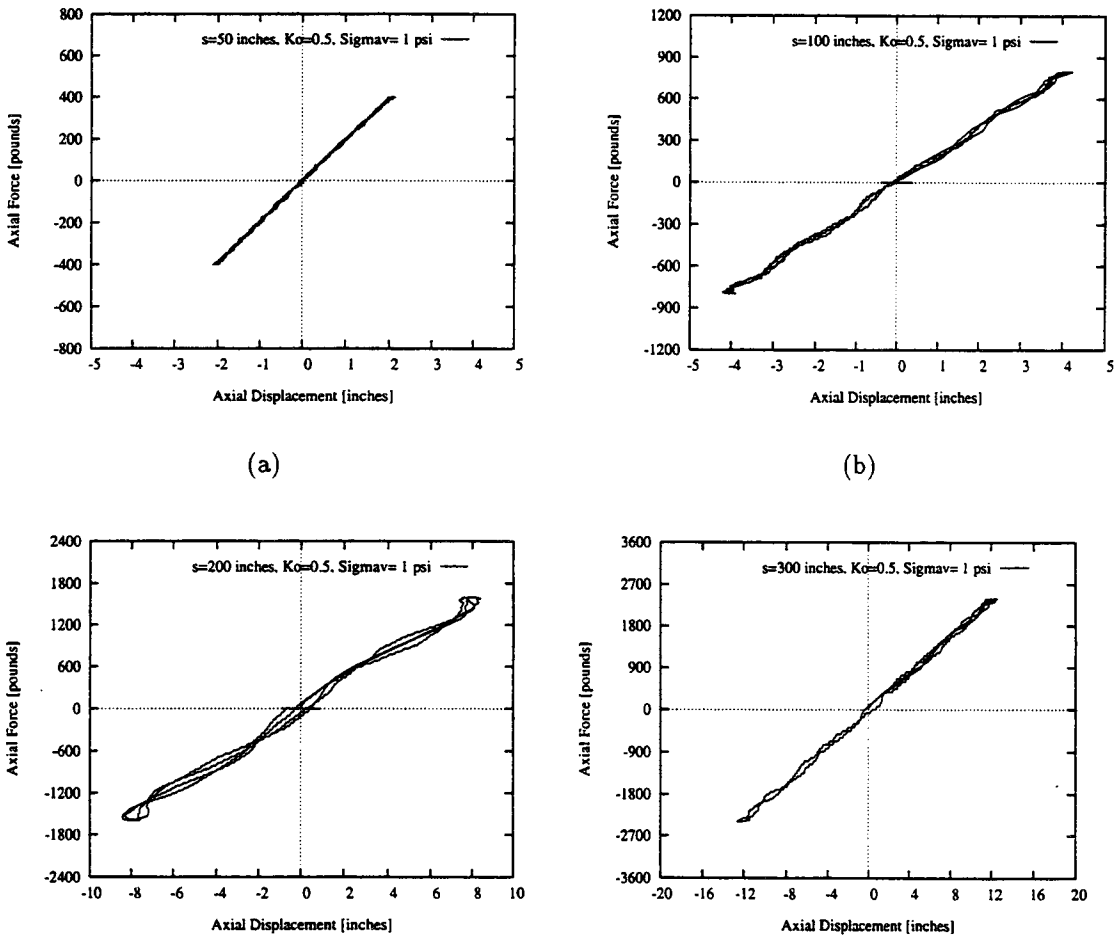

Figure E.54 T_c-Z_c curves for square pile-caps of different sizes vibrating axially. [$K_0' = 0.50$, isotropic hardening, drained condition]

Appendix F: HRZ Lumping of Soil Mass

F. 1 Introduction

A mass matrix is a discrete representation of a continuous mass. A consistent mass matrix is defined by the equation,

$$[m] = \int_v \rho [N]^T [N] dV. \qquad [F.1]$$

It is termed "consistent" because $[m]$ represents the same shape functions as those used to generate the element stiffness matrix. A simpler and historically earlier formulation is the "lumped" mass matrix, which is obtained by placing particle masses m_i at node i of an element, such that Σm_i is the total element mass. Particle "lumps" have no rotary inertia unless they are arbitrarily assigned, as is sometimes done for the rotational d.o.f. of beams and plates. A lumped mass matrix is diagonal, but a consistent mass matrix is not. The two formulations have different merits, and various considerations enter into deciding which one, or what combination of them, is best suited to a particular analysis procedure. In wave propagation problems using linear-displacement field elements, lumped masses give greater accuracy because of fewer spurious oscillations. Lumped masses are simpler to form, occupy less storage, and require less computational effort. Indeed, some methods of dynamic analysis are practical only with lumped mass matrices. The lumped mass matrices are effective and widely used. There are three ways to get a lumped mass matrix, as discussed below.

F.2 Ad hoc Lumping Scheme

This scheme is guided by intuition and physical insight. However, for higher-order elements or elements of triangular shape, intuition can be risky. Accordingly, systematic schemes for lumping are necessary.

F.3 HRZ Lumping Scheme

The HRZ (Hinton, Rock, and Zienkiewicz 1976; Surana 1978) scheme is an effective method for producing a diagonal mass matrix. It can be used for arbitrary elements. The idea is to use only the diagonal terms of the consistent matrix, but to scale them in such a way that the total mass of the element is preserved (Cook et al. 1989). The nodal lumped mass is proportional to the corresponding diagonal element of the consistent matrix, as expressed in the following equation:

$$M_i = \frac{m_{ii}}{\sum m_{jj}} M_{total} \qquad [F.2]$$

F.4 Optimal Lumping Scheme

Mass lumping can be thought of as the result of applying an appropriate quadrature rule to evaluate Equation F.2. If the integration points of a quadrature rule coincide with nodal locations of an element having translational d.o.f. only, then no off-diagonal terms are generated and the mass matrix is diagonal. If the element also has rotational d.o.f., then the lumping by quadrature produces block-diagonal matrices that are of lesser practical usefulness because they are not diagonal. In this report, only lumping by quadrature for elements with translational d.o.f. is considered.

Nodes of Lagrangian elements coincide with integration points of the Lobatto quadrature rule having positive weights only. Hence, optimal lumping for Lagrangian elements results in positive definite diagonal mass matrices, i.e., each node in the element has a positive mass associated with it. But optimally lumped diagonal mass matrices for triangular and serendipity quadrilateral elements (particularly for quadratic or higher elements) frequently have some zero or negative nodal masses.

For low order elements, such as the linear-displacement bar, the constant-strain triangle, and the bilinear quadrilateral, ad hoc lumping usually gives the same result as the optimal lumping. Also, for the quadratic Lagrange element, HRZ lumping and optimal lumping produces the same diagonal mass matrix. For cubic and higher order Lagrange

elements, HRZ lumping and optimal lumping may be different. For quadratic and higher order triangular and serendipity quadrilateral elements, HRZ lumping and optimal lumping are markedly different, and the HRZ lumped model can be less accurate for some problems (Malkus & Plesha 1986, Malkus et al. 1988).

F.5 Conclusion

Lumped masses based on exact integration is recommended, rather than the use of numerical integration with gauss points at the nodes. Because the assumed shape functions are of low order, the consistent matrix can be easily obtained, leading to the HRZ lumped mass matrix.